

Density Functional Theory for Superconductors: Extension to a Pairing Mediated by Spin-Fluctuations

Dissertation

zur Erlangung des akademischen Grades
Doctor rerum naturalium (Dr. rer. nat.)

vorgelegt der

Naturwissenschaftlichen Fakultät II – Chemie, Physik und Mathematik
der Martin-Luther-Universität Halle-Wittenberg

von Frank Essenberger
geboren am 12.11.1984 in Berlin, Deutschland

Gutachter:

Prof. Dr. Eberhard K. U. Gross, MPI Halle (Saale)
Prof. Dr. Giovanni Vignale, University of Missouri
Prof. Dr. Jamal Berakdar, MLU Halle-Wittenberg

Halle (Saale), den 28.10.2014

Table of Contents

List of Figures and Tables	viii
List of Acronyms	ix
List of Symbols	xi
1. Introduction	1
2. Introduction to Green's Functions	5
2.1. The Matsubara Green's Function	6
2.2. The Response Function	7
2.3. Perturbation Expansion	10
2.4. The Feynman Diagrams	14
3. Introduction to Density Functional Theory for Superconductors	17
3.1. Foundation of DFT for Superconductors	18
3.2. The Kohn-Sham Bogoliubov-de Gennes Equations	19
3.2.1. Real Space Form	19
3.2.2. Change to Bloch Representation	20
3.3. Construction of Δ^{xc} Including Spin-Fluctuation Effects – The next Steps	23
4. Hedin Equations for Superconductors	25
4.1. The Equation of Motion	25
4.2. Introduction of the Hedin Cycle	27
4.3. Extension of the Diagrammatic Rules	29
4.4. Perturbation Theory \leftrightarrow DFT – The Sham-Schlüter Equation	30
4.5. Summary	31
5. Finding the Spin-Fluctuations	33
5.1. Simplification of the Hedin Equations	34
5.1.1. Simplify the Vertex	34
5.1.2. Locate the Magnetic Fluctuations	35
5.1.3. Rewrite the Self-Energy	37
5.2. Reduction to an Effective Interaction	42
5.2.1. Preparation	42
5.2.2. Construction Effective Interaction	44
5.3. Self-Energy with Effective Interaction	46
5.4. Discussion of the Effective Interaction	48
5.4.1. The Approximations	48
5.4.2. Comparison with other Effective Interactions	50
5.5. The Question of Self-Consistency	52
5.6. Summary	53
6. The SCDFE Functional Containing Spin-Fluctuations	55
6.1. Construction of the Functional	55
6.1.1. Evaluation of Matsubara Summation	57

6.1.2. Inclusion of Phonons	58
6.1.3. Final Expression	59
6.2. Discussion of the Gap Equation for two Bands	60
6.3. Model Calculation	63
6.3.1. Comparison to Conventional Systems	63
6.3.2. Interplay between Spin-Fluctuations, Phonons and Coulomb Contributions	65
6.4. Summary	67
7. Results – Fe Bases Superconductors	69
7.1. Non-Superconducting Ground State	71
7.2. A Phenomenological Connection	73
7.3. Contributions to the SC Pairing	76
7.3.1. Phonon Contributions	76
7.3.2. Electronic Contributions	79
7.4. SCDFE Calculation	84
7.5. Summary	85
8. Summary, Conclusion and Outlook	87
Appendices	
A. Transformations	A-1
A.1. Fourier Transformation – No Boundary Conditions	A-1
A.1.1. Space	A-1
A.1.2. Time	A-1
A.2. Fourier Transformation – Boundary Conditions	A-1
A.2.1. Space	A-1
A.2.2. Time	A-3
A.3. Spin Space Transformation	A-3
B. Normal State Green’s and Response Functions	B-1
B.1. Properties of the Green’s Function and Response Function	B-1
B.1.1. Time Independent System	B-1
B.1.2. Periodic Hamiltonian	B-2
B.1.3. Collinear Hamiltonian	B-3
B.1.4. The Spectral Representation	B-3
B.2. Coupling Constant Integration	B-5
B.3. Non-SC Response Function	B-6
B.3.1. χ^M – Many-Body Approach	B-6
B.3.2. χ^M – DFT Approach	B-7
B.4. Adiabatic Local Density Approximation	B-8
C. DFT for Superconductors	C-1
C.1. The Pairing Potential	C-1
C.2. KS-Bogoliubov-de Gennes Transformation	C-2
C.2.1. Introduction of the Bogoliubons	C-2
C.2.2. Commutator Relations for the Bogoliubons	C-2
C.2.3. Decoupling Approximation	C-3
C.2.4. Eigenvalues and Vectors of the KS-BdG Equations	C-4
C.3. Group Theory for the Gap	C-4
C.4. The Kohn-Sham Green’s function	C-8
C.4.1. The Kohn-Sham Green’s function – Real Space	C-8
C.4.2. The Kohn-Sham Green’s Function – Bloch Representation	C-9

D. Hedin Equations for Superconductors	D-1
D.1. Nambu Green's Function	D-1
D.1.1. Equation of Motion	D-1
D.1.2. Single-Particle Contributions	D-1
D.1.3. Two-Particle Contributions	D-2
D.1.4. Schwinger's Functional Derivative Approach	D-3
D.2. The Loop Rule	D-4
D.3. Different Reference Systems	D-5
E. Sham-Schlüter Equation	E-1
E.1. Frequency Sums – Residue Theorem	E-1
E.2. Various Terms in the Sham-Schlüter Equation	E-2
E.2.1. The GG^\dagger Term	E-2
E.2.2. The I Term	E-3
E.2.3. Preparation for the Self-Energy Terms	E-3
E.2.4. The $G^{\text{KS}}\Sigma_{12}G^{\text{KS}\dagger}$ Term	E-5
E.2.5. The $G^{\text{KS}}\Sigma_{11}F^{\text{KS}}$ Term	E-6
E.3. Approximations to the Gap Equation	E-7
E.3.1. The Fully Linearized Gap Equation and Isotropic Approximation	E-7
E.3.2. Alternative Gap Equation	E-8
E.4. Details for the Implementation of the Matrix Elements	E-10
Index	I
Bibliography	V
Acknowledgments	XVII
Curriculum Vitae	XVIII
Eidesstattliche Erklärung	XVIII

List of Figures

2.1. Example of the translation between diagrams and equations	14
2.2. Dyson equation for the Green's function	15
2.3. Dyson equation for the response function	15
2.4. Dyson equation for the screened Coulomb interaction	15
2.5. Self-energy	16
2.6. Example of the diagrammatic expansion for some important sets.	16
3.1. Occupation of the two branches in the superconducting system.	22
4.1. Different ways to evaluate the functional derivative in the expression for the vertex.	28
4.2. Extension of the diagrammatic rules in the superconducting case.	30
4.3. Exact superconducting Hedin equations and the Gw approximation.	30
5.1. Vertex in the ladder approximation.	33
5.2. Dyson equation for the vertex	34
5.3. Creation of the direct and crossed contribution by the functional derivative.	35
5.4. Each contribution to the particle-hole propagator is either direct or crossed.	36
5.5. Direct and crossed particle-hole propagators.	36
5.6. Crossed and direct contribution in the vertex	37
5.7. Dyson equation for Λ^P	37
5.8. T -matrix self-energy contribution.	38
5.9. Approximation for the self-energy including magnetic fluctuations.	39
5.10. Direct and crossed contribution in the normal part of the self-energy.	39
5.11. Creation of the self-energy contribution related to the T -matrix.	40
5.12. Comparison between the exact and approximated self-energy.	40
5.13. Overview of the approximation applied to the Hedin equations.	41
5.14. Hartree potential	42
5.15. Double counting errors induced by the T -matrix self-energy.	48
5.16. Intrinsic double counting errors created by GT	49
5.17. Double counting errors related to $G\Lambda^d$	49
5.18. Particle-particle variant of the T -matrix.	50
5.19. Self-energy corresponding to T_{pp}	50
5.20. Difference of an interaction between test particles and "physical electrons".	52
5.21. Hedin cycle with the effective interaction.	53
6.1. Final approximation to the self-energy.	60
6.2. Discussion of the Coulomb and spin-fluctuation contribution in the two band system.	62
6.3. Comparison of the model calculation to the Eliashberg trends.	64
6.4. Effect of Coulomb range on the critical temperature.	66
6.5. Comparison between the one and two band case.	67
7.1. Structural families in the iron based superconductors	69
7.2. Fermi surface in the iron based superconductors.	70
7.3. Experimental critical temperature as a function of pressure for FeSe and LiFeAs	70
7.4. Experimental results for the unit cell parameter in FeSe and LiFeAs	71
7.5. The checkerboard and stripe magnetic structure	72

7.6. Principle form of the magnetic phase transition.	73
7.7. Magnetic moment as a function of the lattice position.	74
7.8. Change of the magnetic susceptibility close to a phase transition.	74
7.9. Possible gap symmetries for singlet pairing in the tetragonal lattice.	77
7.10. Overview of the phononic contribution in the FeSe and LiFeAs.	78
7.11. Overview of the Coulomb contribution in FeSe and LiFeAs.	80
7.12. Overview of the spin-fluctuation contribution.	83
7.13. Critical temperature as a function of pressure for FeSe and LiFeAs.	84
7.14. Gap function close to the phase transition for FeSe and LiFeAs.	85
D.1. Picture explaining the loop rule.	D-5
E.1. Poles of the Fermi and Bose function in the complex plane.	E-1
E.2. Different contours in the analytic evaluation of the Matsubara sum.	E-2
E.3. Spin fluctuation interaction in plane wave representation.	E-11
E.4. Comic in the acknowledgments	XVII

List of Tables

1.1. Overview of the critical temperatures in the iron based superconductors.	3
7.1. Results of the structural relaxation.	71
7.2. Values of the control parameter used in the calculation.	75
C.1. Representations and basis functions of the tetragonal point group.	C-7

List of Acronyms

A

AFM anti ferro magnetic.
ALDA adiabatic local density approximation.
ARPES angle resolved photon emission spectroscopy.
ASA Atomic Sphere Approximation.

B

BCS Bardeen, Cooper and Schrieffer.
BdG Bogoliubov-de Gennes.
BZ Brillouin zone.

C

CB checkerboard.
CPA coherent potential approximation.

D

DC double counting.
DFT density functional theory.
DLM disordered local moments.
DMF dynamical mean field.
DOS density of states.

F

FeSC iron based superconductors.
FT Fourier transformation.

G

GF Green's function.
GGA generalized gradient approximation.

H

HEG homogenous electron gas.

K

KKR Korringa-Kohn-Rostoker.
KS Kohn-Sham.
KS-BdG Kohn-Sham Bogoliubov-de Gennes.

L

LDA local density approximation.
LR linear response.
LRDFT linear response density functional theory.

M

MBPT many-body-perturbation theory.

N

NM non-magnetic.

NMR nuclear magnetic resonance.

O

OEP optimized effective potential.

P

Ph phonons.

Ph.D. philosophiae doctor.

PM paramagnetic.

PW plane wave.

Q

QP quasi particle.

R

RPA random phase approximation.

S

SC superconductivity.

SCDFT superconducting density functional theory.

SF spin-fluctuations.

SQUID superconducting quantum interference device.

SSEq Sham-Schlüter equation.

T

T_c critical temperature.

X

XC exchange-correlation.

List of Symbols

constants

π circ. circumference / diameter	A-1
i imaginary unit $i^2 = -1$	A-1
k_B Boltzman constant	6
a_0 Bohr radius	73
T_c critical temprature	63
$\sigma_{\alpha\beta}^i$ Pauli matrix $i = 0, x, y, z$	A-3
τ^z Nambu matrix $\tau^z = \sigma^z$	25
τ^0 Nambu matrix $\tau^0 = \sigma^0$	26
$\mathbf{1}$ unit matrix	D-5
\mathbf{q}_M vector in inverse space $(\frac{p_i}{a}, \frac{p_i}{a}, 0)$	83
\mathbf{q}_X vector in inverse space $(\frac{2\pi}{a}, 0, 0)$	83
\mathbf{q}_Γ vector in inverse space $(0, , 0)$	83
\mathbf{q}_C vector for which response is singular	63
Ω_{WS} volume Wigner Seitz cell	A-1
N number of unit cells	A-1
a edge length of the tetragonal base area	69
c height of the tetragonal cell	69
Z_G^0 partition func. of non-interact. system	6
Z_G^{KS} part. func. of KS system	C-8
Z_{GS} partition function of full system	6

variables

μ chemical potential	6
T temperature	6
β inverse temperature $1/(k_B T)$	6
N particle number	6
P pressure	71
V volume	71
E energy	E-8
\mathbf{r} vector in space (x, y, z)	6
σ, β, α spin coordinate	6
t real time	B-1
ω real frequency	B-1
τ complex time	B-2
ω_n Matsubara frequency	B-2
\mathbf{x}_1 combined variable $\{\mathbf{r}_1, \tau_1\}$	7
\mathbf{l} combined variable $\{\mathbf{r}_1, \sigma_1, \tau_1\}$	7
$\bar{\mathbf{r}}$ vector in the unit cell	A-1
\mathbf{T} translational vector	A-1
\mathbf{k}, \mathbf{q} vector in the BZ	A-1
n, m, i, j band index	20
k collective index $\{n, \mathbf{k}\}$	20
\mathbf{G}, \mathbf{G}' vec. outside the 1st BZ	A-1

operators

$h.c.$ hermitian conj. of the op. left to $h.c.$	C-1
$\sum_k O_k$ sum with respect to k	20
$\hat{\sum}_k O_k$ sum over one branch of the KS GF	22
$\Delta d1O(1)$ integral with respect to 1	7
$\text{ff } d\gamma O$ curvature integral along γ	E-1
$\langle \hat{O} \rangle_0$ thermal average with respect to $\hat{\rho}_0$	6
$\langle \hat{O} \rangle_{KS}$ ther. aver. with respect to $\hat{\rho}_{KS}$	C-8
$\langle \hat{O} \rangle$ ther. aver. with respect to the full $\hat{\rho}$	6
\hat{A}, \hat{B} generic operators	B-3
\hat{A}_S operator in Schrödinger picture	7
$\hat{A}_D(\tau)$ operator in Dirac picture	10
$\hat{A}_H(\tau)$ operator in Heisenberg picture	7
$U(\tau_1, \tau_2)$ time evolution operator	10
$\hat{\rho}_\beta^0$ non-interacting statistical op.	6
$\hat{\rho}_\beta^{KS}$ statistical op. of KS system	C-8
$\hat{\rho}_\beta$ statistical operator	6
$\hat{\rho}_\beta^\lambda$ statistical operator of \hat{H}_λ	B-5
$\hat{\rho}^{LR}$ stat. op. in linear response theory	8
\hat{T} time ordering operator	7
$\hat{\mathcal{P}}$ principle value integral	B-5
$\hat{A}\hat{B}$ contraction of the operators \hat{A} and \hat{B}	12
\hat{H}_0 non-interacting Hamiltonian	6
\hat{T} kinetic energy operator	6
\hat{V}_0 local potential operator	6
\hat{N} particle number operator	6
\hat{K}_0 operator difference: $\hat{K}_0 - \mu\hat{N}$	6
\hat{K}_{KS} operator difference: $\hat{K}_{KS} - \mu\hat{N}$	C-8
\hat{K} operator difference: $\hat{K} - \mu\hat{N}$	6
\hat{W} Coulomb interaction	6
\hat{W}_{el-ph} electron-phonon coupling	23
\hat{H} full Hamilton operator	6
\hat{H}_λ Hamiltonian with scaled interaction	B-5
\hat{H}_{SC} condensation energy op.	25
$\hat{\Phi}(\mathbf{r})_t$ external field operator	i
$\hat{b}_{\lambda\mathbf{q}}, \hat{b}_{\lambda\mathbf{q}}^\dagger$ Phonon creation/annihilation op.	23
$\hat{\Phi}_{\lambda\mathbf{q}}, \hat{\Phi}_{\lambda\mathbf{q}}^\dagger$ momentum cons. ph. op. $\hat{\Phi}_{\lambda\mathbf{q}} := \hat{b}_{\lambda\mathbf{q}} - \hat{b}_{\lambda-\mathbf{q}}^\dagger$	23
$\hat{\Psi}_\sigma(\mathbf{r}), \hat{\Psi}_\sigma^\dagger(\mathbf{r})$ field operators	6
$\hat{\rho}(\mathbf{r})$ charge density operator	19
$\hat{\mathbf{m}}(\mathbf{r})$ magnetic moment density op.	25
$\hat{\chi}(\mathbf{r}, \mathbf{r}')$ anomalous density operator	17

Hedin equation

\bar{A} Nambu matrix	25
\bar{A}_{ij} ij -element of a Nambu matrix	28
$\bar{G}^{\text{HEG}}(12)$ free GF	D-5
$\bar{G}^0(12)$ non-interacting GF	D-5
$\bar{G}^{\text{H}}(12)$ Hartree GF	D-5
$\bar{G}^{\text{KS}}(12)$ Kohn-Sham GF	D-6
$\bar{G}(12)$ full Nambu GF	7
$G(12), G^\dagger(12)$ diagonal elements of $\bar{G}(12)$	25
$F(12), F^\dagger(12)$ off-dia. elements of $\bar{G}(12)$	25
$G^{\text{R}}(12)$ retarded GF	9
$G^{\text{A}}(12)$ advanced GF	10
$G^{\text{M}}(12)$ Matsubara GF	7
$\bar{G}^{\text{app}}(12)$ approximation to the full $\bar{G}(12)$	31
$\chi_{ij}^{\text{KS}}(12)$ KS density-density response	B-7
$\chi_{ij}(12)$ density-density response	9
$F_{AB}^{\text{R,A,T,M}}$ either GF or response func.	B-1
$D_{\lambda\mathbf{q}}(\omega)$ phonon propagator	58
$\bar{M}(12)$ self-energy with Hartree terms	14
$\Sigma(12)$ self-energy without Hartree terms	27
$\bar{\Sigma}^{\text{app}}(12)$ approximation to $\bar{\Sigma}(12)$	31
$\Gamma(123)$ vertex function	i
$P(12)$ polarization propagator	29
$w(12)$ screened Coulomb interaction	29
$w^{\text{RPA}}(12)$ w in random phase app.	40
$w^{\text{G}}(12)$ dia. Coulomb: $w - 4(f_{\uparrow\uparrow}^F + f_{\uparrow}^F)$	47
$w^{\text{F}}(12)$ off-dia Coulomb: $w - 4(f_{\uparrow\downarrow}^F + f_{\uparrow}^F)$	47
$A_{\sigma\sigma'}$ short for $A_{\sigma\sigma\sigma'\sigma'}$	44
A_{σ}^F short for $A_{\sigma-\sigma\sigma-\sigma}$	44
$\epsilon^{-1}(12)$ dielectric function	27
$v(12)$ bare Coulomb interaction	6
$\bar{h}_{\alpha\beta}^0$ matrix element \hat{H}_0	26
$\bar{h}_{\alpha\beta}^{\text{H}}$ matrix element $\hat{H}_0 + \text{Hartree term}$	27

functions

$\theta(t - t')$ unit-step function	9
δ_{ij} flexible Kronecker δ or δ -distribution	A-1
$\text{Re}[z]$ real part of z	B-4
$\text{Im}[z]$ imaginary part of z	B-4
$\Re[A]$ Hermitian part of A	B-4
$\Im[A]$ anti Hermitian part of A	B-4
$\mathcal{O}[v^n]$ terms higher order than n in v	12
z_{σ} spin sign function $\{\uparrow, \downarrow\} \rightarrow \{+, -\}$	25
$f_{\beta}(E)$ Fermi function	E-1
$b_{\beta}(E)$ Bose function	E-1
$I_{\beta}(EE'\omega)$ result Matsubara summation	E-3
Z_{G} partition function	6
$S(UVN)$ interacting entropy	6
$\Omega_0(\mu NT)$ non-interacting grand kan. pot.	6
$\Omega_{\text{KS}}(\mu NT)$ KS grand kan. pot.	18
$\Omega(\mu NT)$ interacting grand kan. potential	6
$N(E)$ DOS	63

$\rho(\mathbf{r})$ electronic density	20
$\chi(\mathbf{r}, \mathbf{r}')$ anomalous density	20
$\mathbf{m}(\mathbf{r})$ magnetic moment	25
$v_0(\mathbf{r})$ nuclei potential	6
$g_{\lambda\mathbf{q}}^{\text{el-ph}}$ electron-phonon coupling	23
$v^{\text{H}}(\mathbf{r})$ Hartree potential	27
$\varphi_i(\mathbf{r}t)$ external potential	26
$\Phi_0(\mathbf{r}t)$ total field $\varphi_0(\mathbf{r}t) + v_{\text{H}}(\mathbf{r})$	27

spin-fluctuation functional

$T(1234)$ T -matrix	33
$T_{\text{pp}}(1234)$ particle-particle T -matrix	49
$\Lambda^{\text{P}}(1234)$ proper part.-hole propagator	37
$\Lambda^{\text{c}}(1234)$ crossed part.-hole propagator	35
$\Lambda^{\text{d}}(1234)$ direct part.-hole propagator	35
$\Lambda^{\text{c-d}}(1234)$ the difference: $\Lambda^{\text{c}} - \Lambda^{\text{d}}$	35
$\Lambda^{\text{Ph}}(\mathbf{x}_1\mathbf{x}_2)$ phonon effective interaction	58
$\Lambda^{\text{SF}}(\mathbf{x}_1\mathbf{x}_2)$ SF effective interaction	42
$a_{\text{C}}, a_{\text{D}}$ coefficient for C and D -term	55
T symmetry operation	C-5
$P(T)$ trans. op. corresponding to T	C-5
$\Gamma_{nm}^r(T)$ irreducible representation r	C-5
$\chi^r(T)$ trace of irr. representation	C-5
$f_{ij}^{\text{xc}}(\mathbf{x}, \mathbf{x}')$ $\bar{x}\text{c}$ kernel	B-7
$f_{ij}^{\text{ALDA}}(\mathbf{x}, \mathbf{x})$ XC kernel in ALDA	B-8
$f_{ij}^{\text{HEG}}(\mathbf{x}, \mathbf{x})$ XC kernel in HEG	B-8
$G_i(\mathbf{q}\omega)$ local field factor	52
$\bar{\Sigma}^{\text{Gw}}(12)$ self-energy in Gw app.	33
$\bar{\Sigma}^{\text{T}}(12)$ self-energy related to the T -matrix	40
$\bar{\Sigma}^{\text{SF}}(12)$ SF self-energy	38
$\bar{\Sigma}^{\text{CF}}(12)$ charge fluctuation self-energy	38
$\bar{\Sigma}^{\text{H}}(12)$ Hartree self-energy	42
$\bar{\Sigma}^{\text{xc}}(12)$ XC self-energy	43
$\bar{\Sigma}^{\text{V}}(12)$ self-energy for the vertex creation	43
$\bar{\Sigma}^{\text{*}}(12)$ self-energy difference: $\bar{\Sigma} - \bar{\Sigma}_{\text{xc}}$	55
$\bar{\Sigma}_{\text{DC}}(12)$ double counting correction	49

density functional theory of superconductors

$\alpha^2 F$ effective ph. int. at the Fermi level	62
P^{SF} analogon to $\alpha^2 F$ for the SF int.	62
$M(\mathbf{r}, \mathbf{r}', \omega)$ generic interaction matrix element in real space (Ph, Coulomb and SF)	E-3
$M_{kk'}(\omega)$ generic interaction matrix element in Bloch representation	E-4
$A_n(E)$ scalar A_k in isotropic app.	E-9
$M_{nn}(EE')$ matrix $M_{kk'}$ in isotropic app.	E-9
$\mathcal{K}_{kk'}^{\text{C}}$ C -term of the gap equation	58
\mathcal{Z}_k^{D} D -term of the gap equation	58
$M_{kk'}^{\beta}$ matrix of the Sham-Schlüter eq.	E-9
$\psi_{\text{nk}}(\mathbf{r})$ normal state KS wave function	20
ϵ_{nk} KS energy eigenvalue	20

$\zeta_{n\mathbf{k}}$ KS energy relative to Fermi level	C-4
$E_{n\mathbf{k}}^{\pm}$ eigenvalue corresponding to $\hat{\gamma}_{n\mathbf{k}\sigma}$	C-4
$u_l(\mathbf{r})$ particle amplitude	19
$v_l(\mathbf{r})$ hole amplitude	19
$\Delta_{\pm}(E)$ pair. pot. in isotropic 2 band case .	61
$v^{\text{xc}}(\mathbf{r})$ XC potential	18
$v^{\text{KS}}(\mathbf{r})$ KS potential	18
$\mathbf{B}^{\text{ext}}(\mathbf{x})$ external magnetic field	25
$\mathbf{B}^{\text{xc}}(\mathbf{x})$ XC magnetic field	D-6
$\Delta_i(\mathbf{r}, \mathbf{r}')$ pairing potential $i = s, tx, ty, tz$..	C-1
$\Delta^{\text{ext}}(\mathbf{r}, \mathbf{r}')$ external pairing potential	25
$\Delta^{\text{xc}}(\mathbf{r}, \mathbf{r}')$ XC pairing potential	18
$\Delta^{\text{KS}}(\mathbf{r}, \mathbf{r}')$ KS pairing potential	18
Δ_k pairing potential in Bloch space	20

1. Introduction

Most of the works regarding superconductivity start their introduction with the first observation of superconductivity in mercury in the year 1911 by H. Kamerling-Onnes [1]. It then took over 40 years, until Bardeen, Cooper and Schrieffer (BCS) proposed their “Theory of Superconductivity” [2]. The theory is based on an attractive interaction between electrons, which is created by phonons. The pairing provided by the interaction leads to an instability of the normal state to the BCS state and to the formation of superconductivity.

However, for this work the discovery of superconductivity (SC)¹ in the copper oxide family (“cuprates”) in 1986 marks the important date [3]. The critical temperature (T_c) in this class of materials is remarkable, and today’s absolute record holder for T_c with 134 K at ambient pressure is (still) a cuprate [4]. Such high critical temperatures had never been measured before in any material. In the sixties and seventies the record for T_c was increasing very slowly and stagnated around 25 K [5]. This led to the assumption that there is a fundamental limit for T_c around 30 K well captured by a phononic pairing mechanism².

This assumption was proven wrong by the high critical temperature of the cuprates. The term “high temperature superconductivity” became common for materials above the former fundamental limit of 25 K. Quite quickly after the discovery of the cuprates, it became clear that the existing microscopic theory is not able to describe the newly discovered materials. Calculations of the phonon coupling strength showed [7] that the coupling is too weak to explain the high critical temperatures in the cuprates, implying that an alternative mechanism has to be present.

After decades of intense research on the cuprates, the question about the underlying mechanism remains unanswered and under strong debate. Since the critical temperature in the cuprates is outstanding, many researchers focused their theories on the unique features of the cuprates compared to the conventional SC. This changed twenty years after the discovery of the cuprates because a second class of high temperature superconductors was found in 2008: The “pnictides” [8]. The name pnictides was coined in the first months after the discovery, where all compounds contained iron and pnictides (mostly arsenic). However, later also compounds containing chalcogens instead of pnictides were found, so the name iron based superconductors (FeSC) seems more appropriate [9]. The FeSC proved that high temperature superconductivity is not unique to the cuprates. Ideally, a microscopic theory should work for both known classes and for all classes discovered in the future.

For the phonon based superconductors described by the conventional BCS theory, the isotope effect was an early experimental hint for the connection between phonons and superconductivity [10]. Unfortunately, there is no such clear experimental hint for the mechanism in the cuprates or pnictides. Especially, the cuprates are very “difficult” materials, due to the strongly localized d electrons of the copper atoms resulting in an insulating ground state [11]. The FeSC are less strongly correlated and are metallic. The fact that the cuprates and FeSC are very different, is advantageous on one hand because it shows that high temperature superconductivity is not limited to very specific conditions. On the other hand, the big difference between the two groups complicates the derivation of a unified theory. The review articles of I. Mazin provide a much more detailed discussion of the arguments given in this introduction and are highly recommended [12, 13].

Despite all differences between the cuprates and FeSC there are also similarities. In order to find a unified theory for the high temperature superconductors, one should focus on the similarities:

- The compounds show an anti ferro magnetic (AFM) phase.

¹The acronym SC is used flexibly also for superconducting, superconductor, *etc.*

²Note that BCS theory is derived for a weak electron-phonon coupling, but has been extended to the strong coupling regime by the Eliashberg theory [6].

- Magnetic fluctuations (paramagnons) are measured in the superconducting and non-superconducting phase [14, 15].
- Before superconductivity appears, the magnetic ordering is suppressed and the critical temperature often follows a dome-like structure as a function of a control parameter (doping, pressure) [12].

These similarities point in the direction that high temperature superconductivity is connected to a magnetic phase. A pairing mediated by magnetic fluctuations became a widely used theory in the cuprates and there are entire books summarizing model calculations using this approach [16], but also other model theories like polarons and orbital fluctuations have been proposed for the unconventional superconductors [17, 18]. Note that the relevance of magnetism in the context of superconductivity was recognized already in 1966, when the effect of **spin-fluctuations (SF)** on conventional systems like palladium was discussed [19, 20]. For the **FeSC** additional experimental results have been found, supporting the idea of a connection between the suppressed magnetic phase and **unconventional SC**:

- The resonance frequency ω_{res} of the magnetic excitations is related to the critical temperature for a wide range of materials $\frac{\omega_{\text{res}}}{k_{\text{B}}T_{\text{c}}} \approx 5$. An overview of the experimental results is given in Table 1.1.
- In FeSe it has been observed that pressure enhances the magnetic fluctuations as well as the critical temperature [21].

Due to the experimental results, the following scenario is more or less well established within the scientific community: The **AFM** long range order has been suppressed as a function of a control parameter. The control parameter may be (hole, electron, isovalent) doping or pressure (see Tab. 1.1). Due to the proximity to a magnetic phase, strong magnetic fluctuations (**paramagnons**) are present in the material. The fluctuations have finite momentum because they correspond to an **AFM** order and allow for electron scattering between different regions of the **Brillouin zone (BZ)**. These fluctuations may provide the glue for the formation of superconductivity. Note that the paramagnons are collective electronic excitations created by multiple Coulomb scattering: So the glue is repulsive, in contrast to the attractive phonon coupling [22, 2]. This may sound odd at first, but the next sections will explain and clarify this concept.

The present work is devoted to the inclusion of the paramagnon mediated pairing in the framework of **superconducting density functional theory (SCDFT)**. **SCDFT** is the extension of the standard **density functional theory (DFT)** to superconducting systems and a brief introduction is given in chapter 3. The theory was proposed by Olivera, Gross and Kohn in 1988 and is based on the total electronic density and an additional density characterizing the **SC** state [23]. The additional density is called anomalous density and is the order parameter of the **SC** phase. The theory contains no adjustable parameters and is a formally exact theory for **SC**. The theory is only in principle exact because the functional for the **exchange-correlation (XC)**-energy is only known in some approximation.

The successful functionals in **SCDFT** are constructed using **many-body-perturbation theory (MBPT)**. **MBPT** provides a perturbative expansion of the full electronic **Green's function (GF)** in orders of the Coulomb interaction and the phonon propagator. In chapter 2 an introduction to the **GF** technique at finite temperatures is given. Like **DFT** also the Green's function approach can be extended to superconducting systems, by the introduction of an anomalous **GF**[24]. This anomalous **GF** is closely related to the anomalous density in the **SCDFT** treatment. This extension is presented in chapter 4, in the context of the **SC** version of the famous Hedin equations.

The equations have been derived first by Hedin and are a set of five coupled equations [25]. A fully self-consistent treatment would lead the exact normal and anomalous electronic **GF**. In particular, it also leads the exact electronic self-energy. The self-energy provides a connection between **SCDFT** and **MBPT**. The connection has been found by Sham and Schlüter and the central integral equation is named **Sham-Schlüter equation (SSEq)** [26]. This equation relates a given approximation for the self-energy to an xc-potential. In their work Marques *et. al.* truncate the expansion of the self-energy after the first order in the screened Coulomb interaction and the phonon propagator and use the **SSEq**

Material	AFM GS	SF measured	T_c	T_c Doping	T_c Pressure
FeSe	no	yes ^q (6meV)	8 ^g	10 ^h (80% Te)	37 ^g (P=7)
FeTe	yes	yes ^q (6meV)	0.0 ⁱ	9 ⁱ (15% S)	0.0
LiFeAs	no	yes ^r (8-17meV)	18 ^j	negative	18 ^j (P=0)
Na _{1-δ} FeAs	yes	no	21 ^a	33 ^f (20% P)	31 ^d (P=3)
CaFe ₂ As ₂	yes	yes ^k (25 meV)	0.0 ^a	38 ^e (50% Ni)	10 ^a (P=0.5)
BaFe ₂ As ₂	yes	yes ^s (1.5-6meV)	0.0 ^a	38 ^b (40% K)	29 ^a (P=4)
SrFe ₂ As ₂	yes	no	0.0 ^a	38 ^c (20% K)	27 ^a (P=3)
LaFePO	no	indication ^v	3.2 ^u	6 ^u (6% F)	8.8 ^w (P=0.8)
LaOFeAs	yes	yes(9-15meV)	0.0 ^l	25 ^t (10% F)	43 ⁿ (P=3)
CeOFeAs	yes	yes ^p (1meV)	0.0 ^m	35 ^m (10% F)	12 ^o (P=0.4)

Table 1.1.: Overview of the critical temperatures as a function of doping and pressure for various FeSC.

The column “AFM GS” indicates whether the undoped ground state at ambient pressure is magnetic.

^a[29], ^b[30], ^c[31], ^d[32], ^e[33], ^f[34], ^g[21]^h[35], ⁱ[36], ^j[37], ^k[38], ^l[39], ^m[40], ⁿ[41], ^o[42], ^p[43], ^q[44], ^r[45], ^s[46], ^t[47], ^u[48], ^v[49], ^w[50].

to derive an XC-potential [27]. This approximation leads to satisfying results for the conventional superconductors, but fails for the unconventional superconductors.

This is not surprising since the paramagnons are not included in the expansion for the self-energy. By using only the first order in the screened Coulomb interaction *i.e.* the Gw approximation[28], all the vertex corrections in the self-energy have been neglected. In chapter 5 the vertex corrections are investigated and the relevant contributions representing the magnetic fluctuations or paramagnons are selected. The magnetic fluctuations are related to very complicated four point functions and a simpler local form is suggested. In this local form the magnetic fluctuations appear within an effective interaction and the corresponding self-energy contribution is reminiscent to the Gw contribution.

In the expression for the self-energy, the Coulomb, paramagnon and phonon contributions enter on an equal footing. In chapter 6 the XC-potential using the SSEq is derived. The derivation is in analogy to the derivation done by Marques *et. al.* and leads a universal XC-functional containing an extra contribution related to the magnetic excitations. The new term is strictly repulsive which, requires a sign change of the XC-potential in order to find a SC state. The conditions for a SC solution and applications of the new functional to model systems are presented at the end of chapter 6.

In chapter 7 the field of model calculations is left and the functional is applied to FeSe and LiFeAs, which are two representatives of the FeSC. The calculation of the correct magnetic ground state in these material turns out to be difficult and one parameter is necessary to enforce the experimentally observed non-magnetic ground state. With this one parameter the framework is not fully *ab-initio* anymore. The critical temperature is investigated as a function of pressure and the new contribution related to the magnetic fluctuations is the key ingredient to explain the high critical temperatures in this class of materials.

This work features an extended appendix. For a better reading flow, all extensive algebraic transformations have been shifted to the appendix and interested readers may look up details there.

2. Introduction to Green's Functions

In this chapter the GF method is introduced. The formalism is presented for a non-superconducting state, but in chapter 4 an extension to superconducting systems is presented. The section gives only a brief overview of the GF formalism and many-body perturbation theory. A more detailed and didactic introduction may be found in standard text books like Nolting 7 or the Fetter Walecka [51, 52]. Essentially, two functions are introduced in this chapter:

1. The single particle GF which contains an expectation value of two Fermionic operators. It is possible to define four different versions of this function: The retarded, advanced, time ordered and Matsubara GF. Among the four, the
 - Matsubara single particle GF G^M [Eq. (2.11)]is the relevant one in this work.
2. The response function which contains an expectation value of two observables \hat{A} and \hat{B} . Also for the response function the four different versions exist, but only the
 - retarded response function χ_{AB}^R [Eq. (2.21)] and the
 - Matsubara response function χ_{AB}^M [Eq. (2.22)]are used in the derivations.

Why is it necessary to define so many functions? The different functions provide different information about a system:

- The Matsubara GF is a time ordered quantity. It provides expectation values of single particle operators and the total energy of the interacting many-body system [Eqs. (2.12) and (2.13)]. G^M is the most convenient choice for calculations at finite temperature. Since a treatment of systems at finite temperature is essential in the context of SC, the Matsubara GF is mainly used in this work.
- The linear response of the observable \hat{A} , due to a probing field coupling to the internal quantity \hat{B} of the system, is described by the retarded response function (see Sec. 2.2). The singularities or peaks of this function describe phase transitions or excitations of the system due to the external field. Since the response is a measurable quantity, the retarded response function is a real and causal quantity.
- The advanced response function is the “anti-causal” analogous to the retarded one. It is mainly required for mathematical completeness and has no simple physical interpretation like the retarded counterpart.
- The Matsubara response function is the time ordered variant of the response function.

After G^M and χ_{AB}^R have been introduced in Sec. 2.1 and 2.2, a perturbation expansion for the time ordered objects is formulated in Sec. 2.3. A very efficient and descriptive way to present the different orders in this expansion are the so called Feynman diagrams which are introduced in Sec. 2.4. All the different Green's and response functions are connected to each other via the spectral representations (Appendix B.1.4) which simplifies the work essentially.

2.1. The Matsubara Green's Function

The final goal of this work is the description of superconducting systems and the most convenient ensemble for this purpose should be chosen. A superconductor will be cooled down by a large cryostat, so the temperature T is a variable of the thermodynamical potential. The BCS wave function describing superconducting systems has no fixed particle number *i.e.* the corresponding Hamiltonian does not commute with the electron number operator \hat{N} . Hence, the **grand canonical potential** is the most convenient choice:

$$\Omega(\mu TV) = U - TS - \mu N = \left\langle \hat{H} - \frac{1}{\beta} \ln[\hat{\rho}_\beta] - \mu \hat{N} \right\rangle, \quad (2.1)$$

where μ is the chemical potential, \hat{N} the particle number, S the entropy, β the inverse temperature $\beta = \frac{1}{k_B T}$, k_B the Boltzmann constant and $\hat{\rho}_\beta$ the statistical operator. The Hamiltonian \hat{H} contains the following contributions:

$$\hat{H} = \hat{H}_0 + \hat{W} = \hat{T} + \hat{V}_0 + \hat{W} \quad (2.2)$$

$$\hat{T} = - \sum_{\sigma} \Delta dr \hat{\Psi}_{\sigma}^{\dagger}(\mathbf{r}) \frac{\nabla^2}{2} \hat{\Psi}_{\sigma}(\mathbf{r})$$

$$\hat{V}_0 = \sum_{\sigma\sigma'} \Delta dr \hat{\Psi}_{\sigma}^{\dagger}(\mathbf{r}) \left[v_0(\mathbf{r}) \delta_{\sigma\sigma'} + \sum_i \sigma_{\sigma\sigma'}^i \varphi_i(\mathbf{r}) \right] \hat{\Psi}_{\sigma'}(\mathbf{r}) \quad (2.3)$$

$$\hat{W} = \frac{1}{2} \sum_{\sigma\sigma'} \Delta d^3 r d^3 r' v(\mathbf{r}\mathbf{r}') \hat{\Psi}_{\sigma}^{\dagger}(\mathbf{r}) \hat{\Psi}_{\sigma'}^{\dagger}(\mathbf{r}') \hat{\Psi}_{\sigma'}(\mathbf{r}') \hat{\Psi}_{\sigma}(\mathbf{r}). \quad (2.4)$$

The kinetic energy operator is labeled with \hat{T} and \hat{W} is the Coulomb interaction between electrons. The $\hat{\Psi}_{\sigma}(\mathbf{r})$ and $\hat{\Psi}_{\sigma}^{\dagger}(\mathbf{r})$ are the usual annihilation and creation operators of an electron at point \mathbf{r} and spin σ . The single particle potential V_0 consists of the spin independent, background potential created by the nuclei v_0 and some external contribution $\sum_i \sigma_{\sigma\sigma'}^i \varphi_i(\mathbf{r})$. Throughout the whole thesis atomic units $e = \hbar = m_e = 1$ are used. The thermal average of an operator \hat{A} is given by:

$$\langle \hat{A} \rangle := \text{tr} [\hat{\rho}_\beta \hat{A}] = \sum_n \langle n | \hat{\rho}_\beta \hat{A} | n \rangle. \quad (2.5)$$

The trace runs over a complete basis of the Fock space. The statistical operator in the equilibrium minimizes the grand canonical potential *i.e.* $\frac{\delta \Omega}{\delta \hat{\rho}_\beta} = 0$. This condition determines the form of the statistical operator: $\hat{\rho}_\beta \propto e^{-\beta \hat{K}}$. The normalization condition $\langle 1 \rangle \stackrel{!}{=} 1$ leads:

$$\hat{\rho}_\beta = \frac{1}{Z_G} e^{-\beta \hat{K}} \quad \text{with } Z_G := \text{tr} [e^{-\beta \hat{K}}], \quad (2.6)$$

where the operator \hat{K} is given by $\hat{H} - \mu \hat{N}$. For a non-interacting system³ the eigenstates are known and the grand canonical potential reads:

$$\begin{aligned} \Omega_0(\mu TV) &= \left\langle \hat{H}_0 - k_B \ln[\hat{\rho}_\beta^0] - \mu \hat{N} \right\rangle_0 = \text{tr} \left[\hat{\rho}_\beta^0 \left(\hat{H}_0 - k_B \ln[\hat{\rho}_\beta^0] - \mu \hat{N} \right) \right] \\ \hat{\rho}_\beta^0 &= \frac{1}{Z_G^0} e^{-\beta \hat{K}_0} \quad \text{with } Z_G^0 := \text{tr} [e^{-\beta \hat{K}_0}] = \text{tr} [e^{-\beta(\hat{H}_0 - \mu \hat{N})}]. \end{aligned} \quad (2.7)$$

The **grand canonical potential** of the interacting system is connected to the non-interacting one by a **coupling constant** integration (Sec. B.2):

$$\Omega(\mu TV) = \Omega_0(\mu TV) + \Delta_0^1 d\lambda \left\langle \hat{W} \right\rangle_{\lambda}. \quad (2.8)$$

³Non interacting systems are labeled with a subscript 0.

The expectation value on the right hand side can be expressed in terms of a single particle expectation value. This is done using the equation of motion of the operator $\hat{\Psi}_\sigma(\mathbf{r})$ in the Heisenberg picture. The **Heisenberg picture** of an operator is defined as:

$$\hat{O}(\tau)_H := e^{\hat{K}\tau}\hat{O}_S e^{-\hat{K}\tau} \quad \hat{O}(\tau)_H^\dagger := e^{\hat{K}\tau}\hat{O}_S^\dagger e^{-\hat{K}\tau}, \quad (2.9)$$

where τ is a real time argument often called Matsubara time and \hat{O}_S is the operator in the “standard” picture in general referred to as **Schrödinger picture**. Note that $(\hat{O}_H^\dagger)^\dagger$ is not equal to \hat{O}_H . For convenience, combined variables for the electronic coordinates are introduced:

$$\begin{aligned} 1 &:= \{\mathbf{r}_1, \tau_1, \sigma_1\} & \Delta d1 &:= \sum_{\sigma_1} \Delta d^3 r_1 \Delta d\tau_1 \\ \mathbf{x}_1 &:= \{\mathbf{r}_1, \tau_1\} & \Delta dx_1 &:= \sum_{\sigma_1} \Delta d^3 r_1. \end{aligned} \quad (2.10)$$

The equation of motion of the operator $\partial_{\tau_1} \hat{\Psi}(1)_H$ [Eq. (B.14)] leads naturally to an expression for the expectation value $\langle \hat{W} \rangle_\lambda$ [Eq. (B.15)] in terms of the **Matsubara GF**:

$$\begin{aligned} \Omega_\lambda(\mu TV) &= \Omega_0(\mu TV) + \frac{1}{2} \Delta_0^\lambda d\lambda \lim_{\substack{\mathbf{r}_2 \rightarrow \mathbf{r}_1 \\ \sigma_2 \rightarrow \sigma_1}} \lim_{\tau_2 \searrow \tau_1} \sum_{\sigma_1} \Delta d^3 r_1 [-\partial_{\tau_1} - K_0(\mathbf{r}_1)] G_\lambda^M(12) \\ G_\lambda^M(12) &:= - \left\langle \hat{T} \left[\hat{\Psi}_{\lambda H}(1) \hat{\Psi}_{\lambda H}^\dagger(2) \right] \right\rangle_\lambda = -\text{tr} \left[\hat{\rho}_\beta^\lambda \hat{T} \left[\hat{\Psi}_{\lambda H}(1) \hat{\Psi}_{\lambda H}^\dagger(2) \right] \right]. \end{aligned} \quad (2.11)$$

This is an important result because once the Green’s function G_λ^M is known (in some approximation), this provides the grand canonical potential which contains the ground state (or at finite temperature the equilibrium) information of the system. For the Matsubara Green’s function of the fully interacting system ($\lambda = 1$) the index λ is left. The operator \hat{T} is the **time ordering operator** defined in Eq. (B.16). In addition, the Green’s function also provides any single particle ground state expectation value directly:

$$\begin{aligned} \langle \hat{O} \rangle &= \sum_{\sigma_1 \sigma_2} \Delta d^3 r_1 d^3 r_2 \left\langle O_{\sigma_1 \sigma_2}(\mathbf{r}_1 \mathbf{r}_2) \hat{\Psi}_{\sigma_1}^\dagger(\mathbf{r}_1) \hat{\Psi}_{\sigma_2}(\mathbf{r}_2) \right\rangle \\ &= \sum_{\sigma_1 \sigma_2} \Delta d^3 r_1 d^3 r_2 O_{\sigma_1 \sigma_2}(\mathbf{r}_1 \mathbf{r}_2) G(12^+) \end{aligned} \quad (2.12)$$

and as a special case also the expectation value of $\langle K \rangle$ which contains two-particle operators:

$$\begin{aligned} \langle K \rangle &= \langle \hat{H} \rangle - \mu \langle \hat{N} \rangle = \langle \hat{K}_0 \rangle + \langle \hat{W} \rangle \\ &= \sum_{\sigma_1} \Delta d^3 r_1 \lim_{\substack{\mathbf{r}_2 \rightarrow \mathbf{r}_1 \\ \sigma_2 \rightarrow \sigma_1}} \lim_{\tau_2 \searrow \tau_1} \left(K_0(\mathbf{r}_1) - \frac{1}{2} [\partial_{\tau_1} + K_0(\mathbf{r}_1)] \right) G^M(12) \\ &= - \sum_{\sigma_1} \Delta d^3 r_1 \lim_{\substack{\mathbf{r}_2 \rightarrow \mathbf{r}_1 \\ \sigma_2 \rightarrow \sigma_1}} \lim_{\tau_2 \searrow \tau_1} \frac{1}{2} [\partial_{\tau_1} - K_0(\mathbf{r}_1)] G^M(12), \end{aligned} \quad (2.13)$$

This shows the importance of the Matsubara Green’s function with respect to ground state properties. The information about excitation on top of a ground state are given by the response function. This quantity is the central object in linear response theory introduced in Sec. 2.2.

2.2. The Response Function

The retarded **response function** is the central quantity in **linear response (LR)** theory. This theory describes the response of a system related to a (small) perturbation or probing field called $\hat{\Phi}_t$. The

perturbation is created by an external Field $\mathbf{F}(t)$ which couples to an internal observable $\hat{\mathbf{B}}$ of the system. The Hamiltonian in the Schrödinger picture of such a system reads:

$$\hat{H}_S(t) = \hat{K} + \hat{\Phi}_t = \hat{H} - \mu\hat{N} + \Delta d^3r \mathbf{F}(\mathbf{x}) \cdot \hat{\mathbf{B}}(r). \quad (2.14)$$

The statistical operator for a time dependent system and its time derivative are given by:

$$\hat{\rho}_S(t) = \sum_n p_n |\Psi_n(t)\rangle_S \langle \Psi_n(t)|_S \quad \frac{d}{dt} \hat{\rho}_S(t) = i \left[\hat{\rho}_S(t), \hat{H}_S(t) \right]_-. \quad (2.15)$$

The time dependence of the wave function $|\Psi_n(t)\rangle_S$ indicates that the system is not in an equilibrium and the weights are **not** given by $e^{-\beta\hat{K}}$. The weights p_n of the statistical operator are assumed to be time independent. This assumption is valid for small perturbations which do not change the occupation numbers. The statistical operator in the ‘‘unperturbed picture’’ (label U) is:⁴

$$\hat{\rho}_U(t) := e^{i\hat{K}t} \hat{\rho}_S(t) e^{-i\hat{K}t}.$$

The equation of motion for $\hat{\rho}_U(t)$ leads with Eq. (2.15) to:

$$\frac{d}{dt} \hat{\rho}_U(t) = e^{i\hat{K}t} \left(\frac{d}{dt} \hat{\rho}_S(t) + i \left[\hat{K}, \hat{\rho}_S(t) \right]_- \right) e^{-i\hat{K}t} = -i \left[\hat{\Phi}_t(t)_U, \hat{\rho}_U(t) \right]_-.$$

The equation is integrated with respect to t :

$$\Rightarrow \hat{\rho}_U(t) = \lim_{t' \rightarrow -\infty} \hat{\rho}_U(t') - i \Delta_{-\infty}^t dt' \left[\hat{\Phi}_{t'}(t')_U, \hat{\rho}_U(t') \right]_-. \quad (2.16)$$

The perturbation is switched on at a certain time. Hence, in the limit $t \rightarrow -\infty$ the statistical operator $\hat{\rho}(t)_U$ becomes the one of the unperturbed non-time dependent system $\hat{K} = \hat{K}_0 + \hat{W}$. Since the system is in equilibrium at this time, the statistical operator has the form $\hat{\rho}_S(t \rightarrow -\infty) = \frac{1}{Z_G} e^{-\beta\hat{K}} = \hat{\rho}_\beta$ and the time dependence vanishes in this limit:

$$\lim_{t \rightarrow -\infty} \hat{\rho}_U(t) = \lim_{t \rightarrow -\infty} e^{i\hat{K}t} \hat{\rho}_S(t) e^{-i\hat{K}t} = \lim_{t \rightarrow -\infty} e^{i\hat{K}t} e^{-\beta\hat{K}} e^{-i\hat{K}t} = \hat{\rho}_\beta.$$

The Dyson like equation for the statistical operator [Eq. (2.16)] is approximated by the first (linear) order in the perturbation, *i.e.*:

$$\begin{aligned} \hat{\rho}_U^{\text{LR}}(t) &:= \hat{\rho}_\beta - i \Delta_{-\infty}^t dt' \left[\hat{\Phi}_{t'}(t')_U, \hat{\rho}_\beta \right]_- \\ \hat{\rho}_S^{\text{LR}}(t) &= e^{-i\hat{K}t} \hat{\rho}_U^{\text{LR}}(t) e^{i\hat{K}t} = \hat{\rho}_\beta - i \Delta_{-\infty}^t dt' e^{-i\hat{K}t} \left[\hat{\Phi}_{t'}(t')_U, \hat{\rho}_\beta \right]_- e^{i\hat{K}t}. \end{aligned} \quad (2.17)$$

Due to this truncation in the first order of the perturbation, the theory will only work for small perturbing fields or ‘‘in the linear response regime’’. The change of an observable \hat{A}_β created by the perturbation is given by:

$$\Delta A^i(\mathbf{r}t) = \text{tr} \left[\hat{\rho}_S(t) \hat{A}^i \right] - \text{tr} \left[\hat{\rho}_\beta \hat{A}^i \right] = \left\langle \hat{A}^i \right\rangle(t) - \left\langle \hat{A}^i \right\rangle.$$

Using the statistical operator in the linear response approximation [Eq. (2.17)], the expression for ΔA^i reads:

$$\Delta A^i(\mathbf{r}t) = -i \sum_{j=1}^3 \Delta_{-\infty}^\infty dt' \Delta d^3r' \theta(t-t') \left\langle \left[\hat{A}_U^i(\mathbf{r}t), \hat{B}_U^j(\mathbf{r}'t') \right]_- \right\rangle F^j(\mathbf{r}'t').$$

⁴Often the term **Dirac picture** is used here [51], but this name should be reserved to a time propagation including no interaction in my opinion.

The change in the observable is only non-zero for times t after the perturbation, *i.e.* $t > t'$, like it should be in our causal picture of the world. The “unperturbed picture” is identical to the [Heisenberg picture](#) introduced in Eq. (2.9). The expression of the right hand side leads to the definition of the [response function](#):

$$\chi_{A_i B_j}^R(\mathbf{x}, \mathbf{x}') := -i\theta(t - t') \left\langle \left[\hat{A}_H^i(\mathbf{x}), \hat{B}_H^j(\mathbf{x}') \right]_- \right\rangle. \quad (2.18)$$

The change in the observable A is determined by $\chi_{A_i B_j}^R(\mathbf{x}, \mathbf{x}')$ of the unperturbed system:

$$\Delta A^i(\mathbf{x}) = \sum_{j=1}^3 \Delta d^A x' \chi_{A_i B_j}^R(\mathbf{x}, \mathbf{x}') F^j(\mathbf{x}').$$

In other words, the important information about [phase transitions](#) (singularities in χ_{AB}^R) and excitations (peaks in χ_{AB}^R) are accessible via the **ground state**. The theory can only describe excitations related to small external fields. All important excitations in a solid like the collective magnetic modes ([magnons](#)), lattice vibrations ([phonons](#)) and charge density waves ([plasmons](#)) are in most cases well captured within linear response theory. Thus, linear response theory has become a very important tool in the investigation of excitations in solids [53, 54, 55]. If the following density operators

$$\hat{\rho}_i(\mathbf{r}) = \sum_{\alpha\beta} \sigma_{\alpha\beta}^i \hat{\Psi}_\alpha^\dagger(\mathbf{r}) \hat{\Psi}_\beta(\mathbf{r}) = \sum_{\alpha\beta} \sigma_{\alpha\beta}^i \hat{\rho}_{\alpha\beta}(\mathbf{r})$$

are used for the operators \hat{A}_i and \hat{B}_j , the $\chi_{A_i B_j}^R$ is called “density-density response” [$\vec{\sigma}$ is the [Pauli matrix](#) vector given in Eq. (A.4)]. Alternatively, the names, response or [susceptibility](#) are common. The standard label for the density-density response is χ_{ij}^R . The quantity describes the change of the charge/magnetic-moment densities due to an external coulomb potential/magnetic fields. The coupling between the external fields and the densities is given by:

$$\hat{\Phi}(\tau) = \sum_{\alpha\beta} \Delta d^3 \mathbf{r} \vec{\varphi}(\mathbf{x}) \cdot \vec{\sigma}_{\alpha\beta} \hat{\Psi}_\alpha^\dagger(\mathbf{r}) \hat{\Psi}_\beta(\mathbf{r}) = \sum_{i=1}^4 \Delta d^3 \mathbf{r} \varphi_i(\mathbf{x}) \hat{\rho}_i(\mathbf{r}) \quad (2.19)$$

$$\vec{\varphi}(\mathbf{x}) = \begin{pmatrix} v_{\text{ext}}^0(\mathbf{x}) \\ B_{\text{ext}}^x(\mathbf{x}) \\ B_{\text{ext}}^y(\mathbf{x}) \\ B_{\text{ext}}^z(\mathbf{x}) \end{pmatrix} \quad \vec{\rho}(\mathbf{r}) = \begin{pmatrix} \hat{\rho}(\mathbf{r}) \\ \hat{m}^x(\mathbf{r}) \\ \hat{m}^y(\mathbf{r}) \\ \hat{m}^z(\mathbf{r}) \end{pmatrix}, \quad (2.20)$$

where \mathbf{B}_{ext} is the external magnetic field and v_{ext} the external Coulomb potential and $\vec{\sigma}$ is the set of Pauli matrices defined in Eq. (A.4). The $16 = 4 \times 4$ elements of the response function are given by:

$$\chi_{ij}^R(\mathbf{x}, \mathbf{x}') := i\theta(t - t') \left\langle \left[\Delta \hat{\rho}_i(\mathbf{x})_H, \Delta \hat{\rho}_j(\mathbf{x}')_H \right]_- \right\rangle = \chi_{\Delta \rho_i(\mathbf{r}) \Delta \rho_j(\mathbf{r}')}^R(t, t') \quad (2.21)$$

$$\Delta \hat{\rho}_i(\mathbf{x})_H := \sum_{\alpha\beta} \sigma_{\alpha\beta}^i \left[\hat{\Psi}_\alpha(\mathbf{x})_H \hat{\Psi}_\beta^\dagger(\mathbf{x}^+)_H - \rho_{\alpha\beta}(\mathbf{r}) \right].$$

In section A.3 the transformation relation between the notation in spin and Pauli matrix components are given. Depending on the magnetic ground state of the system, the 4×4 matrix can be very sparse [Eq. (B.5)]. Note that before the χ_{ij}^R can be included a perturbative expansion, a change from the retarded to the time ordered or Matsubara response function has to be performed using Eq. (B.11). The details on the perturbative expansion are discussed in the next section (Sec. 2.3). The time

ordered versions are also the reason why the $\Delta\rho$ has been introduced to the expression for χ_{ij}^R . In the commutator of the retarded function a scalar number does not matter. However, the natural definition of the Matsubara response leads to the form with $\Delta\hat{\rho}$ [Eq. (B.18)]:

$$\begin{aligned}\chi_{ij}^M(\mathbf{x}_1\mathbf{x}_2) &:= -\frac{\delta\rho_i(\mathbf{x}_1)}{\delta\varphi_j(\mathbf{x}_2)} = \left\langle \hat{T} [\Delta\hat{\rho}_i(\mathbf{x}_1)_H \Delta\hat{\rho}_j(\mathbf{x}_2)_H] \right\rangle \\ &= \left\langle \hat{T} [\hat{\rho}_i(\mathbf{x}_1) \hat{\rho}_j(\mathbf{x}_2)] \right\rangle - \left\langle \hat{T} [\hat{\rho}_i(\mathbf{x}_1)] \right\rangle \left\langle \hat{T} [\hat{\rho}_j(\mathbf{x}_2)] \right\rangle.\end{aligned}\quad (2.22)$$

The second term $\left\langle \hat{T} [\hat{\rho}_i(\mathbf{x}_1)] \right\rangle \left\langle \hat{T} [\hat{\rho}_j(\mathbf{x}_2)] \right\rangle$ removes all uncorrelated parts from χ^M . In the diagrammatic language introduced in Sec. 2.4 this means that only connected contributions are present in the expansion for χ^M .

Finally the **advanced** response function is defined:

$$\chi_{A_i B_j}^A(\mathbf{x}, \mathbf{x}') := -i\theta(t' - t) \left\langle \left[\hat{A}_H^i(\mathbf{x}), \hat{B}_H^j(\mathbf{x}') \right]_- \right\rangle.\quad (2.23)$$

This function is the anti-causal analogon of the retarded response function.

2.3. Perturbation Expansion

After the importance of the Matsubara GF and the response function have been shown, it would be highly desirable to have a scheme to obtain approximations for these objects. In this section a **perturbation expansion** for the Matsubara GF in terms of the interaction and the free propagator is presented [52, 51].⁵ This is an advantage compared to the DFT framework (presented in Sec. 3), where no straightforward way for the construction of approximations is available.

The Schrödinger equation for a **non-interacting** system [drop \hat{W} in Eq. (2.2)] is solvable on modern computers [56]. Hence, the evaluation of the trace is not a problem and the non-interacting Green's function

$$G_0^M(12) := \epsilon \left\langle \hat{T} \left[\hat{\Psi}_D(1) \hat{\Psi}_D^\dagger(2) \right] \right\rangle_0 = \epsilon \text{tr} \left[\hat{\rho}_0 \hat{T} \left[\hat{\Psi}_D(1) \hat{\Psi}_D^\dagger(2) \right] \right]\quad (2.24)$$

is known. In this section always the Matsubara Green's function is considered and the subscript M is left out for simplicity. For an interacting system on the other hand, the differential equations are coupled and the dimensionality of the problem increases exponentially with the number of electrons in the system. This means a direct solution of the Schrödinger equation is not feasible for large systems [57]. In order to overcome this problem, the interaction \hat{W} is considered as a perturbation and the full GF is expanded in orders of the interaction and the known G_0 . The perturbation series is based on the Matsubara **time evolution operator**:

$$U(\tau_1\tau_2) := e^{\hat{K}_0\tau_1} e^{-\hat{K}(\tau_1-\tau_2)} e^{-\hat{K}_0\tau_2}\quad (2.25)$$

This operator is **not** unitary, but has the same properties as the (unitary) time evolution operator:

$$U(\tau_1, \tau_2) = U(\tau_1, \tau) U(\tau, \tau_2) \quad U(\tau, \tau) = \mathbf{1}.$$

The **Dirac picture** is introduced:

$$\hat{O}(\tau)_D := e^{\hat{K}_0\tau} \hat{O}_s e^{-\hat{K}_0\tau}.$$

The equation of motion for the time evolution operator

$$\frac{dU(\tau_1, \tau_2)}{d\tau_1} = -W(\tau_1)_D U(\tau_1, \tau_2) \Rightarrow U(\tau_1, \tau_2) = e^{-\Delta\tau_1^2 d\tau \hat{W}_D(\tau)}$$

leads to an expansion of U in orders of the interaction \hat{W} :

$$U(\beta, 0) = \mathbf{1} - \Delta_0^\beta d\tau \hat{W}_D(\tau) + \frac{1}{2!} \Lambda_0^\beta d\tau d\tau' \hat{W}_D(\tau) \hat{W}_D(\tau') + \dots \quad (2.26)$$

⁵An analogous expression could be derived for the response function which is not done here.

The Heisenberg picture [Eq. (2.9)] is connected to the Dirac picture via the Matsubara time evolution operator:

$$\hat{A}_H(\tau) = U(0, \tau) \hat{A}_D U(\tau, 0). \quad (2.27)$$

This connection is the essential point in the derivation of a perturbation expansion. The single particle Matsubara GF is rewritten and the case $\tau_1 > \tau_2$ is considered. The real time arguments in Eq. (2.25) allow for a connection between the statistical operator and the time propagation:⁶

$$G(12) = -\frac{1}{Z_G} \text{tr} \left[e^{-\beta \hat{K}_0} U(\beta, \tau_1) \hat{\Psi}(1)_D U(\tau_1, \tau_2) \hat{\Psi}^\dagger(2)_D U(\tau_2, 0) \right].$$

In Sec. B.1.1 it is shown that the Green's function depends only on $\tau_1 - \tau_2 \in [-\beta, \beta]$. Hence it is sufficient to investigate the properties with respect to $\tau_1, \tau_2 \in [0, \beta]$. This means that the operators in the last equation are already time ordered and the operator \hat{T} is added:

$$G(12) = -\frac{1}{Z_G} \text{tr} \left[e^{-\beta \hat{K}_0 \hat{T}} \left[U(\beta, \tau_1) \hat{\Psi}(1)_D U(\tau_1, \tau_2) \hat{\Psi}^\dagger(2)_D U(\tau_2, 0) \right] \right].$$

Since the operator U always contains an even number of fermionic operators, the U 's are exchanged within the time ordered product without picking up extra minus signs:

$$G(1, 2) = -\frac{Z_G^0}{Z_G} \left\langle \hat{T} \left[U(\beta, 0) \hat{\Psi}(1)_D \hat{\Psi}^\dagger(2)_D \right] \right\rangle_0$$

The grand canonical partition function Z_G is also related to the time evolution operator (see the definition of the time evolution operator 2.25):

$$Z_G = \text{tr} \left[e^{-\beta \hat{K}} \right] = \text{tr} \left[e^{-\beta \hat{K}_0} U(\beta, 0) \right] \quad (2.28)$$

and the expression for the GF is cast to:

$$G(12) = -\frac{Z_G^0}{\text{tr} \left[e^{-\beta \hat{K}_0} U(\beta, 0) \right]} \left\langle \hat{T} \left[U(\beta, 0) \hat{\Psi}(1)_D \hat{\Psi}^\dagger(2)_D \right] \right\rangle_0 = -\frac{\left\langle \hat{T} \left[U(\beta, 0) \hat{\Psi}(1)_D \hat{\Psi}^\dagger(2)_D \right] \right\rangle_0}{\left\langle U(\beta, 0) \right\rangle_0}.$$

For $\tau_1 < \tau_2$ the same result is obtained. The expectation value has been changed from the interacting to the non-interacting one and the time dependence of the operators is trivial, if eigenstates of the non-interacting system are used in the trace. The operator $U(\beta, 0)$ now contains all the interaction *i.e.* the difficulties. In terms of the series expansion for the time evolution operator Eq. (2.26) the expression for the full GF reads:

$$\begin{aligned} G(12) &= -\frac{\left\langle \hat{T} \left[U(\beta, 0) \hat{\Psi}(1)_D \hat{\Psi}^\dagger(2)_D \right] \right\rangle_0}{\left\langle \hat{T} U(\beta, 0) \right\rangle_0} \\ &= -\frac{\left\langle \hat{T} \left[\left(1 - \Delta_0^\beta d\tau \hat{W}_D(\tau) + \dots \right) \hat{\Psi}(1)_D \hat{\Psi}^\dagger(2)_D \right] \right\rangle_0}{\left\langle \hat{T} \left[1 - \Delta_0^\beta d\tau \hat{W}_D(\tau) + \frac{1}{2!} \Lambda_0^\beta d\tau d\tau' \hat{W}_D(\tau) \hat{W}_D(\tau') + \dots \right] \right\rangle_0}. \end{aligned} \quad (2.29)$$

If the expansion for $U(\beta, 0)$ is truncated after the first term, the $G^M(1, 2)$ reduces to the non-interacting GF. The evaluation of the perturbation series is done in a efficient way using Wick's Theorem and the linked cluster theorem. The proof for these theorems can be found in every many-body theory text book [52, 51]:

⁶In the zero temperature limit the time evolution operator is given by $e^{i\hat{K}_0 t_1} e^{-i\hat{K}(t_1-t_2)} e^{-i\hat{K}_0 t_2}$ and the thermal average reduces to $\langle \Psi_0 | \dots | \Psi_0 \rangle$. In this case the adiabatic connection is used $\Psi_0 = U(t, -\infty) \Phi_0$ [52].

Wick's Theorem: The expectation value of a time ordered product of the operators $\langle \hat{T} [A_1(\tau_1)_D \dots A_N(\tau_N)_D] \rangle_0$ is equal to the sum of all possible totally contracted products.

A product of operators is fully contracted, if all operators in the product are contracted with one another. A **contraction** between two operators \hat{A} and \hat{B} will be denoted by $\underline{\hat{A}\hat{B}}$ and is defined by:

$$\underline{\hat{A}\hat{B}} := \langle \hat{T} [\hat{A}\hat{B}] \rangle_0. \quad (2.30)$$

Note that no normal ordered term is present in the definition of the contraction. This is only necessary in the zero temperature case [52]. From the definition it is obvious that $\underline{\hat{\Psi}(1)_D \hat{\Psi}(2)_D} = \underline{\hat{\Psi}^\dagger(1)_D \hat{\Psi}^\dagger(2)_D} = 0$ and $\underline{\hat{\Psi}(1)_D \hat{\Psi}^\dagger(2)_D} = -G_0^M(12)$. This changes in the superconducting state and an extension to Wick's theorem for the superconducting state is necessary. This point is discussed in more detail in the Ph.D. of S. Kurth [58]. In order to illustrate the total contraction procedure, the first order term in the numerator of Eq. (2.29)

$$G = G_0(12) + \Lambda d3d4 \langle \hat{T} [v(34) \hat{\Psi}^\dagger(3) \hat{\Psi}^\dagger(4) \hat{\Psi}(4) \hat{\Psi}(3) \hat{\Psi}(1) \hat{\Psi}^\dagger(2)] \rangle + \mathcal{O}[v^2] \quad (2.31)$$

is fully contracted. The Coulomb interaction is spin-independent and static, but it is convenient to introduce an interaction $v(12)$ given by $v(12) = \delta_{\tau_1 \tau_2} v(\mathbf{r}_1 \mathbf{r}_2)$:

$$\begin{aligned} G(12) &= G_0(12) + \Lambda d3d4 v(34) \underline{\hat{\Psi}^\dagger(3)_D \hat{\Psi}^\dagger(4)_D \hat{\Psi}(4)_D \hat{\Psi}(3)_D \hat{\Psi}(1)_D \hat{\Psi}^\dagger(2)_D} \\ &\quad + \Lambda d3d4 v(34) \underline{\hat{\Psi}^\dagger(3)_D \hat{\Psi}^\dagger(4)_D \hat{\Psi}(4)_D \hat{\Psi}(3)_D \hat{\Psi}(1)_D \hat{\Psi}^\dagger(2)_D} \\ &\quad + \Lambda d3d4 v(34) \underline{\hat{\Psi}^\dagger(3)_D \hat{\Psi}^\dagger(4)_D \hat{\Psi}(4)_D \hat{\Psi}(3)_D \hat{\Psi}(1)_D \hat{\Psi}^\dagger(2)_D} + \mathcal{O}[v^2] \\ &= G_0(12) + \Lambda d3d4 v(34) \underline{\hat{\Psi}^\dagger(3)_D \hat{\Psi}(3)_D \hat{\Psi}^\dagger(4)_D \hat{\Psi}(4)_D \hat{\Psi}(1)_D \hat{\Psi}^\dagger(2)_D} \\ &\quad + \Lambda d3d4 v(34) \underline{\hat{\Psi}(1)_D \hat{\Psi}^\dagger(3)_D \hat{\Psi}^\dagger(4)_D \hat{\Psi}(4)_D \hat{\Psi}(3)_D \hat{\Psi}^\dagger(2)_D} \\ &\quad + \Lambda d3d4 v(34) \underline{\hat{\Psi}(4)_D \hat{\Psi}^\dagger(3)_D \hat{\Psi}^\dagger(4)_D \hat{\Psi}(1)_D \hat{\Psi}^\dagger(2)_D \hat{\Psi}(3)_D} + \mathcal{O}[v^2] \\ G(12) &= G_0(12) - \Lambda d3d4 \rho(3) \rho(4) v(34) G_0(1, 2) \\ &\quad + \Lambda d3d4 G_0(13) v(34) \rho(4) G_0(32) + \\ &\quad - \Lambda d3d4 G_0(14) v(34) G_0(43) G_0(32) + \mathcal{O}[v^2]. \end{aligned}$$

The factor $1 - \Lambda d3d4 \rho(3) \rho(4) v(34)$ does not depend on the coordinates of the Green's function (12). Such contributions are called not linked and following theorem makes a statement with respect to these constant terms [51, 52].

Linked Cluster Theorem: The non-linked contributions in the expansion of the numerator of Eq. (2.29) cancel with the denominator.

Hence, the perturbation expansion in Eq. (2.29) simplifies to:

$$G(1, 2) = - \left\langle \hat{T} \left[U(\beta, 0) \hat{\Psi}(1)_D \hat{\Psi}^\dagger(2)_D \right] \right\rangle_0^{\text{Linked}}.$$

Note that also the difference between the **grand canonical potential** of the interacting and non-interacting system is expandable in diagrams [Eq. (2.28)]:

$$\begin{aligned} \Delta \Omega &= \Omega - \Omega_0 = -\frac{1}{\beta} \ln [Z_G] + \frac{1}{\beta} \ln [Z_G^0] = -\frac{1}{\beta} \ln \left[\frac{Z_G}{Z_G^0} \right] \\ &= -\frac{1}{\beta} \ln \left[\frac{\text{tr} \left[e^{-\beta \hat{H}_0} U(\beta, 0) \right]}{Z_G^0} \right] = -\frac{1}{\beta} \ln \langle U(\beta, 0) \rangle_0 = -\frac{1}{\beta} \langle U(\beta, 0) \rangle_0^{\text{Linked}}. \end{aligned} \quad (2.32)$$

Already the first order contributions of G are quite complicated. However, all contributions contain only the non-interacting Green's function G_0 and the bare Coulomb interaction v . Fortunately R. Feynman invented a very effective way to illustrate the different contributions: The so called "Feynman diagrams" which are beautifully discussed by R.D. Mattuck [59].

2.4. The Feynman Diagrams

The **Feynman diagrams** are a replacement of the more complicated perturbative equation by simple images. There exists a set of translation rules for going from a picture to the corresponding equation and *vice versa*:

1. Each non-interacting Green's function G_0 (12) is represented by a single line arrow pointing from $2 \rightarrow 1$. The full Green's function is given by a double line.
2. Each interaction v is represented by a wiggled line. The screened interaction [Eq. (2.36)] is given by a double wiggled line.
3. It is integrated over all internal coordinates, besides the two lose ends.
4. Only linked diagrams are considered, due to the linked cluster theorem.
5. For a contribution with n interaction lines, a factor $(-1)^n$ is introduced, related to the expansion of the exponential function [Eq. (2.29)].⁷
6. For each **Fermionic loop**, a factor of (-1) is added. (Sec. D.2).

In Fig. 2.1 examples of diagrams and the corresponding representation in conventional equation form are given. The not linked terms appearing in the contraction have been left due to rule number 4. The green factors are related to the number of interaction lines (rule 5) and the blue ones to the number of loops (rule 6). It becomes immediately clear that for higher order contribution the diagrammatic representation is much easier to read. The full Green's function G (12) is given by drawing all possible connected diagrams with an arrow starting from the open coordinate 2 leading to the point 1 in spin space time.

Figure 2.1.: Example of the translation between diagrams and equations

very natural in the diagrammatic language. Also the group of diagrams containing “ladders”, “bubbles” and “loops” makes only sense in the new language. For the classification of diagrams it is convenient to define two new vocabularies:

Reducible Diagram: A diagram is called **reducible** with respect to something, if one can cut/remove something in order to get two not linked diagrams. The term **irreducible** is used for diagrams which are not reducible.

Proper Diagram: A diagram is called **proper**, if it is irreducible with respect to an interaction line. The term **improper** is used for diagrams which are not proper.

These definitions are very useful in the expansion of quantities. For example is it possible to obtain the full Green's function, by the solution of the equation:

⁷From the expansion you would expect a factor of $\frac{(-1)^n}{n!}$, but for each connected diagram it is possible to create $n!$ equivalent contribution by permutation of internal coordinates and a diagram represents all these contribution [52]. An example of such a permutation is to interchange $3 \leftrightarrow 4$ in the second order diagram in Fig. 2.1.

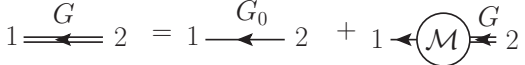
$$G(12) = G_0(12) + \Lambda d^3d^4 G_0(13) \mathcal{M}(34) G(42), \quad (2.33)$$


Figure 2.2.: Dyson equation for $G(12)$

where $\mathcal{M}(12)$ is defined by all diagrams with an outgoing/incoming GF at 2/1 which are irreducible with respect to G_0 . The definition of \mathcal{M} is chosen in such a way that all possible contributions to the GF are created by iterating the Eq. (2.33):

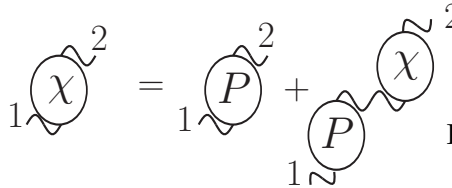
$$G(12) = G_0(12) + \Lambda d^3d^4 G_0(13) \mathcal{M}(34) G_0(42) + \Lambda d^3 \dots d^6 G_0(13) \mathcal{M}(34) G_0(45) \mathcal{M}(56) G_0(62) + \dots$$

The function \mathcal{M} describes the change from the known G_0 to the fully interacting G . Since this transition is extremely important, the object \mathcal{M} is given a special name: **self-energy**. An equation of the kind $A = X + XYA$ is called a **Dyson equation**. Such an equation is solved either by iteration or by a matrix inversion:

$$G_0(12) = \Delta d^4 [\delta_{41} - \Delta d^3 G_0(13) \mathcal{M}(34)] G(42) \\ \Rightarrow G(12) = \Delta d^4 [\delta_{14} - \Delta d^3 G_0(13) \mathcal{M}(34)]^{-1} G_0(42)$$

The two ways should lead to the same result. A finite order approximation for \mathcal{M} leads to a summation of an infinite number of contributions. This is a clear advantage of the Dyson equation compared to truncating the expansion implied by Eq. (2.29). After a summation has been carried out, the resulting set is often called renormalized or dressed [59].


The density response function $\chi^M(12)$ is a very important quantity. In this section always the Matsubara response function is used and the subscript M is left. The response function is the central object in linear response theory which is discussed in more detail in section 2.2. The Dyson equation for the response function reads:



$$\chi(12) = P(12) - \Lambda d^3d^4 P(13) v(34) \chi(42) \quad (2.34)$$

Figure 2.3.: Dyson equation for $\chi(12)$

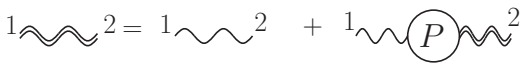
where $P(12)$ contains all proper diagrams which can be connected at 1 and 2 to an interaction line (Fig. 2.6). In Sec. 2.2 it is shown that the retarded version of this function describes the response of the density to external fields. Like the self-energy, the set P receives its own name: **Polarization propagator**. The simplest approximation to the polarization is the bubble:



$$P(12) \approx -G(12) G(21) \quad (2.35)$$

and the corresponding approximation for χ is called the **random phase approximation (RPA)**.

Besides the sets \mathcal{M} and P two more important sets are defined in general. The first one is the **screened Coulomb interaction** given by



$$-w(12) = -v(12) + \Lambda d^3d^4 v(13) P(34) w(42) \quad (2.36)$$

Figure 2.4.: Dyson Equation for $w(12)$

and represented by a double wiggly line. The screened Coulomb interaction takes multiple scattering processes of the electrons (screening) into account. The second one is the vertex function $\Gamma(123)$ depicted by a triangle (Fig. 2.6). The **vertex function** appears naturally in the derivation of the Hedin equations (Sec. 4) and determines the self-energy [Eq. (4.14)]:

$$\mathcal{M}(12) = \int d^3d^5 w(31) G(15) \Gamma(523) + \delta_{12} \Delta d^3 v(13) G(33^+).$$

Figure 2.5.: Self-energy $\mathcal{M}(12)$

Some authors call only the non-local part in the previous equation self-energy and the full object is referred to as **mass operator** [60]. From the previous definitions of \mathcal{M} and w , it can be concluded that the vertex must contain only proper contributions and is irreducible with respect to G_0 .

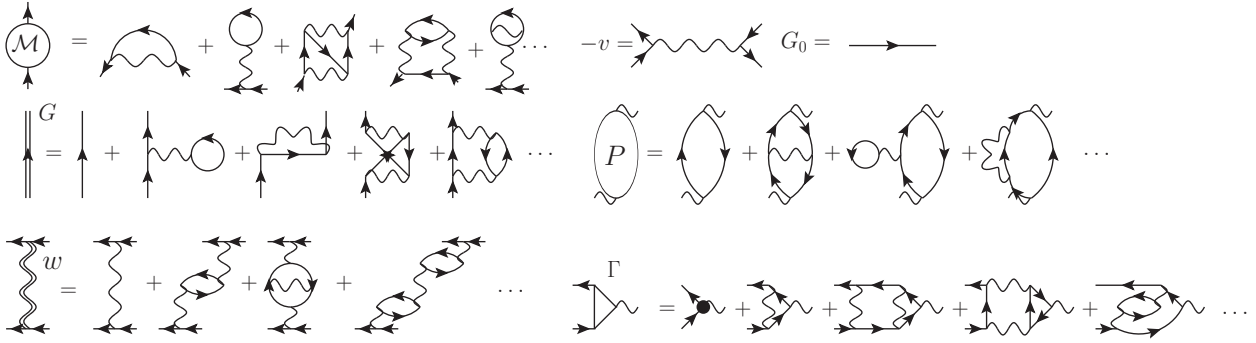


Figure 2.6.: Expansion of the relevant objects appearing in MBPT. In the first line the self-energy is expanded in terms of G_0 and v like discussed in Eq. (2.29). In the next lines the first orders of the Green's function G , Response function χ , screened Coulomb interaction w and vertex function Γ are shown.

3. Introduction to Density Functional Theory for Superconductors

Density functional theory (DFT) is an alternative *ab-initio* approach for treating interacting many-body systems. A detailed overview of the concepts and ideas behind DFT is presented in the book by Gross [61]. Instead of the electronic Green's function (GF) in many-body-perturbation theory (MBPT), the electronic density is the central object in DFT. The foundation of DFT was laid by Hohenberg and Kohn, who showed that every ground state expectation value is a functional of the electronic density $\rho(\mathbf{r})$ [62]. In particular the total energy is also a functional of the electronic density. For this functional a variational principle holds and the exact ground state density is found by minimizing the energy. The theory proposed by Hohenberg and Kohn is exact only in principle because the exact form of the total energy functional is unknown.

The DFT formalism is universal and may be applied to any electronic system: magnetic, superconducting, containing currents *etc.*. However, it is easier to construct concrete approximations for the energy functional, if the relevant densities are explicitly included in the functional. A standard example for this procedure is the inclusion of the spin magnetic density $m(\mathbf{r}) := \rho_{\uparrow}(\mathbf{r}) - \rho_{\downarrow}(\mathbf{r})$ to the energy functional [63, 64]. This theory is called spin DFT and all expectation values become functionals of ρ and m and the energy is minimal for the ground state densities. The magnetic density is the order parameter of the magnetic phase and couples to external magnetic fields.⁸

In the same spirit Oliveira, Gross and Kohn included an additional density for the treatment of superconductivity (SC) [23]. For SC the relevant density is the so called anomalous density. In analogy to the magnetic case, the anomalous density is the order parameter of the superconducting phase. The anomalous density is defined by two annihilation operators with different spin:

$$\hat{\chi}(\mathbf{r}\mathbf{r}') := \hat{\Psi}_{\uparrow}(\mathbf{r})\hat{\Psi}_{\downarrow}(\mathbf{r}'). \quad (3.1)$$

The anomalous density, should not be confused with the density-density response (Sec. 2.2). It couples to an external pairing potential $\Delta_s^{\text{ext}}(\mathbf{r}\mathbf{r}')$ and the term $\Lambda\hat{\chi}\Delta_s^{\text{ext}} + h.c.$ is added to the interacting Hamiltonian in Eq. (2.2). If the anomalous density is non-zero *i.e.*:

$$\langle\hat{\chi}\rangle \neq 0$$

the system is considered superconducting at this temperature [23]. The contribution $\Lambda\hat{\chi}\Delta_s^{\text{ext}} + h.c.$ describes only singlet pairing, where electrons with opposite spin are coupled by the pairing potential. An extension to pairing of electrons with identical spin (triplet pairing) is not considered in this work because the pairing in the cuprates and iron based superconductors (FeSC) takes place mainly in the singlet channel [67, 13]. However, the ruthenates are an example of a system, where the triplet pairing is important [68].

As discussed in the introduction, the magnetic phase is suppressed first and then superconductivity appears. Hence, it is not necessary to include the magnetic density as an additional density in the DFT framework of SC, if the goal is the description of the SC phase alone.

The additional densities are not limited to electronic contributions. In order to introduce the phonons in a proper way, the diagonal part of the N -particle density matrix of the nuclei is included as a further density. In this case the framework is called multi component DFT [27]. This leads to a formally exact description of the superconducting electronic-nuclear system. However, the focus of this work lies on a purely electronic pairing mechanism and the nuclear degrees of freedom are left out for simplicity in this chapter.

⁸ Note that non-uniqueness problems of spin DFT at zero temperature are fixed at finite temperature [65, 66].

3.1. Foundation of DFT for Superconductors

Superconducting density functional theory (SCDFT) is based on three pillars [69]:

1. There is a 1:1 correspondence between the densities $\{\rho, \chi\}$ and the corresponding potentials $\{v_0 + v_{\text{ext}}, \Delta_s^{\text{ext}}\}$ [70].
2. The statistical operator $\hat{\rho}_\beta$ [Eq. (2.6)] is fully determined by the external potentials and due to the 1:1 correspondence every expectation value is a functional of the densities. In particular this is true for the **grand canonical potential** [Eq. (2.1)]:

$$\Omega(\mu, V, T) = \Omega(\mu, V, T)[\rho, \chi].$$

3. A variational principle for the grand canonical potential holds:

$$\Omega[\rho_{\text{GS}}, \chi_{\text{GS}}] \leq \Omega[\rho, \chi],$$

where ρ_{GS} and χ_{GS} are the densities of the system in thermal equilibrium.

The grand canonical potential is formally rewritten:

$$\Omega[\rho, \chi] = T_0[\rho, \chi] + \Delta \int d^3r (v_0 + v_{\text{ext}} - \mu) \rho + \Lambda \int d^3r d^3r' \Delta_s^{\text{ext}} \chi + E_{\text{H}}[\rho] + \frac{1}{\beta} S_0[\rho, \chi] + E_{\text{xc}}[\rho, \chi] \quad (3.2)$$

$$E_{\text{H}}[\rho] = \frac{1}{2} \Lambda \int d^3r d^3r' \frac{\rho(\mathbf{r}) \rho(\mathbf{r}')}{|\mathbf{r} - \mathbf{r}'|}$$

$$S_0[\rho, \chi] = -\frac{1}{\beta} \langle \ln [\hat{\rho}_\beta^0] \rangle_0 = -\frac{1}{\beta} \text{tr} [\hat{\rho}_\beta^0 \ln [\hat{\rho}_\beta^0]] \quad \text{remember that } \hat{\rho}_\beta = \hat{\rho}_\beta[\rho, \chi]$$

$$T_0[\rho, \chi] = -\left\langle \Delta \int d^3r \hat{\Psi}^\dagger(\mathbf{r}) \frac{\nabla^2}{2} \hat{\Psi}(\mathbf{r}) \right\rangle_0$$

$$E_{\text{xc}}[\rho, \chi] := \left(\langle \hat{T} \rangle - T_0[\rho, \chi] \right) - \left(\frac{1}{\beta} \langle \ln [\hat{\rho}_\beta] \rangle - \frac{1}{\beta} \langle \ln [\hat{\rho}_\beta^0] \rangle_0 \right) + \left(\langle \hat{W} \rangle - E_{\text{H}}[\rho] \right),$$

where E_{xc} is the **exchange-correlation (XC)**-energy, E_{H} the Hartree energy, S_0 the non-interacting entropy, T_0 the non-interacting kinetic energy and the statistical operators $\hat{\rho}_\beta$ and $\hat{\rho}_\beta^0$ are given in Eqs. (2.6) and (2.7), respectively. The electronic potentials $v_0 + v_{\text{ext}}$ and pairing potential Δ_s^{ext} couple to the electronic and anomalous density, respectively. The occurrence of an external pairing potential may have two reasons: (1) The system is located near another **SC** material (proximity effect) or (2) an infinitesimal external field is introduced as a mathematical trick to break the degeneracy in analogy to an external **B**-field in magnetic calculations.

The **XC**-energy is the only unknown part and the main task in **DFT** is to construct good approximations to E_{xc} . For the exact functional a minimization would lead to the exact ground state densities ρ_{GS} and χ_{GS} for a given temperature T . If χ_{GS} is zero at this temperature, the system is not superconducting.

The minimization of the grand canonical potential is done using a non-interacting auxiliary system which has the same density as the interacting system. The idea to introduce such an auxiliary system goes back to Kohn and Sham and therefore the system is called the **Kohn-Sham (KS)** system [71]. The condition that the density of the **KS** and interacting system are equal, leads to the following expression for the potential in the **KS** system:

$$v_{\text{KS}}[\rho, \chi](\mathbf{r}) = v_0(\mathbf{r}) + v_{\text{ext}} + \Delta \int dr' \frac{\rho(\mathbf{r}')}{|\mathbf{r} - \mathbf{r}'|} + \underbrace{\frac{\delta E_{\text{xc}}[\rho, \chi]}{\delta \rho(\mathbf{r})}}_{:=v_{\text{xc}}(\mathbf{r})} \quad (3.3)$$

$$\Delta_s^{\text{KS}}[\rho, \chi](\mathbf{r}\mathbf{r}') = \Delta_s^{\text{ext}}(\mathbf{r}\mathbf{r}') + \underbrace{\frac{\delta E_{\text{xc}}[\rho, \chi]}{\delta \chi(\mathbf{r}\mathbf{r}')}}_{:=\Delta_s^{\text{xc}}(\mathbf{r}\mathbf{r}')}, \quad (3.4)$$

where the **XC-potentials** v_{xc} and Δ_s^{xc} are given by the functional derivative with respect to the corresponding density. In the present work **only** singlet superconductivity is considered and the subscript s at the pairing potential is dropped. Eqs. (3.3) and (3.4) together with $\rho(\mathbf{r}) = \sum_{\sigma} \langle \hat{\Psi}_{\sigma}^{\dagger}(\mathbf{r}) \hat{\Psi}_{\sigma}(\mathbf{r}) \rangle$ and $\chi(\mathbf{r}\mathbf{r}') = \langle \hat{\Psi}_{\uparrow}(\mathbf{r}) \hat{\Psi}_{\downarrow}(\mathbf{r}') \rangle$ lead to a fix point iteration. For the exact **XC-energy** the fix point leads to the exact ground state densities [72]. Note that the difference between the grand canonical potential of the interacting and the **KS** system is given by the exchange-correlation energies:

$$\begin{aligned} \Omega_{\text{KS}}[\rho, \chi] &= \langle \hat{H}_{\text{KS}} \rangle - \mu \langle \hat{N} \rangle - TS_0[\rho, \chi] \\ &= T_0[\rho, \chi] + \Delta \int d^3r (v^{\text{KS}}[\rho, \chi] - \mu) \rho + \Lambda \int d^3r d^3r' \Delta^{\text{KS}}[\rho, \chi] \chi - TS_0 \\ \Omega[\rho\chi] - \Omega_{\text{KS}}[\rho, \chi] &= E_{\text{xc}}[\rho, \chi] - \Lambda \int d^3r d^3r' \Delta^{\text{xc}} \chi - \Delta \int d^3r v^{\text{xc}} \rho - E_{\text{H}}[\rho]. \end{aligned} \quad (3.5)$$

3.2. The Kohn-Sham Bogoliubov-de Gennes Equations

3.2.1. Real Space Form

The Kohn-Sham Hamiltonian for a **non-magnetic (NM)** electronic system with **singlet pairing** reads [69]:

$$\begin{aligned} \hat{K}_{\text{KS}} &= \sum_{\sigma} \Delta \int d^3r \hat{\Psi}_{\sigma}^{\dagger}(\mathbf{r}) \left(-\frac{\nabla^2}{2} + v^{\text{KS}}(\mathbf{r}) - \mu \right) \hat{\Psi}_{\sigma}(\mathbf{r}) \\ &\quad + \Lambda \int d^3r d^3r' \left[\Delta^{\text{KS}}(\mathbf{r}, \mathbf{r}') \hat{\Psi}_{\uparrow}(\mathbf{r}) \hat{\Psi}_{\downarrow}(\mathbf{r}') - \Delta^{\text{KS}*}(\mathbf{r}, \mathbf{r}') \hat{\Psi}_{\uparrow}^{\dagger}(\mathbf{r}) \hat{\Psi}_{\downarrow}^{\dagger}(\mathbf{r}') \right] \end{aligned} \quad (3.6)$$

$$v^{\text{KS}}(\mathbf{r}) = v_0(\mathbf{r}) + \Delta \int d^3r' \frac{\rho(\mathbf{r}')}{|\mathbf{r} - \mathbf{r}'|} + v^{\text{xc}}(\mathbf{r}) \quad (3.7)$$

$$\Delta^{\text{KS}}(\mathbf{r}\mathbf{r}') = \Delta^{\text{ext}}(\mathbf{r}\mathbf{r}') + \Delta^{\text{xc}}(\mathbf{r}\mathbf{r}'). \quad (3.8)$$

An elegant way to diagonalize a Hamilton operator containing $\hat{\Psi}_{\uparrow} \hat{\Psi}_{\downarrow}$ contributions, is to introduce new fermionic operators γ_k defined by [52]:

$$\hat{\Psi}_{\sigma}(\mathbf{r}) = \sum_l \left(u_l(\mathbf{r}) \hat{\gamma}_{l\sigma} - z_{\sigma} v_l^*(\mathbf{r}) \hat{\gamma}_{l-\sigma}^{\dagger} \right) \quad (3.9)$$

$$\hat{\gamma}_{l\sigma} = \Delta \int d^3r \left(u_l^*(\mathbf{r}) \hat{\Psi}_{\sigma}(\mathbf{r}) - z_{-\sigma} v_l^*(\mathbf{r}) \hat{\Psi}_{-\sigma}^{\dagger}(\mathbf{r}) \right), \quad (3.10)$$

where $z_{\uparrow} = +1$ and $z_{\downarrow} = -1$. In Sec. C.2.2 it is shown that the operators γ are indeed fermionic, if the transformation matrix is unitary. The u_l, v_l are **chosen** in such a way that the operator \hat{H}_e^{KS} becomes diagonal in terms of the new operators $\hat{\gamma}$:

$$\hat{K}_{\text{KS}} \stackrel{!}{=} \sum_{k\sigma} E_k \hat{\gamma}_{k\sigma}^{\dagger} \hat{\gamma}_{k\sigma}. \quad (3.11)$$

By evaluating the commutators $[\hat{\Psi}_{\sigma}(\mathbf{r}), \hat{K}_{\text{KS}}]_{-}$ once using Eq. (3.6) and once Eq. (3.11) an eigenvalue equation for the functions $u_l(\mathbf{r})$ and $v_l(\mathbf{r})$ is obtained (Sec. C.2):

$$\Delta \int d^3r' \begin{pmatrix} \left(-\frac{\nabla^2}{2} + v^{\text{KS}}(\mathbf{r}) - \mu \right) \delta_{\mathbf{r}\mathbf{r}'} & \Delta^{\text{KS}*}(\mathbf{r}\mathbf{r}') \\ \Delta^{\text{KS}}(\mathbf{r}\mathbf{r}') u_l(\mathbf{r}') & - \left(-\frac{\nabla^2}{2} + v^{\text{KS}}(\mathbf{r}) - \mu \right) \delta_{\mathbf{r}\mathbf{r}'} \end{pmatrix} \begin{pmatrix} u_l(\mathbf{r}') \\ v_l(\mathbf{r}') \end{pmatrix} = E_l \begin{pmatrix} u_l(\mathbf{r}) \\ v_l(\mathbf{r}) \end{pmatrix}. \quad (3.12)$$

The set of these two coupled single particle equations is called **Kohn-Sham Bogoliubov-de Gennes (KS-BdG)** equations [69]. The densities ρ and χ in terms of the eigenvector $(u_l(\mathbf{r}), v_l(\mathbf{r}))$ are given

by:

$$\rho(\mathbf{r}) := \sum_{\sigma} \left\langle \hat{\Psi}_{\sigma}(\mathbf{r}) \hat{\Psi}_{\sigma}^{\dagger}(\mathbf{r}) \right\rangle = 2 \sum_l \left[|u_l(\mathbf{r})|^2 f_{\beta}(E_l) + |v_l(\mathbf{r})|^2 f_{\beta}(-E_l) \right] \quad (3.13)$$

$$\chi(\mathbf{r}\mathbf{r}') := \left\langle \hat{\Psi}_{\uparrow}(\mathbf{r}) \hat{\Psi}_{\downarrow}(\mathbf{r}') \right\rangle = \sum_l \left[u_l(\mathbf{r}) v_l^*(\mathbf{r}') f_{\beta}(-E_l) - v_l^*(\mathbf{r}) u_l(\mathbf{r}') f_{\beta}(E_l) \right]. \quad (3.14)$$

where $f_{\beta}(E)$ is the Fermi function. Remember that the KS potentials are functionals of the densities ρ and χ and the equations have to be solved self-consistently to find the ground state or at finite temperature the equilibrium densities.

3.2.2. Change to Bloch Representation

For an application in solid state physics, it is advantageous to rewrite the problem from real space to a representation in terms of Bloch states. As a basis set for the Bloch space, the eigenstates of the non-superconducting KS system at zero temperature are used:

$$\begin{aligned} \psi_k(\mathbf{r}) &= \left\langle \mathbf{r} \left| \hat{c}_k^{\dagger} \right| \text{vac} \right\rangle \\ \epsilon_k \psi_k(\mathbf{r}) &= \left[-\frac{\nabla^2}{2} + v^{\text{KS}}[\rho_{\text{GS}}^{T=0}, \chi = 0, T = 0](\mathbf{r}) \right] \psi_k(\mathbf{r}) \\ v^{\text{KS}}[\rho\chi T](\mathbf{r}) &= v_0(\mathbf{r}) + v^{\text{ext}}(\mathbf{r}) + v^{\text{H}}[\rho](\mathbf{r}) + v^{\text{xc}}[\rho\chi T](\mathbf{r}). \end{aligned} \quad (3.15)$$

The index k is a combined index describing the band n and the momentum \mathbf{k} of the Bloch electron and $-k$ denotes $(n, -\mathbf{k})$. The functions $u_l(\mathbf{r})$, $v_l(\mathbf{r})$ and $\Delta(\mathbf{r}, \mathbf{r}')$ are expanded in terms of the Bloch basis functions:

$$u_l(\mathbf{r}) := \sum_k u_{lk} \psi_k(\mathbf{r}) \quad (3.16)$$

$$v_l(\mathbf{r}) := \sum_k v_{lk} \psi_k(\mathbf{r}) \quad (3.17)$$

$$\Delta_{qk}^{\text{KS}} := \Lambda d^3 r d^3 r' \psi_q^*(\mathbf{r}) \Delta^{\text{KS}}(\mathbf{r}\mathbf{r}') \psi_k(\mathbf{r}') \quad (3.18)$$

$$\Delta_{qk}^{\text{KS}*} := \Lambda d^3 r d^3 r' \psi_q(\mathbf{r}) \Delta^{\text{KS}*}(\mathbf{r}\mathbf{r}') \psi_k^*(\mathbf{r}'). \quad (3.19)$$

Note that for a system without time reversal symmetry Eq. (3.17) changes to $v_l(\mathbf{r}) = \sum_k v_{lk} \psi_{-k}^*(\mathbf{r})$. Due to the symmetric singlet pairing and the time reversal symmetry the pairing potential in Bloch space is invariant with respect to $(k, k') \rightarrow (-k', -k)$:

$$\begin{aligned} \Delta_{qk}^{\text{KS}} &= \Lambda d^3 r d^3 r' \psi_q^*(\mathbf{r}) \Delta^{\text{KS}}(\mathbf{r}\mathbf{r}') \psi_k(\mathbf{r}') \\ &= \Lambda d^3 r d^3 r' \psi_{-q}(\mathbf{r}) \Delta^{\text{KS}}(\mathbf{r}\mathbf{r}') \psi_{-k}^*(\mathbf{r}') = \Delta_{-k, -q}^{\text{KS}}. \end{aligned} \quad (3.20)$$

Using the definitions given in Eqs. (3.16), (3.17), (3.18) and (3.19) the KS-BdG equations in real space read

$$\begin{aligned} \sum_k \left[\left(-\frac{\nabla^2}{2} + v^{\text{KS}}(\mathbf{r}) - \mu \right) u_{lk} \psi_k(\mathbf{r}) + \Delta d^3 r' \Delta^{\text{KS}*}(\mathbf{r}\mathbf{r}') v_{lk} \psi_k(\mathbf{r}') \right] &= E_l \sum_k u_{lk} \psi_k(\mathbf{r}) \\ \sum_k \left[-\left(-\frac{\nabla^2}{2} + v^{\text{KS}}(\mathbf{r}) - \mu \right) v_{lk} \psi_k(\mathbf{r}) + \Delta d^3 r' \Delta^{\text{KS}}(\mathbf{r}\mathbf{r}') u_{lk} \psi_k(\mathbf{r}') \right] &= E_l \sum_k v_{lk} \psi_k(\mathbf{r}). \end{aligned}$$

The operator $\Delta d^3 r \psi_q^*(\mathbf{r})$ is applied from left. The Bloch states are orthogonal and a set of coupled equations in Bloch space is found:

$$(\epsilon_q - \mu) u_{lq} + \sum_k \Delta_{-q-k}^{\text{KS}*} v_{lk} = E_l u_{lq} \quad (3.21)$$

$$\sum_k \Delta_{qk}^{\text{KS}} u_{lk} - (\epsilon_q - \mu) v_{lq} = E_l v_{lq}. \quad (3.22)$$

The last step used the fact that ψ_k is an eigenfunction of $\left(-\frac{\Delta}{2} + v^{\text{KS}}(\mathbf{r}) - \mu\right)$ with eigenvalue ϵ_k . This is only true, if the functional v^{KS} is evaluated for the zero temperature ground state density of the non-superconducting system [Eq. (3.15)]. It is assumed that the effects induced by temperature and superconductivity on the KS -potential are small [69]:

$$v^{\text{KS}}[\rho, \chi, T](\mathbf{r}) \approx v^{\text{KS}}[\rho_{\text{GS}}^{T=0} \chi = 0, T = 0](\mathbf{r}).$$

In this approximation the same basis functions ψ_k and chemical potential μ can be used in every step of the iteration. Now the **decoupling approximation** is introduced. In the decoupling approximation it is assumed that the relevant part of the pairing is created by states with identical quantum numbers⁹ and hence only the diagonal part of the **pairing potential** is considered [69]:

$$\Delta_{qk}^{\text{KS}} \approx \delta_{qk} \Delta_k^{\text{KS}}. \quad (3.23)$$

This approximation breaks down if bands are crossing close to the Fermi level. In appendix C.2.3 it is shown that the decoupling approximation leads to diagonal coefficients

$$u_{lm} = \delta_{lm} u_l \text{ and } v_{lm} = \delta_{lm} v_l. \quad (3.24)$$

The coefficients are determined by a two-dimensional eigenvalue problem and the eigenvectors are calculated in Sec. C.2.4 of the appendix:

$$\begin{pmatrix} \epsilon_l - \mu & \Delta_l^{\text{KS}*} \\ \Delta_l^{\text{KS}} & \mu - \epsilon_l \end{pmatrix} \begin{pmatrix} u_l \\ v_l \end{pmatrix}_{\pm} = E_l^{\pm} \begin{pmatrix} u_l \\ v_l \end{pmatrix}_{\pm} \quad (3.25)$$

$$E_l^{\pm} = \pm \sqrt{(\epsilon_l - \mu)^2 + |\Delta_l^{\text{KS}}|^2} =: \pm R_l \quad \begin{pmatrix} u_l \\ v_l \end{pmatrix}_{\pm} = \frac{1}{\sqrt{2}} \begin{pmatrix} \pm \frac{\Delta_l^{\text{KS}*}}{|\Delta_l^{\text{KS}}|} \left[1 + \frac{\epsilon_l - \mu}{E_l^{\pm}}\right]^{\frac{1}{2}} \\ \left[1 - \frac{\epsilon_l - \mu}{E_l^{\pm}}\right]^{\frac{1}{2}} \end{pmatrix}. \quad (3.26)$$

The function Δ_l^{KS} determines the gap in the excitation spectrum associated with the $\hat{\gamma}$ operators. That is the reason why the pairing potential coupling to the **anomalous density** is also called **gap function**. Note that $\Delta_l^{\text{KS}} = \Delta_{-l}^{\text{KS}}$ [Eq. (3.20)] and $\epsilon_l = \epsilon_{-l}$ (time reversal symmetry) lead to:

$$E_l = E_{-l}, \quad u_l = u_{-l} \text{ and } v_l = v_{-l}. \quad (3.27)$$

For each quantum number l there is a positive and negative eigenvalue. In the equations for the densities [Eqs. (3.13) and (3.14)] a sum with respect to the quantum number l appears and the question arises, how these sums have to be evaluated. Obviously the summation over the positive **and** negative branch *i.e.* $\sum_l e^{-\beta E_l} \rightarrow \sum_l (e^{-\beta R_l} + e^{+\beta R_l})$ would lead to many contributions and would diverge.

⁹For a lattice periodic system the gap is translation invariant $\Delta(\mathbf{r}_1, \mathbf{r}_2) = \Delta(\mathbf{r}_1 + \mathbf{T}, \mathbf{r}_2 + \mathbf{T})$ which leads in Bloch space to $\Delta_{n\mathbf{k}m\mathbf{q}} = \delta_{\mathbf{k}\mathbf{q}} \Delta_{nm}(\mathbf{k})$. So the decoupling approximation neglects pairing between different bands.

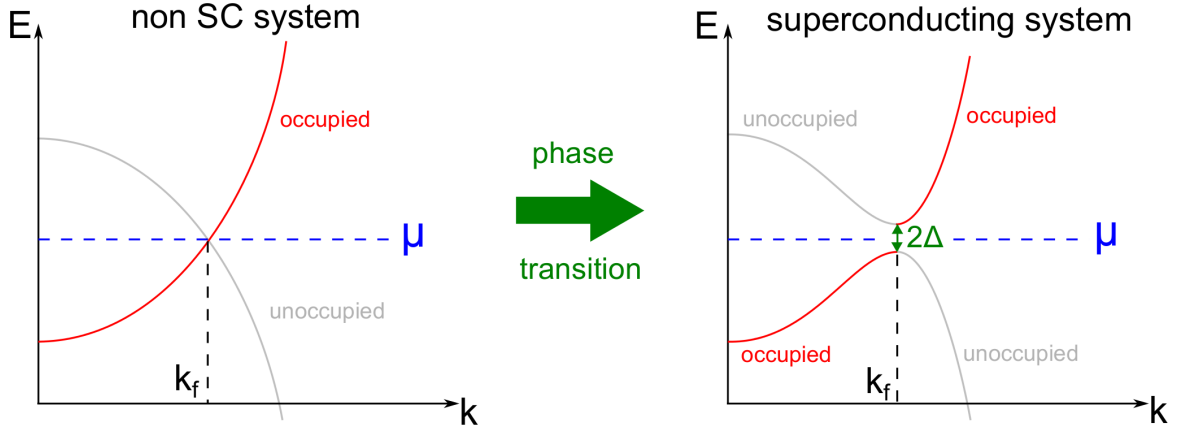


Figure 3.1.: (left) For a non-superconducting system one eigenvalue branch is occupied. (right) In the superconducting phase a gap opens and one branch is occupied above and the other one below μ

In the non-superconducting limit the equations should reduce to the non-superconducting expressions: The eigenvalue problem is one dimensional, and only one branch is present with a finite number of states below the chemical potential and an infinite number of states above. This weight $\frac{1}{Z_G} e^{-\beta(\epsilon_l - \mu)}$ leads to a finite number of particles per unit cell (left hand side of Fig. 3.1). Since the sign of $\epsilon_l^{\text{KS}} - \mu$ is lost in Eq. (3.26), it is enforced by evaluating the sums in the following way:

$$\sum_l A(E_l^\pm) \rightarrow \hat{\sum}_l A(E_l^\pm) := \sum_{l, \epsilon_l < \mu} A(-R_l) + \sum_{l, \epsilon_l > \mu} A(R_l), \quad (3.28)$$

where μ is the chemical potential of the non-superconducting system. On the right hand side of Fig. 3.1 this occupation rule is shown. The convention fixes also the ground state energy E_{GS} of the superconducting KS system which has been undetermined due to the commutator in Eq. (3.11):

$$\begin{aligned} \hat{\sum}_k E_k \hat{\gamma}_k^\dagger \hat{\gamma}_k &= \sum_{k, \epsilon_k < \mu} (-R_k) \hat{\gamma}_{k-}^\dagger \hat{\gamma}_{k-} + \sum_{k, \epsilon_k > \mu} R_k \hat{\gamma}_{k+}^\dagger \hat{\gamma}_{k+} = \sum_{k, \epsilon_k < \mu} (-R_k) (1 - \hat{\gamma}_{k-} \hat{\gamma}_{k-}^\dagger) + \sum_{k, \epsilon_k > \mu} R_k \hat{\gamma}_{k+}^\dagger \hat{\gamma}_{k+} \\ &= \sum_{k, \epsilon_k < \mu} (-R_k) + \sum_{k, \epsilon_k < \mu} R_k \hat{\gamma}_{k-} \hat{\gamma}_{k-}^\dagger + \sum_{k, \epsilon_k > \mu} R_k \hat{\gamma}_{k+}^\dagger \hat{\gamma}_{k+} = \underbrace{\sum_{k, \epsilon_k < \mu} (-R_k)}_{\text{GS energy}} + \underbrace{\sum_{k, \epsilon_k > \mu} R_k \hat{c}_k^\dagger \hat{c}_k}_{\text{excitations } R_k > 0}, \end{aligned}$$

where the operators \hat{c}_k and \hat{c}_k^\dagger are defined as:

$$\hat{\gamma}_k^\dagger := \begin{cases} \hat{c}_k & \text{if } E_k < 0 \\ \hat{c}_k^\dagger & \text{if } E_k > 0 \end{cases} \quad \hat{\gamma}_k := \begin{cases} \hat{c}_k & \text{if } E_k > 0 \\ \hat{c}_k^\dagger & \text{if } E_k < 0 \end{cases}.$$

Note that different rules for the evaluation of the sum only affect the ground state energy. If for example the complete negative branch is chosen for each k , the ground state energy changes to:

$$\begin{aligned} \sum_k^{(-)} E_k \hat{\gamma}_k^\dagger \hat{\gamma}_k &= \sum_{k, \epsilon_k < \mu} (-R_k) \hat{\gamma}_{-k}^\dagger \hat{\gamma}_{-k} + \sum_{k, \epsilon_k > \mu} (-R_k) \hat{\gamma}_{k-}^\dagger \hat{\gamma}_{k-} \\ &= \sum_{k, \epsilon_k < \mu} (-R_k) + \sum_{k, \epsilon_k < \mu} (-R_k) + \sum_{k, \epsilon_k < \mu} (R_k) \hat{\gamma}_{-k} \hat{\gamma}_{-k}^\dagger + \sum_{k, \epsilon_k > \mu} (R_k) \hat{\gamma}_{k-} \hat{\gamma}_{k-}^\dagger \\ &= \underbrace{\sum_{k, \epsilon_k < \mu} (-R_k) + \sum_{k, \epsilon_k < \mu} (-R_k)}_{\text{GS energy}} + \underbrace{\sum_{k, \epsilon_k > \mu} R_k \hat{c}_k^\dagger \hat{c}_k}_{\text{excitations } R_k > 0}. \end{aligned}$$

In the thermal average the explicit value of the ground state energy is irrelevant ($\langle \hat{O} \rangle = \frac{\text{tr}[e^{-\beta E_{\text{GS}}} e^{-\beta \hat{H}_0} \hat{O}]}{\text{tr}[e^{-\beta E_{\text{GS}}} e^{-\beta \hat{H}_0}]}$) and the same results are found, if for each k **either** the positive or the negative eigenvalue is used or the rule given in Eq. (3.28).

3.3. Construction of Δ^{xc} Including Spin-Fluctuation Effects – The next Steps

A way to construct an approximation for Δ^{xc} is provided by many-body perturbation theory. In the previous section the diagram rules for a non-superconducting system with Coulomb interaction have been presented. The **phonons** (Ph) have been left out for simplicity here, but the lattice dynamics would show up as an additional interaction term in the Hamiltonian [69]:

$$\begin{aligned} \hat{W} &= \frac{1}{2} \sum_{\sigma\sigma'} \Lambda \int d^3r d^3r' \frac{\hat{\Psi}_{\sigma}^{\dagger}(\mathbf{r}) \hat{\Psi}_{\sigma'}^{\dagger}(\mathbf{r}') \hat{\Psi}_{\sigma'}(\mathbf{r}') \hat{\Psi}_{\sigma}(\mathbf{r})}{|\mathbf{r} - \mathbf{r}'|} + \hat{W}_{\text{e-ph}} \\ \hat{W}_{\text{e-ph}} &= \sum_{\lambda\mathbf{q}} \Delta \int dr g_{\lambda\mathbf{q}}^{\text{e-ph}}(\mathbf{r}) \hat{\Psi}^{\dagger}(\mathbf{r}) \hat{\Psi}(\mathbf{r}) \underbrace{[\hat{b}_{\lambda\mathbf{q}} + \hat{b}_{\lambda-\mathbf{q}}^{\dagger}]}_{:=\Phi_{\lambda\mathbf{q}}}, \end{aligned} \quad (3.29)$$

where $g_{\lambda\mathbf{q}}^{\text{e-ph}}$ are the electron-phonon coupling matrix elements and $\hat{b}_{\lambda\mathbf{q}}$ and $\hat{b}_{\lambda\mathbf{q}}^{\dagger}$ are the phonon operators. The additional term leads in first non-vanishing order to an electron-electron interaction mediated by phonons. This effective interaction is not instantaneous like the Coulomb interaction and may be attractive. Two approaches are available for the construction of Δ^{xc} :

- In the **Ph.D.** thesis of Lüders, the difference $\Omega - \Omega_{\text{KS}}$ [Eqs. (2.32) and (3.5)] is expanded and **functional derivatives** are used to obtain Δ^{xc} [69].
- In the work of Marques, the self-energy [Eq. (2.33)] is expanded and the **Sham-Schlüter equation** (SSEq) is used to find Δ^{xc} [73]. The SSEq connects an approximation of the self-energy to the corresponding Kohn-Sham potential (see Sec. 4.4 for details).

If the expansion is done up to first order in the Coulomb interaction and the phonon propagator, both ways lead to the same expression for Δ^{xc} . This approximation for Δ^{xc} has been used so far and leads to reasonable results for many materials, *i.e.* the predicted critical temperatures are close to the measured ones [27]. However, for materials like the iron based superconductors or cuprates this approach fails [74]. As discussed in chapter 1, the magnetic fluctuations are most likely the glue for pairing the electrons in these materials and an inclusion is essential for the correct description of superconductivity in these materials [12, 13, 75]. The derivation of a functional containing dynamic effects like fluctuations is not straight forward. In this work the inclusion is based on a diagrammatic expansion of the self-energy and is split into two chapters:

1. In the next chapter (chapter 4) the Hedin equations for a superconducting system are derived. A fully self-consistent treatment of these equations would lead to the exact electronic self-energy which contains all many-body effects including the low lying collective excitations (**paramagnons**). However, a fully self-consistent treatment of the Hedin equations is computationally not feasible.
2. Hence, in chapter 5 the relevant diagrams in the self-energy containing the magnetic fluctuations are selected. After various transformations the contribution in the self-energy related to the magnetic fluctuations are transformed to an effective interaction which is used along with the phonon and Coulomb interaction to construct a functional.

The functional construction and application to two representatives are done in chapter 6 and 7, respectively.

4. Hedin Equations for Superconductors

In this chapter the [Hedin equations](#) for superconducting systems are derived. The Hedin equations were first obtained by Lars Hedin in the sixties [25], for electrons interacting via the Coulomb interaction. To this day various extensions of the original Hedin equations have been derived. In the original work, the nuclei are frozen and create only a static background potential. A proper treatment of the nuclei was proposed by R. Leeuwen *et. al.* [76]. Recently the Hedin equations have been extended to spin dependent interactions [60].

The focus of this work lies on the inclusion of the magnetic fluctuations *i.e.* a purely electronic pairing mechanism in a [DFT](#) functional and the excitations of the nuclear lattice ([phonons](#)) are neglected. As in the previous section, only [singlet pairing](#) is considered. In contrast to the previous section, an external magnetic field B^{ext} along the z -axis is considered in order to allow for the description of collinear magnetism and superconductivity. The Hamiltonian for such a system reads:

$$\begin{aligned} \hat{K} &= \hat{H} - \mu\hat{N} = \hat{H}_0 + \hat{H}_{\text{sc}} + \hat{H} - \mu\hat{N} \\ \hat{H}_0 &= \sum_{\alpha\beta} \Delta dr \hat{\Psi}_\alpha^\dagger(\mathbf{r}) \left[\left[-\frac{\nabla^2}{2} + v_0(\mathbf{r}) \right] \delta_{\alpha\beta} - \sigma_z^{\alpha\beta} B^{\text{ext}}(\mathbf{r}) \right] \hat{\Psi}_\beta(\mathbf{r}) \end{aligned} \quad (4.1)$$

$$\hat{H}_{\text{sc}} = \Lambda d^3r d^3r' \left[\Delta^{\text{ext}}(\mathbf{r}\mathbf{r}') \hat{\Psi}_\uparrow(\mathbf{r}) \hat{\Psi}_\downarrow(\mathbf{r}') + \Delta^{\text{ext}*}(\mathbf{r}\mathbf{r}') \hat{\Psi}_\downarrow^\dagger(\mathbf{r}') \hat{\Psi}_\uparrow^\dagger(\mathbf{r}) \right] \quad (4.2)$$

$$\hat{W} = \frac{1}{2} \sum_{\alpha\beta} \Lambda d^3r d^3r' v(\mathbf{r}\mathbf{r}') \hat{\Psi}_\sigma^\dagger(\mathbf{r}) \hat{\Psi}_{\sigma'}^\dagger(\mathbf{r}') \hat{\Psi}_{\sigma'}(\mathbf{r}') \hat{\Psi}_\sigma(\mathbf{r}). \quad (4.3)$$

Here a short remark on the sign convention for the magnetic field is made. The energy term in the Hamiltonian is written as $\hat{\mathbf{m}}_z B^{\text{ext}}$ and the magnetic density $\hat{\mathbf{m}}_z$ is given by $-\hat{\Psi}_\alpha^\dagger \hat{\Psi}_\beta \sigma_z^{\alpha\beta}$. In this convention the moments will align anti-parallel to the external magnetic field which is a bit counterintuitive, but the [XC](#)-fields $\frac{\delta E}{\delta \mathbf{m}} = \mathbf{B}^{\text{xc}}$ are defined without any extra minus signs.

4.1. The Equation of Motion

The starting point for the derivation of the Hedin equations is the [equation of motion](#) of the Green's function. The definition of the [GF](#) given in Eq. (2.11) is extended in order to account for superconductivity. The scalar function G becomes a matrix object indicated as a \bar{G} and is called [Nambu GF](#) [24]:

$$\begin{aligned} \bar{G}(12) &:= \tau^z \begin{pmatrix} G(12) & F(12) \\ F^\dagger(12) & G^\dagger(12) \end{pmatrix} = \tau^z \begin{pmatrix} G_{\sigma_1\sigma_2}(\mathbf{x}_1\mathbf{x}_2) & F_{\sigma_1\sigma_2}(\mathbf{x}_1\mathbf{x}_2) \\ F_{\sigma_1\sigma_2}^\dagger(\mathbf{x}_1\mathbf{x}_2) & G_{\sigma_1\sigma_2}^\dagger(\mathbf{x}_1\mathbf{x}_2) \end{pmatrix} \\ &= -\tau^z \begin{pmatrix} \left\langle \hat{T} \left[\Psi_{\sigma_1}(\mathbf{x}_1) \Psi_{\sigma_2}^\dagger(\mathbf{x}_2) \right] \right\rangle & \left\langle \hat{T} \left[\Psi_{\sigma_1}(\mathbf{x}_1) z_{\sigma_2} \Psi_{\sigma_2}(\mathbf{x}_2) \right] \right\rangle \\ \left\langle \hat{T} \left[z_{\sigma_1} \Psi_{\sigma_1}^\dagger(\mathbf{x}_1) \Psi_{\sigma_2}^\dagger(\mathbf{x}_2) \right] \right\rangle & \left\langle \hat{T} \left[z_{\sigma_1} \Psi_{\sigma_1}^\dagger(\mathbf{x}_1) z_{\sigma_2} \Psi_{\sigma_2}(\mathbf{x}_2) \right] \right\rangle \end{pmatrix}. \end{aligned} \quad (4.4)$$

The matrix τ^z is identical to the Pauli matrix σ^z [Eq. (A.4)]. The new symbol is introduced to avoid confusion between the spin and Nambu space and z_σ is the spin sign function: $z_\uparrow = 1$ and $z_\downarrow = -1$. The diagonal elements are referred to as normal parts of the Green's function and the off-diagonal parts are the [anomalous Green's function](#). The off diagonal terms determine the [anomalous density](#) χ [Eq. (3.1)] and are zero for a non-superconducting system. If in the thermal average [Eq. (2.5)] the eigenstates correspond to a fixed particle number N , the off diagonal terms are strictly zero. If the eigenstates in the trace have the form of a [Bardeen, Cooper and Schrieffer \(BCS\)](#) wave function one gets a non-trivial result [2]. The definition including the τ^z and the z_σ is a convenient choice:

- The τ^z simplifies a relation between the two-particle contributions $\langle \hat{\Psi}^\dagger \hat{\Psi}^\dagger \hat{\Psi} \hat{\Psi} \rangle$ and the functional derivative of \bar{G} with respect to an external field φ (Sec. D.1.4)
- The z_σ cancels with the other z_σ in the definition of the operators $(\hat{\gamma}, \hat{\gamma}^\dagger)$ given in Eq. (3.9) which leads to a KS Green's functions of a NM system without any z_σ .

The equation of motion for the Nambu GF reads [Eq.(D.1)]:

$$-\partial_{\tau_1} \bar{G}(12) := \delta_{12} \tau^0 + \left(\begin{array}{l} \langle \hat{T} [\hat{K}, \hat{\Psi}_{\sigma_1}(\mathbf{r}_1)](\tau_1) \hat{\Psi}_{\sigma_2}^\dagger(\mathbf{x}_2) \rangle \quad \langle \hat{T} [\hat{K}, \hat{\Psi}_{\sigma_1}(\mathbf{r}_1)](\tau_1) z_{\sigma_2} \hat{\Psi}_{\sigma_2}(\mathbf{x}_2) \rangle \\ \langle \hat{T} [\hat{K}, z_{\sigma_1} \hat{\Psi}_{\sigma_1}^\dagger(\mathbf{r}_1)](\tau_1) \hat{\Psi}_{\sigma_2}^\dagger(\mathbf{x}_2) \rangle \quad \langle \hat{T} [\hat{K}, z_{\sigma_1} \hat{\Psi}_{\sigma_1}^\dagger(\mathbf{r}_1)](\tau_1) z_{\sigma_2} \hat{\Psi}_{\sigma_2}(\mathbf{x}_2) \rangle \end{array} \right). \quad (4.5)$$

All the necessary commutators are worked out in Sec. D.1.1 of the appendix. The single particle contributions in \hat{H} give rise to [Eq. (D.2)]:

$$-\tau^z \partial_{\tau_1} \bar{G}^0(12) = \delta_{12} \tau^0 + \Delta d3 \bar{h}^0(13) \bar{G}^0(32) \\ \bar{h}^0(12) := \delta_{\tau_1 \tau_2} \delta_{\mathbf{r}_1 \mathbf{r}_2} \delta_{\sigma_1 \sigma_2} \tau^0 \left[-\frac{\nabla^2}{2} + v_0(\mathbf{r}_1) - \mu + z_\alpha B^{\text{ext}}(\mathbf{r}_1) \right] \\ + \delta_{\tau_1 \tau_2} \delta_{\sigma_1, -\sigma_2} \left(\begin{array}{cc} 0 & \Delta^{\text{ext}*}(\mathbf{r}_1 \mathbf{r}_2) \\ \Delta^{\text{ext}}(\mathbf{r}_1 \mathbf{r}_2) & 0 \end{array} \right). \quad (4.6)$$

This is the equation of motion for a non-interacting system. The interaction \hat{W} gives rise to an extra term which couples the $\partial_\tau \bar{G}$ to the two-particle propagator $\bar{G}^{(2)} \propto \langle \hat{\Psi} \hat{\Psi} \hat{\Psi}^\dagger \hat{\Psi}^\dagger \rangle$ [Eq. (D.4)]:

$$-\tau^z \partial_{\tau_1} \bar{G}(12) = \delta_{12} \tau^0 + \Delta d3 \bar{h}^0(13) \bar{G}(32) \\ + \left(\begin{array}{l} \langle \hat{T} [\hat{W}, \hat{\Psi}_{\sigma_1}(\mathbf{r}_1)](\tau_1) \hat{\Psi}_{\sigma_2}^\dagger(\mathbf{x}_2) \rangle \quad \langle \hat{T} [\hat{W}, \hat{\Psi}_{\sigma_1}(\mathbf{r}_1)](\tau_1) z_{\sigma_2} \hat{\Psi}_{\sigma_2}(\mathbf{x}_2) \rangle \\ \langle \hat{T} [\hat{W}, z_{\sigma_1} \hat{\Psi}_{\sigma_1}^\dagger(\mathbf{r}_1)](\tau_1) \hat{\Psi}_{\sigma_2}^\dagger(\mathbf{x}_2) \rangle \quad \langle \hat{T} [\hat{W}, z_{\sigma_1} \hat{\Psi}_{\sigma_1}^\dagger(\mathbf{r}_1)](\tau_1) z_{\sigma_2} \hat{\Psi}_{\sigma_2}(\mathbf{x}_2) \rangle \end{array} \right).$$

It is possible to connect the two-particle propagator with the single particle one, by using a **functional derivative** with respect to an external probing field φ_0 [Eq. (D.5)]:

$$-\Delta d3 [\tau^z \partial_{\tau_1} \delta_{13} + \bar{h}^0(13)] \bar{G}(32) = \delta_{12} \tau^0 + \Delta d^3 r v(\mathbf{r}_1 \mathbf{r}) \left[\rho(\mathbf{r} \tau_1) \bar{G}(12) - \frac{\delta \bar{G}(12)}{\delta \varphi_0(\mathbf{r} \tau_1)} \right].$$

The Coulomb interaction is formally written as a time dependent interaction *i.e.* $v(12) = \delta_{\tau_1 \tau_2} v(\mathbf{r}_1 \mathbf{r}_2)$. This simplifies the expression for \bar{G} to:

$$-\Delta d3 [\tau^z \partial_{\tau_1} \delta_{13} + \bar{h}^0(13)] \bar{G}(32) = \delta_{12} \tau^0 + \Delta d3 v(13) \left[\rho(3) \bar{G}(12) - \frac{\delta \bar{G}(12)}{\delta \varphi_0(3)} \right].$$

where the total charge $\rho(\mathbf{x}_1)$ is given by $\sum_{\sigma_1} \rho(1)$. Inserting a one $\mathbf{1} = \bar{G}^0 (\bar{G}^0)^{-1}$ between the \bar{G} and the operator on the left hand side and using the identity $0 = \frac{\delta(\bar{G} \bar{G}^{-1})}{\delta \varphi_0} = \bar{G} \frac{\delta \bar{G}^{-1}}{\delta \varphi_0} + \frac{\delta \bar{G}}{\delta \varphi_0} \bar{G}^{-1}$ for the derivative on the right hand side leads to:

$$\bar{G}(12) = \bar{G}^0(12) + \Lambda d3 d4 \bar{G}^0(13) v(34) \left[\rho(4) \bar{G}(32) + \Lambda d5 d6 \bar{G}(35) \frac{\delta \bar{G}^{-1}(56)}{\delta \varphi_0(4)} \bar{G}(62) \right].$$

The inverse \bar{G}^{-1} denotes the inverse of the full Nambu matrix: $\bar{G}_{ij}(12)$ where ij are the components in Nambu space and 1, 2 are the combined variables defined in Eq. (2.10). In analogy to the non-superconducting GF in Eq. (2.33) one can define the **self-energy** $\bar{\mathcal{M}}$:

$$\bar{\mathcal{M}}(12) = \delta_{12} \tau^0 \Delta d3 v(13) \rho(3) + \Lambda d4 d5 \bar{G}(15) v(14) \frac{\delta \bar{G}^{-1}(52)}{\delta \varphi_0(4)} \\ \bar{G}(12) = \bar{G}^0(12) + \Lambda d3 d4 \bar{G}^0(13) \bar{\mathcal{M}}(34) \bar{G}(42). \quad (4.7)$$

The positive sign of the local contribution $v(\mathbf{r}_1\mathbf{r})\rho(\mathbf{r}\tau_1) = v(\mathbf{r}_1\mathbf{r})\hat{\Psi}^\dagger(\mathbf{r}\tau_1^+)\hat{\Psi}(\mathbf{r}\tau_1)$ is in line with the diagrammatic rules for the Hartree diagram, requiring a (-1) for the first order in the interaction and (-1) for each fermionic loop (see Sec. 2.4). This local contribution is called [Hartree potential](#)

$$v^{\text{H}}(1) = \Delta d2v(12)\rho(2) \quad (4.8)$$

and is added to the single particle \bar{h}^0 operator:

$$\bar{h}^{\text{H}}(12) := \bar{h}^0(12) + \tau^0\delta_{12}v^{\text{H}}(1). \quad (4.9)$$

We define the Hartree Green's function by:

$$-\Delta d3[\tau^z\partial_{\tau_1}\delta_{13} + \bar{h}^{\text{H}}(13)]\bar{G}_{\sigma\sigma_2}^{\text{H}}(32) = \tau_0\delta_{12}.$$

In terms of the Hartree Green's function \bar{G}^{H} the Dyson equation for the full [GF](#) changes:

$$\bar{G}(12) = \bar{G}^{\text{H}}(12) + \Lambda d3d4\bar{G}^{\text{H}}(13)\bar{\Sigma}(34)\bar{G}(42) \quad (4.10)$$

$$\bar{\Sigma}(12) := \Lambda d4d5\bar{G}(15)v(14)\frac{\delta\bar{G}^{-1}(52)}{\delta\varphi_0(4)}. \quad (4.11)$$

The Eqs. (4.7) and (4.11) lead to the same full Green's function \bar{G} , but the underlying non-interacting system is different: For \bar{M} the non-interacting system is \bar{h}^0 and for $\bar{\Sigma}$ it is \bar{h}^{H} . The freedom of choosing a single particle Hamiltonian as a [reference system](#) is discussed in more detail in Sec. D.3. The Eqs. (4.10) and (4.11) are a coupled set of equations leading to the exact self-energy and Green's function. However, the derivative $\frac{\delta\bar{G}^{-1}}{\delta\varphi_0}$ is almost impossible to evaluate. Hence, the goal of the next sections is to rewrite the equations to a form without difficult functional derivatives. The rewriting process leads more or less naturally to the set of five [Hedin equations](#).

4.2. Introduction of the Hedin Cycle

The first element in the set of Hedin equations has been derived already. It is simply the Dyson equation for the full Green's function:

$$\bar{G}(12) = \bar{G}^{\text{H}}(12) + \Lambda d3d4\bar{G}^{\text{H}}(13)\bar{\Sigma}(34)\bar{G}(42).$$

As a next step the total field is defined:

$$\Phi_0(1) := \varphi_0(1) + v^{\text{H}}(1) = \varphi_0(\mathbf{x}_1) + \Delta d2v(12)\rho(2).$$

Using the chain rule, the [self-energy](#) is rewritten:

$$\bar{\Sigma}(12) = \Lambda d4d5\bar{G}(15)v(14)\frac{\delta\bar{G}^{-1}(52)}{\delta\varphi_0(4)} = \Pi d3d4d5v(14)\bar{G}(15)\frac{\delta\Phi_0(3)}{\delta\varphi_0(4)}\frac{\delta\bar{G}^{-1}(52)}{\delta\Phi_0(3)}.$$

The new quantities: [dielectric constant](#) (ϵ^{-1}), [vertex function](#) ($\bar{\Gamma}$) and [screened Coulomb interaction](#) (w) are introduced and the self-energy is rewritten in term of these new quantities:

$$\epsilon^{-1}(34) := \frac{\delta\Phi_0(3)}{\delta\varphi_0(4)} = \delta_{34} + \Delta d1v(31)\frac{\delta\rho(1)}{\delta\varphi_0(4)} \quad (4.12)$$

$$\bar{\Gamma}(523) := -\frac{\delta\bar{G}^{-1}(52)}{\delta\Phi_0(3)} \quad w(31) := \Delta d4\epsilon^{-1}(34)v(41) \quad (4.13)$$

$$\bar{\Sigma}(12) = -\Lambda d3d4\bar{G}(14)w(13)\bar{\Gamma}(423). \quad (4.14)$$

Note that there is a certain degree of freedom in the distribution of the minus signs: The minus sign in front of $\bar{\Sigma}$ may be moved to the expression of the screened interaction. The next step is the derivation of Dyson like equations for $\bar{\Gamma}$ and w . The inverse of the Green's function given in Eq. (4.10) is inserted:

$$\begin{aligned}\bar{\Gamma}(123) &= -\frac{\delta\bar{G}^{-1}(12)}{\delta\Phi_0(3)} = \frac{\delta[\tau^z\partial_{\tau_1} + \bar{h}^H(12) + \tau^0\delta_{12}\varphi_0(1) + \bar{\Sigma}(12)]}{\delta\Phi_0(3)} \\ &= \frac{\delta[\tau^z\partial_{\tau_1} + \bar{h}_0(12) + \tau^0\delta_{12}\Phi_0(1) + \bar{\Sigma}(12)]}{\delta\Phi_0(3)} = \delta_{12}\delta_{23}\tau_0 + \frac{\delta\bar{\Sigma}(12)}{\delta\Phi_0(3)}.\end{aligned}$$

The chain rule and the relation $\bar{G}\frac{\delta\bar{G}^{-1}}{\delta\varphi_0}\bar{G} = -\frac{\delta\bar{G}}{\delta\varphi_0}$ are used to obtain a **Dyson equation** for the **vertex function**:

$$\begin{aligned}\bar{\Gamma}(123) &= \tau^0\delta_{12}\delta_{23} + \sum_{ij} \Lambda d4d5 \frac{\delta\bar{\Sigma}(12)}{\delta\bar{G}(45)_{ij}} \frac{\delta\bar{G}(45)_{ij}}{\delta\Phi_0(3)} \\ &= \tau^0\delta_{12}\delta_{23} - \sum_{ij} \Upsilon d4d5d6d7 \frac{\delta\bar{\Sigma}(12)}{\delta\bar{G}(45)_{ij}} \left[\bar{G}(46) \frac{\delta\bar{G}^{-1}(67)}{\delta\Phi_0(3)} \bar{G}(75) \right]_{ij} \\ &= \tau^0\delta_{12}\delta_{23} - \sum_{ij} \Upsilon d4d5d6d7 \frac{\delta\bar{\Sigma}(12)}{\delta\bar{G}(45)_{ij}} [\bar{G}(46) \Gamma(673) \bar{G}(75)]_{ij}.\end{aligned}\quad (4.15)$$

The index ij indicates a summation with respect to a Nambu matrix and should not be confused with a spin summation. Note that the quantities are now matrices so \bar{G} does in general not commute with $\bar{\Gamma}$. The **functional derivative** in the equation for $\bar{\Gamma}$ is the **only** one remaining in the set of Hedin's equations. For a given approximation of the self-energy in terms of the Green's function and Coulomb interaction the derivative can be done analytically. The object $\frac{\delta\bar{\Sigma}(12)}{\delta\bar{G}(34)}$ is also referred to as **irreducible particle-hole propagator**. Depending on the approximation for $\bar{\Sigma}$, it may be advantageous to rewrite the derivative in terms of the Hartree Green's function [77]:

$$\begin{aligned}\bar{\Gamma}(123) &= \tau^0\delta_{12}\delta_{23} + \sum_{ij} \Lambda d4d5 \frac{\delta\bar{\Sigma}(12)}{\delta\bar{G}^H(45)_{ij}} \frac{\delta\bar{G}^H(45)_{ij}}{\delta\Phi_0(3)} \\ &= \tau^0\delta_{12}\delta_{23} - \sum_{ij} \Upsilon d4d5d6d7 \frac{\delta\bar{\Sigma}(12)}{\delta\bar{G}^H(45)_{ij}} \left[\bar{G}^H(46) \frac{\delta\bar{G}^{H-1}(67)}{\delta\Phi_0(3)} \bar{G}^H(75) \right]_{ij} \\ &= \tau^0\delta_{12}\delta_{23} + \sum_{ij} \Upsilon d4d5d6d7 \frac{\delta\bar{\Sigma}(12)}{\delta\bar{G}^H(45)_{ij}} [\bar{G}^H(43) \bar{G}^H(35)]_{ij}.\end{aligned}\quad (4.16)$$

In this form a Dyson equation is avoided, but the self-energy has to be reexpanded in terms of the non-interacting Hartree Green's function to calculate the interaction. In Fig. 4.1 it is shown that this procedure mimics the Dyson equation in Eq. (4.15).

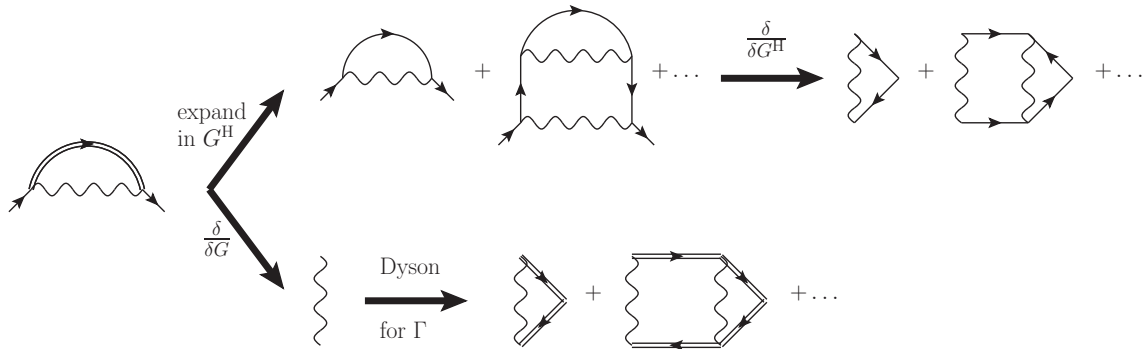


Figure 4.1.: The two possible ways to obtain the vertex function. (top line) The derivative is evaluated with respect to G^H . In this case Σ has to be expanded in terms of G^H . (bottom line) The derivative is evaluated with respect to the full GF followed by the solution of a Dyson equation.

The derivative in the vertex is the key for the creation of all possible diagrams. The [Dyson equation](#) for the [screened Coulomb interaction](#) is found by using the chain rule:

$$\begin{aligned}
 w(12) &= \Delta d3\epsilon^{-1}(13)v(32) = v(12) + \Lambda d3d4v(13) \frac{\delta\rho(3)}{\delta\varphi_0(4)}v(42) \\
 &= v(12) + \Pi d3d4d5v(13) \frac{\delta\rho(3)}{\delta\Phi_0(4)} \underbrace{\frac{\delta\Phi_0(4)}{\delta\varphi_0(5)}}_{=\epsilon^{-1}v=w} v(52) \\
 -w(12) &= -v(12) + \Pi d3d4d5v(13) P(34)w(42)
 \end{aligned} \tag{4.17}$$

$$P(34) := -\frac{\delta\rho(3)}{\delta\Phi_0(4)}. \tag{4.18}$$

The function $P(12)$ is the [polarization propagator](#), already introduced in Eq. (2.34). It can be written in terms of known objects like the vertex and Green's function:

$$P(12) = -\frac{\delta\rho(1)}{\delta\Phi_0(2)} = -\frac{\delta G(11^+)}{\delta\Phi_0(2)} = -\frac{\delta\bar{G}(11^+)_{11}}{\delta\Phi_0(2)} = \left[\Lambda d3d4\bar{G}(13) \frac{\delta\bar{G}^{-1}(34)}{\delta\Phi_0(2)} \bar{G}(31) \right]_{11}.$$

The index 11 denotes the element of the Nambu matrix. The definition of the vertex function is inserted:

$$\begin{aligned}
 P(12) &= -\left[\Lambda d3d4\bar{G}(13) \bar{\Gamma}(342) \bar{G}(41) \right]_{11} = -\sum_{ij} \Lambda d3d4\bar{G}(13)_{1i} \bar{\Gamma}(342)_{ij} \bar{G}(41)_{j1} \\
 &= -G(12)G(21) + F(12)F^\dagger(21) + \dots
 \end{aligned} \tag{4.19}$$

Here the additional contributions compared to the normal state expression [Eq. (2.35)] due to [SC](#) are clearly seen (terms like FF^\dagger , *etc.*).

4.3. Extension of the Diagrammatic Rules

The basic [diagram rules](#) have been introduced in Sec. 2.4. However, the quantities \bar{G} , $\bar{\Sigma}$ and $\bar{\Gamma}$ are now 2×2 matrices and the [irreducible particle-hole propagator](#) has even 16 elements. The elements of the Nambu Green's function and self-energy are represented by arrows with two pointers [69, 73]. In a diagram a $G(12)_{11}$ and a $G(21)_{22}$ are indistinguishable which is unproblematic [Eq. (4.4)]:

$$\bar{G}(12)_{11} = -\left\langle \hat{T} \left[\hat{\Psi}(1) \hat{\Psi}^\dagger(2) \right] \right\rangle = \left\langle \hat{T} \left[\hat{\Psi}^\dagger(2) \hat{\Psi}(1) \right] \right\rangle = \bar{G}(21)_{22}. \tag{4.20}$$

The basic rules regarding the prefactor $(-1)^n$ related to the order of a diagram and the integration with respect to internal coordinates remain unchanged in the superconducting formalism. Also the full Nambu Green's function is found by drawing all connected topological distinct diagrams with two open ends at the coordinates 1 and 2. The conventions for in and outgoing Green's function lines are shown in Fig. 4.2. Remember that at each coordinate of the Coulomb interaction $w(12)$ one line comes in and one goes out.

Only the rule for the [Fermionic loop](#) has to be used carefully in the superconducting formalism. Loops containing anomalous Green's functions do **not** lead to a factor of (-1) (Sec. D.2).

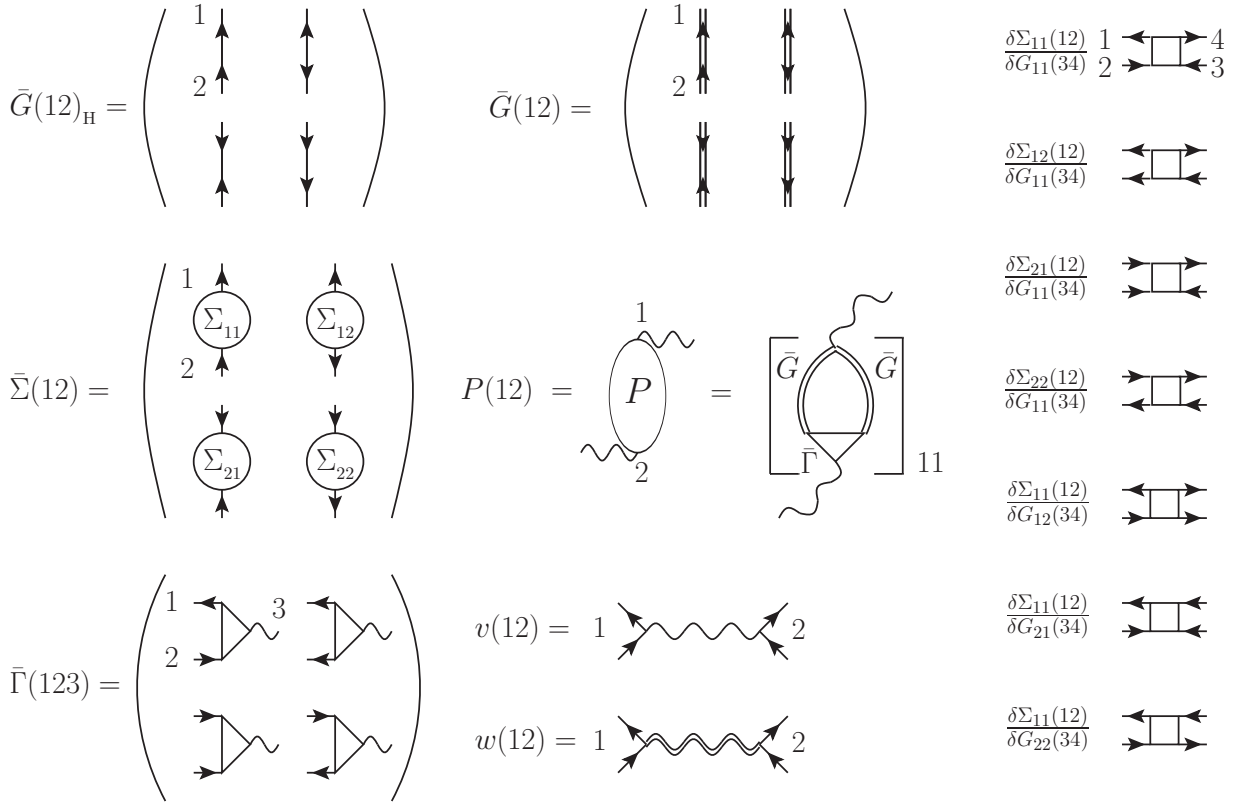


Figure 4.2.: Extension of the diagrammatic rules in the superconducting case. The Green's function, self-energy and vertex become 2×2 dimensional Nambu matrices. The derivative $\frac{\delta \bar{\Sigma}}{\delta \bar{G}}$ has sixteen different elements in total, of which only a few are shown here. The polarization propagator couples to the Coulomb interaction and stays a scalar object. However, within the polarization propagator, anomalous terms appear [Eq. (4.19)]

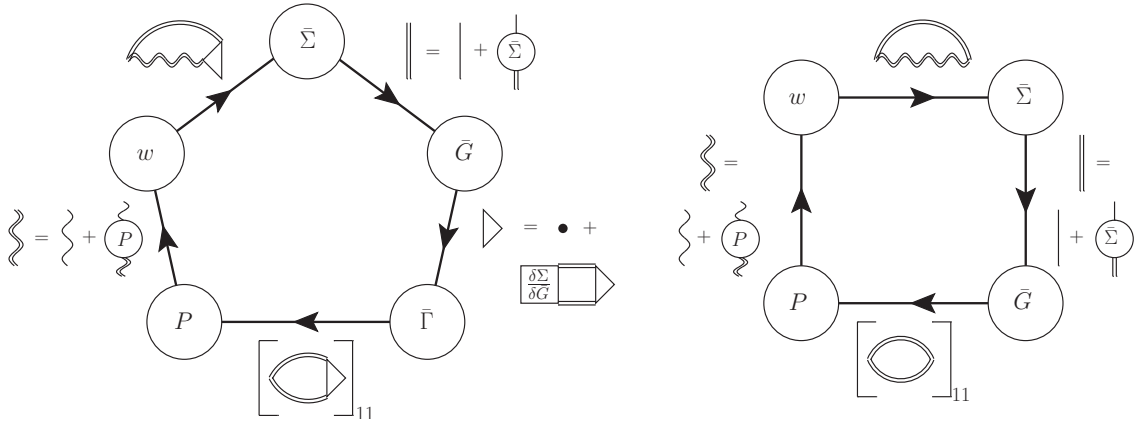


Figure 4.3.: (left) Exact self-consistent cycle for solving the five Hedine equations. (right) If the vertex corrections are neglected the pentagon becomes a square. This approximation is called the *Gw* approximation [28].

4.4. Perturbation Theory \leftrightarrow DFT – The Sham-Schlüter Equation

After this preparation, the SSEq is introduced [26]. The fact that the KS Green's function reproduces the density of the exact system is also used in linear response DFT [Eq. (B.3.2)]. Now it is applied to obtain a connection between MBPT and DFT. The normal and anomalous densities defined in Eqs.

(3.13) and (3.14) are expressed using the Nambu GF [Eq. (4.4)]:

$$\begin{aligned}\rho(\mathbf{r}) &= \sum_{\alpha} \lim_{\tau' \searrow \tau} G_{\alpha\alpha}(\mathbf{r}\tau\mathbf{r}\tau') = \frac{1}{\beta} \sum_{\alpha} \lim_{\tau' \searrow \tau} \lim_{N \rightarrow \infty} \sum_{n=-N}^N e^{-i\omega_n(\tau-\tau')} G_{\alpha\alpha}(\mathbf{r}\mathbf{r}\omega_n) \\ &= \frac{1}{\beta} \sum_{\alpha} \sum_n e^{i\omega_n 0^+} G_{\alpha\alpha}(\mathbf{r}\mathbf{r}\omega_n) \\ \chi(\mathbf{r}\mathbf{r}') &= \lim_{\tau \searrow \tau'} F_{\uparrow\downarrow}(\mathbf{r}\tau\mathbf{r}'\tau') = \frac{1}{\beta} \lim_{\tau \searrow \tau'} \lim_{N \rightarrow \infty} \sum_{n=-N}^N e^{-i\omega_n(\tau-\tau')} F_{\uparrow\downarrow}(\mathbf{r}\mathbf{r}'\omega_n) \\ &= \frac{1}{\beta} \sum_n e^{i\omega_n 0^+} F_{\uparrow\downarrow}(\mathbf{r}\mathbf{r}'\omega_n).\end{aligned}$$

The Dyson equation for the full GF using the KS system as a reference system reads [the $\bar{v}_{\sigma\sigma'}^{\text{xc}}$ is given in Eq. (D.9)]:

$$\bar{G}(12) = \bar{G}^{\text{KS}}(12) + \Lambda 34' \bar{G}^{\text{KS}}(13) [\bar{\Sigma}(34) - \bar{v}^{\text{xc}}(34)] \bar{G}(42). \quad (4.21)$$

By taking the limits as discussed above, \bar{G}_{11} becomes the electronic density and \bar{G}_{12} the anomalous density. The density of the interacting system is reproduced by the KS system and the two terms cancel out. This leads to the SSEq corresponding to the normal [Eq. (4.22)] and the anomalous density [Eqs (4.23)]:

$$0 = \frac{1}{\beta} \sum_{\sigma_1} \left[\sum_n \sum_{\sigma\sigma'} e^{i\omega_n 0^+} \Lambda d^3 r d^3 r' \bar{G}_{\sigma_1\sigma}^{\text{KS}}(\mathbf{r}_1\mathbf{r}\omega_n) \bar{\Sigma}_{\sigma\sigma'}^*(\mathbf{r}\mathbf{r}'\omega_n) \bar{G}_{\sigma'\sigma_1}(\mathbf{r}'\mathbf{r}_1\omega_n) \right]_{11} \quad (4.22)$$

$$0 = \frac{1}{\beta} \left[\sum_n \sum_{\sigma\sigma'} e^{i\omega_n 0^+} \Lambda d^3 r d^3 r' \bar{G}_{\uparrow\sigma}^{\text{KS}}(\mathbf{r}_1\mathbf{r}\omega_n) \bar{\Sigma}_{\sigma\sigma'}^*(\mathbf{r}\mathbf{r}'\omega_n) \bar{G}_{\sigma'\downarrow}(\mathbf{r}'\mathbf{r}_2\omega_n) \right]_{12} \quad (4.23)$$

$$\bar{\Sigma}_{\sigma_1\sigma_2}^*(\mathbf{r}_1\mathbf{r}_2\omega_n) := \bar{\Sigma}_{\sigma_1\sigma_2}(\mathbf{r}_1\mathbf{r}_2\omega_n) - \bar{v}_{\sigma_1\sigma_2}^{\text{xc}}(\mathbf{r}_1\mathbf{r}_2).$$

The SSEq has to be understood in the following way: Every given approximation for the self-energy $\bar{\Sigma}^{\text{app}}$ is associated with a Green's function \bar{G}^{app} via the solution of the Dyson equation:

$$\bar{G}^{\text{app}} = \bar{G}^{\text{app}} [\bar{\Sigma}^{\text{app}}] = \frac{\bar{G}_0}{1 - \bar{G}_0 \bar{\Sigma}^{\text{app}}}.$$

This approximated Green's function implies a density and therefore also the density can be viewed as a functional of the approximation to the self energy:

$$\begin{aligned}\rho(\mathbf{r}_1) &= \bar{G}_{11}^{\text{app}}(11^+) \Rightarrow \rho = \rho[\bar{\Sigma}^{\text{app}}] \\ \chi(\mathbf{r}_1\mathbf{r}_2) &= \bar{G}_{12}^{\text{app}}(\mathbf{r}_1 \uparrow \tau_1^+, \mathbf{r}_2 \downarrow \tau_1^+) \Rightarrow \chi = \chi[\bar{\Sigma}^{\text{app}}].\end{aligned}$$

By solving the SSEq [Eqs. (4.23) and (4.22)] the XC-potential, corresponding to this density $\rho[\bar{\Sigma}^{\text{app}}]$ and $\chi[\bar{\Sigma}^{\text{app}}]$ is found. If the approximation of the self-energy leads to a physical density¹⁰, the 1:1 mapping between potentials and densities ensures a unique solution of the SSEq [70, 78]. The benefit of the SSEq is based on the following assumption: If some processes are included in the self-energy, they also enter the XC-potential by solving the SSEq. For corrections to the densities induced by $\bar{\Sigma}^{\text{app}}$ this is clear.

4.5. Summary

In this chapter the Hedin equations for a superconducting system have been presented. The contribution related to the dynamics of the nuclei have been neglected. The derivation is based on the

¹⁰The density should be real, positive and integrate to a finite number.

equation of motion for the 2×2 Nambu Green's function [Eq. (4.5)] and on Schwinger's functional derivative approach (Sec. D.1.4). The diagrammatic rules presented in chapter 2 have been extended to the superconducting case (Fig. 4.2) and the **SSEq** has been introduced. The **SSEq** connects the **MBPT** with the **DFT** world: Given an approximation to the self-energy (Σ^{app}) the **SSEq** leads the related **XC**-potential. In the next section (chapter 5) the diagrams describing the magnetic fluctuations are located in the exact expression for the self-energy and an approximation Σ^{app} including them is suggested.

5. Finding the Spin-Fluctuations

In the last chapter the Hedin equations for a superconducting system have been derived. The [Hedin equations](#) are an exact scheme: Starting with any approximation for $\bar{\Sigma}$ from cycle to cycle all possible diagrams are appearing and if magnetic fluctuations are present in a material the corresponding diagrammatic contributions should become large and dominate the self-energy.

However, a full self-consistent treatment is at the moment only realizable for simplified model systems and not for a realistic materials [79]. With this in mind, the aim of this chapter can be formulated in the following way:

1. Identify the set of diagrams representing the magnetic excitations and find Dyson equations to compute them.
2. Construct an approximation for the self-energy including these contributions.
3. Simplify the self-energy to extract an effective interaction to be used in the [SCDFT](#) framework along with the Coulomb and phonon contributions.

The exact equation of the self-energy is given in Eq. (4.14). Already in the original work of Hedin [25] it is suggested to neglect the vertex contribution as an initial approximation for the self-energy:

$$\Sigma^{Gw}(12) \approx -G(12)w(12) \text{ with } -w = -v + v\chi_{00}v, \quad (5.1)$$

where χ_{00} is the charge-charge response function introduced in Sec. 2.2. Today this approximation is known as the Gw approximation [28]. In this simple approximation only the charge component of the susceptibility (Sec. 2.2) enters explicitly, not its magnetic counterpart χ_{zz} . Therefore this approximation is not likely to describe spin fluctuations. Since the Hedin equations are an exact self-consistent scheme, the diagrams related to the magnetic response will appear in higher orders in the self-consistent iteration. If in the functional derivative $\frac{\delta \Sigma^{Gw}}{\delta G}$ appearing in the vertex equation [Eq. (4.15)] only the explicit G in Σ^{Gw} is considered, the Dyson equation for the vertex leads to the set of ladder diagrams shown in Fig. 5.1.

The ladder diagrams are the simplest vertex correction and are used in calculations of the magnetic response function since the sixties [20, 80]. Many researchers refer to the set of ladder diagrams as the T -matrix. The diagrams corresponding to the T -matrix are shown in the second line of Fig. 5.1.

In early calculations, the screened Coulomb interaction in the ladder diagrams was approximated by a local model parameter [20, 81]. Recently, the T -matrix has been calculated for ferro magnets like iron, cobalt or nickel, from first principles without using model parameters[82, 83]. The expression for the magnetic response function in terms of the T -matrix reads:

$$\chi_{ij}(12) \approx - \sum_{\alpha\beta\gamma\delta} \sigma_{\beta\alpha}^i G_{\alpha\gamma}^{\text{KS}}(\mathbf{x}_1\mathbf{x}_2) G_{\delta\beta}^{\text{KS}}(\mathbf{x}_2\mathbf{x}_1) \sigma_{\gamma\delta}^j \quad (5.2)$$

$$T(1234) = -\delta_{13}\delta_{24}w(12) - \Lambda d5d6w(12) G^{\text{KS}}(15) G^{\text{KS}}(62) T(5634). \quad (5.3)$$

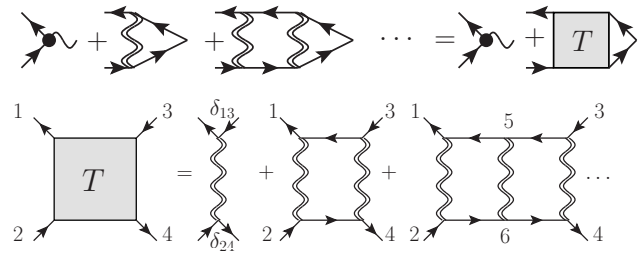


Figure 5.1.: Vertex in the ladder approximation with G approximated by a non-interacting GF.

The agreement between the calculated response using the T -matrix approximation and experiment is reasonable [82]. This observation indicates that magnetic fluctuations are represented by multiple scattering between particle and hole pairs and contributions like this should appear explicitly in the self-energy. The origin of these diagrams is the vertex function and to go beyond the well established Gw approximation is essential to include the magnetic fluctuations in a proper way.

The chapter has the following outline: In the first section 5.1, the Hedin equations are simplified and the expression of the self-energy is adjusted according to point 1. and 2. In Sec. 5.3 the complexity of the self-energy containing the magnetic fluctuations is reduced. The resulting expression contains an **effective interaction** related to magnetic fluctuations and is reminiscent of the $\bar{G}w$ expression. The derivation of this effective interaction and proper incorporation in a self-energy is an important result of this work. The derived self-energy will be used in the next section to construct a functional for **SCDFT**, but it could also be used within **Eliashberg theory** [6]. The applied approximations and different effective interactions in the literature are discussed in Secs. 5.4.1 and 5.4.2, respectively.

5.1. Simplification of the Hedin Equations

5.1.1. Simplify the Vertex


The starting point is an investigation of the vertex function. The vertex is created by the functional derivative of the self-energy [Eq. (4.13)]. In general the self-energy is a Nambu matrix and a functional of the full Nambu Green's function $\bar{\Sigma}^v = \bar{\Sigma}^v[\bar{G}]$ (the label $\bar{\Sigma}^v$ is given to the self-energy used in the construction of the vertex function). A self-energy of this form takes all effects related to **SC** into account. The calculation of the vertex corrections is a computationally demanding task. In particular, this calculation cannot be done in every iteration of the **KS-BdG** equations [Eq. (3.12)] and the vertex function is approximated by an expression in the non-superconducting state:

$$\bar{\Sigma}^v(12) \approx \begin{pmatrix} \bar{\Sigma}_{11}^v(12)[G] & 0 \\ 0 & \bar{\Sigma}_{22}^v(12)[G^\dagger] \end{pmatrix}. \quad (5.4)$$

This approximation neglects the effects of **SC** on the magnetic excitations and is in complete analogy to the phonons, where the excitation are also calculated only once in the non-superconducting phase and are kept fixed for the rest of the **SCDFT** calculation [84, 85, 86]. The approximation is discussed in Sec. 5.4.1 and is shown diagrammatically in Fig. 5.13. Due to the symmetry between G and G^\dagger [Eq. (4.20)], every functional is expressible in either the 11 or 22 component of the Green's function. The vertex related to $\bar{\Sigma}^v$ is diagonal in Nambu space

$$\bar{\Gamma}(125) \approx \delta_{12}\delta_{25}\tau_0 + \begin{pmatrix} \bar{\Gamma}(125)_{11} & 0 \\ 0 & \bar{\Gamma}(125)_{22} \end{pmatrix} = \delta_{12}\delta_{25}\tau_0$$

and the Dyson equations for the two components of the vertex are decoupled:

$$\bar{\Gamma}_{ii} = 1 + \bar{\Lambda}_{ii}^0 \bar{G}_{ii} \bar{G}_{ii} \bar{\Gamma}_{ii} \quad \text{with} \quad \frac{\delta \bar{\Sigma}_{ii}^v(12)}{\delta \bar{G}_{ii}(34)} = \bar{\Lambda}_{ii}^0(1234). \quad (5.5)$$


The vertex is created by multiple scattering between particle and hole pairs and hence the object $\bar{\Lambda}_{ii}^0$ is called **irreducible particle-hole propagator**.

Figure 5.2.: Dyson equation for the vertex

The symmetry between \bar{G}_{11} and \bar{G}_{22} [Eq. (4.20)] also connects the two contributions of the self-energy:

$$\bar{\Sigma}_{11}^v(12) = \bar{\Sigma}_{22}^v(21).$$

With the two symmetries for $\bar{\Sigma}$ and \bar{G} , the two components of the irreducible particle-hole propagator are related:

$$\frac{\delta \bar{\Sigma}_{11}^v(12)}{\delta \bar{G}_{11}(34)} = \frac{\delta \bar{\Sigma}_{22}^v(21)}{\delta \bar{G}_{22}(43)} \implies \bar{\Lambda}_{11}^0(1234) = \bar{\Lambda}_{22}^0(2143),$$

which transfers via the Dyson Eq. (5.5) also to the vertex function:

$$\xrightarrow{\text{Dyson Eq.}} \bar{\Gamma}_{11}(123) = \bar{\Gamma}_{22}(213). \quad (5.6)$$

Hence, it is sufficient to calculate only the 11 component and from now on only the 11 component is considered and $\bar{\Sigma}_{11}^V$, $\bar{\Gamma}_{11}$ and $\bar{\Lambda}_{11}^0$ are called Σ^V , Γ and Λ_0 , respectively.

5.1.2. Locate the Magnetic Fluctuations

At this point it is necessary to investigate Λ_0 in more detail. A restriction to systems with collinear magnetism is made, leading to Green's functions which are diagonal in spin space. The four-point function Λ_0 contains two disjoint sets of diagrams [87]:

- The **crossed contributions** Λ_0^c which have a path connecting the coordinates $1 \leftrightarrow 3$ and $2 \leftrightarrow 4$. The spin contributions in this set are

$$\Lambda_0^c(1234) \equiv \delta_{\sigma_1\sigma_3} \delta_{\sigma_2\sigma_4} \Lambda_0^c(1234). \quad (5.7)$$

Note, that the contributions to the T -matrix are of the crossed type.

- The **direct contributions** Λ_0^d which have a path connecting the coordinates $1 \leftrightarrow 2$ and $3 \leftrightarrow 4$. The spin contributions in this set are

$$\Lambda_0^d(1234) \equiv \delta_{\sigma_1\sigma_2} \delta_{\sigma_3\sigma_4} \Lambda_0^d(1234). \quad (5.8)$$

The kernels Λ_0^c and Λ_0^d are created by the **functional derivative** of the self-energy $\bar{\Sigma}^V$ with respect to G . By the functional derivative $\frac{\delta}{\delta G(34)}$ one GF within the self-energy is removed and the open connections get the indices 3 and 4 resulting in the four-point function $\Lambda_0(1234)$. If the removed function was part of a loop, the resulting contribution is direct and crossed otherwise (Fig. 5.3). Since a loop was destroyed in the derivative, an extra minus sign is necessary to compensate for this:

$$\Lambda_0^c(1234) = \frac{\delta \bar{\Sigma}^V(12)}{\delta G(34)} \text{ with } G \text{ not in loop} \quad (5.9)$$

$$\Lambda_0^d(1234) = -\frac{\delta \bar{\Sigma}^V(12)}{\delta G(34)} \text{ with } G \text{ in loop} \quad (5.10)$$

The total irreducible particle-hole propagator is given by the difference between the crossed and direct contribution:

$$\Lambda_0(1234) = \frac{\delta \bar{\Sigma}^V(12)}{\delta G(34)} = \Lambda_0^c - \Lambda_0^d =: \Lambda_0^{c-d}.$$

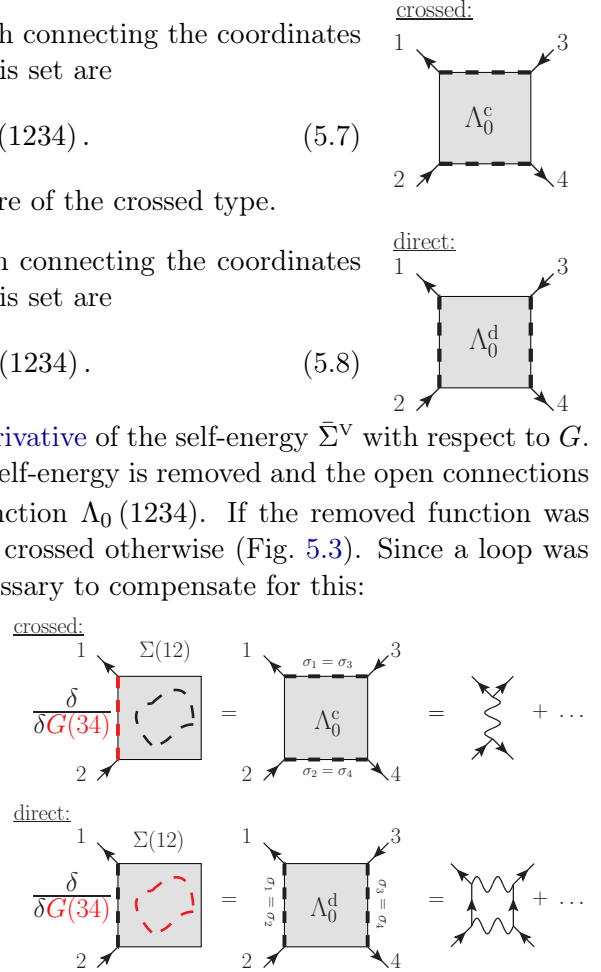


Figure 5.3.: Creation of the direct and crossed contribution by the functional derivative.

The Λ_0^c and Λ_0^d contain all four-point functions which are proper and irreducible with respect to the particle-hole propagator. For the creation of the vertex function, larger sets are needed, namely all proper four-point functions. Also within this large set all contributions are either crossed or direct.

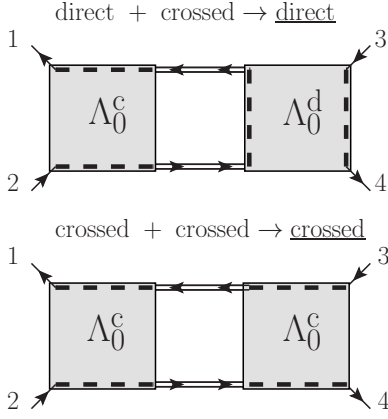


Figure 5.4.: Each contribution to the particle-hole propagator is either direct or crossed.

This is seen by starting with an irreducible contribution and creating the reducible contributions by a product consisting of: Λ_0^c , Λ_0^d and pairs of GFs GG connecting two irreducible parts. This procedure has been used already for the creation of the T -matrix in Eq. (5.3) using the most simple irreducible part: $\Lambda_0 = \Lambda_0^c = -\omega$. In the example shown in Fig. 5.4 it is started with a crossed contribution represented by the gray box. If a direct contribution is multiplied to the crossed one, the whole product becomes direct and it stays crossed otherwise. For each further step, the same argument is true always leading either to a crossed or to a direct contribution. If it is started with a direct contribution the product will always stay direct. The sets containing all crossed and direct terms are called Λ^c and Λ^d , respectively.

Having the previous arguments in mind, Dyson equations for the direct and crossed part are derived. The situation for the crossed contribution is simple because each single factor has to be crossed leading to the following Dyson equation:

$$\Lambda^c = \Lambda_0^c + \Lambda_0^c G G \Lambda^c$$

Labeling the n -th order with respect to GG inside Λ^c by $\Lambda_{(n)}^c$, the Dyson equation may be written as:

$$\Lambda_{(n+1)}^c = \Lambda_0^c G G \Lambda_{(n)}^c \quad \text{and} \quad \Lambda^c = \sum_{n=0}^{\infty} \Lambda_{(n)}^c, \quad (5.11)$$

where the zero order $\Lambda_{(0)}^c$ is given by the irreducible part Λ_0^c . This rewriting is necessary for the Dyson equation of the direct contribution, where a $\Lambda_{(n)}^c$ will appear. This equation has to create all possible products containing at least one direct term, but without creating multiple times the same contribution (double counting). This is done by the following equation:

$$\Lambda^d = \sum_{n=0}^{\infty} \Lambda_{(n)}^d \quad \text{and} \quad \Lambda_{(n+1)}^d = \Lambda_0^d G G \Lambda_{(n)}^c + \Lambda_0^c G G \Lambda_{(n)}^d - \Lambda_0^d G G \Lambda_{(n)}^d. \quad (5.12)$$

The last term $\Lambda_0^d G G \Lambda_{(n)}^d$ alone would create a product of pure direct terms only. The minus sign in front is due to a loop created by the connection of two direct terms. The first two other terms create mixed products starting with a direct or crossed term, respectively. The series Λ^d reads (the GG between two irreducible contribution has been left for simplicity):

$$\begin{aligned} \Lambda_{(1)}^d &= \Lambda_0^d \\ \Lambda_{(2)}^d &= \Lambda_0^d \Lambda_0^c + \Lambda_0^c \Lambda_0^d - \Lambda_0^d \Lambda_0^d \\ \Lambda_{(3)}^d &= \Lambda_0^d \Lambda_{(2)}^c + \Lambda_0^c \Lambda_{(2)}^d - \Lambda_0^d \Lambda_{(2)}^d \\ &= \Lambda_0^d \Lambda^c \Lambda^c + \Lambda_0^c \Lambda_0^d \Lambda_0^c + \Lambda_0^c \Lambda_0^c \Lambda_0^d - \Lambda_0^c \Lambda_0^d \Lambda_0^d - \Lambda_0^d \Lambda_0^d \Lambda_0^c - \Lambda_0^d \Lambda_0^c \Lambda_0^d + \Lambda_0^d \Lambda_0^d \Lambda_0^d \\ &\vdots \end{aligned}$$

In Fig. 5.5 some crossed and direct contributions are shown. The two sets together contain all four-point functions which are proper and irreducible with respect to a single GF.

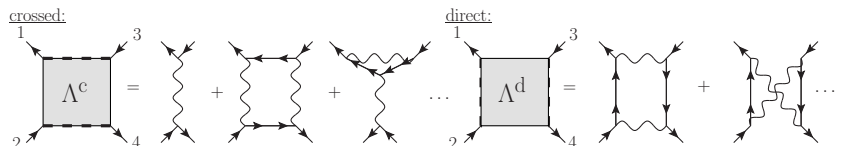


Figure 5.5.: Direct and crossed particle-hole propagators.

With these two sets it is possible to create the vertex function without using the Dyson Eq. (5.5).

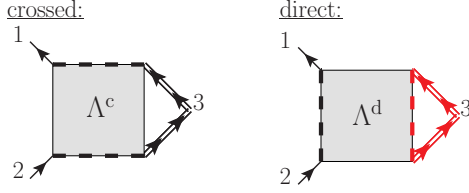


Figure 5.6.: Crossed and direct contribution in the vertex

In the equation for the vertex function the direct and crossed contribution enter with a different sign: For the direct term a loop is created which is not present for the crossed contribution (Fig. 5.6). This leads to the following expression for the vertex in terms of Λ^c and Λ^d :

$$\Gamma(123) = \delta_{12}\delta_{23} + \Lambda d4d5 [\Lambda^c(1245) - \Lambda^d(1245)] G(43) G(35). \quad (5.13)$$

It is possible to derive a Dyson equation for $\Lambda^{c-d} := \Lambda^c - \Lambda^d$, by subtracting the Dyson equation of the direct part [Eq. (5.12)] from the crossed one [Eq. (5.11)] :

$$\begin{aligned} \Lambda_{(n+1)}^{c-d} &= \Lambda_0^c G G \Lambda_{(n)}^c - \left(\Lambda_0^d G G \Lambda_{(n)}^c + \Lambda_0^c G G \Lambda_{(n)}^d - \Lambda_0^d G G \Lambda_{(n)}^d \right) \\ &= \Lambda_0^{c-d} G G \Lambda_{(n)}^c - \Lambda_0^{c-d} G G \Lambda_{(n)}^d = \Lambda_0^{c-d} G G \Lambda_{(n)}^{c-d} \\ \Rightarrow \Lambda^{c-d} &= \Lambda_0^{c-d} + \Lambda_0^{c-d} G G \Lambda^{c-d} \end{aligned} \quad (5.14)$$

The set Λ^{c-d} contains direct and crossed contributions. It is given by a Dyson Eq. (5.14) and leads to the vertex functions Eq. (5.13). From now on this important set is called the **particle-hole propagator** and labeled with:

$$\Lambda^P(1234) := \Lambda^{c-d}(1234) \quad (5.15)$$

$$\Lambda^P = \Lambda_0 + \Lambda_0 G G \Lambda^P \quad \text{with } \Lambda_0 = \frac{\delta \Sigma^v}{\delta G} \quad (5.16)$$

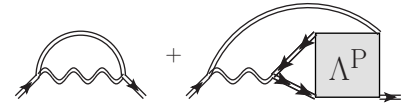
Figure 5.7.: Dyson equation for Λ^P

The set Λ^P contains a huge number of diagrams. The T -matrix is only a small subset of crossed contributions contained in Λ^P . If in Eq. (5.2) the full Λ^P is used instead of the T -matrix, the exact polarization is found. This means the particle-hole propagator contains the complete information about the magnetic fluctuations in the system.

5.1.3. Rewrite the Self-Energy

The particle-hole propagator Λ^P enters the Hedin equations in two places shown in Fig. 5.13a:

1. In the **vertex function** $\bar{\Gamma}$ within the self-energy.



2. In the **polarization propagator** P within the screened Coulomb interaction.



Remember, that the effects of superconductivity in the vertex have been neglected (Sec. 5.1.1) and only the 11 element of the Green's function appears in the vertex function. In order to reduce the complexity of the figures only the 11 element of the self-energy is shown in most figures in the following discussion. First, the contributions related to P are discussed. These contributions are coupled to the equations via the Coulomb interaction which does not depend on spin. The summation of the spin degrees of freedom leads to the charge-charge part of the proper polarization propagator [Eq. (4.17)]:

$$-w(\mathbf{x}_1\mathbf{x}_2) = -v(\mathbf{x}_1\mathbf{x}_2) + \Lambda d\mathbf{x}_3 d\mathbf{x}_4 v(\mathbf{x}_1\mathbf{x}_3) P_{00}(\mathbf{x}_3\mathbf{x}_4) w(\mathbf{x}_4\mathbf{x}_2).$$

The calculation of P_{00} is easier in the **linear response density functional theory (LRDFT)** formalism compared to **MBPT** because the Dyson equation for the full response function (Sec. B.3.2):

$$\chi_{ij}(\mathbf{x}_1\mathbf{x}_2) = \chi_{ij}^{\text{KS}}(\mathbf{x}_1\mathbf{x}_2) - \sum_{lk} \Lambda d\mathbf{x} d\mathbf{x}' \chi_{il}^{\text{KS}}(\mathbf{x}_1\mathbf{x}) [\delta_{k0}\delta_{0l}v(\mathbf{x}\mathbf{x}') + f_{lk}^{\text{xc}}(\mathbf{x}\mathbf{x}')] \chi_{kj}(\mathbf{x}'\mathbf{x}_2). \quad (5.17)$$

contains only two-point objects: Namely the **KS** response χ_{ij}^{KS} (12), the **XC**-kernel f_{ij}^{xc} (12)

$$\chi_{ij}^{\text{KS}}(\mathbf{x}_1\mathbf{x}_2) := - \sum_{\alpha\beta\sigma\sigma'} \sigma_{\beta\alpha}^i G_{\alpha\sigma}^{\text{KS}}(\mathbf{x}_1\mathbf{x}_2) G_{\sigma'\beta}^{\text{KS}}(\mathbf{x}_2\mathbf{x}_1^+) \sigma_{\sigma\sigma'}^j, \quad (5.18)$$

$$f_{lk}^{\text{xc}}(\mathbf{x}_1\mathbf{x}_2) := \frac{\delta v_l^{\text{xc}}[\rho](\mathbf{x}_1)}{\delta \rho_k(\mathbf{x}_2)} \quad (5.19)$$

and the bare Coulomb interaction v (12) $\delta_{i0}\delta_{j0}$. The indices i and j run over x, y, z and 0 , corresponding to the three directions of a magnetic field in real space and the electric field coupling to the charge. The equation for the proper part of the charge-charge polarization reads:

$$P_{00} = \chi_{00}^{\text{KS}} - \sum_{ij} \chi_{0i}^{\text{KS}} f_{ij}^{\text{xc}} \chi_{0i}^{\text{KS}} + \sum_{ijmn} \chi_{0i}^{\text{KS}} f_{ij}^{\text{xc}} \chi_{jm}^{\text{KS}} f_{mn}^{\text{xc}} \chi_{n0}^{\text{KS}} - \dots$$

The off diagonal elements of the **XC**-kernel *i.e.* f_{0x}^{xc} , f_{0y}^{xc} and f_{0z}^{xc} introduce the magnetic contributions to the charge-charge part. If the size of f_{0x}^{xc} , f_{0y}^{xc} and f_{0z}^{xc} is comparable to the size of the magnetic terms f_{xx}^{xc} , f_{xy}^{xc} , f_{zz}^{xc} ... the contribution of the magnetic response *i.e.* vertex corrections within the screened Coulomb interaction become an important contribution and should be considered. However, from experiments it is known, that usually the magnetic phase is suppressed before superconductivity appears *i.e.*, magnetism and superconductivity normally do not coexist (chapter 1). For a non-magnetic system the \uparrow and \downarrow components are degenerate and all off diagonal terms in the kernel or response vanish [Sec. A.3] (A_{ij} represents χ_{ij} , χ_{ij}^{KS} or f_{ij}^{xc}):

$$\begin{aligned} A_{0z} &= A_{\uparrow\uparrow\uparrow\uparrow} + A_{\downarrow\downarrow\uparrow\uparrow} - A_{\uparrow\uparrow\downarrow\downarrow} - A_{\downarrow\downarrow\downarrow\downarrow} = 0 \\ A_{xy} &= -i(A_{\uparrow\downarrow\uparrow\downarrow} + A_{\downarrow\uparrow\uparrow\downarrow} - A_{\downarrow\uparrow\downarrow\uparrow} - A_{\uparrow\downarrow\downarrow\uparrow}) = 0. \\ &\vdots \qquad \qquad \qquad \vdots \end{aligned} \quad (5.20)$$

Hence, the screened Coulomb interaction contains **only** multiples of χ_{00}^{KS} , v and f_{00}^{xc} :

$$\begin{aligned} -w &= -v + v\chi_{00} \\ \chi_{00}^{\text{NM}} &\stackrel{\text{NM}}{=} \chi_{00}^{\text{KS}} - \chi_{00}^{\text{KS}}(v + f_{00}^{\text{xc}})\chi_{00}^{\text{KS}} + \chi_{00}^{\text{KS}}(v + f_{00})\chi_{00}^{\text{KS}}(v + f_{00}^{\text{xc}})\chi_{n0}^{\text{KS}} - \dots \end{aligned} \quad (5.21)$$

This means for a non-magnetic ground state, the screened Coulomb interaction includes no magnetic fluctuations in the self-energy.

From these arguments it is concluded that vertex corrections included in the screened Coulomb interaction are **not sufficient** to include the magnetic fluctuations in the self-energy.

The explicit vertex correction in the self-energy are the second place where the particle-hole propagator enters the Hedin equations. Now these contributions are discussed. The exact expression for the self-energy in terms of the vertex is given in Eq. (4.14). To go beyond the Gw approximation it would be natural to iterate these equation as shown in Fig. 4.3. If this is done, all possible self-energy contribution are created and the magnetic excitation are included in the self-energy.

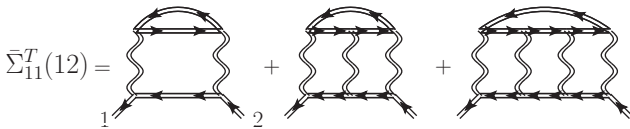


Figure 5.8.: T -matrix self-energy contribution.

However, a self-consistent iteration of the exact equations is very demanding and is also not systematic in the sense that it is not obvious in which iteration the relevant diagrammatic contribution are included and how fast the results will improve compared to Gw . Hence, the field of exact expressions is left and the self-energy is approximated by a manageable expression including **some** vertex corrections. In the introduction of this section, it has been pointed out that the particle-hole contributions are the relevant set of diagrams containing the magnetic contribution. The simplest self-energy contributions related to the crossed particle-hole channel are shown in Fig. 5.8. In order to include these and also direct contributions with respect to the particle-hole channel, the following form of the self-energy is proposed:



$$\bar{\Sigma} \approx -\bar{G}w + \bar{G}\Lambda^P \quad (5.22)$$

$$\bar{\Sigma}^{\text{CF}} := -\bar{G}w \quad \bar{\Sigma}^{\text{SF}} := \bar{G}\Lambda^P. \quad (5.23)$$

Figure 5.9.: Approximation for the self-energy including magnetic fluctuations.

This is an *ad-hoc* approximation selecting only a subset of all possible self-energy contributions. Admittedly, this approximation comes out of the sky, but this is a way many-body perturbation theory has been applied successfully in the past: The relevant physical processes (in this case magnetic fluctuations) are included by selecting a class of diagrams capturing these processes [59]. In Sec. 5.4.1 the double counting errors and the groups of neglected diagrams are discussed.

In the context of Hubbard models various approximations for Σ containing terms like Gw , $Gw\Gamma$ or GT have been used in the past [88, 89, 90]. In the Hubbard model the GT approximation describes the low density limit of particles or holes *i.e.* close to completely filled or empty bands, whereas the Gw approximation works well at half filling. More recently, the approximation $Gw + GT$ has been applied to Pd, Ta and Al [91].

At this point the expression for the self-energy in Eq. (5.22) is worked out in more detail. For the anomalous terms in Eq. (5.23) the loop rule (Sec. D.2) does not apply and the crossed and direct contribution in the self-energy enter with the same sign:

$$\bar{\Sigma}_F^{\text{SF}} := \Lambda d3d4\tau^z \begin{pmatrix} 0 & F(34)\Lambda^{c+d}(1342) \\ F^\dagger(34)\Lambda^{c+d}(3124) & 0 \end{pmatrix}. \quad (5.24)$$

For the normal contribution the situation is a bit more complicated because the loop rule has to be considered. If a crossed contribution is inserted, a loop is created (Fig. 5.10) leading to a minus sign. For the direct terms on the other hand no additional loops appear. Taking the signs related to the loops into account, the equation for the normal contributions in $\bar{\Sigma}^{\text{SF}}$ reads:

$$\bar{\Sigma}_G^{\text{SF}} := \Lambda d3d4\tau^z \begin{pmatrix} G(34)\Lambda^{d-c}(1324) & 0 \\ 0 & G^\dagger(34)\Lambda^{d-c}(3142) \end{pmatrix}. \quad (5.25)$$

Figure 5.10.: Direct and crossed contribution in the normal part of the self-energy.

Collecting the two parts related to the normal and anomalous Green's function in $\bar{\Sigma}^{\text{SF}}$ and adding the $\bar{\Sigma}^{\text{CF}}$, leads to the detailed form of the self-energy containing charge and magnetic fluctuations:

$$\bar{\Sigma}(12) = -w(12)\bar{G}(12) + \Lambda d3d4\tau^z \begin{pmatrix} -G(34)\Lambda^{c-d}(1324) & F(34)\Lambda^{c+d}(1342) \\ F^\dagger(34)\Lambda^{c+d}(3124) & -G^\dagger(34)\Lambda^{c-d}(3142) \end{pmatrix}. \quad (5.26)$$

In the discussion of the gap equation in Sec. 6.2, the different signs of $\Lambda^{c\pm d}$ on the diagonal and off diagonal part turn out to be **crucial** in order to find a finite solution of the gap equation. Note that the self-energy derived from the Berk-Schrieffer interaction has the same sign convention, like the $\Lambda^{c\pm d}$ presented here [19]. In case the vertex corrections are set to zero *i.e.* $\Lambda^{c\pm d} = 0$, the self-energy given in Eq. (5.26) reduces to the Gw approximation, with a **random phase approximation (RPA)** for the screening of the Coulomb interaction ($\chi_{00}^{\text{RPA}} = \chi_0 + \chi_0 v \chi_{00}^{\text{RPA}}$).

This chapter concludes with an investigation, how the contribution contained in Σ^{SF} are created within the exact Hedin equations.¹¹ Assume that $\bar{\Sigma}_{11}^{\text{V}}$ in Eq. (5.4) is approximated by Gv . In this case

¹¹For simplicity of the figures the non-superconducting diagrams are used here.

the proper particle-hole propagator reduces to an unscreened ($w = v$) T -matrix [Eq. (5.3)]:

$$\Lambda^c = T^{\text{bare}} \quad \Lambda^d = 0. \quad (5.27)$$

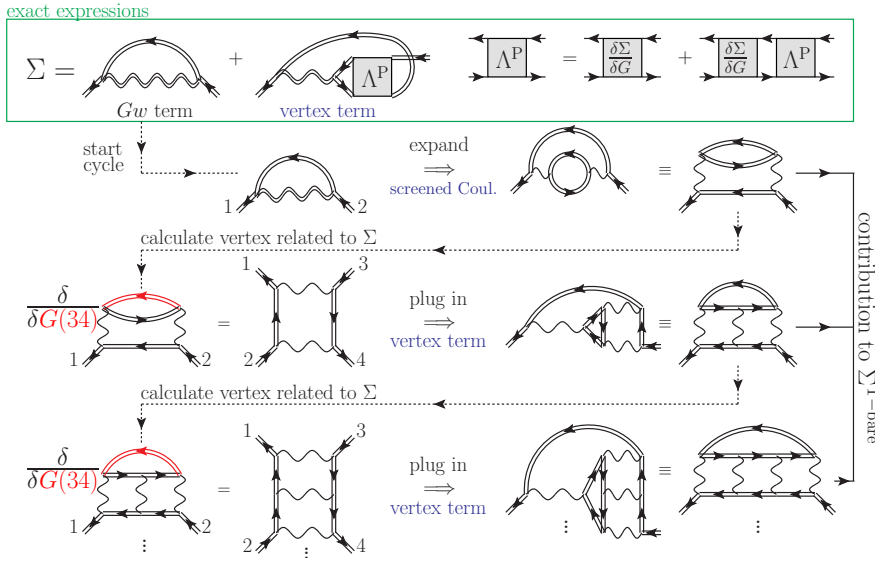


Figure 5.11.: Creation of the self-energy contribution related to the T -matrix in the iteration of the Hedin cycle. For simplicity only the normal state Green's function is considered in this and the next picture.

5.11 the removed Green's function is colored in red. The resulting four-point function is inserted in the vertex entering the self-energy. This process is repeated for the two next contributions of $\bar{\Sigma}^{T\text{-bare}}$ and all higher orders are created in an analogous way.

If the Hedin equations are iterated all orders related to $\bar{\Sigma}^{T\text{-bare}}$ will appear. However, already in the original work of Hedin [25], it is pointed out that the slow summation of a set like $\bar{\Sigma}^{T\text{-bare}}$ in the cycle does not seem like "a systematic improvement of the self-energy". This problem is not present in the approximate form of the self-energy given in Eq.

(5.26) and all orders of $\bar{\Sigma}^{T\text{-bare}}$ appear within one iteration (Fig. 5.12). In Fig. 5.13 an overview of the approximations applied so far to the exact Hedin equation is given.

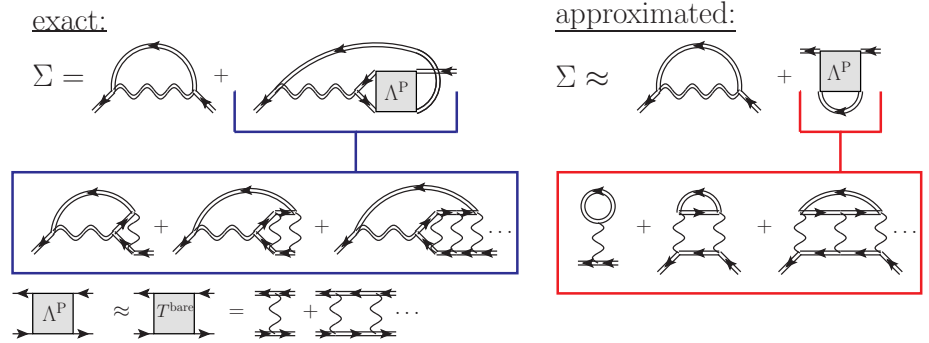
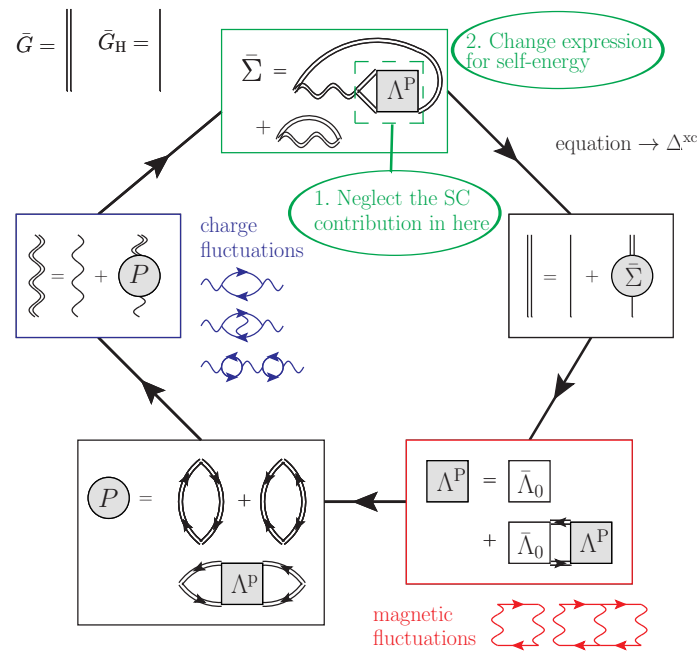
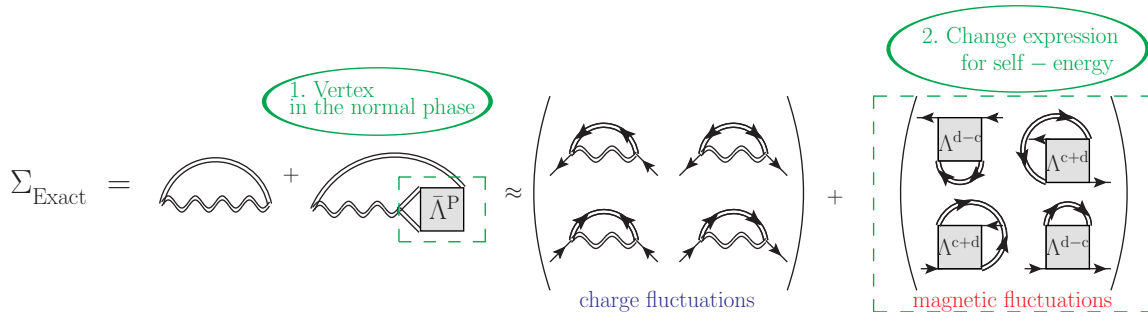


Figure 5.12.: Comparison between the contribution in the self energy related to the simple particle-hole propagator T^{bare} [Eq. (5.27)]. One iteration of the exact expression [Eq. (4.14)] does not lead the desired contribution shown in Fig. 5.8, but the approximated form [Eq. (5.26)] does.



- (a) The two approximations in the Hedin cycle are indicated by the green boxes. As a first approximation, the effect of superconductivity on the fluctuations is neglected by considering a vertex in the normal state Eq. 5.4. The magnetic excitations have been located in the vertex correction as multiple scattering between particles and holes (red box). The vertex enters the cycle in two places: In the polarization propagator and the self-energy. The contribution in the polarization propagator contributes to the screening of the bare Coulomb interaction (blue box). The contribution in the self-energy are the essential ones, leading to an interaction between electrons and (para)magnons. In order to avoid a full self-consistent treatment of the Hedin equation, and still get the diagrammatic contributions representing the electron-magnon interaction, the exact expression for the self-energy is approximated. This is the second approximation and is shown in more detail in the subfigure (b) below. In this form the self-energy may be used directly (without iterating) in the SSEq for the construction of a pairing potential Δ^{xc}



- (b) The details on the two approximations of the self-energy. Like discussed above the magnetic fluctuations represented by Λ^P are calculated in the non-superconducting phase and only normal Green's functions appear in the expansion. The second approximation was to change the exact expression of the self-energy containing a vertex function to the form $\bar{G}\Lambda^P$. This step has to be done carefully considering the loops shown in Eq. 5.25 and 5.24. The resulting self-energy contains two terms: The $\bar{G}w$ representing the interaction of an electron with charge fluctuations and the new $\bar{G}_{ij}\Lambda_{ij}^P$ describing the interaction of electrons to magnetic fluctuations. If the vertex corrections are neglected the Λ^P becomes zero and the expression reduces to the well known $\bar{G}w$ approximation.

Figure 5.13.: Overview of the approximation applied to the Hedin equations: The top figure shows the two approximations embedded in the Hedin equations. The lower figure gives the details of the approximations applied to the self-energy.

5.2. Reduction to an Effective Interaction

5.2.1. Preparation

In the last section the Hedin equations have been approximated. An overview of the two approximations is presented in Fig. 5.13 and the final result for the self-energy reads [Eq. (5.26)]:

$$\bar{\Sigma}(12) = -w(12)\bar{G}(12) + \Lambda d3d4\tau^z \begin{pmatrix} -G(34)\Lambda^{c-d}(1324) & F(34)\Lambda^{c+d}(1342) \\ F^\dagger(34)\Lambda^{c+d}(3124) & -G^\dagger(34)\Lambda^{c-d}(3142) \end{pmatrix}. \quad (5.28)$$

However, these simplifications are still not sufficient to do calculations for real materials. The dimensionality of the four-point object $\Lambda^{c\pm d}$ and the resulting integrals in Eq. (5.28) are simply too difficult to handle. A two-point form is necessary *i.e.*

$$\bar{\Sigma}^{\text{SF}}(12)_{ij} \stackrel{!}{=} \bar{G}(12)_{ij} \Lambda^{\text{SF}}(12)_{ij}. \quad (5.29)$$

The expression is reminiscent of the contribution related to the charge fluctuations ($\bar{\Sigma}^{\text{CF}} = -\bar{G}(12)w(12)$). A definition is made to distinguish the two:


Effective interactions are all two-point functions with an incoming and outgoing GF line at 1 and 2, beyond the screened Coulomb interaction.

The equation for the self-energy [Eqs. (5.26) and (5.29)] can be inverted for the effective interaction containing the spin-fluctuations (SF):

$$\Lambda^{\text{SF}}(12)_{ij} = \frac{\bar{\Sigma}(12)_{ij}}{\bar{G}(12)_{ij}} = \frac{1}{\bar{G}(12)_{ij}} \Lambda d3d4 \begin{pmatrix} -G(34)\Lambda^{c-d}(1324) & F(34)\Lambda^{c+d}(1342) \\ -F^\dagger(34)\Lambda^{c+d}(3124) & G^\dagger(34)\Lambda^{c-d}(3142) \end{pmatrix}_{ij}.$$

This relation is not useful in practice because one would need the four-point object $\Lambda^{c\pm d}$ in the first place to construct the Λ^{SF} . However, this trivial equation for Λ^{SF} has dire consequences. It shows that there is a **unique** way to go from the four-point object $\Lambda^{c\pm d}$ to the effective interaction and the two-point object Λ^{SF} is defined rigorously.

In this work, simplifications to the self-energy Σ^V creating the vertex correction [Eq. (5.4)] are used to construct an effective interaction. It is instructive to investigate local potentials as a contribution to Σ^V . An example of such a local contribution is the Hartree potential [Eqs. (4.8) and (D.8)]:

$$G^{\text{H}} = G_0 + G_0 \Sigma^{\text{H}} G^{\text{H}} \quad \Sigma^V(12) = \Sigma^{\text{H}}(12) := \delta_{12} \Delta d^3 r_3 \frac{\rho(\mathbf{r}_3)}{|\mathbf{r}_2 - \mathbf{r}_3|}. \quad \text{Figure 5.14.: Hartree potential}$$


The functional derivative of Σ^V leads to a **direct contribution** because the Green's function in Σ^V was part of a fermionic loop [Eq. (5.10)]:

$$\Lambda_0^{\text{d}}(1234) = \frac{\delta \Sigma^V(12)}{\delta G(34)} = -\delta_{12} \delta_{34} v(13).$$

The solution of the Dyson equation [Eq. (5.12)] creates an **improper** particle-hole propagator which is equivalent to the screened Coulomb interaction in the RPA:

$$\Lambda^{\text{d}}(1234) = -\delta_{12} \delta_{34} [v(12) + \Lambda d3d4 v(13) G(34) G(43) v(42) + \dots] = -w^{\text{RPA}}(12).$$

This term is already present in the expansion given in Eq. (5.26) and using Λ^{d} in Eq. (5.26) would lead to double counting errors. This is not surprising because the Hartree system is the **reference system** in the Hedin equations (Eq. (4.10) and Sec. D.3) and therefore the Hartree potential is not a correct self-energy contribution.

However, the discussion leads to the insight that two-point irreducible particle-hole propagators are related to local self-energies. This will be used to construct an effective interaction containing SF. The

Kohn-Sham potential [Eq. (D.9)] is used as an approximation for the self-energy creating the vertex correction *i.e.*:

$$\bar{\Sigma}^v(12) = \bar{\Sigma}^{\text{xc}}(12).$$

This has been done by various other researchers in the context of band structure calculations [92, 93, 90]. The potential is local in space, but non-diagonal in spin:

$$\bar{\Sigma}^v(12) = \sum_i \delta_{\mathbf{x}_1 \mathbf{x}_2} \begin{pmatrix} \sigma_{\sigma_1 \sigma_2}^i v_i^{\text{xc}} [\{\rho_j\}] (\mathbf{x}_1) & 0 \\ 0 & \sigma_{\sigma_1 \sigma_2}^{i*} z_{\sigma_1} z_{\sigma_2} v_i^{\text{xc}*} [\{\rho_j\}] (\mathbf{x}_1) \end{pmatrix}. \quad (5.30)$$

The **XC**-energy is defined as the difference between the exact expectation value $\langle \hat{T} + \hat{W} \rangle$ minus the Hartree contributions $T_s + \Lambda \frac{\rho(\mathbf{r})\rho(\mathbf{r}')}{|\mathbf{r}-\mathbf{r}'|}$. So by definition there is no overlap between the Hartree potential and the **XC**-potential and double counting cannot occur. On the ground state level, the $\bar{\Sigma}^{\text{xc}}$ usually improves the Hartree results. This is seen for example by the fact that the **KS** Green's function (corresponding to the exact v_i^{xc} .)

$$G^{\text{KS}} = G^{\text{H}} + G^{\text{H}} \bar{\Sigma}^{\text{xc}} G^{\text{KS}}$$

reproduces the exact many-body density. Also the quasi particle energies of the **KS** system are in general closer to the experimental quasi particle energies, than the Hartree results for metals [94, 95]. But not only the ground state properties are improved going from G^{H} to G^{KS} . Also the information of the excitations are provided by $\bar{\Sigma}^{\text{xc}}$: Within time dependent density functional theory, it is possible to obtain the exact (magnetic) **response function** [Eq. (5.17)]. Since the expression for the self-energy is local in space and time, the irreducible particle-hole propagator becomes a two-point function:

$$\begin{aligned} \frac{\delta \bar{\Sigma}^{\text{xc}}(12)}{\delta G(34)} &= \sum_i \delta_{\mathbf{x}_1 \mathbf{x}_2} \sigma_{\sigma_1 \sigma_2}^i \frac{\delta v_i^{\text{xc}} [\{\rho_j\}] (\mathbf{x}_1)}{\delta G(34)} \\ &= \delta_{\mathbf{x}_1 \mathbf{x}_2} \sum_{ij} \sum_{\sigma_5 \sigma_6} \Delta d_{\mathbf{x}_5} \sigma_{\sigma_1 \sigma_2}^i \frac{\delta v_i^{\text{xc}} [\{\rho_j\}] (\mathbf{x}_1)}{\delta \rho_j(\mathbf{x}_5)} \frac{\sigma_{\sigma_6 \sigma_5}^j \delta G_{\sigma_5 \sigma_6}(\mathbf{x}_5 \mathbf{x}_5^+)}{\delta G(34)} \\ &= \delta_{\mathbf{x}_1 \mathbf{x}_2} \sum_{ij} \sigma_{\sigma_1 \sigma_2}^i f_{ij}^{\text{xc}}(\mathbf{x}_1 \mathbf{x}_3) \sigma_{\sigma_4 \sigma_3}^j \delta_{\mathbf{x}_3 \mathbf{x}_4} = 4 \delta_{\mathbf{x}_1 \mathbf{x}_2} \delta_{\mathbf{x}_3 \mathbf{x}_4} f_{\sigma_1 \sigma_2 \sigma_4 \sigma_3}^{\text{xc}}(\mathbf{x}_1 \mathbf{x}_3) \end{aligned} \quad (5.31)$$

and is given by the exchange-correlation kernel f_{ij}^{xc} . The relation for the change between spin and Pauli components is given in Sec. A.3. The only problematic point in choosing the $\bar{\Sigma}^{\text{xc}}$ is the separation in **direct** and **crossed contributions**. The separation in direct and crossed terms is necessary for the construction of the self-energy in Eq. (5.26) because the two sets enter with different sign on the diagonal and off diagonal part of the equation.

However, the successful **XC**-potentials like **local density approximation (LDA)** or **generalized gradient approximation (GGA)** are explicit functionals of the densities $\rho(\mathbf{r})$ and $\mathbf{m}(\mathbf{r})$ [96, 97] and are not constructed by a perturbative expansion using **MBPT**. The functional derivative of $\bar{\Sigma}^{\text{xc}}$ is evaluated with the chain rule [Eq. (5.31)], but whether the resulting contribution is direct or crossed is not a meaningful question for a **non**-perturbative expression like $\rho^{\frac{4}{3}}$ or $\nabla \rho$.

This problem is only relevant for the term $\Lambda^{\text{c+d}}$ in the self-energy expression. For the other contribution $\Lambda^{\text{p}} = \Lambda^{\text{c-d}}$, the Dyson Eq. (5.16) exists which contains the full kernel (crossed and direct terms). The problem of determining $\Lambda^{\text{c+d}}$ for a non-separable kernel is circumvented by the **assumption** that the spin conditions based on the diagram expansion given in Eqs. (5.7) and (5.8) also hold for the **XC**-kernel:

$$f_{\sigma-\sigma\sigma-\sigma}^{\text{xc}} : \text{only crossed} \quad (5.32)$$

$$f_{\sigma\sigma-\sigma-\sigma}^{\text{xc}} : \text{only direct} \quad (5.33)$$

$$f_{\sigma\sigma\sigma\sigma}^{\text{xc}} : \text{crossed and direct.}$$

5.2.2. Construction Effective Interaction

A separate calculation of Λ^c and Λ^d by the Dyson Eq. (5.11) or (5.12) is not possible because the kernels Λ_0^c and Λ_0^d given in Eqs. (5.10) and (5.9) are not known for the usual XC-potentials. However, it is possible to solve the combined Dyson Eq. (5.16) containing direct and crossed terms:

$$\Lambda^P = \Lambda_0 + \Lambda_0 G G \Lambda^P \text{ with } \Lambda_0 = \frac{\delta \Sigma^{\text{xc}}}{\delta G} = 4f_{\text{xc}} \quad (5.34)$$

and use the assumption made in the previous section to construct the missing contribution. The kernel is a two-point function in space time, but a four-point object in spin space *i.e.* $\Lambda_{\sigma_1 \sigma_2 \sigma_3 \sigma_4}^0(\mathbf{x}_1 \mathbf{x}_3)$:

$$\begin{aligned} \Lambda_{\sigma_1 \sigma_2 \sigma_3 \sigma_4}^P(\mathbf{x}_1 \mathbf{x}_3) &= \Lambda_{\sigma_1 \sigma_2 \sigma_3 \sigma_4}^0(\mathbf{x}_1 \mathbf{x}_3) \\ &+ \sum_{\sigma_5 \dots \sigma_8} \Lambda d\mathbf{x}_6 \dots d\mathbf{x}_8 \Lambda_{\sigma_1 \sigma_2 \sigma_5 \sigma_6}^0(\mathbf{x}_1 \mathbf{x}_6) G_{\sigma_8 \sigma_6}(\mathbf{x}_6 \mathbf{x}_8) G_{\sigma_5 \sigma_7}(\mathbf{x}_8 \mathbf{x}_6) \Lambda_{\sigma_7 \sigma_8 \sigma_3 \sigma_4}^P(\mathbf{x}_8 \mathbf{x}_3). \end{aligned}$$

For a collinear system the Green's function is diagonal in spin: $G_{\sigma_1 \sigma_2} = \delta_{\sigma_1 \sigma_2} G_{\sigma_1}$. The kernel [Eq. (5.31)] is inserted for Λ_0 and the product $-G_{\sigma_5}(\mathbf{x}_8 \mathbf{x}_6) G_{\sigma_6}(\mathbf{x}_6 \mathbf{x}_8)$ is approximated by χ^{KS} given in Eq. (5.18). This means the full Green's function is approximated by the KS one. Also this approximation is discussed in Sec. 5.4.1. These steps lead to the following expression for the proper particle-hole propagator:

$$\Lambda_{\sigma_1 \sigma_2 \sigma_3 \sigma_4}^P = 4f_{\sigma_1 \sigma_2 \sigma_4 \sigma_3}^{\text{xc}} - 16 \sum_{\sigma_5 \dots \sigma_8} f_{\sigma_1 \sigma_2 \sigma_6 \sigma_5}^{\text{xc}} \chi_{\sigma_5 \sigma_6 \sigma_6 \sigma_5}^{\text{KS}} \Lambda_{\sigma_5 \sigma_6 \sigma_3 \sigma_4}^P.$$

All quantities are functions of \mathbf{x}_1 and \mathbf{x}_2 . For simplicity, this dependence and the corresponding integrals are left out in most places. By comparison with Eq. (5.17) it is seen that Λ^{c-d} contains parts of the [response function](#):

$$\Lambda^P = 4f^{\text{xc}} - 16f^{\text{xc}} \chi^{\text{KS}} f^{\text{xc}} + 64f^{\text{xc}} \chi^{\text{KS}} f^{\text{xc}} \chi^{\text{KS}} f^{\text{xc}} + \dots = 4f^{\text{xc}} - 16f^{\text{xc}} \left[\underbrace{\chi^{\text{KS}} - 4\chi^{\text{KS}} f^{\text{xc}} \chi^{\text{KS}} + \dots}_{=\text{proper response function}} \right] f^{\text{xc}}.$$

The effective interaction contains only the proper parts of the response function [Eq. (B.20)] which are identical to the polarization propagator P introduced in Eq. (4.18):

$$\Lambda_{\sigma_1 \sigma_2 \sigma_3 \sigma_4}^P = 4f_{\sigma_1 \sigma_2 \sigma_4 \sigma_3}^{\text{xc}} - 16 \sum_{\sigma_5 \dots \sigma_8} f_{\sigma_1 \sigma_2 \sigma_6 \sigma_5}^{\text{xc}} P_{\sigma_6 \sigma_5 \sigma_7 \sigma_8} f_{\sigma_7 \sigma_8 \sigma_3 \sigma_4}^{\text{xc}} \quad (5.35)$$

$$P_{\alpha\beta\gamma\delta} = \frac{1}{4} \sum_{ij} \sigma_{\alpha\beta}^i P_{ij} \sigma_{\gamma\delta}^j \text{ with } P_{ij} = \chi_{ij}^{\text{KS}} - \sum_{kl} \chi_{ik}^{\text{KS}} f_{kl}^{\text{xc}} P_{lj}. \quad (5.36)$$

For the XC-kernel, adiabatic approximations (Sec. B.4) are used and therefore the object has no structure in frequency space. The proper response function on the other hand has poles at the excitation energies of the magnetic fluctuations. This is the relevant contribution in the scenario of pairing mediated by fluctuations. The flat kernels are put to a separate self-energy term called $\bar{G}f^{\text{xc}}$:

$$\Lambda_{\sigma_1 \sigma_1 \sigma_2 \sigma_2}^P = \underbrace{4f_{\sigma_1 \sigma_1 \sigma_2 \sigma_2}^{\text{xc}}}_{\text{move to } \bar{G}f^{\text{xc}}} - 16 \sum_{\sigma_6 \sigma_7} f_{\sigma_1 \sigma_1 \sigma_6 \sigma_6}^{\text{xc}} P_{\sigma_6 \sigma_6 \sigma_7 \sigma_7} f_{\sigma_7 \sigma_7 \sigma_2 \sigma_2}^{\text{xc}} \quad (5.37)$$

$$\Lambda_{\sigma-\sigma\sigma-\sigma}^P = \underbrace{4f_{\sigma-\sigma-\sigma\sigma}^{\text{xc}}}_{\text{move to } \bar{G}f^{\text{xc}}} - 16 f_{\sigma-\sigma-\sigma\sigma}^{\text{xc}} P_{\sigma-\sigma-\sigma\sigma} f_{\sigma-\sigma-\sigma\sigma}^{\text{xc}}, \quad (5.38)$$

which is discussed separately from now on. For a collinear system there are only six independent contributions with respect to spin. In order to keep the equations simpler, the six terms receive a shorter name:

$$\begin{aligned} f_{\sigma\sigma'} &:= f_{\sigma\sigma'\sigma'\sigma}^{\text{xc}} & P_{\sigma\sigma'} &:= P_{\sigma\sigma\sigma'\sigma'} \\ f_{\sigma}^F &:= f_{\sigma-\sigma-\sigma\sigma}^{\text{xc}} & P_{\sigma}^F &:= P_{\sigma-\sigma-\sigma\sigma}. \end{aligned} \quad (5.39)$$

The equations for the **effective interaction** become more transparent if the response quantities are rewritten in components of the Pauli matrix [Eq. (A.4)] because these are the response functions corresponding to magnetic fields in x , y , or z direction. The change between the spin and $i, j \in \{x, y, z, 0\}$ components is done via the following matrix transformation:

$$\begin{pmatrix} A_{00} \\ A_{zz} \\ A_{z0} \\ A_{0z} \end{pmatrix} = \begin{pmatrix} 1 & 1 & 1 & 1 \\ 1 & 1 & -1 & -1 \\ 1 & -1 & -1 & 1 \\ 1 & -1 & 1 & -1 \end{pmatrix} \begin{pmatrix} A_{\uparrow\uparrow} \\ A_{\downarrow\downarrow} \\ A_{\downarrow\uparrow} \\ A_{\uparrow\downarrow} \end{pmatrix} \quad \begin{pmatrix} A_{\uparrow\uparrow} \\ A_{\downarrow\downarrow} \\ A_{\downarrow\uparrow} \\ A_{\uparrow\downarrow} \end{pmatrix} = \frac{1}{4} \begin{pmatrix} 1 & 1 & 1 & 1 \\ 1 & 1 & -1 & -1 \\ 1 & -1 & -1 & 1 \\ 1 & -1 & 1 & -1 \end{pmatrix} \begin{pmatrix} A_{00} \\ A_{zz} \\ A_{z0} \\ A_{0z} \end{pmatrix}.$$

For the xx and xy block the transformation matrix becomes block diagonal and the symmetry $A_{xx} = A_{yy}$ and $A_{xy} = A_{yx}$ reduces the transformation relation to a two-dimensional matrix:

$$\begin{pmatrix} A_{xx} \\ A_{xy} \end{pmatrix} = \begin{pmatrix} 1 & 1 \\ -i & i \end{pmatrix} \begin{pmatrix} A_{\uparrow}^F \\ A_{\downarrow}^F \end{pmatrix} \quad \begin{pmatrix} A_{\uparrow}^F \\ A_{\downarrow}^F \end{pmatrix} = \frac{1}{2} \begin{pmatrix} 1 & i \\ 1 & -i \end{pmatrix} \begin{pmatrix} A_{xx} \\ A_{xy} \end{pmatrix}.$$

The spin resolved quantities in the Eqs. (5.37) and (5.38) are replaced:

$$\begin{aligned} \Lambda_{\sigma_1\sigma_2}^P &= -16 \sum_{\sigma_6\sigma_7} f_{\sigma_1\sigma_1\sigma_6\sigma_6}^{\text{xc}}(\mathbf{x}_1\mathbf{x}_6) P_{\sigma_6\sigma_6\sigma_7\sigma_7}(\mathbf{x}_6\mathbf{x}_8) f_{\sigma_7\sigma_7\sigma_2\sigma_2}^{\text{xc}}(\mathbf{x}_8\mathbf{x}_3) \\ &= 16 [f_{\sigma_1\uparrow}^{\text{xc}} P_{\uparrow\uparrow} f_{\uparrow\sigma_2}^{\text{xc}} + f_{\sigma_1\downarrow}^{\text{xc}} P_{\downarrow\downarrow} f_{\downarrow\sigma_2}^{\text{xc}} + f_{\sigma_1\uparrow}^{\text{xc}} P_{\uparrow\downarrow} f_{\downarrow\sigma_2}^{\text{xc}} + f_{\sigma_1\downarrow}^{\text{xc}} P_{\downarrow\uparrow} f_{\uparrow\sigma_2}^{\text{xc}}] \\ &= 4 [f_{\sigma_1\uparrow}^{\text{xc}} (P_{00} + P_{zz} + P_{z0} + P_{0z}) f_{\uparrow\sigma_2}^{\text{xc}} + f_{\sigma_1\downarrow}^{\text{xc}} (P_{00} + P_{zz} - P_{z0} - P_{0z}) f_{\downarrow\sigma_2}^{\text{xc}} \\ &\quad + f_{\sigma_1\uparrow}^{\text{xc}} (P_{00} - P_{zz} + P_{z0} - P_{0z}) f_{\downarrow\sigma_2}^{\text{xc}} + f_{\sigma_1\downarrow}^{\text{xc}} (P_{00} - P_{zz} - P_{z0} + P_{0z})] f_{\uparrow\sigma_2}^{\text{xc}} \\ \Lambda_{\sigma-\sigma\sigma-\sigma}^P &= -16 f_{\sigma}^F P_{\sigma}^F f_{\sigma}^F = -2 (f_{xx} + z_{\sigma} i f_{xy}) (P_{xx} + z_{\sigma} i P_{xy}) (f_{xx} + z_{\sigma} i f_{xy}). \end{aligned}$$

The spin-flip contribution P_{σ}^F in the full response function contain no improper contribution [Eq. (5.17)] and for this component the proper response function is equal to the full one:

$$\Lambda_{\sigma-\sigma\sigma-\sigma}^P = -2 (f_{xx} + z_{\sigma} i f_{xy}) (\chi_{xx} + z_{\sigma} i \chi_{xy}) (f_{xx} + z_{\sigma} i f_{xy}).$$

The contributions of Λ^P related to the charge-charge response would read:

$$\Lambda_{\sigma_1\sigma_2}^P = -4 (f_{\sigma_1\uparrow}^{\text{xc}} + f_{\sigma_1\downarrow}^{\text{xc}}) P_{00} (f_{\sigma_2\uparrow}^{\text{xc}} + f_{\sigma_2\downarrow}^{\text{xc}}).$$

The screened Coulomb interaction in the Gw term of the self energy on the other hand is given by

$$w = v - v P_{00} v + v P_{00} v P_{00} v - \dots$$

From Eq. (5.17) it is seen that for a density of a non-interacting system, the $f_{jk}[\rho_{\text{Non Int}}]$ has to cancel the Coulomb interaction in order to provide the non-interacting χ^{KS} :

$$\chi_{00} = \chi_{00}^{\text{KS}} - \sum_{j,k \in \{0,z\}} \chi_{0j}^{\text{KS}} (v \delta_{0j} \delta_{0k} + f_{jk}[\rho_{\text{Non Int}}]) \chi_{j0} \stackrel{!}{=} \chi_{00}^{\text{KS}}.$$

This indicates the presence of Coulomb contributions within the charge part of the XC-kernel. Hence, in order to avoid double counting problems with the $\bar{G}w$ term [Eq. (5.26)], the P_{00} contributions in Λ^P are dropped:

$$\begin{aligned} \Lambda_{\sigma_1\sigma_2}^P &= -4 [(f_{\sigma_1\uparrow}^{\text{xc}} - f_{\sigma_1\downarrow}^{\text{xc}}) P_{zz} (f_{\uparrow\sigma_2}^{\text{xc}} - f_{\downarrow\sigma_2}^{\text{xc}}) + (f_{\sigma_1\uparrow}^{\text{xc}} - f_{\sigma_1\downarrow}^{\text{xc}}) P_{z0} (f_{\uparrow\sigma_2}^{\text{xc}} + f_{\downarrow\sigma_2}^{\text{xc}}) \\ &\quad + (f_{\sigma_1\uparrow}^{\text{xc}} + f_{\sigma_1\downarrow}^{\text{xc}}) P_{0z} (f_{\uparrow\sigma_2}^{\text{xc}} - f_{\downarrow\sigma_2}^{\text{xc}})] \\ \Lambda_{\sigma-\sigma\sigma-\sigma}^P &= -2 (f_{xx} + z_{\sigma} i f_{xy}) (\chi_{xx} + z_{\sigma} i \chi_{xy}) (f_{xx} + z_{\sigma} i f_{xy}) := -2 f_{\sigma}^{\pm} \chi_{\sigma}^{\pm} f_{\sigma}^{\pm}. \end{aligned}$$

The spin dependent combinations of the kernel are written in a compact form:

$$\begin{aligned} f_{z\sigma}^T &:= z_{\sigma} f_{zz} + f_{0z} = 2 (f_{\uparrow\sigma}^{\text{xc}} - f_{\downarrow\sigma}^{\text{xc}}) & f_{z\sigma} &:= z_{\sigma} f_{zz} + f_{z0} = 2 (f_{\uparrow\sigma}^{\text{xc}} - f_{\downarrow\sigma}^{\text{xc}}) \\ f_{0\sigma}^T &:= f_{00} + z_{\sigma_1} f_{z0} = 2 (f_{\uparrow\sigma}^{\text{xc}} + f_{\downarrow\sigma}^{\text{xc}}) & f_{0\sigma} &:= f_{00} + z_{\sigma} f_{0z} = 2 (f_{\uparrow\sigma}^{\text{xc}} + f_{\downarrow\sigma}^{\text{xc}}) \\ f_{\sigma}^{\pm} &:= f_{xx} + z_{\sigma} i f_{xy} & \chi_{\sigma}^{\pm} &:= \chi_{xx} + z_{\sigma} i \chi_{xy}. \end{aligned}$$

For a non-magnetic system, the kernel and response function becomes diagonal and the expression reduces to:

$$\begin{aligned} f_{z\sigma}^T &= f_{z\sigma} = z_\sigma f_{zz} & f_{0\sigma}^T &= f_{0\sigma} = f_{00} \\ f_\sigma^\pm &= f_{xx} = f_{yy} = f_{zz} & \chi_\sigma^\pm &= \chi_{xx} = \chi_{yy} = \chi_{zz}. \end{aligned}$$

With these definitions the **effective interaction** for a collinear and NM system reads:

$$\text{Collinear: } \Lambda_{\sigma_1\sigma_2}^P = - \sum_{ij \in \{0,z\}} f_{i\sigma_1}^T P_{ij} (1 - \delta_{i0}\delta_{j0}) f_{j\sigma_2} \quad \Lambda_{\sigma-\sigma\sigma-\sigma}^P = -2f_\sigma^\pm \chi_\sigma^\pm f_\sigma^\pm \quad (5.40)$$

$$\text{NM: } \Lambda_{\sigma_1\sigma_2}^P = -z_{\sigma_1} f_{zz} \chi_{zz} f_{zz} z_{\sigma_2} := -z_{\sigma_1} z_{\sigma_2} \frac{\Lambda^{\text{SF}}}{2} \quad \Lambda_{\sigma-\sigma\sigma-\sigma}^P = -2f_{zz} \chi_{zz} f_{zz} = -\Lambda^{\text{SF}}. \quad (5.41)$$

For the collinear system the spin diagonal term contains the magnetic response P_{zz} plus contributions proportional to P_{z0} and P_{z0} describing the coupling between charge and magnetic degrees of freedom. In contrast to the screened Coulomb interaction [Eq. (4.17)], the $\Lambda_{\sigma_1\sigma_2}^P$ shows a real dependence on spin *i.e.*:

$$\Lambda_{\uparrow\downarrow}^P \neq \Lambda_{\downarrow\uparrow}^P \text{ and } \Lambda_{\uparrow\uparrow}^P \neq \Lambda_{\downarrow\downarrow}^P.$$

The spin flip term $\Lambda_{\sigma-\sigma\sigma-\sigma}^P$ contains the transverse response function χ^\pm and is absent in the screened Coulomb interaction. The physical interpretation of this term is an interaction mediated by a quasi-particle (**magnon**) carrying one Bohr magneton: $e_{\uparrow}^- \rightarrow e_{\downarrow}^- + \kappa_{\mu_B}$.

For non-magnetic systems, the coupling between charge and magnetic degrees of freedom vanishes. This is due to the degeneracy of the \uparrow and \downarrow spin [Eq. (5.20)]. The ratio of 1 : 2 for $\Lambda_{\sigma\sigma}^P : \Lambda_{\sigma-\sigma\sigma-\sigma}^P$ and the sign change between the $\Lambda_{\uparrow\uparrow}^P$ and $\Lambda_{\downarrow\downarrow}^P$ is known, from effective interactions in the unpolarized electron gas [87]. Remember that all quantities are functions of \mathbf{x}_1 and \mathbf{x}_2 and the integrals in the expressions

$$\Lambda^{\text{SF}}(\mathbf{x}_1\mathbf{x}_2) = 2 \int d\mathbf{x}_3 d\mathbf{x}_4 f_{zz}(\mathbf{x}_1\mathbf{x}_3) \chi_{zz}(\mathbf{x}_3\mathbf{x}_4) f_{zz}(\mathbf{x}_4\mathbf{x}_2)$$

have been left for simplicity.

5.3. Self-Energy with Effective Interaction

What remains to be done is the evaluation of the self-energy given in Eq. (5.26) containing this effective interaction. The space-time integrals in Eq. (5.26) are trivial for an effective interaction and the summation with respect to spin is simplified by the **collinearity** of the Green's function:

$$\begin{aligned} \bar{\Sigma}^{\text{SF}}(12) &= \tau^z \int d5d6 \begin{pmatrix} -G(56) \Lambda^P(1526) & F(56) \Lambda^{\text{c+d}}(1562) \\ F^\dagger(46) \Lambda^{\text{c+d}}(5126) & -G^\dagger(46) \Lambda^P(4162) \end{pmatrix} \\ &= \tau^z \sum_{\sigma} \begin{pmatrix} -G_{\sigma}(\mathbf{x}_1\mathbf{x}_2) \Lambda_{\sigma_1\sigma\sigma_2\sigma}^P(\mathbf{x}_1\mathbf{x}_2) & F_{\sigma}(\mathbf{x}_1\mathbf{x}_2) \Lambda_{\sigma_1\sigma-\sigma\sigma_2}^{\text{c+d}}(\mathbf{x}_1\mathbf{x}_2) \\ F_{\sigma}^\dagger(\mathbf{x}_1\mathbf{x}_2) \Lambda_{\sigma\sigma_1\sigma_2-\sigma}^{\text{c+d}}(\mathbf{x}_1\mathbf{x}_2) & -G_{\sigma}^\dagger(\mathbf{x}_1\mathbf{x}_2) \Lambda_{\sigma\sigma_1\sigma_2}^P(\mathbf{x}_2\mathbf{x}_1) \end{pmatrix} \\ &= \tau^z \begin{pmatrix} -G_{\sigma_1} (\Lambda_{\sigma_1\sigma_1\sigma_2\sigma_1}^P + \Lambda_{\sigma_1-\sigma_1\sigma_2-\sigma_1}^P) & F_{\sigma_1} (\Lambda_{\sigma_1\sigma_1-\sigma_1\sigma_2}^{\text{c+d}} + \Lambda_{\sigma_1-\sigma_1\sigma_1\sigma_2}^{\text{c+d}}) \\ F_{\sigma_1}^\dagger (\Lambda_{\sigma_1\sigma_1\sigma_2-\sigma_1}^{\text{c+d}} + \Lambda_{-\sigma_1\sigma_1\sigma_2\sigma_1}^{\text{c+d}}) & -G_{\sigma_1}^\dagger (\Lambda_{\sigma_1\sigma_1\sigma_1\sigma_2}^P + \Lambda_{-\sigma_1\sigma_1-\sigma_1\sigma_2}^P) \end{pmatrix}. \end{aligned}$$

The interaction contains two spin components $\Lambda_{\sigma_1-\sigma_1\sigma_1-\sigma_1}^P$ and $\Lambda_{\sigma_1\sigma_1\sigma_2\sigma_2}^P$ [Eq. (5.40)]. This leads to a diagonal spin contribution for the normal part of the self-energy and non-diagonal contribution ($\delta_{\sigma_1-\sigma_2}$) for the anomalous part:

$$\bar{\Sigma}^{\text{SF}}(12) = \tau^z \begin{pmatrix} -\delta_{\sigma_1\sigma_2} G_{\sigma_1} (\Lambda_{\sigma_1\sigma_1\sigma_1\sigma_1}^P + \Lambda_{\sigma_1-\sigma_1\sigma_1-\sigma_1}^P) & \delta_{\sigma_1-\sigma_2} F_{\sigma_1} (\Lambda_{\sigma_1\sigma_1-\sigma_1-\sigma_1}^{\text{c+d}} + \Lambda_{\sigma_1-\sigma_1\sigma_1-\sigma_1}^{\text{c+d}}) \\ \delta_{\sigma_1-\sigma_2} F_{\sigma_1}^\dagger (\Lambda_{\sigma_1\sigma_1-\sigma_1-\sigma_1}^{\text{c+d}} + \Lambda_{-\sigma_1\sigma_1-\sigma_1\sigma_1}^{\text{c+d}}) & -\delta_{\sigma_1\sigma_2} G_{\sigma_1}^\dagger (\Lambda_{\sigma_1\sigma_1\sigma_1\sigma_1}^P + \Lambda_{-\sigma_1\sigma_1-\sigma_1\sigma_1}^P) \end{pmatrix}.$$

The solution of the Eq. (5.34) provides only $\Lambda^P = \Lambda^{c-d}$. For the other term Λ^{c+d} one would in principle need to solve one of the Dyson equations [Eq. 5.11 or 5.12]. Alternatively, one can use the relation given in Eq. (5.32) and (5.33) and the self-energy becomes:

$$\bar{\Sigma}^{\text{SF}} = \tau^z \begin{pmatrix} -\delta_{\sigma_1\sigma_2} G_{\sigma_1} (\Lambda_{\sigma_1\sigma_1\sigma_1\sigma_1}^P + \Lambda_{\sigma_1-\sigma_1\sigma_1-\sigma_1}^P) & \delta_{\sigma_1-\sigma_2} F_{\sigma_1} (-\Lambda_{\sigma_1\sigma_1-\sigma_1-\sigma_1}^P + \Lambda_{\sigma_1-\sigma_1\sigma_1-\sigma_1}^P) \\ \delta_{\sigma_1-\sigma_2} F_{\sigma_1}^\dagger (-\Lambda_{\sigma_1\sigma_1-\sigma_1-\sigma_1}^P + \Lambda_{\sigma_1-\sigma_1\sigma_1-\sigma_1}^P) & -\delta_{\sigma_1\sigma_2} G_{\sigma_1}^\dagger (\Lambda_{\sigma_1\sigma_1\sigma_1\sigma_1}^P + \Lambda_{\sigma_1-\sigma_1\sigma_1-\sigma_1}^P) \end{pmatrix}, \quad (5.42)$$

where the effective interaction is given in Eq. (5.40):

$$\Lambda_{\sigma\sigma}^P = - \sum_{ij=\{0,z\}} f_{i\sigma}^T (\chi_{ij} - \delta_{i0}\delta_{j0}) f_{j\sigma} \quad \Lambda_{\sigma-\sigma\sigma-\sigma}^P = -2f_{\sigma}^{\pm} \chi_{\sigma}^{\pm} f_{\sigma}^{\pm}.$$

In the context of superconductivity the case of a NM system is relevant. In this case the effective interaction [Eq. (5.41)] becomes more simple and the self-energy reduces to:

$$\bar{\Sigma}^{\text{SF}} = \frac{3}{2} \tau^z \begin{pmatrix} \delta_{\sigma_1\sigma_2} G(\mathbf{x}_1\mathbf{x}_2) \Lambda^{\text{SF}}(\mathbf{x}_1\mathbf{x}_2) & -\delta_{\sigma_1-\sigma_2} F(\mathbf{x}_1\mathbf{x}_2) \Lambda^{\text{SF}}(\mathbf{x}_1\mathbf{x}_2) \\ -\delta_{\sigma_1-\sigma_2} F^\dagger(\mathbf{x}_1\mathbf{x}_2) \Lambda^{\text{SF}}(\mathbf{x}_1\mathbf{x}_2) & \delta_{\sigma_1\sigma_2} G^\dagger(\mathbf{x}_1\mathbf{x}_2) \Lambda^{\text{SF}}(\mathbf{x}_1\mathbf{x}_2) \end{pmatrix} \quad (5.43)$$

$$\Lambda^{\text{SF}}(\mathbf{x}_1\mathbf{x}_2) = 2 \Lambda \int d\mathbf{x}_3 d\mathbf{x}_4 f_{zz}^{\text{xc}}(\mathbf{x}_1\mathbf{x}_3) \chi_{zz}(\mathbf{x}_3\mathbf{x}_4) f_{zz}^{\text{xc}}(\mathbf{x}_4\mathbf{x}_2). \quad (5.44)$$

For completeness, the self-energy contribution containing the screened Coulomb interaction is derived [Eq. (5.26)]. Remember that in Eq. (5.37) and (5.38) a term containing the bare kernel was present which is added to the $\bar{\Sigma}^{\text{CF}}$:

$$\bar{\Sigma}^{\text{CF}}(12) = - \begin{pmatrix} \delta_{\sigma_1\sigma_2} G(\mathbf{x}_1\mathbf{x}_2) w^G(\mathbf{x}_1\mathbf{x}_2) & \delta_{\sigma_1-\sigma_2} F(\mathbf{x}_1\mathbf{x}_2) w^F(\mathbf{x}_1\mathbf{x}_2) \\ \delta_{\sigma_1-\sigma_2} F^\dagger(\mathbf{x}_1\mathbf{x}_2) w^F(\mathbf{x}_1\mathbf{x}_2) & \delta_{\sigma_1\sigma_2} G(\mathbf{x}_1\mathbf{x}_2) w^G(\mathbf{x}_1\mathbf{x}_2) \end{pmatrix}, \quad (5.45)$$

where the screened Coulomb interactions w , w_G and w_F are defined as:

$$-w(12) = -v(12) + \Lambda \int d3d4v(13) P_{00}(34) w(42) \quad (5.46)$$

$$w^G(\mathbf{x}_1\mathbf{x}_2) := w(\mathbf{x}_1\mathbf{x}_2) - 4 [f_{\sigma-\sigma-\sigma\sigma}^{\text{xc}}(\mathbf{x}_1\mathbf{x}_2) + f_{\sigma\sigma\sigma\sigma}^{\text{xc}}(\mathbf{x}_1\mathbf{x}_2)] \quad (5.47)$$

$$w^F(\mathbf{x}_1\mathbf{x}_2) := w(\mathbf{x}_1\mathbf{x}_2) - 4 [f_{\sigma-\sigma-\sigma\sigma}^{\text{xc}}(\mathbf{x}_1\mathbf{x}_2) + f_{\sigma\sigma-\sigma-\sigma}^{\text{xc}}(\mathbf{x}_1\mathbf{x}_2)].$$

The charge-charge polarization propagator P_{00} in terms of the local vertex correction is given in Eq. (5.36)

$$P_{00} = \chi_{00}^{\text{KS}} - \sum_{ij=\{0,z\}} \chi_{0i}^{\text{KS}} f_{ij}^{\text{xc}} \chi_{j0}^{\text{KS}} + \dots \quad (5.48)$$

and after slight rearrangement it is found:

$$-w(12) = -v(12) + \Lambda \int d3d4v(13) \chi_{00}(34) v(42),$$

where χ_{00} is the full charge-charge response function [Eq. (5.17)].

5.4. Discussion of the Effective Interaction

5.4.1. The Approximations

In the derivation of the self-energy containing the magnetic fluctuations [Eq. (5.43)], several approximations have been applied. In this section all of them are discussed in the order they appear in the derivation. If there is no likelihood of confusion, the normal part of the Nambu Green's function is depicted with a single arrow in this section.

1.) Non-SC Vertex

As a first approximation, the effect of superconductivity on the vertex *i.e.* the spin fluctuation spectrum was neglected. For conventional superconductors it is well known that the **phonons** are not strongly influenced by the onset of superconductivity: The linewidth and excitation energy may vary, but the structure of the spectrum stays the same [98]. For the charge and magnetic fluctuations the effect could be larger. Static magnetic fields are expelled completely from a **SC** below the critical temperature, regardless of whether the material is first exposed to a magnetic field and then cooled down below the **critical temperature** (T_c) or *vice versa*¹². This phenomenon was first reported by Meissner and Ochsenfeld in 1933 [99] and is described by the phenomenological and macroscopic **London equations** [100]. The **Meissner-Ochsenfeld effect** distinguishes a superconducting system from a perfect conductor.

Not only the static, but also the dynamic response function shows changes induced by superconductivity. In **nuclear magnetic resonance (NMR)** experiments for the **FeSC** and cuprates two changes in the dynamic response are observed [101, 44, 102]:

1. A resonance peak appears below T_c . In the **FeSC** the position of the resonance is proportional to the gap $\omega_{\text{res}}(T) \propto \Delta(T)$ and close to the critical temperature the rule $5k_B T_c \approx \omega_{\text{res}}$ is found.
2. A gap opens in the response function, meaning that $\chi_{zz}(\omega)$ drops to zero even for frequencies above zero.

Model calculations of the **RPA** magnetic response done by P. Hirschfeld *et. al.* [103] indicate that the resonance and gap in the response function are created by the FF^\dagger term in Eq. (4.18). Above the critical temperature magnetic fluctuations are still present, but the resonance energies are higher and the peaks are much broader. Since the effects induced by superconductivity to the response have been neglected in the theory, it is not possible to obtain the resonance below T_c and hence a valid self-energy for this regime.

2.) Change of the Expression for the Self-Energy

As a second approximation the self-energy was changed to a form given in Eq. (5.26) and shown in Fig. 5.13. The reason for changing the self-energy was to include all contributions corresponding to the **T -matrix** (or more general the $\Lambda^{c,d}$) directly in the self-energy. By this change an iteration of the Hedin equations is avoided (Fig. 5.11).

Since the Hedin equations are an exact scheme in the first place, applying approximations may create some artifacts. This is seen by the presence of **double counting (DC)** problems using for example the **T -matrix** for Λ^c and set the direct contribution to zero: $\Lambda^d = 0$. The two problematic contributions are shown in the top row of Fig. 5.15. The Hartree potential is included already in the reference system and the contribution $\delta_{12} \Delta d3w$ (13) $G(33^+)$ fully contains the Hartree contribution. Also the second order term in w is partially contained in the Gw contribution shown in the second line of Fig. 5.15. Also for the anomalous

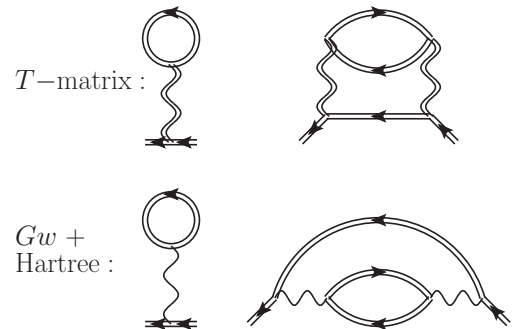


Figure 5.15.: Double counting errors induced by the **T -matrix** self-energy.

¹²Below T_c the system becomes a perfect diamagnet and the static volume response is -1 .

parts **DC** appears: The term $w(12)F(12)$ is created by the $\bar{G}T$ in first order and also by the $\bar{G}\omega$. All these errors are compensated by following double counting correction:

$$\begin{aligned} \bar{\Sigma}_{\text{DC}}^{\text{T}}(12) = \tau^z & \begin{pmatrix} \delta_{12} \Delta d3w(13) G(33^+) & -w(12) F(12) \\ -w(12) F^\dagger(12) & \delta_{12} \Delta d3w(13) G^\dagger(33^+) \end{pmatrix} \\ & - \tau^z \Lambda d3d4 \begin{pmatrix} G(12) w(13) w(24) G(43) G(34) & 0 \\ 0 & G(21) w(13) w(24) G(34) G^\dagger(34) \end{pmatrix}. \end{aligned} \quad (5.49)$$

Note that the normal terms shown in the top line of Fig. 5.15 are also intrinsically wrong. This means each term itself contains multiple copies of the same diagram and the double counting is not created in combination with an other diagram as discussed above. An example is the Coulomb interaction screened with bubbles. The bubbles are also contained in the renormalized Green's function [Eq. (4.10)]. This is shown on the left hand side of Fig. 5.16. Also the second order term in w has intrinsic double counting problems: If the screened interaction is expanded in orders of v , it leads for third and higher orders to multiple times the same contribution. As an example this is shown for the third order term in Fig. 5.16.

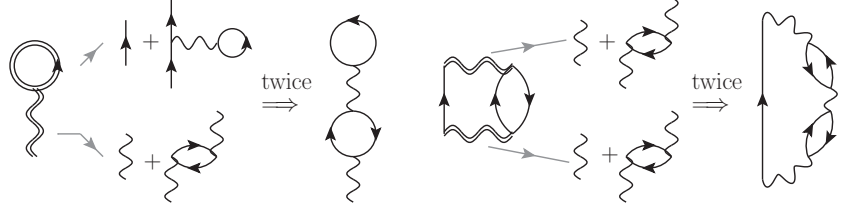


Figure 5.16.: Intrinsic double counting errors created by GT .

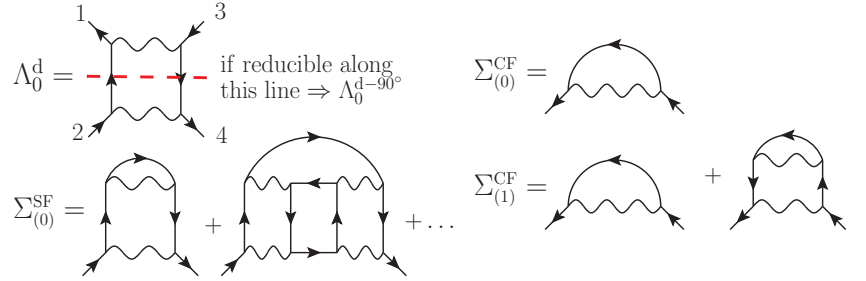


Figure 5.17.: Double counting errors related to $G\Lambda^{\text{d}}$

As an example this is shown for the third order term in Fig. 5.16.

But **DC** errors are not restricted to the crossed diagrams in the particle-hole propagator. Assume the direct second order contribution for the proper particle-hole propagator Λ_0^{d} shown in Fig. 5.17. If this term is used in the self-energy an **DC** error in combination with the Gw term is created. The double counting error originates in direct contribution which are reducible with respect to the particle-hole channel propagating along $1 \rightarrow 2$ and $3 \rightarrow 4$. This is indicated by the dashed red line in Fig. 5.17. Such contribution are called $\Lambda_0^{\text{d}-90^\circ}$ and should be removed form $\bar{\Sigma}^{\text{SF}}$:

$$\bar{\Sigma}_{\text{DC}}^{\text{d}}(12) = \tau^z \Lambda d3d4 \begin{pmatrix} G(56) \Lambda_0^{\text{d}-90^\circ}(1324) & 0 \\ 0 & G^\dagger(34) \Lambda_0^{\text{d}-90^\circ}(3142) \end{pmatrix}.$$

In higher orders of Λ^{d} created by the Dyson Eq. (5.12), no further **DC** errors appear. Fortunately, all the double counting problems are not present for the **effective interaction**. The two-point form leads to a lowest order contribution which is a ‘‘lying object’’, of the form $\delta_{12}\delta_{34}[f_{zz}^{\text{xc}}\chi_{zz}f_{zz}^{\text{xc}}](13)$ and not a ‘‘standing’’ Coulomb interaction $\frac{\delta\Sigma^{(1)}(12)}{\delta G(34)} = \delta_{13}\delta_{24}v(12)$ as in the diagrammatic expansion. This avoids the double counting errors shown in Fig. 5.16. Also the double counting problems in the direct part (Fig. 5.17) are not possible for a two-point function. The **DC** errors appearing in the anomalous part of $\bar{\Sigma}^{\text{T}}$ are avoided because the parts of the effective interaction which contains Coulomb contribution ($f_{00}^{\text{xc}}P_{00}f_{00}^{\text{xc}}$) have been neglected.

In the rewriting of the self-energy given in Eq. (5.26) only the particle-hole propagator is included. The response functions introduced in Sec. 2.2 is based on the particle-hole contributions, so the excitations due to external electric and magnetic fields are included. On the other hand, this means all the particle-particle contributions are entirely neglected in the approximation. A detailed discussion of the particle-particle and particle-hole contributions on the T -matrix level is given in Ref. [104].

However, the fluctuations in the particle-particle channel may become relevant for a pairing mechanism in some systems. The particle-particle analogon to the T -matrix is given by:

$$T_{\text{pp}}(1234) = -\delta_{12}\delta_{34}w(13) - \Lambda d5d6w(12)G^{\text{KS}}(15)G^{\text{KS}}(26)T(5634).$$

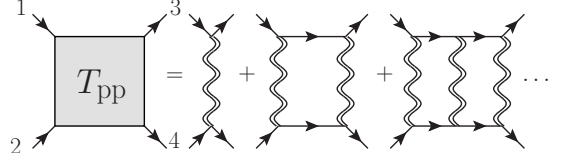


Figure 5.18.: Particle-particle variant of the T -matrix.

It is possible to create two normal self-energy contribution Σ_A and Σ_B by the particle-particle T -matrix shown in Fig. 5.19. The first one contains a Fermionic loop leading to a minus sign:

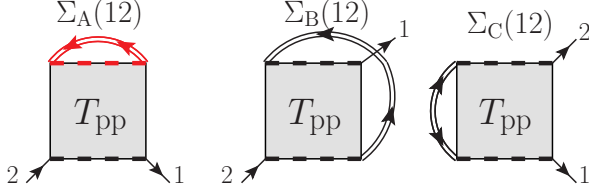


Figure 5.19.: Self-energy corresponding to T_{pp} .

$$\Sigma_A(12) = -\Lambda d3d4T_{\text{pp}}(3214)G(34)$$

$$\Sigma_B(12) = \Lambda d3d3T_{\text{pp}}(3241)G(34).$$

For both contributions, double counting errors of the type discussed in Fig. 5.16 appear. The anomalous part of the self-energy related to T_{pp} has only a single contribution given by:

$$\Sigma_C(12) = \Lambda d3d4T_{\text{pp}}(3412)F(34).$$

Note that a systematic inclusion of the [particle-particle propagator](#) beyond the T_{pp} contribution is not possible. The reason is the lack of an expression for the irreducible particle-particle propagator in terms of $\bar{\Sigma}$ which is present for the [irreducible particle-hole propagator](#) $\Lambda_0 = \frac{\delta\Sigma}{\delta G}$. Only the screened Coulomb interaction w and G within T_{pp} could be updated in a self-consistent treatment, but this will not create all possible particle-particle contributions.

3.) Reduction to Two-Point Function

Eventually, the particle-hole propagator is approximated by an [effective interaction](#). This approximation seems very severe in the first place. However, the resulting effective interaction given in Eq. (5.41) has a very physical or intuitive form: $f^{\text{xc}}\chi f^{\text{xc}}$. Like in the case of the screened Coulomb interaction ($-w = -v + v\chi_0v$) the fluctuations enter explicitly via the corresponding [response function](#) [Eq. (4.17)]. The coupling to the fluctuations is done by the [XC-kernel](#) which is the derivative of the [XC-magnetic field](#) with respect to the magnetization [Eq. (5.19)].

This leads to the following coupling mechanism in complete analogy to the Coulomb screening: A propagating electron creates a change in the magnetic density $\delta\mathbf{m}$ due to its spin. The change leads to a change in the magnetic field via the kernel. The field creates large fluctuations, if the response function is peaked for the corresponding field symmetry. These fluctuations then couple to another propagating electron via the second kernel. This coupling becomes strong if the response function features large excitations and the coupling to the electronic system given by the [XC-kernel](#) is large.

In the derivation of the effective interaction, the full [GF](#) has been approximated by the [KS](#) one, *i.e.* $G(12)G(21) \approx G^{\text{KS}}(12)G^{\text{KS}}(21)$. Nevertheless, the final effective interaction contains the full response function. This is a feature of [LRDFT](#) which reproduces the exact response with an [RPA](#) like equation starting from the [KS](#) response: $\chi_{\text{KS}}(12) = -G^{\text{KS}}(12)G^{\text{KS}}(21)$ [Eq. (5.17)]. So in the end also response functions calculated using [MBPT](#) involving the full [GF](#) may be used in the construction of the effective interaction [Eqs. (B.19)].

5.4.2. Comparison with other Effective Interactions

The derivation of the [effective interaction](#) in this work is based on a local approximation of the self-energy [Eq. 5.30] within the formally exact Hedin equations. In the literature, various ways of deriving

effective interactions or two-point scattering amplitudes are found. The ancestor of all the interactions is most likely the interaction proposed by Berk and Schrieffer [19]. In this interaction the charge (bubble diagrams) and magnetic fluctuations (ladder diagrams) are merged to one interaction. It was designed to treat systems close to a Stoner instability where $U\chi_0 \approx 1$ and U is a local Hubbard like Coulomb matrix element between electrons with opposite spin.

Effective interactions suited for a more general purpose are presented in [105, 106, 87]. Some of the results are comparable (almost identical) to the one presented in Eqs. (5.40) and (5.41). All the different approaches have in common that:

- many-body effects are responsible for a spin dependence of the interaction and
- a local approximation is used.

In the end, all approaches also lead to a form like: coupling \times Fluctuation \times coupling. The charge and magnetic fluctuations are represented either by the response function or a bosonic propagator. For a practical application, the response function is the more convenient object because the extraction of **quasi particle (QP)** energies and lifetimes is not necessary. Although being very similar regarding the form, the derivations of the effective interactions are very different. They follow physical intuition (1), a reformulation of the initial problem (2) or a diagrammatic expansion in the **homogenous electron gas (HEG)** (3).

1. In their work Kukkonen and Overhauser [105] derive an effective interaction between indistinguishable particles. The derivation is **not** based on diagrammatic techniques so the inclusion of the presented effective interaction in the self-energy is not obvious. However, the physical picture is very intuitive. If you bring two test charges e_1^- and e_2^- into the system, they will interact via the bare Coulomb interaction v and via scattering processes in the medium. This processes are given by $v\chi_{00}v$, which is found by the following considerations: The charge e_1^- is related to a potential $v_1 = ve_1^-$ which creates a change in the density of the system given by $\delta\rho = \chi_{00}v_1$. The change in the density is then seen by the other charge $e_2^- v\delta\rho = e_1^- [v\chi_{00}v] e_2^-$ (see top line of Fig 5.20). So the screened Coulomb interaction in the Hedin equation [Eq. (4.17)] is an interaction between test particles.

This picture changes, if instead of test particles, indistinguishable particles are considered. Around an electron with spin \uparrow at point (\mathbf{r}, t) the $\delta\rho_{\uparrow}$ and $\delta\rho_{\downarrow}$ are different due to correlation effects¹³. These many-body effects are taken into account by the so called “field factors” in the effective interaction of Kukkonen and Overhauser. The field factors are spin dependent, dynamic and local. They are the analogon to the **XC**-kernel in our approach. Kukkonen and Overhauser do not consider transverse magnetic fluctuation which allow for a spin-flip and also the inclusion of the effective interaction in the self-energy is not discussed.

2. Yarlagadda *et al.* derive an effective interaction following a different approach. The many-body Hamiltonian [Eq. (4.3)] is rewritten by dividing the electrons into two sets: (1) The electrons close to the **Fermi surface** and (2) the low-lying electrons creating macroscopic fluctuations in the medium [106]. The electrons close to the Fermi energy couple to the electronic fluctuations (bosons) in the medium. The coupling constants are defined *ad-hoc*. In analogy to the electron-phonon coupling, a canonical transformation is used to transform the interaction between fermions and bosons to an effective electron-electron interaction between electrons close to the Fermi energy.

This spin dependent effective interaction could be used in a perturbation expansion for the self-energy. Note that only the first order diagrams in the interaction are allowed due to the minimal coupling in the derivation. The final result is very similar to the effective interaction in this section. Also here no higher order contributions in the Λ^P appear. However in the presented derivation the coupling constants are defined much more rigorously and no separation in two sets of electrons is necessary.

¹³Correlation in this context means that the charge density around e_1^- is reduced due to Coulomb repulsion and the Pauli principle. The Pauli principle introduces the spin dependence of the change density.

3. Vignale and Singwi [87] use a diagrammatic approach to derive the scattering amplitude shown in Eqs. (5.11) and (5.12) for the non-magnetic HEG. The **irreducible particle-hole propagator** contains **direct** and exchange **crossed** terms (Fig. 5.5). The two contributions do not mix and hence the renormalization of $\frac{\delta\Sigma}{\delta G}$ can be done for the two channels separately. Before the renormalization is done, the function $\frac{\delta\Sigma}{\delta G}$ is approximated by a function \tilde{I} related to the **local field factor** or in our approach the **XC-kernel**.

The final result is equivalent to the effective interaction for a non-magnetic system presented in Eqs. (5.41). However, the inclusion of this interaction in the self-energy and the double counting corrections/errors are not considered in their work.

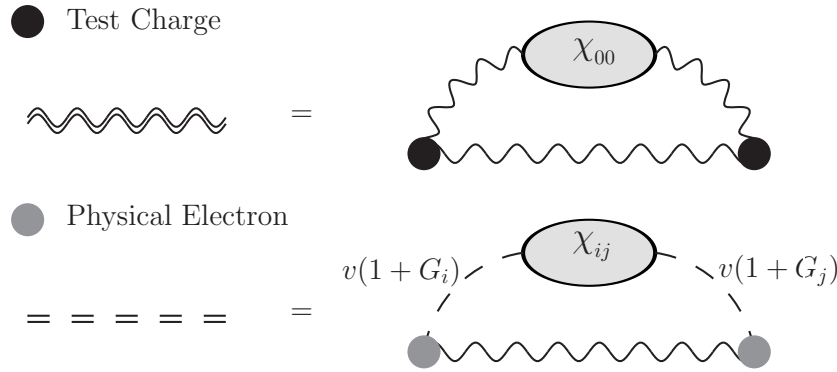


Figure 5.20.: Difference of an interaction between test particles and “physical electrons”. The function $G_i(\mathbf{q}\omega)$ is the local field factor taking care of the many-body effects. The label G is used for historical reasons and the function has nothing to do with the electronic Green’s function.

5.5. The Question of Self-Consistency

Up to now, the **Hedin equations** have been investigated in order to find an approximation to the self-energy containing **SF**. This self-energy will be used in the **SSEq** to construct an approximation for the **pairing potential** Δ_{xc} (see Sec. 4.4). The initial Hedin equations are an exact self-consistent set of equations. Exact means that a fully self-consistent solution converges to the exact Green’s function. The question of convergence and uniqueness of the result is non-trivial and not considered here. At least for limiting cases (weakly interacting limit in the Gw approximation) it can be shown that the cycle converges (a fixpoint is present) and the result is unique (there is only one fixpoint) [79].

The change of the exact expression [Eq. (4.14)] to the expression displayed in Eq. (5.26) was mainly done to avoid a self-consistent treatment of the Hedin equations and still get a self-energy which contains the magnetic fluctuations. This “non-self-consistency” is indicated in Fig. 5.21 by the open cycle ending at either the **SSEq** (**SCDFT** calculation) or the Dyson equation for the normal part of the Green’s function (correction of single particle spectrum). However, one could ask the question to what extent a self-consistent treatment is still possible with the approximated **self-energy**.

- A self-consistent treatment using “ Gw ” is feasible. Recently such calculations have been reported for molecules and solids [107, 108]. The standard Gw approximation for the self-energy has been extended by a term including magnetic excitations: $\Sigma = (w + \Lambda^{\text{SF}})G$. The interactions $w = v + v\chi_{00}v = v \frac{1-f_{00}^{\text{xc}}}{1-(f_{00}^{\text{xc}}+v)\chi^{\text{KS}}}$, $\Lambda^{\text{SF}} = -2f_{zz}^{\text{xc}}\chi_{zz}^{\text{KS}}f_{zz}^{\text{xc}} = -\frac{2f_{zz}^{\text{xc}}\chi^{\text{KS}}f_{zz}^{\text{xc}}}{1-f_{zz}^{\text{xc}}\chi^{\text{KS}}}$ and non-interacting response χ^{KS} are functionals of the density and it is possible to update them with new densities, related to the G in each iteration process. However, the **XC-functional** remains the same in this approach and the functional should describe the excitations (charge and spin) in the system properly. In chapter 7 it is shown for the **FeSC** that already simple approximations like **LDA** lead to reasonable results for the magnetic response function.

- Updating the **XC**-kernel itself is more difficult. The updating must somehow recover the functional derivative $\frac{\delta \Sigma}{\delta G}$ in the vertex, where all diagrams are created from cycle to cycle. The **SSEq** [Eq. (4.21)] can be used directly to construct an **XC**-potential related to a self-energy, *i.e.* update the potential properly, not only evaluating at a changed density. However, the result of the **SSEq** provides only the **XC**-potential and not the functional dependence $v^{\text{xc}} = v^{\text{xc}}[\rho]$ which is needed to calculate the **XC**-kernel. The calculation of the kernel would require a set of self-energies $\{\Sigma_1, \Sigma_2, \dots\}$. This set corresponds to densities $\{\rho_1, \rho_2, \dots\}$ and with the **SSEq** the corresponding potentials $\{v^{\text{xc}}[\rho_1], v^{\text{xc}}[\rho_2], \dots\}$ are found. With this information the derivative $\frac{\delta v^{\text{xc}}}{\delta \rho}$ can be calculated, but this is a very demanding task (see “difficult connection” in Fig. 5.21). Alternatively a closed expression for f^{xc} exists within the linearized Sham-Schlüter equation [109]. Note that even such a treatment would not lead to the exact **XC**-kernel. The reason for this lies in the approximated self-energy: Only the exact expression will lead to the exact Green’s function which leads to the exact density and due to the 1:1 correspondence (Sec. 3.1) to the exact **XC**-potential and **XC**-kernel.

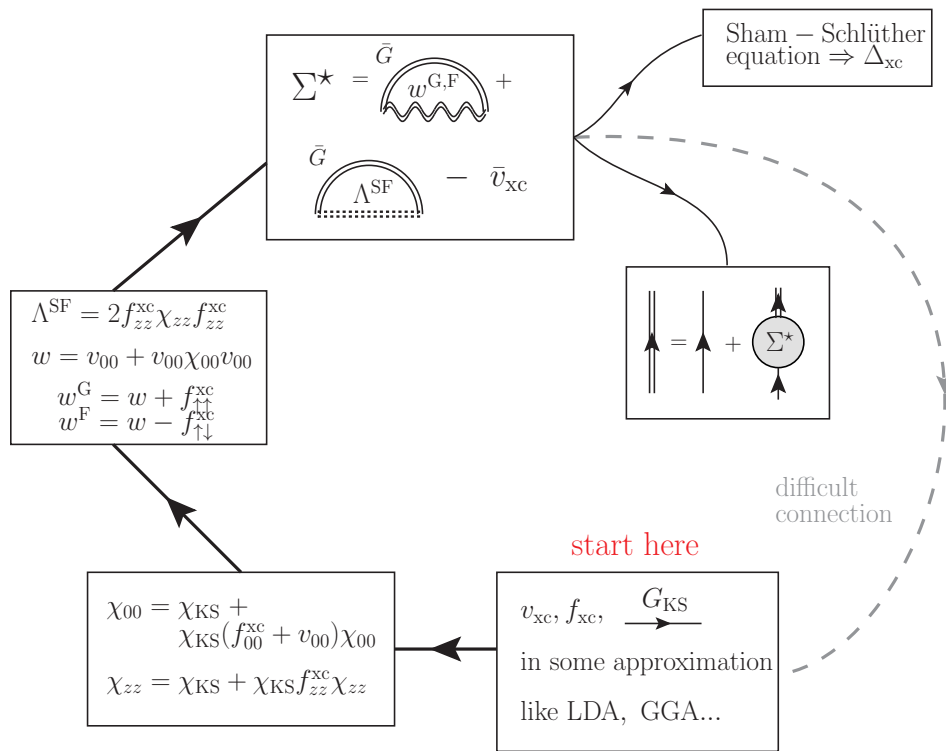


Figure 5.21.: Approximated Hedin cycle for a **NM** system applying the approximation shown in Fig. 5.13. The self-energy contains the well known Gw term and an additional term representing the magnetic fluctuations. The latter contribution originates from vertex corrections and contains the effective interaction given in Eq. (5.44). The change of the exact self-energy containing the vertex function was necessary in order to include the magnetic fluctuations within one cycle of the Hedin equations. Due to this rewriting the loop may end after one iteration in the **SSEq** leading to an approximation for Δ^{xc} .

5.6. Summary

In this chapter the exact expression for the electronic self-energy provided by the Hedin equations for superconductors has been rewritten. This step was necessary because a treatment of the exact equations is not feasible. The derivation is based on **MBPT** and involves several approximations (Sec. 5.4.1) of which the assumption in Eq. (5.22) is the least obvious one. The final result is a self-energy containing two separate terms:

1. The well known Gw contribution [Eq. (5.45)]. This term includes the charge fluctuations and screened Coulomb interaction.
2. An additional term originating from vertex corrections [Eq. (5.43)]. This term contains the magnetic response function and is of the same complexity like the Gw term. The (magnetic) response function can be calculated very efficiently using LRDFE and it is possible to compute the new self-energy contribution for real materials.

The equations have been derived allowing for a collinear magnetic state, but the special case of a non-magnetic system will be the relevant one in the context of SC. In the next chapter the proposed self-energy will be used to construct a SCDFE functional using the Sham-Schlüter connection.

6. The SCDFE Functional Containing Spin-Fluctuations

This chapter consists of two parts. In the first part (Sec. 6.1), the functional containing the SF is constructed. The starting point for the derivation is the approximation to the self-energy (Fig. 6.1) which contains the effective interaction mediated by paramagnons, the screened Coulomb interaction and the phononic contribution [Eqs. (5.41), (5.48) and (6.8)]. This self-energy is then used in the SSEq discussed in Sec. 4.4 to construct a functional $\Delta^{\text{xc}} = \Delta^{\text{xc}}[\rho, \chi]$. One advantage of SCDFE is that the involved Matsubara summation can be worked out analytically. The derivation is in analogy to the previous derivations containing only the Coulomb and phonon term in the work of A. Sanna [110]. The final result is a gap equation shown at the end of Sec. 6.1, where the magnetic fluctuations simply appear as an extra term in the gap equation compared to the old framework [110].

In the second part of the chapter (from Sec. 6.2 on), numerical tests with the new functional are performed. Since the interaction created by the magnetic fluctuations is strictly repulsive, a multi-band system with changing sign of the gap function is necessary to find a superconducting solution. The different form of the phonon, Coulomb and magnetic contribution in momentum space, lead to interesting differences in how the three contributions affect the critical temperature and the shape of the gap function. In the next chapter the functional is applied to the FeSC.

6.1. Construction of the Functional

The XC-potential is constructed starting from the SSEq [Eqs. (4.21)]. The standard phonon terms are left out in the discussion for simplicity and but will be put back in the end. Without the phonon part the SSEq reads:

$$0 = \frac{1}{\beta} \sum_{\omega_n} e^{i\omega_n 0^+} \bar{G}^{\text{KS}} [\bar{\Sigma} - \bar{v}^{\text{xc}}] \bar{G} = \sum_{\omega_n} e^{i\omega_n 0^+} \bar{G}^{\text{KS}} [(\bar{\Sigma}^{\text{SF}} + \bar{\Sigma}^{\text{CF}}) - \bar{v}^{\text{xc}}] \bar{G}.$$

For a NM system the contributions to the self-energy and XC-potential reduce to [Eqs. (5.43) and appendix D]:

$$\begin{aligned} \bar{\Sigma} - \bar{v}^{\text{xc}} := \Sigma^* = \tau^z & \begin{pmatrix} \delta_{\sigma_1\sigma_2} [a_{\mathcal{D}}\Lambda^{\text{SF}} - w^{\text{G}}] G^{\text{KS}} & -\delta_{-\sigma_1\sigma_2} [w^{\text{F}} + a_{\mathcal{C}}\Lambda^{\text{SF}}] F^{\text{KS}} \\ -\delta_{-\sigma_1\sigma_2} [w^{\text{F}} + a_{\mathcal{C}}\Lambda^{\text{SF}}] F^{\text{KS}\dagger} & \delta_{\sigma_1\sigma_2} [a_{\mathcal{D}}\Lambda^{\text{SF}} - w^{\text{G}}] G^{\text{KS}\dagger} \end{pmatrix} \\ & - \begin{pmatrix} \delta_{\sigma_1\sigma_2} v^{\text{xc}} & \delta_{-\sigma_1\sigma_2} \Delta^{\text{xc}*} \\ \delta_{-\sigma_1\sigma_2} \Delta^{\text{xc}} & \delta_{\sigma_1\sigma_2} v^{\text{xc}} \end{pmatrix}. \end{aligned} \quad (6.1)$$

The $a_{\mathcal{C}}$ and $a_{\mathcal{D}}$ are $\frac{3}{2}$, but it is easier to keep track of the various factors of $\frac{1}{2}, \pi$, *ect.*, if symbols are used. In order to invert the SSEq for the XC-potential, two approximations are necessary: (1) The full Green's function on the right hand side is approximated with the non-interacting one and (2) the contribution $\bar{\Sigma}_{ii}^{\text{CF}} - \bar{v}_{ii}^{\text{xc}}$ is neglected. The first approximation is known as linearization of the Sham-Schlüter equation and is found by requiring a stationary Klein functional with respect to the GF [109]. The second approximation is motivated by the fact that the Gw and XC-potential both add correlation effects to the Hartree system. This argumentation has been suggested by A. Sanna [110] and is much more transparent than the transformation given by M. Marques, in which a constant v^{xc} in Bloch representation is assumed [73]. Applying these approximations, the SSEq contains only known quantities and can be inverted to obtain the Δ^{xc} . The 12 component of the equation related to

the anomalous density [Eq. (4.23)] is used for this step:

$$\begin{aligned}
 0 &= \frac{1}{\beta} \sum_{\omega_n} \sum_{\sigma_3 \sigma_4} e^{i\omega_n 0^+} \Lambda d^3 r_3 d^3 r_4 \left[\bar{G}_{\uparrow\sigma_3}^{\text{KS}}(\mathbf{r}_1 \mathbf{r}_3 \omega_n) \bar{\Sigma}_{\sigma_3 \sigma_4}^* (\mathbf{r}_3 \mathbf{r}_4 \omega_n) \bar{G}_{\sigma_4 \downarrow}^{\text{KS}}(\mathbf{r}_4 \mathbf{r}_2 \omega_n) \right]_{12} \\
 &= \frac{1}{\beta} \sum_{\omega_n} \sum_{\sigma_3 \sigma_4} e^{i\omega_n 0^+} \left[G_{\uparrow\sigma_3}^{\text{KS}} \bar{\Sigma}_{\sigma_3 \sigma_4}^{11} F_{\sigma_4 \downarrow}^{\text{KS}} + F_{\uparrow\sigma_3}^{\text{KS}} (\bar{\Sigma}_{\sigma_3 \sigma_4}^{21} - \delta_{\sigma_3 - \sigma_4} \Delta^{\text{xc}}) F_{\sigma_4 \downarrow}^{\text{KS}} \right. \\
 &\quad \left. - G_{\uparrow\sigma_3}^{\text{KS}} (\bar{\Sigma}_{\sigma_3 \sigma_4}^{12} - \delta_{\sigma_3 - \sigma_4} \Delta^{\text{xc}*}) G_{\sigma_4 \downarrow}^{\text{KS}\dagger} - F_{\uparrow\sigma_3}^{\text{KS}} \bar{\Sigma}_{\sigma_3 \sigma_4}^{22} G_{\sigma_4 \downarrow}^{\text{KS}\dagger} \right] \\
 &= \frac{1}{\beta} \sum_{\omega_n} e^{i\omega_n 0^+} \left[G^{\text{KS}} \bar{\Sigma}_{\uparrow\uparrow}^{11} F^{\text{KS}} + F^{\text{KS}} (\bar{\Sigma}_{\downarrow\downarrow}^{21} - \Delta^{\text{xc}}) F^{\text{KS}} - G^{\text{KS}} (\bar{\Sigma}_{\uparrow\downarrow}^{12} - \Delta^{\text{xc}*}) G^{\text{KS}\dagger} - F^{\text{KS}} \bar{\Sigma}_{\downarrow\downarrow}^{22} G^{\text{KS}\dagger} \right].
 \end{aligned}$$

As a further approximation all terms higher than linear order in the gap are neglected. At this point only explicit orders of Δ_k are counted and the contribution related to $E_k^\pm = \pm \sqrt{\zeta_k^2 + |\Delta_k|^2}$ in Eq. (C.22) are not considered. This approach is useful in the derivation of a partially linearized gap equation. Since the anomalous Green's function [Eq. (C.22)] contains only linear and higher orders in Δ , all terms like $F^{\text{KS}} \bar{\Sigma}_{\downarrow\uparrow}^{21} F^{\text{KS}}$ are neglected:

$$0 = \frac{1}{\beta} \sum_{\omega_n} e^{i\omega_n 0^+} \left[G^{\text{KS}} \bar{\Sigma}_{\uparrow\uparrow}^{11} F^{\text{KS}} - F^{\text{KS}} \bar{\Sigma}_{\downarrow\downarrow}^{22} G^{\text{KS}\dagger} - G^{\text{KS}} \bar{\Sigma}_{\uparrow\downarrow}^{12} G^{\text{KS}\dagger} \right] + \sum_{\omega_n} e^{i\omega_n 0^+} G^{\text{KS}} \Delta^{\text{xc}*} G^{\text{KS}\dagger}.$$

For a solid state application a transformation to a representation in **Bloch states** is advantageous. As discussed in Sec. 3.2.2 the equations are transformed using the orbitals of the non-superconducting **KS** system as basis functions. The transformation rules given in Eq. (C.19) are used to transform the Green's functions:

$$\begin{aligned}
 0 &= \frac{1}{\beta} \sum_{\omega_n} e^{i\omega_n 0^+} \left[G^{\text{KS}} \bar{\Sigma}_{\uparrow\uparrow}^{11} F^{\text{KS}} - F^{\text{KS}} \bar{\Sigma}_{\downarrow\downarrow}^{22} G^{\text{KS}\dagger} - G^{\text{KS}} \bar{\Sigma}_{\uparrow\downarrow}^{12} G^{\text{KS}\dagger} \right] \\
 &\quad + \frac{1}{\beta} \sum_{k_1 k_2} \sum_{\omega_n} e^{i\omega_n 0^+} \psi_{k_1}(\mathbf{r}_1) G^{\text{KS}}(k_1 \omega_n) \Delta_{k_1 k_2}^{\text{xc}*} G^{\text{KS}\dagger}(k_2 \omega_n) \psi_{k_2}^*(\mathbf{r}_2).
 \end{aligned}$$

The gap $\Delta_{k_1 k_2}^{\text{xc}}$ is assumed to be diagonal with respect to k_1 and k_2 in the **decoupling approximation** (chapter 3). Hence, it is sufficient to obtain the $k_1 = k_2$ contribution from the **SSEq**. The element is selected by multiplying from left and right with the operators $\Delta d^3 r_1 \psi_k^*(\mathbf{r}_1)$ and $\Delta d^3 r \psi_k(\mathbf{r}_2)$, respectively:

$$\begin{aligned}
 - \sum_{\omega_n} e^{i\omega_n 0^+} G^{\text{KS}} G^{\text{KS}\dagger} \Delta_k^{\text{xc}*}(k) &= \sum_{\omega_n} e^{i\omega_n 0^+} \left[G^{\text{KS}}(k \omega_n) \bar{\Sigma}_{\uparrow\uparrow}^{11}(k \omega_n) - G^{\text{KS}\dagger}(k \omega_n) \bar{\Sigma}_{\downarrow\downarrow}^{22}(k \omega_n) \right] F^{\text{KS}}(k \omega_n) \\
 &\quad - \sum_{\omega_n} e^{i\omega_n 0^+} G^{\text{KS}}(k \omega_n) \bar{\Sigma}_{\uparrow\downarrow}^{12}(k \omega_n) G^{\text{KS}\dagger}(k \omega_n).
 \end{aligned} \tag{6.2}$$

The first two terms related to $\bar{\Sigma}_{\uparrow\uparrow}^{11}$ and $\bar{\Sigma}_{\downarrow\downarrow}^{22}$ lead to identical contributions [see Eq. (E.10)]:

$$\begin{aligned}
 - \frac{1}{\beta} \sum_{\omega_n} e^{i\omega_n 0^+} G^{\text{KS}} G^{\text{KS}\dagger} \Delta_k^{\text{xc}*} &= 2 \frac{1}{\beta} \sum_{\omega_n} e^{i\omega_n 0^+} G^{\text{KS}}(k \omega_n) \bar{\Sigma}_{\uparrow\uparrow}^{11}(k \omega_n) F^{\text{KS}}(k \omega_n) \\
 &\quad - \frac{1}{\beta} \sum_{\omega_n} e^{i\omega_n 0^+} G^{\text{KS}}(k \omega_n) \bar{\Sigma}_{\uparrow\downarrow}^{12}(k \omega_n) G^{\text{KS}\dagger}(k \omega_n).
 \end{aligned}$$

6.1.1. Evaluation of Matsubara Summation

The frequency sum $\frac{1}{\beta} \sum_{\omega_n} e^{i\omega_n 0^+} G^{\text{KS}}(k\omega_n) G^{\text{KS}\dagger}(k\omega_n)$ on the left hand side, is evaluated in the Appendix [Eq. (E.3)]. The resulting hyperbolic tangent is brought to the right hand side of the equation:

$$\begin{aligned} \Delta_k^{\text{xc}*} &= -\frac{4E_k}{\tanh\left(\frac{\beta E_k}{2}\right)} \frac{1}{\beta} \sum_{\omega_n} e^{i\omega_n 0^+} G^{\text{KS}}(k\omega_n) \bar{\Sigma}_{\uparrow\uparrow}^{11}(k\omega_n) F^{\text{KS}}(k\omega_n) \\ &\quad + \frac{2E_k}{\tanh\left(\frac{\beta E_k}{2}\right)} \frac{1}{\beta} \sum_{\omega_n} e^{i\omega_n 0^+} G^{\text{KS}}(k\omega_n) \bar{\Sigma}_{\uparrow\downarrow}^{12}(k\omega_n) G^{\text{KS}\dagger}(k\omega_n). \end{aligned}$$

This expression describes Δ^{xc} in terms of interaction matrix elements (w, Λ^{SF}) and the KS Green's function. Since the GFs are determined by the solution of the KS-BdG equation [Eqs. (3.26) and (C.18)] this expression is a functional:

$$\Delta_k^{\text{xc}} = \Delta_k^{\text{xc}} [\{u_l, v_l, E_l\}]$$

and can be used in a self-consistent calculation of the KS-BdG equation given in Eq. (3.25). This functional is **not** an explicit functional of the electronic density like the LDA or GGA [96, 97]. However, XC-functionals depending on orbitals are well known from the optimized effective potential (OEP) approach [111].

In SCDFT the summation with respect to the Matsubara frequencies can be worked out analytically using the residue theorem. This is one of the main advantages of SCDFT as compared to the Eliashberg theory. In exchange for the analytic evaluation of the double Matsubara sum a single frequency integral on the real frequency axis appears. The appearing retarded quantity on the real axis will have some features at finite energy and the frequency integrals will converge quickly (Fig. 7.12a). The details and the lengthy algebra of this rewriting are shown in Sec. E.1. The final results for the term $G^{\text{KS}} \Sigma_{11} F^{\text{KS}}$ and $G^{\text{KS}} \Sigma_{12} G^{\text{KS}}$ lead to [Eqs. (E.11) and (E.15)]:

$$\begin{aligned} \Delta_k^{\text{xc}*} &= -\frac{\Delta_k^{\text{xc}*}}{\pi \tanh\left(\frac{\beta E_k}{2}\right)} \sum_{k'} \Delta_0^\infty d\omega \Im [a_{\mathcal{D}} \Lambda_{kk'}^{\text{SF}}(\omega)] \times \\ &\quad \left(\left[\frac{\zeta_k}{E_k} + \frac{\zeta_{k'}}{E_{k'}} \right] I'(E_k E_{k'} \omega) + \left[\frac{\zeta_k}{E_k} - \frac{\zeta_{k'}}{E_{k'}} \right] I'(E_k - E_{k'} \omega) - \zeta_k \frac{I(E_k E_{k'} \omega) - I(E_k - E_{k'} \omega)}{E_k^2} \right) \\ &\quad + \frac{1}{\pi \tanh\left(\frac{\beta E_k}{2}\right)} \sum_{k'} \Delta_0^\infty d\omega \frac{\Im [-w_{kk'}^{\text{F}}(\omega) - a_{\mathcal{D}} \Lambda_{kk'}^{\text{SF}}(\omega)]}{E_{k'}} \times \\ &\quad [I_\beta(E_k E_{k'} \omega) - I_\beta(E_k - E_{k'} \omega)] \Delta_k^{\text{xc}*}. \end{aligned} \quad (6.3)$$

The convenient result that the SF interaction Λ_{zz}^{SF} enters with the same functions I as the phonons is related to the adiabatic approximation to the XC-kernel which does not add extra residues in the expression [Eq. (E.9)]. The functions $I(E_k E_{k'} \omega)$ and $I'(E_k E_{k'} \omega)$ are defined as [Eq. (E.5)]:

$$I_\beta(E_k, E_{k'} \omega) := -f_\beta(E_k) f_\beta(E_{k'}) b_\beta(\omega) \left[\frac{e^{\beta E_k} - e^{\beta(E_{k'} + \omega)}}{E_k - E_{k'} - \omega} - \frac{e^{\beta E_{k'}} - e^{\beta(E_k + \omega)}}{E_k - E_{k'} + \omega} \right] \quad (6.4)$$

$$I'_\beta(E_k, E_{k'} \omega) := \frac{\partial}{\partial E_k} I_\beta(E_k, E_{k'} \omega). \quad (6.5)$$

The expression can be written in the form of a BCS like gap equation:

$$\Delta_k^{\text{xc}*} = -Z_k^{\text{D}} \Delta_k^{\text{xc}*} - \sum_{kk'} \mathcal{K}_{kk'}^{\text{C}} \frac{\tanh\left(\frac{\beta E_{k'}}{2}\right)}{2E_{k'}} \Delta_{k'}^{\text{xc}*}.$$

The kernels \mathcal{K}_k^{D} (*D-term*) and $\mathcal{K}_{kk'}^{\text{C}}$ (*C-term*) are found by comparison with Eq. (6.3). The kernels are linearized, *i.e.* $E_k = \zeta_k$, but the hyperbolic function in the gap equation is still evaluated at E_k . This

is the well known partial linearization of the gap equation [27, 110]. This linearization ensures that the relevant nonlinear contributions are those of BCS type. The linearization greatly simplifies the (D) term:

$$\begin{aligned}\Delta_k^{\text{xc}*} &= -\Delta_k^{\text{xc}*} Z_k^D - \sum_{kk'} \mathcal{K}_{kk'}^C \frac{\tanh\left(\frac{\beta E_{k'}}{2}\right)}{2E_{k'}} \Delta_{k'}^{\text{xc}*} \\ Z_k^D &= \Delta_0^\infty d\omega \frac{\Im [a_{\mathcal{D}} \Lambda_{kk'}^{\text{SF}}(\omega)]}{\pi \tanh\left(\frac{\beta \zeta_k}{2}\right)} \sum_{k'} \left[2I'(\zeta_k \zeta_{k'} \omega) - \frac{1}{\zeta_k} (I(\zeta_k \zeta_{k'} \omega) - I(\zeta_k - \zeta_{k'} \omega)) \right] \\ \mathcal{K}_{kk'}^C &= \Delta_0^\infty d\omega \frac{2\Im [w_{kk'}^F(\omega) + a_{\mathcal{C}} \Lambda_{kk'}^{\text{SF}}(\omega)]}{\pi \tanh\left(\frac{\beta \zeta_k}{2}\right) \tanh\left(\frac{\beta \zeta_{k'}}{2}\right)} [I_\beta(\zeta_k \zeta_{k'} \omega) - I_\beta(\zeta_k - \zeta_{k'} \omega)].\end{aligned}\quad (6.6)$$

The kernels are real functions and the complex conjugation of the gap function is left out from now on in the gap equation. Also in this form the equation can be understood as a functional because the gap can be expressed in terms of the particle and hole amplitudes and the eigenvalues [Eq. (3.26)]:

$$\frac{u_l v_l^*}{2E_l} = \frac{\text{sgn}[E_l]}{E_l} \frac{\Delta_l^{\text{KS}}}{|\Delta_l^{\text{KS}}|} \left[1 - \frac{(\varepsilon_l - \mu)^2}{E_l^2} \right]^{\frac{1}{2}} = \frac{\Delta_l^{\text{KS}} |E_l|}{|\Delta_l^{\text{KS}}|} \left[\frac{|\Delta_l^{\text{KS}}|^2}{E_l^2} \right]^{\frac{1}{2}} = \Delta_l^{\text{ext}} + \Delta_l^{\text{xc}}. \quad (6.7)$$

However, one can directly iterate the gap equation for various temperatures. The phase transition is found by the condition $\Delta(T_c) \neq 0$ because all the anomalous terms are linear and higher order in the gap.

6.1.2. Inclusion of Phonons

The difference in the gap equation compared to the work of A. Sanna [110], is the absence of the phonon contributions and of course the new terms related to the SF. The phonons have been left out for simplicity, but are easily added to the equation now. The frequency dependence of the free phonon propagator is known (see Sec. 3.3):

$$\begin{aligned}D_{\lambda_1 \mathbf{q}_1 \lambda_2 \mathbf{q}_2}(\omega_n) &= \left\langle \hat{T} \left[\hat{\Phi}_{\lambda_1 \mathbf{q}_1}(\tau_1) \hat{\Phi}_{\lambda_2 \mathbf{q}_2}(\tau_2) \right] \right\rangle_{\omega_m} - \left\langle \hat{\Phi}_{\lambda_1 \mathbf{q}_1} \right\rangle \left\langle \hat{\Phi}_{\lambda_2 \mathbf{q}_2} \right\rangle \\ &= -\delta_{\lambda_1 \lambda_2} \delta_{\mathbf{q}_1 \mathbf{q}_2} \Delta_0^\infty d\omega \frac{2\omega}{\omega_n^2 + \omega^2} \delta(\omega - \Omega_{\lambda_1 \mathbf{q}_1}) := \delta_{\lambda_1 \lambda_2} \delta_{\mathbf{q}_1 \mathbf{q}_2} D_{\lambda_1 \mathbf{q}_1}(\omega_n).\end{aligned}$$

The term $\left\langle \hat{\Phi}_{\lambda_1 \mathbf{q}_1} \right\rangle \left\langle \hat{\Phi}_{\lambda_2 \mathbf{q}_2} \right\rangle$ is useful in the equations of motion for the full phonon propagator [76]. The contraction of two electron-phonon coupling terms [Eq. (3.29)] leads to an effective interaction mediated by the phonons:

$$\Lambda_{kk'}^{\text{Ph}}(\omega_n) = \sum_{\lambda \mathbf{q}} \left| g_{\lambda \mathbf{q}}^{kk'} \right|^2 D_{\lambda \mathbf{q}}(\omega_n) = \frac{1}{\pi} \Delta_0^\infty d\omega \frac{2\omega}{\omega_n^2 + \omega^2} \underbrace{\left[-\pi \sum_{\lambda \mathbf{q}} \left| g_{\lambda \mathbf{q}}^{kk'} \right|^2 \delta(\omega - \Omega_{\lambda \mathbf{q}}) \right]}_{:= \Lambda^{\text{Ph}}(kk' \omega)}. \quad (6.8)$$

The $g_{\lambda \mathbf{q}}^{kk'}$ are the electron-phonon coupling matrix elements and the interaction related to the phonons is attractive: $\Lambda^{\text{Ph}}(kk' \omega) < 0$. The interaction is identical for all components of the Green's function and it is simple to extend the self-energy given in Eq. (6.1) by a phonon term:

$$\bar{\Sigma} = \tau^z \begin{pmatrix} \delta_{\sigma_1 \sigma_2} a_{\mathcal{D}} \Lambda^{\text{SF}} G^{\text{KS}} & -\delta_{-\sigma_1 \sigma_2} [w^F + a_{\mathcal{C}} \Lambda^{\text{SF}}] F^{\text{KS}} \\ -\delta_{-\sigma_1 \sigma_2} [w^F + a_{\mathcal{C}} \Lambda^{\text{SF}}] F^{\text{KS}\dagger} & \delta_{\sigma_1 \sigma_2} a_{\mathcal{D}} \Lambda^{\text{SF}} G^{\text{KS}\dagger} \end{pmatrix} - \Lambda^{\text{Ph}} \bar{G}.$$

The analytic Matsubara summation leads also for the phonon contribution to the same function I [Eq. (E.4)]:

$$\begin{aligned}\Delta_k^{\text{xc}} &= -\Delta^{\text{xc}}(k) \mathcal{Z}_k^D - \sum_{k'} \mathcal{K}_{kk'}^C \frac{\tanh\left(\frac{\beta E_{k'}}{2}\right)}{2E_{k'}} \Delta_{k'}^{\text{xc}} \\ \mathcal{Z}_k^D &= \sum_{k'} \Delta_0^\infty d\omega \frac{\Im [a_D \Lambda_{kk'}^{\text{SF}}(\omega)] - \Lambda_{kk'}^{\text{Ph}}(\omega)}{\pi \tanh\left(\frac{\beta \zeta_k}{2}\right)} \times \\ &\quad \left[2I'_\beta(\zeta_k, \zeta_{k'}\omega) - \frac{1}{\zeta_k} (I_\beta(\zeta_k, \zeta_{k'}\omega) - I_\beta(\zeta_k - \zeta_{k'}\omega)) \right] \\ \mathcal{K}_{kk'}^C &= 2 \Delta_0^\infty d\omega \frac{\Im [w_{kk'}^F(\omega) + a_C \Lambda_{kk'}^{\text{SF}}(\omega)] + \Lambda_{kk'}^{\text{Ph}}(\omega)}{\pi \tanh\left(\frac{\beta \zeta_k}{2}\right) \tanh\left(\frac{\beta \zeta_{k'}}{2}\right)} [I_\beta(\zeta_k, \zeta_{k'}\omega) - I_\beta(\zeta_k, -\zeta_{k'}\omega)].\end{aligned}$$

In the work of M. Marques [73], two changes of the D -term are suggested: (1) A particle-hole symmetric form for $2I'_\beta - \frac{1}{\zeta_k} (I_\beta - I_\beta)$ is used (2) a factor of $\frac{1}{2}$ is introduced. The first change is necessary due to a divergence of the k' summation in the anti-symmetric part. The divergence appears only if k averaged interactions like an $\alpha^2 F$ [Eq. (6.15)] are used instead of the fully k dependent matrix elements. The second approximation is done because for the conventional superconductors the critical temperatures are systematically underestimated by SCDFT.

6.1.3. Final Expression

Applying these approximations, the gap equation reads:

$$\Delta_k^{\text{xc}} = -\Delta_k^{\text{xc}} \mathcal{Z}_k^D - \sum_{k'} \mathcal{K}_{kk'}^C \frac{\tanh\left(\frac{\beta E_{k'}}{2}\right)}{2E_{k'}} \Delta_{k'}^{\text{xc}} \quad (6.9)$$

$$\mathcal{Z}_k^D = \frac{1}{\pi} \sum_{k'} \Delta_0^\infty d\omega \frac{\Im [a_D \Lambda_{kk'}^{\text{SF}}(\omega)] - \Lambda_{kk'}^{\text{Ph}}(\omega)}{2 \tanh\left(\frac{\beta \zeta_k}{2}\right)} \frac{d}{d\zeta_k} J^+(\zeta_k, \zeta_{k'}\omega) \quad (6.10)$$

$$\mathcal{K}_{kk'}^C = \frac{2}{\pi} \Delta_0^\infty d\omega \frac{\Im [w_{kk'}^F(\omega) + a_C \Lambda_{kk'}^{\text{SF}}(\omega)] + \Lambda_{kk'}^{\text{Ph}}(\omega)}{\tanh\left(\frac{\beta \zeta_k}{2}\right) \tanh\left(\frac{\beta \zeta_{k'}}{2}\right)} J^-(\zeta_k, \zeta_{k'}\omega) \quad (6.11)$$

$$J_\beta^\pm(\zeta_k, \zeta_{k'}\omega) := I_\beta(\zeta_k, \zeta_{k'}\omega) \pm I_\beta(\zeta_k, -\zeta_{k'}\omega).$$

The contributions in the kernels \mathcal{Z}_k^D and $\mathcal{K}_{kk'}^C$ represent different physical processes due to bosonic QP in the system:

1. The $\Lambda_{kk'}^{\text{Ph}}(\omega)$ term describes pairing between electrons due to **phonons**. The interaction is attractive: $\Lambda_{kk'}^{\text{Ph}}(\omega) < 0$.
2. The $w_{kk'}^F(\omega)$ term is the scattering of electrons due to Coulomb interaction. The bare Coulomb interaction is reduced by intermediate scattering processes (screening) $w = v\epsilon^{-1}$ [Eq. (4.12)]. **Plasmons** may also enter via this term.
3. The last term $\Lambda_{kk'}^{\text{SF}}(\omega)$ contains basically the magnetic response function χ_{zz} and hence becomes important, if the system is close to a magnetic phase transition. In such a case the **response function** features sharp excitations which represent **paramagnons**.

The last two terms originate both from the bare Coulomb interaction and are **repulsive**¹⁴

$$\Im [\Lambda_{kk'}^{\text{SF}}(\omega)] > 0 \text{ and } \Im [w_{kk'}^F(\omega)] > 0$$

¹⁴This is not obvious and is a results for all k and k' in the calculation for the FeSC.

for $\omega > 0$ [the spectral function swaps sign at $\omega = 0$, see Eq. (B.8)]. The final result is very intuitive and includes the magnetic fluctuations with an explicit contribution on the same footing as the phonons and charge fluctuations. In the next section the solutions of the gap equation are discussed. In Fig. 6.1 the three contribution in the self-energy used in the construction of the Δ_k^{xc} are shown.

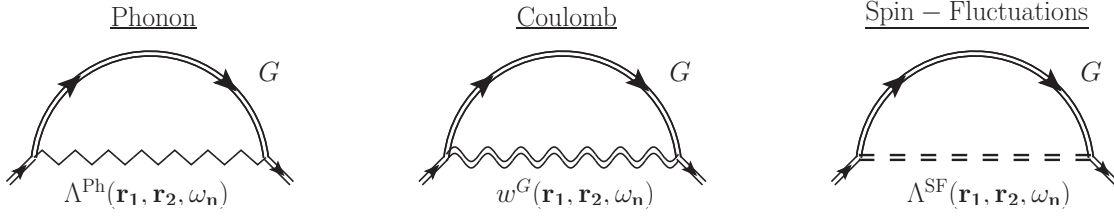


Figure 6.1.: Final approximation to the self-energy containing the phonon, Coulomb and SF contribution. The Λ^{Ph} , w and Λ^{SF} are given in Eq. (6.16), (5.48) and (5.44), respectively. The screened Coulomb and effective interaction are renormalized quantities which is indicated by a double line.

6.2. Discussion of the Gap Equation for two Bands

Before turning to calculations, it is instructive to analyze the solutions of the gap equation [Eq. (6.9)]. One possible solution is **always** the trivial solution ($\Delta_k \equiv 0$) which means the system is not superconducting. Any different solution will be highly peaked around the Fermi energy. The reasons for this behavior are: (1) scattering elements are largest for k and k' with similar band energies. Due to the Pauli principle scattering is possible from full \leftrightarrow empty states leading for low temperature to large scattering at the Fermi level and (2) the $\frac{1}{\tanh[x]}$ becomes large for small x *i.e.* $\epsilon_k - \mu$ close to zero. Whether or not a non-trivial solution is found depends on the topology of the Fermi surface (entering the function I in the gap equation) and the values of the interaction matrix elements.

In case a non-zero solution is found, two situations are possible: The gap Δ_k has the same symmetry like the underlying Fermi surface or it has a lower symmetry. These two disjunct cases lead to the most general definition of conventional and unconventional¹⁵ SC [16]:

Conventional SC are systems where the gap function at the Fermi level contains a global phase which is set to one *i.e.*: $\Delta_k = e^{i\phi} |\Delta_k| \stackrel{\text{gauge}}{=} |\Delta_k|$ with $k = k_{\text{F}}$.

Unconventional SC are systems where Δ_k at the Fermi level contains a k dependent phase: $\Delta_k = e^{i\phi(k)} |\Delta_k|$ with $k = k_{\text{F}}$.

Note that these definitions do not imply any kind of pairing mechanism. However, in the literature the terms conventional and unconventional are mostly used in a less strict way: In general all systems which are well described by a phononic pairing mechanism and moderate T_c are called conventional and the rest unconventional. Before the two types of superconductivity are discussed, it is necessary to investigate the signs of the functions appearing in the kernels \mathcal{Z}_k^D and $\mathcal{Z}_{kk'}^C$. For $\omega > 0$ and all E_k and β , the inequalities

$$\frac{I_\beta(E_k, E_{k'}, \omega) - I_\beta(E_k, -E_{k'}, \omega)}{\tanh\left(\frac{\beta E_k}{2}\right) \tanh\left(\frac{\beta E_{k'}}{2}\right)} \geq 0 \quad \frac{\tanh\left(\frac{\beta E_{k'}}{2}\right)}{2E_{k'}} \geq 0 \quad \frac{I'_\beta(\zeta_k, \zeta_{k'}, \omega) + I'_\beta(\zeta_k, -\zeta_{k'}, \omega)}{\tanh\left(\frac{\beta \zeta_k}{2}\right)} \geq 0$$

hold [see Eqs. (6.4) and (6.5) for the definitions of I and I']. Hence, the signs of the kernels are determined by the sign of the interactions. The phonon contributions are attractive, whereas the Coulomb and SF terms are repulsive. Strictly **positive** kernels $\mathcal{D}_k^{\text{Ph,SF,C}}$ and $\mathcal{C}_{kk'}^{\text{Ph,SF,C}}$ are introduced for

¹⁵In this work a restriction to systems without currents is made. This implies $\nabla_{\mathbf{k}}\phi(\mathbf{k}) = 0$ and the phase $\phi(\mathbf{k})$ is either 0 or π leading to a real gap function with a sign change.

the different contributions in $\mathcal{K}_{kk'}^C$ and \mathcal{Z}_k^D [Eqs. (6.11) and (6.10)] The label **Ph** indicates the phonon, **SF** the spin-fluctuations and **C** the screened Coulomb contribution. The sign of the contributions appears now explicitly in the gap equation:

$$\Delta_k^{\text{xc}} = -(\mathcal{D}_k^{\text{Ph}} + \mathcal{D}_k^{\text{SF}}) \Delta^{\text{xc}}(k) + \sum_{k'} (\mathcal{C}_{kk'}^{\text{Ph}} - \mathcal{C}_{kk'}^{\text{SF}} - \mathcal{C}_{kk'}^{\text{C}}) \Delta_{k'}^{\text{xc}}.$$

First, a conventional superconductor is considered. This means that the phase of the gap is the same for all k on the Fermi surface and without loss of generality it is set to +1. Such a symmetry of the gap is called s -symmetry. Other possible symmetries are discussed in detail in section C.3 and the allowed gap symmetries in a tetragonal structure are shown in Fig. 7.9. In order to find a non-trivial solution, the left hand side of the gap equation has to be positive. The diagonal contributions, Coulomb and SF contributions are all negative pushing towards the trivial solution and the phonon term alone must compensate all the negative contributions:

$$\underbrace{\Delta_k^{\text{xc}}}_{\text{positive}} = -(\mathcal{D}_k^{\text{Ph}} + \mathcal{D}_k^{\text{SF}}) \Delta_k^{\text{xc}} - \underbrace{\sum_{k'} (\mathcal{C}_{kk'}^{\text{SF}} + \mathcal{C}_{kk'}^{\text{C}}) \Delta_k^{\text{xc}}}_{\text{negative}} + \underbrace{\sum_{k'} \mathcal{C}_{kk'}^{\text{Ph}} \Delta_{k'}^{\text{xc}}}_{\text{positive}}.$$

Note that the **SF** are reducing the critical temperature for a gap with s -symmetry. An example of a system where the strong **SF** suppress **SC** is Palladium [19, 112]. This was already pointed out 1966 by Berk and Schrieffer and in their paper they estimate the effect of a T -matrix self-energy on the critical temperature [19]. Calculations in the cuprates or iron based superconductors using an s -symmetry for the gap and neglecting the **SF** predict very small critical temperatures or no phase transition at all [74, 7]. In other words, the phonon contributions are too small to explain the large critical temperature in these compounds. Hence, the phonon contributions are left out for the further discussion and the gap equation becomes more simple:

$$\underbrace{\Delta_k^{\text{xc}}}_{\text{positive}} = -\mathcal{D}_k^{\text{SF}} \Delta^{\text{xc}}(k) - \underbrace{\sum_{k'} (\mathcal{C}_{kk'}^{\text{SF}} + \mathcal{C}_{kk'}^{\text{C}}) \Delta_{k'}^{\text{xc}}}_{\text{negative}}.$$

It is obvious that this equation can only lead to the trivial solution, unless there is a **sign change** of the gap on the Fermi surface. This means that superconductors based on a low energy repulsive pairing are unconventional by definition. For the present analysis a very simple two-dimensional Fermi surface with two well separated bands is considered:

1. One band around the Γ point with a positive sign (+) of the gap function.
2. The other band around the M point [$\mathbf{q}_M = (\frac{\pi}{a}, \frac{\pi}{a}, 0)$] with a negative sign (-).

This example is similar to the situation in the **FeSC** with their tetragonal unit cell and two groups of bands at the Fermi level (the results for the **FeSC** are presented in Sec. 7). A principle picture of such a Fermi surface is shown in Fig. 6.2 and Mazin proposed the name s_{\pm} for a symmetry like this [113]. For an analysis of the possible solutions to the gap equation it is sufficient to replace the k quantum number with a (+) if k is close to Γ and with a (-) if the k was close to \mathbf{q}_M :

$$\underbrace{\Delta_+^{\text{xc}}}_{\text{positive}} = -\mathcal{D}_+^{\text{SF}} \Delta_+^{\text{xc}} - \underbrace{(\mathcal{C}_{++}^{\text{SF}} + \mathcal{C}_{++}^{\text{C}}) \Delta_+^{\text{xc}}}_{\text{negative}} + \underbrace{(\mathcal{C}_{+-}^{\text{SF}} + \mathcal{C}_{+-}^{\text{C}}) |\Delta_-^{\text{xc}}|}_{\text{positive}}. \quad (6.12)$$

First, the contribution of the screened Coulomb interaction is analyzed in more detail. Assume the magnetic fluctuations ($\chi_{zz} \approx 0$) are weak in the system which leads to a negligible \mathcal{D}^{SF} and \mathcal{C}^{SF} and only Coulomb contributions are present in the gap equation:

$$\underbrace{\Delta_+^{\text{xc}}}_{\text{positive}} = \underbrace{-\mathcal{C}_{++}^{\text{C}} \Delta_+^{\text{xc}}}_{\text{negative}} + \underbrace{\mathcal{C}_{+-}^{\text{C}} |\Delta_-^{\text{xc}}|}_{\text{positive}}. \quad (6.13)$$

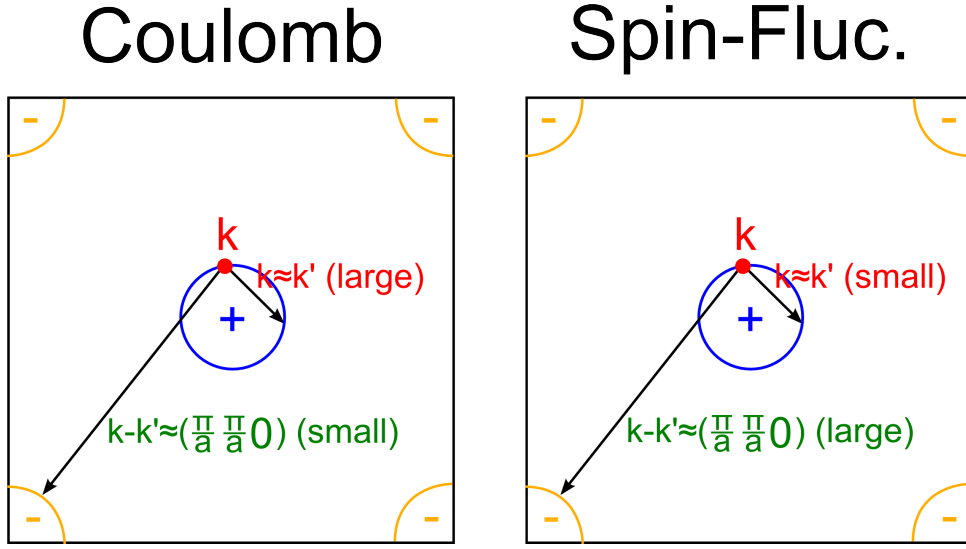


Figure 6.2.: Contribution to the gap equation due to the Coulomb interaction (left) and SF (right). Red are contributions destroying superconductivity and green contributions pushing towards the non-trivial solution of the gap equations.

The $\mathcal{C}_{++}^{\text{Coul}}$ corresponds to small momentum transfer and the $\mathcal{C}_{+-}^{\text{Coul}}$ to large transfer around $|\mathbf{q}_M|$. The adiabatic and local approximation for the XC-kernel does not depend on the momentum transfer (Sec. B.4) and will cancel for a gap containing a sign change. Hence, the kernel in $w_{kk'}^F$ in Eq. (5.47) is neglected from now on and $w_{kk'}^F$ is just the screened Coulomb interaction. The Coulomb interaction is isotropic in \mathbf{k} space and becomes weaker for larger momentum transfer. This can be seen, by the Thomas Fermi interaction which is a simple and static approximation to the screened Coulomb interaction [Eq. (E.12)]:

$$w(\mathbf{k} - \mathbf{k}') \approx \frac{4\pi}{|\mathbf{k} - \mathbf{k}'|^2 + \mathbf{k}_{\text{TF}}^2}. \quad (6.14)$$

Hence, the negative $\mathcal{C}_{+-}^{\text{Coul}}$ is larger than the $\mathcal{C}_{++}^{\text{Coul}}$ and the trivial solution will be found (see left hand side of Fig. 6.2). Due to its structure in momentum space, the Thomas-Fermi Coulomb contributions cannot lead to superconductivity in the s_{\pm} symmetry. This may change close to an instability to a charge density wave, where the full $w_{\mathbf{k}\mathbf{k}'}(\omega)$ features peaks at low energy.

The situation changes, if the system features strong magnetic fluctuations. The fluctuations have to be low lying in energy (the function $I_{\beta}(E_k, E_{k'}; \omega)$ goes to zero for $\omega \rightarrow \infty$) and strongly peaked for specific momenta. To be more specific, the fluctuations must support a scattering between the parts of the Fermi surface with different sign:

$$\mathcal{C}_{kk'}^{\text{SF}} = \begin{cases} \text{large for} & kk' = +- \quad (\text{interband}) \\ \text{small for} & kk' = ++ \quad (\text{intraband}). \end{cases}$$

If the fluctuations lead to such a form of the kernel, the positive contributions in Eq. (6.12) can overcome the negative ones. Note once more that the **sign change** of the pairing potential is essential to get a non-trivial solution of the gap equation. If the system is close to a magnetic phase transition, the magnetic response function features precisely strong fluctuations for discrete momenta at low energies which makes this scenario very plausible.

This section concludes with an introduction of an effective coupling related to the SF. The standard Eliashberg function $\alpha^2 F$ is the averaged phonon interaction at the Fermi level and the effective coupling

is just the frequency integral of this quantity:

$$\alpha^2 F(\omega) = \frac{1}{N(\mu)} \sum_{kk'} \sum_{\lambda} \left| g_{\lambda \mathbf{q}}^{kk'} \right|^2 \delta(\omega - \Omega_{\mathbf{q}\lambda}) \delta(\epsilon_k - \mu) \delta(\epsilon_{k'} - \mu) \quad (6.15)$$

$$\lambda^{\text{Ph}} = 2 \Delta_0^\infty d\omega \frac{\alpha^2 F(\omega)}{\omega}. \quad (6.16)$$

The corresponding quantities for the **SF** are found by comparing Eqs. (6.11), (6.15) and (6.16). In analogy to the phonon case the equations read:

$$P^{\text{SF}}(\omega) = \frac{1}{N(\mu)} \frac{a\mathcal{C}}{\pi} \sum_{kk'} \Im \left[\Lambda^{\text{SF}}(kk'\omega) \right] \delta(\epsilon_k - \mu) \delta(\epsilon_{k'} - \mu)$$

$$\lambda^{\text{SF}} = 2 \Delta_0^\infty d\omega \frac{P^{\text{SF}}(\omega)}{\omega}. \quad (6.17)$$

A dimensional analysis of the averaged isotropic interaction shows that the object is dimensionless:

$$\begin{aligned} [M_{nm'}(E, E', \omega)] &= \left[\frac{1}{N_n(E)} \right] \sum_{\mathbf{k}\mathbf{k}'} [M(kk'\omega)] [\delta(E - \epsilon_{\mathbf{k}})] [\delta(E' - \epsilon_{\mathbf{k}'})] \\ &= \frac{1}{\frac{\text{states}}{\text{Ryd}}} \text{Ryd} \frac{1}{\text{Ryd}} \frac{1}{\text{Ryd}} = 1 \end{aligned}$$

and all effective coupling constants are positive real numbers.

6.3. Model Calculation

6.3.1. Comparison to Conventional Systems

For the conventional superconductors driven by an attractive phonon interaction, the critical temperature is well captured by the McMillan formula [114]. The original expression is found by fitting the critical temperature as a function of the phonon coupling strength λ^{Ph} , characteristic phonon frequency and effective Coulomb repulsion μ^* [115, 116]. For the calculation of the critical temperature the **Eliashberg theory** theory is used. Later, the fitting procedure was reanalyzed by Allen and Dynes and a more sophisticated fitting function was proposed [117]. With the more sophisticated fitting function also the large coupling limit ($\lambda^{\text{Ph}} > 1.5$) is well captured. For the characteristic phonon frequency a logarithmic weight is introduced putting a larger weight to smaller frequencies:

$$\bar{\omega}_{\text{Log}} = \exp \left[\frac{2}{\lambda^{\text{Ph}}} \Delta d\omega \log(\omega) \frac{\alpha^2 F(\omega)}{\omega} \right]. \quad (6.18)$$

From the analytic expression for the T_c the following limiting cases are found for the critical temperature:

- For small coupling the T_c depends exponentially on λ^{Ph} : $T_c \propto e^{-\frac{1}{\lambda^{\text{Ph}}}}$.
- In the large coupling limit the critical temperature grows with $\sqrt{\lambda^{\text{Ph}}}$.
- The T_c is linear in the average phonon frequency $\bar{\omega}_{\text{Log}}$.

The question now arises how the unconventional **SC** based on a repulsive interaction behaves as a function of coupling strength and characteristic frequency. In Sec. (E.3.1) a fully linearized and isotropic form of the gap equation is discussed. In this section this equation is solved. For a first investigation, the Coulomb and phonon parts are neglected. This means only the repulsive interaction related to magnetic excitations is present. For this purely repulsive interaction a sign change of the gap function is mandatory to find a non-zero solution in the gap equation. For the calculation two bands labeled with + and - corresponding to the sign of the gap function are considered at the Fermi level.

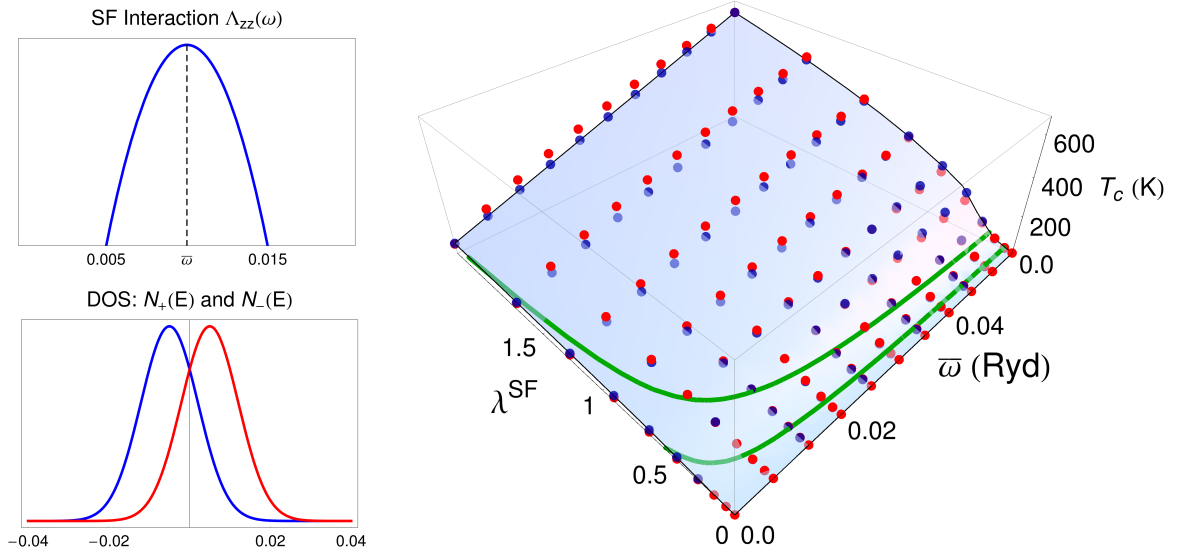


Figure 6.3.: (left) Model isotropic interaction related to the SF given in Eq. (6.19) and model density of states representing the two bands around the Γ and M point. All energies are in Rydberg. (right) SCDF calculation of the critical temperature as a function of the coupling strength λ^{SF} and characteristic frequency $\bar{\omega}$ using the model interaction and density of states. The green lines are iso lines for $T_c = 10$ K and 50 K, the red dots indicate calculated points and the surface is a fit using the function given in Eq. (6.20). The blue dots are a guide for the eye sitting on top of the surface.

It is assumed that the system is close to an **anti ferro magnetic (AFM)** instability which leads to strong fluctuations (paramagnons) for a finite momentum vector \mathbf{q}_c . It is assumed that the fluctuations are weak for other vectors and that the two bands at the Fermi level are nested by \mathbf{q}_c (Fig. 6.2). In such a situation the isotropic effective interaction is small for intraband scattering ($\Lambda_{\pm\pm}^{\text{SF}} \approx 0$) and peaked for interband scattering ($\Lambda_{\pm\mp}^{\text{SF}}$). This situation is modeled by a simple parabola centered around a characteristic frequency $\bar{\omega}$:

$$\Lambda_{IJ}^{\text{SF}}(EE'\omega) = \begin{cases} c_1 N_J(E') \left[1 - \left(\frac{\omega - \bar{\omega} - \frac{c_2}{2}}{c_2} \right)^2 \right] & \text{if } |\omega - \bar{\omega}| \leq c_2 \text{ and } I \neq J \\ 0 & \text{elsewhere.} \end{cases} \quad (6.19)$$

The width c_2 is fixed to a value of 0.01 Ryd and the **density of states (DOS)** of the two sets $N_I(E)$ is modeled by two Gaussian peaks around the Fermi energy (left side of Fig. 6.3). The peak height c_1 is determined by requiring a value for the effective coupling strength λ^{SF} [Eq. (6.17)]. On the right hand side of Fig. 6.3, the critical temperature as a function of $\bar{\omega}$ and λ^{SF} is shown. The red dots are the solution of the fully linearized gap equation together with a fitting function f . The function f is designed to reproduce the limits imposed by the fit to the conventional superconductors:

$$f(\lambda^{\text{SF}}\bar{\omega}) = \bar{\omega} \left[\Theta(\lambda^{\text{SF}} - A_3) e^{-\frac{A_1}{\lambda^{\text{SF}}}} + \Theta(A_3 - \lambda^{\text{SF}}) \sqrt{B_1 \lambda^{\text{SF}} - B_2} \right]. \quad (6.20)$$

The parameters B_1 and B_2 are chosen to get a continuous and smooth function at the crossover $\lambda^{\text{SF}} = A_3$. The remaining parameters $\{A_1, A_2, A_3\}$ are found by fitting to the calculated points. For large λ^{SF} the calculated T_c shows a systematic deviation from the linear behavior in $\bar{\omega}$. For smaller coupling (below 1) this is not the case and it can be seen that the overall agreement between the fit and the calculation is reasonable. This means that the two band system with a sign changing gap function and a purely repulsive interaction behaves identical to the conventional case with a single band and an attractive interaction created by phonons. This result is not accidental because the sign change of the gap leads effectively to an attractive interaction between the two bands.

The A_3 gives the crossover between the square-root and exponential dependence *i.e.* between the high and **weak coupling** limit. A value for A_3 around 0.5 is found which is smaller than the value for a single band conventional (*i.e.* phonon driven) superconductors.

In the plot also two green iso lines are drawn which mark $T_c = 10$ K and 50 K, respectively. The critical temperature for the iron based superconductors lies in this regime. Experiments indicate (Tab. 1.1) that the paramagnon have a very low characteristic energies $\bar{\omega}$ of ~ 10 meV = $7 \cdot 10^{-4}$ Ryd. The model calculations imply a effective couplings above 0.5 for this $\bar{\omega}$ in order to reproduce the experimental T_c . In this regime the critical temperature depends exponentially on the coupling and the critical temperature will depend strongly on the size of the effective interaction.

6.3.2. Interplay between Spin-Fluctuations, Phonons and Coulomb Contributions

In the previous section a model calculation containing two bands at the Fermi level and the SF interaction has been presented. In this section the interplay between the Coulomb, spin and phonon contributions in a two band system is investigated. Different shapes in frequency space are considered for the phonon and spin interaction contribution (Fig. 6.4a). But the dependence on E and E' is neglected like in Eq. (6.19) which is a valid approximation due to the small characteristic magnon or phonon frequencies. The function $I(EE'\omega)$ given in Eq. (6.4) becomes small for $E \gg \omega$ and ω is limited by the QP energy. As in the previous section, it is assumed that the bands at the Fermi level are separated by some finite vector \mathbf{q}_c and only off diagonal elements are considered for the SF term.

For the Coulomb contribution the situation is different. The characteristic frequencies are not small and it is assumed that the Coulomb contribution is flat in frequency space and the dependence with respect to ω is neglected. Since the Coulomb interaction decays like $\frac{1}{q^2}$, the contribution for small momentum transfer (intraband) are usually larger then the interband contribution corresponding to $\mathbf{k} - \mathbf{k}' \approx \mathbf{q}_c$. For higher energies away from the Fermi level the contributions become equal. This situation is modeled by the following expression:

$$w_{IJ}(EE') = \begin{cases} N_J(E') \left(U_0 + U_1 e^{-\kappa(E^2+E'^2)} \right) & \text{if } I = J \\ N_J(E') U_0 & \text{if } I \neq J. \end{cases} \quad (6.21)$$

The $N_I(E)$ is the density of states of the band I and originates from the averaging process of the interaction Eq. (E.19). In the beginning the Phonon contribution are neglected which implies a gap with different sign on the two bands. Like in the previous section the gap function is labeled as $\Delta_I(E)$ and I is either + or -. Note that the sign changing two band system is a special case: For a symmetric DOS $N_+(E) = N_-(E)$ and a symmetric gap function *i.e.* $\Delta_+(E) = -\Delta_-(E)$ the constant Coulomb term U_0 cancels out completely in the C-term [Eq. (E.21)]:

$$\Delta dE \begin{pmatrix} U_0 N_+(E) & U_0 N_-(E) \\ U_0 N_+(E) & U_0 N_-(E) \end{pmatrix} \begin{pmatrix} \Delta_+(E) \\ \Delta_-(E) \end{pmatrix} = U_0 \Delta dE \begin{pmatrix} N_+(E) \Delta_+(E) + N_-(E) \Delta_-(E) \\ N_+(E) \Delta_+(E) + N_-(E) \Delta_-(E) \end{pmatrix}$$

$$U_0 \Delta dE [N_+(E) \Delta_+(E) + N_+(-E) \Delta_-(E)] = U_0 \Delta dE [N_+(E) \Delta_+(E) - N_+(E) \Delta_+(E)] = 0$$

and the Coulomb interaction for a symmetric system reduces effectively to:

$$w_{IJ}(EE') = \begin{cases} N_J(E') U_1 e^{-\kappa(E^2+E'^2)} & \text{if } I = J \\ 0 & \text{if } I \neq J. \end{cases} \quad (6.22)$$

The parameter space for a calculation containing three independent model calculation is very large. For reasons of simplicity, in the beginning a flat DOS $N_+(E) = N_-(E) = \text{const.}$ is assumed. The fully linearized equation introduced in Sec. E.3.1 is solved. As discussed in the previous section, the critical temperature is increasing with the characteristic frequency $\bar{\omega}$ of the SF and the effective coupling strength λ^{SF} . These trends are not reinvestigated here and λ^{SF} is fixed to 1.2. and $\bar{\omega}$ to 0.01 Ryd. For the Coulomb interaction $N_J(\epsilon_F) U_0$ a value of 0.2 is used and U_1 is set to $\frac{U_0}{2}$. The critical temperature and gap structure is not influenced by different shapes of the SF interaction (left side of Fig. 6.4a). The relevant quantity is the characteristic frequency $\bar{\omega}$. With increasing $\bar{\omega}$ the critical temperature becomes larger and the gap becomes broader.

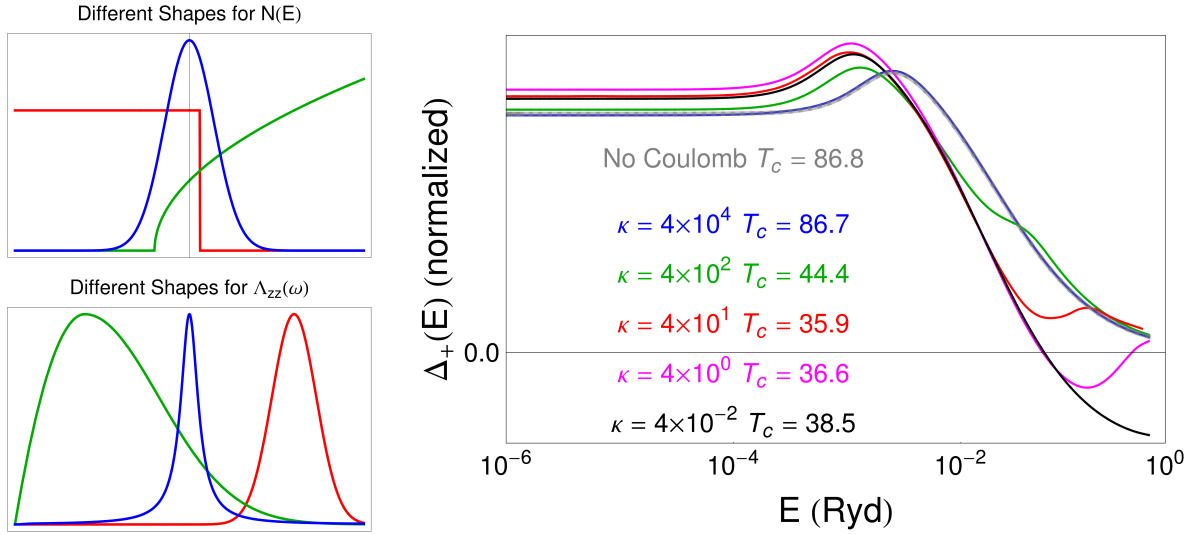


Figure 6.4.: (left) Density of states considered in the model calculation. (right) Gap symmetry for a flat DOS and different values for the parameter κ determining the decay of the Coulomb interaction in Eq. (6.22)

The parameter κ in Eq. (6.22) can be used to control the Coulomb interaction: If κ is large the Coulomb interaction decays very quickly. In Fig. 6.4a the gap as a function of κ is plotted. Since the gap is totally symmetric $\Delta_I(E) = \Delta_I(-E)$ and $\Delta_+(E) = -\Delta_-(E)$ only the positive branch $\Delta_+(E)$ is shown. The gap shows the typical form being constant close to the Fermi level, followed by an extremum and a decay for larger energies [110]. For large κ the results are identical to a calculation neglecting the Coulomb interaction completely. By decreasing the value of κ the Coulomb contribution starts to influence the results. The critical temperature goes down, due to repulsion within one band [Eq. (6.13)] and the gap starts to show dips. The dips indicate the regime, where the Coulomb interaction competes with the SF. For $\kappa < 1$ the Coulomb contribution is strong enough to flip the sign of the gap function for certain energies. The sign change of the gap function at higher energies **reduces** the effect related to the repulsive Coulomb term in the gap equation [Eq. (6.13)]. Effectively, the Coulomb contribution on the full energy scale may be mapped to a reduced effective Coulomb term on a smaller energy scale due to the sign change of the gap function. Hence, the sign change of the gap function is referred to as **Coulomb renormalization** [86]. Note that the sign change of the gap happens far away from the Fermi level and is compatible with conventional and unconventional SC defined in Sec. 6.2.

However, for $\kappa = 4$ the Coulomb contribution still decays faster in energy, than the SF term which leads to one more sign change in the large energy regime (magenta line in Fig. 6.4a). If κ is decreased further the Coulomb contribution dominates also in the large energy range and the gap changes sign only once. Note that the critical temperature converges quickly with respect to κ . This indicates that the Coulomb interaction influences the critical temperature only within a small energy window in the symmetric two band system and the sign change of the gap does not affect the critical temperature.

In a real material, the density of states is of course **not** flat. In order to investigate the effect of the DOS two things are there to be done: (1) The ratio of the DOS at the Fermi level is changed *i.e.* $\frac{N_+(\epsilon_F)}{N_-(\epsilon_F)} \neq 1$ and (2) Non-flat functions are used. The results are shown in Fig. 6.5. The tested functions are step and square root functions which represent a two and three dimensional system, respectively and a Gaussian peak (left hand side of Fig. 6.4a). First, the ratio is set to one and different functions are tried. The effect on the critical temperature with respect to the used function is very small for two band system. The smooth functions used to model the DOS, start to differ beyond the maximum of the gap (note the logarithmic energy scale). However, the symmetry $\Delta_+(E) = -\Delta_-(E)$ is broken by the unsymmetric DOS with respect to the Fermi level.

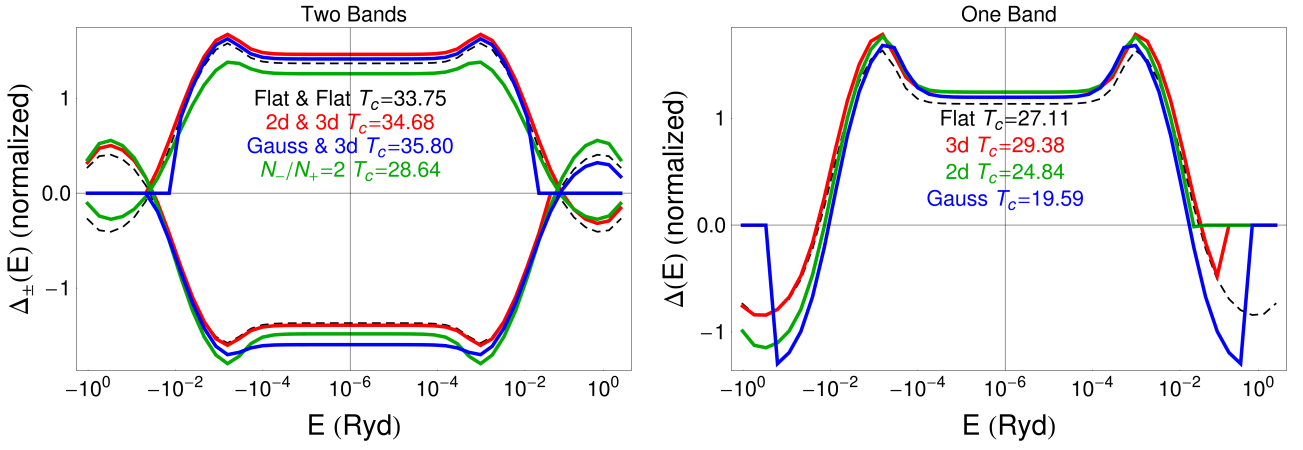


Figure 6.5.: (left) Calculations for a two band system with no phonons, $\lambda^{\text{SF}} = 1.2$ and $U_0 = 0.3$. The κ is set to 1 in both calculations. (right) Model calculation using a single band with an attractive Phonon and a repulsive Coulomb interaction for various DOS. The λ^{Ph} is set to 1.2 and U_0 to 0.3.

What seems to matter in the two band case is only the value of the Coulomb interaction at the Fermi level. Up to now, this value is identical for the two bands: $w_{12} = w_{21}$ and $w_{11} = w_{22}$. By changing the ratio $\frac{N_+(\epsilon_F)}{N_-(\epsilon_F)}$ from one, the Coulomb interaction becomes different for the two sets. This has a strong effect on the critical temperature (green line in Fig. 6.5b) compared to the changes in the shape of the DOS. These findings are very different from a one band system with an attractive interaction (left side of Fig. 6.5b). In such a system the Coulomb renormalization in the large energy regime is **essential** for the critical temperature. If a Gaussian DOS is used to cut away the renormalization, the T_c is reduced very strongly and the T_c becomes zero for functions with a smaller width (*cf.* the change in T_c in the one and two band case). In summary it can be said that in a two band system with a sign changing gap function the ratio of the Coulomb interaction at the Fermi level is very important, but not the large energy tails.

Finally, a comment on the phonon contribution is made. Adding the phonons introduces a repulsive contribution in the D -term [Eq. (6.10)] and two contributions in the \mathcal{C} term: $\mathcal{C}_{+-}\Delta_-$ and $\mathcal{C}_{++}\Delta_+$ [Eq. (6.11)]. If the gap changes sign *i.e.* $\Delta_-\Delta_+ < 0$ the contribution with respect to the \mathcal{C} term cancel and only the repulsive term is left. This means for a system in the sign changing state a band independent phonon contribution will reduce the critical temperature. If the phonons are further increased and dominate the gap equation, the symmetry of the gap changes. The s_{\pm} state favored by the repulsive interactions is suppressed and an s_{++} state with $\Delta_-\Delta_+ > 0$ is found.

6.4. Summary

In this chapter a SCDFT functional containing magnetic fluctuations along with the Coulomb and phononic contributions has been derived [Eq. (6.9)]. The functional has been applied to a model system with two bands at the Fermi level. The critical temperature is sensitive to the characteristic frequency of the magnetic fluctuation and effective coupling strength provided by the paramagnons. The T_c follows the trends implied by Eliashberg theory (Fig. 6.3). In contrast to the one band system, only a small energy range around the Fermi level of the Coulomb interaction is important for the critical temperature (Fig. 6.5). However, the results are sensitive to the parameters of the model like DOS at the Fermi level, Coulomb repulsion, λ^{SF} , λ^{Ph} , *ect.*. In the next section all these parameters will be calculated from first principles for two representatives of the iron based superconductors and a SCDFT calculation will be performed for the two compounds.

7. Results – Fe Bases Superconductors

In the previous chapters a functional containing SF has been derived. The derivation was based on MBPT Sec. 4 and 5. The MBPT is connected to the DFT framework using the SSEq. This procedure leads to a universal functional in Sec. 6.1. The ground state properties enter the functional via the KS energies ζ_k and the excitations are included via the linear response function [Eq. (E.17)].

After the general derivation and model calculation it is essential to check the functional in real materials. Like discussed in the introduction (chapter 1), the iron based superconductors are the perfect candidate to test the functional for two reasons: (1) There is strong experimental evidence for a connection between magnetic fluctuations and superconductivity [118] and (2) the ground state does not involve complicated Mott physics as in the cuprates [11]. However, even in the FeSC the determination of the correct electronic ground state is problematic (see Sec. 7.2).

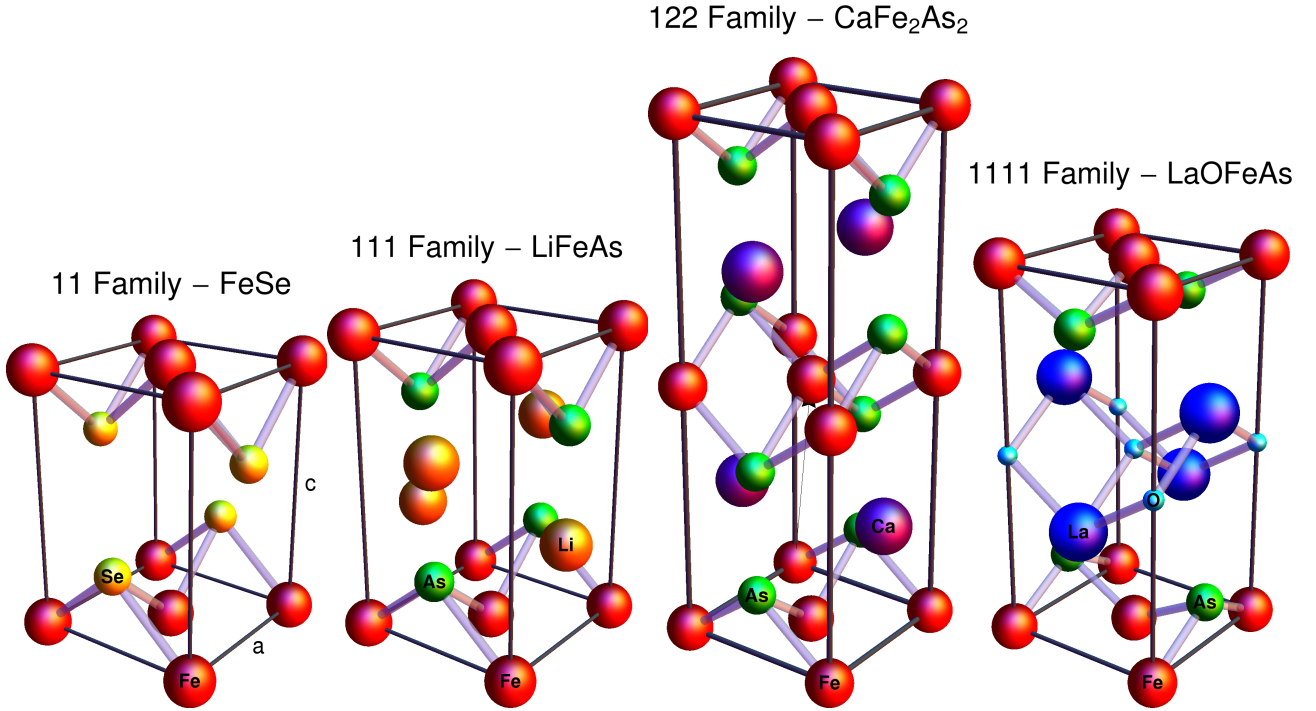


Figure 7.1.: Representatives of the four structural families of iron based superconductors. The unit cell of CaFe_2As_2 (122 family) is non-tetragonal indicated by the third unit cell vector point in the $(\frac{a}{2}, \frac{a}{2}, \frac{c}{2})$ direction.

The FeSC split into four main structural families, the so called 11, 111 122 and 1111 family [75]. The building blocks in all groups are layers composed of a Fe square lattice, where each Fe atom is surrounded by a tetragonal of Se or As atoms (Fig. 7.1). The various families are created by putting different spatial layers between the building blocks. The simplest family (11) is created by simply using no spatial layer at all [9]. For the 111 family light alkali metals like lithium or sodium are used as spatial layers [119, 120]. The unit cells become more and more complicated with increasing the number of different layers. Also the 122 family has only one spatial layer for example Ca, Sr or Ba, but the layer is rotated by 90° from one iron layer to the next one. In the last important group (1111) two spatial layers are present consisting for example of lanthanum and oxygen. There are more complicated structures like the 32522 family which are left here for simplicity [75].

The electronic structure close to the Fermi level is mainly given by the d states of the iron atoms

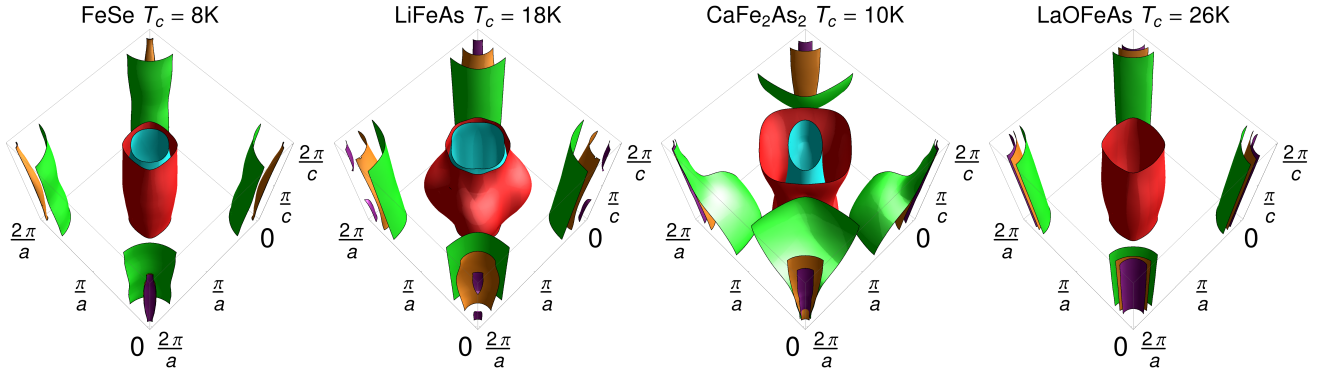


Figure 7.2.: Fermi surface of: FeSe , LiFeAs, CaFe₂As₂ and LaOFeAs representing the 11, 111, 122, 1111 family of the iron based superconductors, respectively. The Fermi surface has been calculated in the non-magnetic phase with an all electron linear augmented plane wave code [125].

and hence the Fermi surface is rather similar in all the materials [13]: There are one or two electron bands crossing the Fermi energy around the M -point $(\frac{\pi}{a}, \frac{\pi}{a}, 0)$ and two or three hole bands crossing the Fermi level near the Γ -point. The Fermi surface corresponding to these bands is shown in Fig. 7.2. For most materials the topology is two-dimensional with two “barrels” centered around the Γ and M point. In the Li compound small electron “pockets” around the Γ -point are present. These theoretical results are in reasonable agreement with angle resolved photon emission spectroscopy (ARPES) experiments [121, 122, 123, 124].

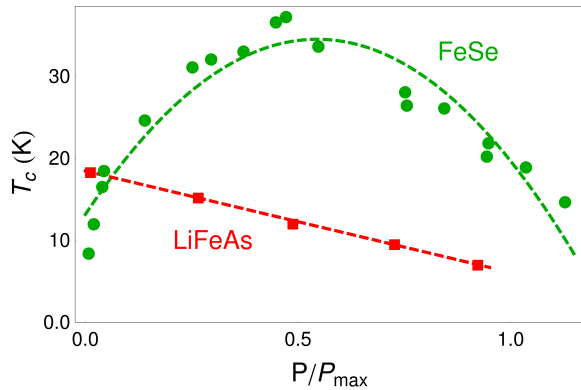


Figure 7.3.: Experimental critical temperature as a function of pressure [9, 126]. P_{\max} is 9 GPa for LiFeAs and 18 GPa for FeSe.

structural phase transition superconductivity vanishes [9].

In LiFeAs on the other hand, the critical temperature reduces with pressure. The decay in T_c is measured for pressures up to 2 GPa and a decay rate between $-1.5 \frac{\text{K}}{\text{GPa}}$ and $-2.0 \frac{\text{K}}{\text{GPa}}$ depending on the sample quality is found [37, 127, 126]. The experimentalists explain the negative decay rate with the small size of the lithium atom. This atom creates chemical pressure which results in the small lattice parameters of LiFeAs compared to the 122 and 1111 compound. However, the 11 compounds for example FeSe has an even smaller unit cell and show a different temperature behavior with respect to pressure. A comparison of the critical temperature as a function of pressure is shown in Fig. 7.3. In this figure the pressure is normalized by the maximum value investigated in this work which is 18 GPa for FeSe and 9 GPa for LiFeAs.

This chapter features a complete study of the two compounds with respect to pressure and has the following outline: First the ground state results are presented (Sec. 7.1). Unfortunately, the magnetic ground state is **not** predicted correctly by the DFT calculation within all known functionals. In Sec. 7.2 this problem is discussed and a simple solution is suggested. In the last part of this chapter the excitations and SCDFD calculations are presented and discussed (Secs. 7.3 and 7.4).

P (GPa)	FeSe				P (GPa)	LiFeAs				
	a	c	$z_{\text{Fe-Se}}$	m_{Fe}		a	c	$z_{\text{Fe-As}}$	$z_{\text{Fe-Li}}$	m_{Fe}
0	7.09	10.37	4.395	2.20	0	7.12	11.99	4.475	5.2855	1.89
6	6.88	9.65	4.338	1.64	1	7.09	11.91	4.467	5.267	1.85
12	6.77	9.52	4.318	1.45	3	7.02	11.78	4.452	5.330	1.79
18 ^(s)	6.73	9.63	4.320	1.46	6	6.94	11.59	4.434	5.168	1.72
					9	6.87	11.44	4.420	5.108	1.66

Table 7.1.: Results of the relaxation obtained with the experimental unit cell parameters a and c as a function of pressure. The $z_{\text{Fe-X}}$ is the relaxed distance between the Fe and $X = \{\text{Se,As}\}$ atoms, m_{Fe} is the magnetic moment per Fe atom and $z_{\text{Fe-X}}^{\text{crit}}$ is the critical distance .

7.1. Non-Superconducting Ground State

The preliminary step before the investigation of SC is to characterize and understand the non-SC ground state from which SC originates. For this purpose spin DFT calculations of the electronic ground state of FeSe and LiFeAs as a function of pressure are performed. For FeSe pressures up to 18 GPa are considered and for LiFeAs the relevant pressure regime is smaller and a maximum value of 9 GPa is used in the calculation (Fig. 7.3). The effect of pressure is modeled in the ground state calculation via the edge length a and the height of the unit cell c . The values are taken from the X-ray diffraction experiments performed under pressure. In Fig. 7.4 the experimental lattice constants as a function of pressure are shown, together with the interpolation leading the values for a and c ¹⁶. In experiments no unified trends for the internal lattice parameters are found (compare [129, 130] and [128]) and the crystal symmetry does also not require a specific value for the distance of the Se or As atoms to the iron layer. Hence, the internal lattice positions are obtained by a structural **relaxation**, and the distance between an atom X and the nearest Fe atom is labeled with $z_{\text{Fe-X}}$.

The relaxation is performed with a state of the art **plane wave (PW)** code [131]¹⁷. In general the relaxation in the magnetic cell leads to better agreement with experiment (this point is explained later). Hence, the relaxation is done in the **stripe** magnetic phase. The stripe magnetic structure is shown in Fig. 7.5 and the magnetic unit cell size is twice the chemical one. The results of the relaxation for the two materials together with the magnetic properties are summarized in Tab. 7.1.

At all pressures for both materials a magnetic ground state is found. This is in **contradiction** with the experimental results finding both materials to be NM [9, 121]. It also contradicts with the scenario of the pairing induced by **paramagnetic (PM)** fluctuations related to a suppressed magnetic phase

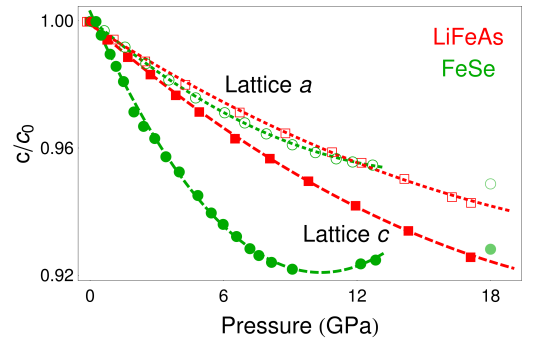


Figure 7.4.: Unit cell parameter with respect to pressure [128, 37].

¹⁶The test calculation indicate that the orthorhombic distortions do not effect the results significantly and the tetragonal structure is used in the calculation. For FeSe at the highest pressure (18 GPa) no experimental data was available. A calculation with a variable cell size and the minimization of the free enthalpy

$$\left. \frac{\partial H(S, PV)}{\partial V} \right|_{\substack{P = 18 \text{ GPa} \\ S = \text{const.}}} = 0$$

under the pressure of 18 GPa leads the optimal unit cell volume in terms of a and c . The simulated points are shown in light green in Fig. 7.4.

¹⁷The **XC-potential** is approximated by a norm conserving **GGA** functional [97] The cutoffs for the **PWs** and charge density are set to 100 Ryd and 400 Ryd, respectively. Sixty bands are included per \mathbf{k} point and a \mathbf{k} point mesh of $14 \times 14 \times 10$ points is used. The calculation is stopped, if the forces acting on the atoms are below a cutoff of $5 \times 10^{-5} \frac{\text{Ryd}}{a_0}$. It is very important to use always the same setup (like cutoffs, functional, basis set *etc.*) in the calculation in order to achieve consistent results.

discussed in the introduction (chapter 1). The magnetic ground state explains, why the relaxation in the NM phase gives less good agreement with experiment than the relaxation considering the magnetic state.

In principle, DFT is an exact scheme and should lead the correct ground state, so the mistake lies (like always) in the approximation for the XC-potential. Many researchers believe [132, 133] that the magnetic fluctuations are also essential for finding the correct ground state and the standard functionals like LDA or GGA do not take AFM fluctuations into account [96, 97]. So one solution would be the improvement of the existing XC-potentials in such a way that the ground state is correctly predicted. However, the inclusion of dynamic effects in a static XC-potential is a highly non-trivial task and has not been solved in general and is also not in this work. Simpler candidates to overcome this problem are either dynamical mean field (DMF) or disordered local moments (DLM) [134]. The latter one has been tried, but the energy of the DLM state does not lie below the stripe structure of all pressures. The DMF enjoys great popularity nowadays in treating dynamical effects on a simple level [133], but the common frameworks contain parameters and the derivation of an XC-kernel related to a DMF ground state is not obvious [134].

In the present work a phenomenological approach is used to overcome the wrongly predicted ground state. This approach is discussed in more detail in the next section (Sec. 7.2) and this section is closed with a discussion of the energetic stability of the magnetic phase with respect to pressure.

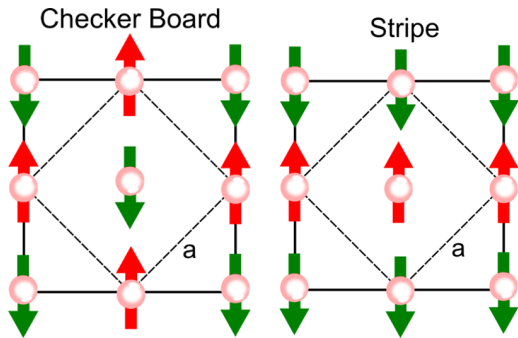


Figure 7.5.: The CB and stripe magnetic structure.

pressure is -4.7 mRyd for FeSe and -11.0 mRyd for LiFeAs. The difference between the CB and NM structure becomes smaller with pressure and reaches a minimum value of $|E_{CB} - E_{NM}| \sim 2.5$ mRyd in both materials. The change in the latter difference is stronger than the decrease between the Stripe and CB structure which leads in total to a shirking $|E_{Stripe} - E_{NM}|$ for the two materials with respect to pressure. The only exception from this trends is the highest pressure in FeSe, where the $|E_{Stripe} - E_{NM}|$ goes up a little bit by half a mRyd compared to 12 GPa which is also seen by a small increase in the size of the magnetic moment. However, the energy difference for all pressures $|E_{Stripe} - E_{NM}|$ never goes below ~ 9 mRyd which is quite a solid energy amount.

Both LiFeAs and FeSe follow the general trend that by reducing the unit cell size the tendency for a magnetic phase is suppressed. This is seen by the reduction of the on site magnetic moment for the two materials with respect to pressure. In order to investigate the stability of the stripe magnetic structure, also calculations in the NM and CB phase are performed (Fig. 7.5). The energetic order of the three configurations is $E_{Stripe} < E_{CB} < E_{NM}$. The energy difference between the stripe and CB configuration increases in magnitude with pressure by $\frac{E_{Stripe} - E_{CB}}{P_{max} - P_0} \sim -2$ mRyd in both materials. The starting value for ambient

7.2. A Phenomenological Connection

In order to include the effect of spin fluctuations into **SCDFT** we need a reliable estimation of the magnetic response function χ_{zz} . Due to the ground state problem χ_{zz} cannot be computed straightforwardly from the **GGA** or **LDA** ground state. As discussed in the previous section no proper *ab-initio* tools to come across the obstacle have been developed. Therefore, a phenomenological method is used in this work. The idea is to find an adjustable external control parameter ξ to push the system in the non-magnetic regime. Only in this phase it is possible to compute the χ_{zz} containing the paramagnons.

In Fig. 7.6 a generic cartoon of the phase space is shown. The magnetic moment undergoes a **phase transition** as a function of the control parameter. The magnetic response χ_{zz} is given by the derivative $-\frac{\delta m}{\delta B^{\text{ext}}}|_{B^{\text{ext}}=0}$ and diverges at $\xi = \xi_{\text{crit}}$. Some distance away from the transition $|\xi - \xi_{\text{crit}}| > 0$ the values are finite. The sign of the response function is **always** negative, if the **KS** Green's function and density corresponding to the ground state at this ξ is used in Eq. (5.18). If not the ground state **GF** is used, the static response becomes positive at the \mathbf{q} corresponding to the magnetic ground state ordering vector \mathbf{q}_{GS} . For the stripe magnetic structure in the **FeSC** (Fig. 7.5) the \mathbf{q}_{GS} is $\mathbf{q}_{\text{M}} = (\frac{\pi}{a}, \frac{\pi}{a}, 0)$. The sign changes to a positive response function leads to an energy gain,

$$\Delta E = - \lim_{\mathbf{q} \rightarrow \mathbf{q}_{\text{GS}}} \lim_{\omega \rightarrow 0} B_z(\mathbf{q}\omega) \cdot \mathfrak{Im} [\chi_{zz}(\mathbf{q}\omega)] \cdot B_z(\mathbf{q}\omega) < 0$$

if the system is exposed to external magnetic fields matching the ground state symmetry. The energy gain is indicating that the systems wants to go to the real ground state and static external perturbation are sufficient to do this. Once more this is in total analogy to the phonons. The positive sign of the response leads also to an attractive (positive) interaction related to the magnetic fluctuations [see Eq. (5.41)]. An attractive interaction created by the Coulomb repulsion is highly unphysical and the integral in Eq. (B.11) would diverge due to the finite value of $\chi(\omega = 0)$.

This means a linear response calculation on top of non-ground state (for example **NM** state in the **FeSC**) leads to **wrong** results. What one has to do is to adjust the external control parameter ξ to enforce the correct or desired ground state (**NM**) and perform a linear response calculation for this value of ξ .

One candidate for the control parameter is the distance of the Se or As atom to the iron layer labeled with $z_{\text{Fe-Se}}$ and $z_{\text{Fe-As}}$, respectively. The on site magnetic moment is strongly affected by the $z_{\text{Fe-Se}}$ or $z_{\text{Fe-As}}$, as shown in Fig. 7.7. For sufficiently small distances the magnetic phase is suppressed for all pressures in the considered regime and the phase transition is second order. The values for $z_{\text{Fe-Se}}$ and $z_{\text{Fe-As}}$ obtained by the structural relaxation (dashed lines in Fig. 7.7) lie all above the critical point an large shifts of $\sim \frac{1}{4} a_0$ from the relaxed position are necessary to obtain a non-magnetic state.

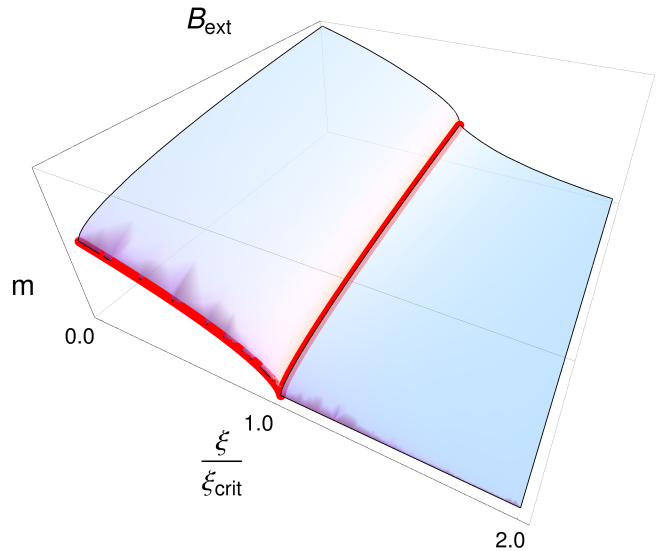


Figure 7.6.: Magnetic moment as a function of $\frac{\xi}{\xi_{\text{crit}}}$ and the external magnetic field.

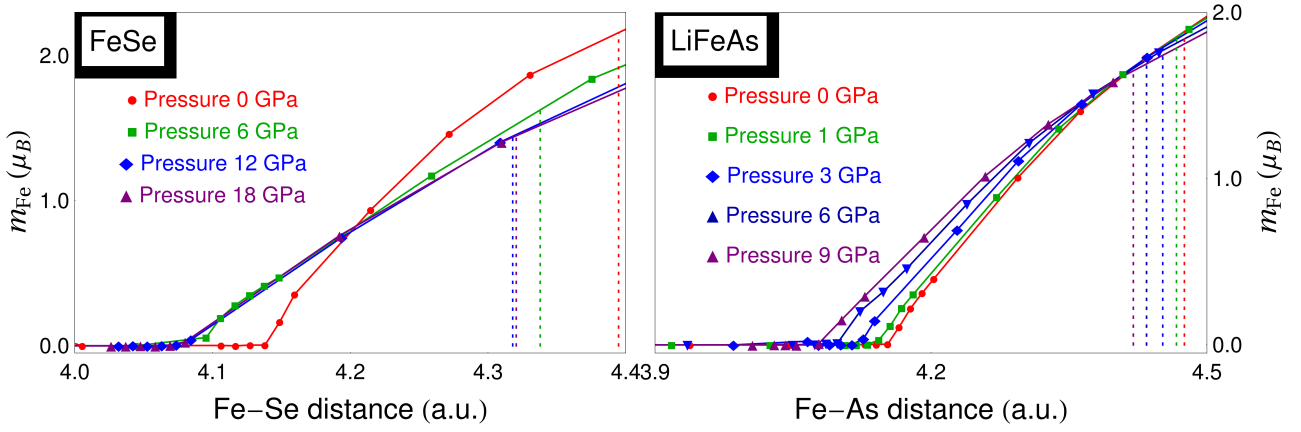


Figure 7.7.: Magnetic moment as a function of the distance between the As or Se to the Fe atom for the different pressures. The relaxed values are indicated as a dotted line.

But also doping, pressure or external magnetic fields are possible choices for ξ . However, all these control parameters strongly affect the underlying electronic and structural properties which will prove to be a disadvantage in the further discussion. It is also possible to keep the ground state unchanged and introduce the control parameter in the Dyson Eq. (5.17) for the response function:

$$\chi_{zz}(\mathbf{q}\omega) = \frac{\chi^{\text{KS}}(\mathbf{q}\omega)}{1 - \chi^{\text{KS}}(\mathbf{q}\omega) \alpha f_{zz}^{\text{xc}}(\mathbf{q}\omega)}.$$

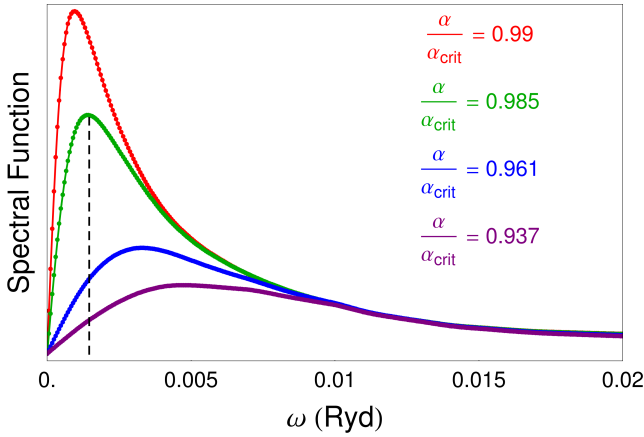


Figure 7.8.: The spectral function [Eq. (B.13)] for $\mathbf{q} = \mathbf{q}_M$ in LiFeAs. The dashed line indicates 20 meV which is roughly the energy of the fluctuation in the non-SC phase[102]

The response function of LiFeAs for various α is shown in Fig. 7.8. Due to the scaled kernel the sign change of the response function is avoided and χ starts correctly at zero as it should in a non-magnetic groundstate. The results are very sensitive to the value of α which is well known from early calculation of S. Doniach of the magnetic response in the electron gas [135]. The use of the parameter α has been suggested by I. Mazin and in Ref. [136, 132] arguments for the rescaling of the kernel in a magnetic system are given. The reduction of the XC-kernel and potential can be connected to magnetic fluctuations. This is in line with the picture that the absence of the fluctuations in the used functionals leads to the overestimation of magnetism. Note that constrained field calculations (often called fixed spin moment calculation) enforce a vanishing moment, but the

response depends then on the external constraining field.

From the discussed control parameters, only the scaling of the kernel and the internal lattice position $z_{\text{Fe-Se}}$ and $z_{\text{Fe-As}}$ are undetermined by experiment and could be freely chosen in calculations. In this work the scaling of the kernel is used as the control parameter in order to fix the problem of the wrongly predicted ground state. There are two reasons for this choice: One is practical and the other one is physical. The physical one is that the Fermi surface is in reasonable agreement with the observed ARPES data (*cf.* Fig. 7.2 and [121, 122, 123, 124]) and parameters like the $z_{\text{Fe-Se}}$ and $z_{\text{Fe-As}}$ would change the shape of the Fermi surface in an unphysical way. As the role of the Fermi surface is essential in the context of superconductivity (Sec. 6.2) this should be avoided. The practical advantage is the much lower computational work associated in a change of the parameter α compared to a change in the internal lattice coordinates. The latter one would involve a recalculation of the ground state and χ^{KS} , where as a change in the scaling only requires to re-solve the Dyson equation [Eq. (5.17)].

More important than the choice of the control parameter itself is the procedure how to fix the value of the parameter. If one is very close to the critical value, the fluctuation strength becomes infinitely strong, and the characteristic frequency of the fluctuations goes to zero (Fig. 7.6). In Sec. 6.3.1 an exponential dependence of the critical temperature on the coupling strength has been observed in the weak coupling regime. This means that big changes in T_c are created by small change in the value of the control parameter. The dependence on the parameter means that the framework is not *ab-initio* anymore. A principle solution to this problem would be a self-consistent feedback of the fluctuations, converging to a non-magnetic ground state 5.5. Like the improvement of the ground state functional itself, also the self-consistent treatment starting from a magnetic state and hopefully converging in a non-magnetic state due to magnetic fluctuations is beyond the scope of this work.

The initial idea was to estimate the value of α in order to reproduce the experimentally observed critical temperature as a first step. This leads to one scaling value α for **each** separate calculation *i.e.*

$$\alpha = \alpha [\text{Material, Pressure}].$$

In Tab. 7.2 the value for the two materials at each pressure are shown. The values are all below

one, indicating that the ground state is magnetic except for LiFeAs at 9 GPa. At this point no down scaling of the kernel is necessary to get a finite response. This seems strange because in Sec. 7.1 a finite moment *i.e.* a magnetic ground state was found. The reason for this inconsistency lies in the usage of different codes. The response function and critical values are found using a multiple scattering Korringa-Kohn-Rostoker (KKR)¹⁸ code, whereas the results in the ground state section are obtained using DFT methods within a PW basis set. However, the tendency to magnetism is overestimated in both approaches and the critical value for α is increasing with pressure. This implies that the magnetic state is suppressed by pressure, with FeSe at 18 GPa being an exception of this trend. Precisely the same results have been found with the DFT methods in the previous section.

Once the values of α are settled, it is tried to find an empirical formula to reproduce the estimated values of α . With this approach the theory would leave the field of first-principle calculations and become semi-empirical. The information available for the empirical expression contain ground state properties as the unit cell volume, the energy differences between the three magnetic structures, the electronic structure in \mathbf{k} space (DOS, nesting...), the coefficients $\{a_i\}$ of a fixed spin moment calculation $E = a_0 + a_2 M^2 + a_4 M^4 + \dots$ as well as response quantities like the α_{crit} or a fluctuation strength $\Delta dw_{\chi_{zz}}(\mathbf{q}_M \omega \alpha_1)$ where the scaling value $\alpha_1 < \alpha_{\text{crit}}$ is chosen to create an excitation energy of ~ 20 meV found in experiment (Fig. 7.8).

All these quantities have been calculated and collected for the two compounds at each pressure. Unfortunately it was not possible to find a simple correlation between some of the collected information and the estimated values for α . The reason for this failure is most likely related to the fact that one tries to correct the wrong ground state (no information about the fluctuations), with the information provided by this wrong ground state. This means the scaling of the kernel stays a parameter, **chosen** to reproduce the experimental results.

FeSe			LiFeAs		
Pressure	$\alpha [P]$	α_{crit}	Pressure	$\alpha [P]$	α_{crit}
0 GPa	0.668	0.686	0 GPa	0.890	0.909
6 GPa	0.737	0.755	1 GPa	0.890	0.924
12 GPa	0.738	0.770	3GPa	0.900	0.948
18 GPa	0.720	0.765	6GPa	0.91	0.984
			9GPa	0.905	1.011

Table 7.2.: Values for the rescaling of the kernel used in the calculation for the effective interaction. The values are chosen to obtain reasonable agreement with experiment.

¹⁸Details on the KKR calculation are given in Sec. 7.3.2.

7.3. Contributions to the SC Pairing

After the ground state results have been discussed in detail, it is time to investigate the excitations in the system. In the gap equation [Eqs. (6.11) and (6.10)] three different excitations are present:

1. The vibration modes of the nuclear lattice (Phonons.)
2. The collective excitation of the electronic spin (Paramagnons.)
3. The screening of the Coulomb interaction

All three terms are accessible via **LRDFT**. The results of the linear response calculation lead to fully anisotropic interactions in \mathbf{k} space: $\Lambda(n\mathbf{k}n'\mathbf{k}'\omega)$. These high dimensional objects are very difficult to investigate and the solution of the gap equation becomes very demanding. Fortunately, the Fermi surface of the iron based superconductors is split into two sets: one group of bands around the Γ -point and the other one around the M -point (Figs. 7.2 and 7.11a). The bands around the Γ -point are merged in one band called $\{+\}$ and the bands around the M -point go into the set $\{-\}$. This means the interactions become:

$$\Lambda(n\mathbf{k}n'\mathbf{k}'\omega) \longrightarrow \Lambda_{IJ}(E, E', \omega) \text{ with } I, J \in \{+, -\}.$$

In this approximation it is only possible to find isotropic gap structures like the s_{\pm} or s_{++} in the irreducible representation A_{1g} (Fig. 7.9) and also the anisotropy of the gap with respect to the different bands around Γ or M is neglected [137]. Also d wave structures with nodes on the sheets of the Fermi surface are excluded. To find such structures (like B_{1g} , B_{2g} and A_{1g}) or oscillations of the gap in \mathbf{k} space [138] one has to keep the isotropy in \mathbf{k} space. However, as discussed in the Sec. C.3 there are experimental hints in favor of a s_{\pm} symmetry and the missed d symmetries (due to the constrained symmetry) are energetically close to the s state.

The **DOS** with respect to the bands is important for the averaging process and is shown in Fig. 7.10. The region in \mathbf{k} space close to the Fermi energy is the essential one for the averaging because this is the region where the gap function is highly peaked and varies strongly. Since the electronic energies change along the normal vector of the **Fermi surface** a very dense sampling along this direction is necessary. The energy resolution $\epsilon(\mathbf{k}_1) - \epsilon(\mathbf{k}_2)$ should be in the regime of 10^{-6} Ryd. This resolution is achieved by a dense grid of random \mathbf{k} points with uniform weights and a precise interpolation of the electronic energies is used to obtain the $\epsilon(\mathbf{k})$ at each random grid point. This integration technique is called Metropolis algorithm [139]. It is not feasible to calculate the electronic or nuclei response on such a dense grid and the functions are evaluated on a rougher regular \mathbf{q} grid. In the summation of the random grid points in the calculation of the isotropic interaction [Eq. E.19] always the closest \mathbf{q} is assigned to a pair of random points: $\min_{\mathbf{q}} [(\mathbf{k} - \mathbf{k}') - \mathbf{q}]$. In Fig. 7.11a the regular \mathbf{q} grid and the random grid used for the calculation of the electronic response function are shown.

7.3.1. Phonon Contributions

First the phonon contributions are discussed. For the calculation of the phononic contribution the Sternheimer equation is solved which is the linear response equation for the nuclear degrees of freedom [53]. The implementation within the **PW** code quantum espresso is used [131]. The phonons and isotropic interaction have been calculated by A. Sanna. An ultra soft pseudo potential within the **GGA** has been used [97]. For the **PW** a cutoff of 40 Ryd was sufficient and for the charge a ten times larger value is used. The \mathbf{k} and \mathbf{q} grid for the calculation of the $g_{\lambda\mathbf{q}}^{kk'}$ and $\Omega_{\lambda\mathbf{q}}$ [Eq. (6.8)] are set to $8 \times 8 \times 6$ and $6 \times 6 \times 4$ in LiFeAs and to $10 \times 10 \times 6$ and $6 \times 6 \times 4$ in FeSe, respectively. The averaging of the \mathbf{k} resolved quantity involves a random grid integration and is discussed above. The dependence with respect to E and E' is neglected for the phonons and always the value at the Fermi level $E = E' = 0$ is used in the **gap equation**. This is justified by the small energy ω of the phononic excitations which will induce a quick decay in the function $I(E, E', \omega)$ defined in Eq. (6.4) with respect to larger E and E' .

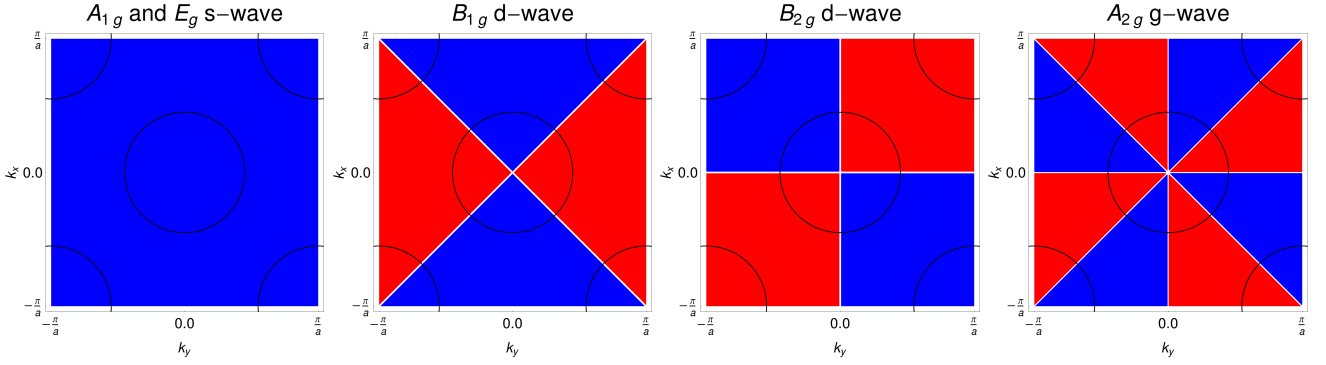


Figure 7.9.: Possible gap symmetries for singlet pairing in the tetragonal lattice. A detailed derivation of the groups is found in Sec. C.3. The red and blue areas indicate regions where the gap switches sign if a symmetry operations is applied. The black lines indicate the two groups of bands at the Fermi level.

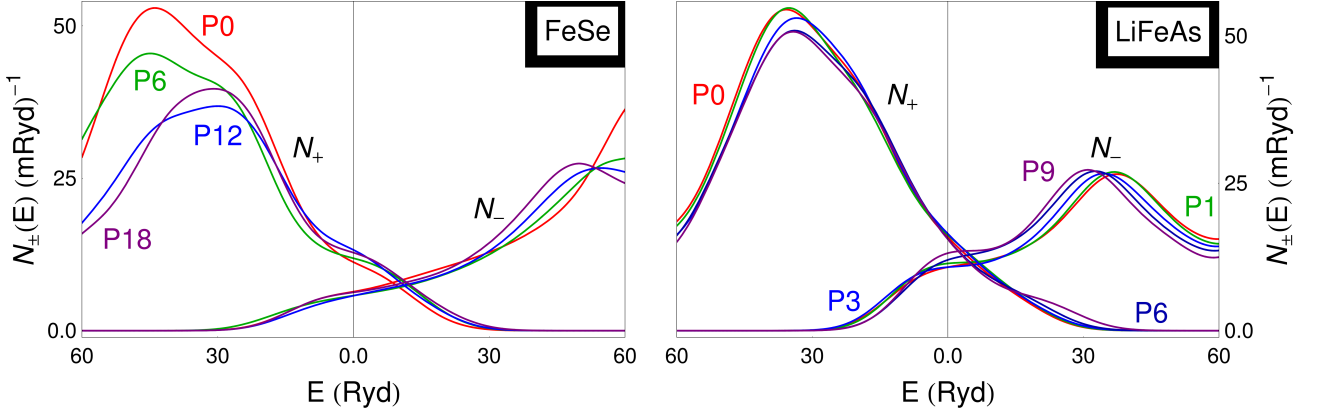
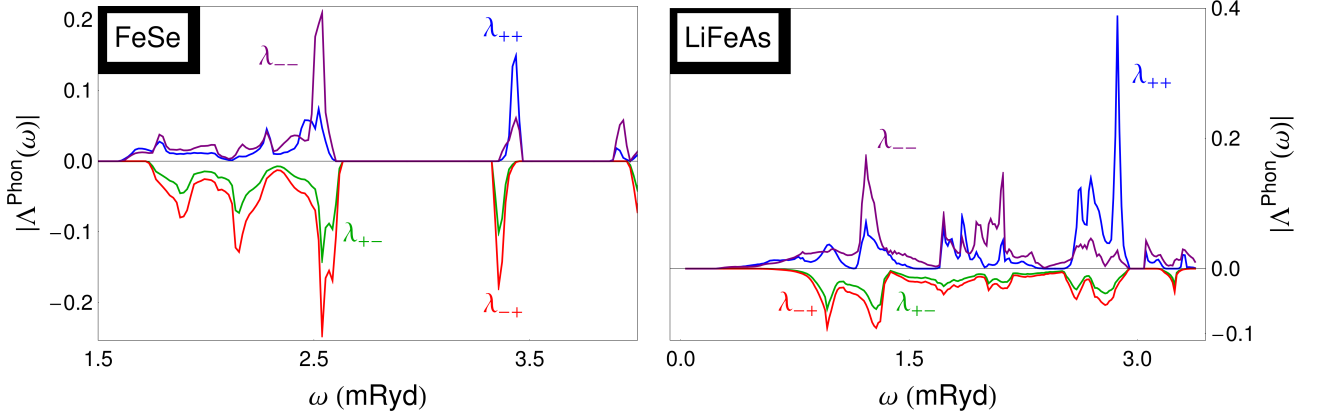
As an example the $\Lambda_{IJ}^{\text{Ph}}(\omega)$ at ambient pressure for FeSe and LiFeAs is shown in Fig. 7.10b. As a function of pressure the phonon spectrum changes a little bit, but the overall structure stays the same. The off diagonal contributions $\Lambda_{\pm\mp}(\omega)$ have almost the same form with respect to frequency and differ only in magnitude due to a different DOS at the Fermi level. For the diagonal contribution $\Lambda_{\pm\pm}(\omega)$ this is not the case and the spectrum is different for the two bands. This difference is stronger in LiFeAs, where already the Fermi surface indicates a stronger difference between the $\{+\}$ and $\{-\}$ band, compared to FeSe (Fig. 7.2). The characteristic frequency ω_{\log} is larger for FeSe compared to LiFeAs. Since the coupling strength is weighted with $\frac{1}{\omega}$ [see Eq. (6.16)] the coupling becomes then stronger in LiFeAs.

However, the general level of the phononic coupling is low and the average coupling strength is around 0.1. This indicates that the phonons cannot be the essential contribution in the iron based superconductors. Besides being too small, the phononic coupling also shows no dome like (FeSe) or declining (LiFeAs) shape with respect to pressure which would be necessary to explain the experimental trends in T_c (Fig. 7.3). This result is in line with the previous calculations of the phononic coupling in the 1111 compound [74]. In these calculations a coupling of 0.2 was predicted, leading to a maximum T_c of less than one Kelvin using the Allen and Dynes Formula with $\mu^* = 0$ [117].

Assuming a s_{\pm} symmetry in the gap equation the contribution $C_{\pm\pm}^{\text{Ph}}\Delta_{\pm}$ pushes the system towards a non-trivial solution, whereas the term $C_{\mp\pm}^{\text{Ph}}\Delta_{\pm}$ fights superconductivity [Eq. (6.12)]. In order to give a quick overview which terms enhance or destroys superconductivity the sign function $\text{sgn}[\Delta_I]\text{sgn}[\Delta_J]$ is added in the Fig. 7.10b to the effective interaction $\Lambda_{IJ}^{\text{Ph}}(\omega)$. A positive value indicates a good contribution for superconductivity and a negative value a destructive one. This convention will also be used in all plots of all the other contribution to the gap. Note that this sign only is induced within the gap equation and plots, but the phonon coupling is always attractive: $\Lambda_{IJ}^{\text{Ph}} < 0$ for all ω, I and J . Finally an average coupling is defined:

$$\bar{\lambda} := \frac{1}{N(\epsilon_F)} \sum_{IJ} N_I(\epsilon_F) \lambda_{IJ} \text{sgn}[\Delta_I] \text{sgn}[\Delta_J]. \quad (7.1)$$

Also this quantity takes into account the sign convention discussed above. Since for the low pressure in FeSe the average phonon coupling is stronger for interband scattering the average value becomes negative. This is not the case for LiFeAs, where the the average value is constant at $\sim +0.02$ with respect to pressure. Our results agree with the recent calculation for LiFeAs at ambient pressure done by R.A. Jishi and D. Scalapino [140].


 (a) Density of states of the two bands N_+ and N_- as a function of Pressure.

 (b) The effective interaction related to phonons $\Lambda_{IJ}^{\text{Phon}}(\omega)$. The sign of the $\Lambda_{IJ}^{\text{Phon}}(\omega)$ is given by $\text{sgn}[\Delta_I] \text{sgn}[\Delta_J]$.

FeSe					LiFeAs				
	0 GPa	6 GPa	12 GPa	18 GPa	0 GPa	1 GPa	3 GPa	6 GPa	9GPa
λ_{++}^{ph}	0.020	0.081	0.059	0.054	0.081	0.079	0.081	0.083	0.089
ω_{\log}	2.367	1.257	2.383	2.578	1.447	1.474	1.508	1.593	1.595
λ_{+-}^{ph}	0.030	0.100	0.043	0.039	0.056	0.055	0.057	0.063	0.068
ω_{\log}	2.326	0.769	2.054	2.332	1.409	1.429	1.458	1.505	1.530
λ_{-+}^{ph}	0.052	0.206	0.100	0.080	0.082	0.078	0.086	0.047	0.079
ω_{\log}	2.326	0.769	2.054	2.332	1.409	1.429	1.458	1.505	1.530
λ_{--}^{ph}	0.030	0.164	0.078	0.054	0.103	0.096	0.108	0.058	0.096
ω_{\log}	2.370	0.339	2.051	2.419	1.339	1.352	1.375	1.421	1.420
λ^{ph}	-0.014	-0.029	0.005	0.003	0.023	0.022	0.022	0.019	0.019

 (c) Table showing the relevant effective coupling strength and logarithmic frequency defined in Eq. (6.18). The ω_{\log} is given in (mRyd) and $\bar{\lambda}^{\text{ph}}$ is the average coupling value defined in Eq. (7.1).

Figure 7.10.: Overview of the phononic contribution in the FeSe and LiFeAs.

7.3.2. Electronic Contributions

In the gap equation [Eqs. (6.11) and (6.10)] a screened Coulomb term w and a SF term Λ^{SF} are present. The full density-density response function χ_{ii} is calculated with LRDFE [Eq. (5.17)]. The charge part χ_{00} leads to the screening of the Coulomb interaction and the magnetic response χ_{zz} the effective interaction due to paramagnons [Eqs. (4.17) and (5.41)]. The KS Green's function is obtained using a KKR multiple scattering code, implemented by P. Buczek, A. Ernst *et. al.* [56, 141]. The calculation of the KS Green's function $G^{\text{KS}}(\bar{\mathbf{r}}_1\bar{\mathbf{r}}_2\mathbf{k}\omega)$ is done on a mesh of $20 \times 20 \times 20$ \mathbf{k} points and in the Atomic Sphere Approximation (ASA). The XC-energy is approximated by the local density approximation [96]. The corresponding adiabatic XC-kernel is frequency-independent and local in space (Sec. B.4). The computationally expensive part within the linear response calculation is the convolution of the two G^{KS} in the non-interacting response. The convolution is calculated with the GF transformed to frequency and inverse space:

$$\chi^{\text{KS}}(\bar{\mathbf{r}}_1\bar{\mathbf{r}}_2\mathbf{q}\omega) = \Delta d\nu \sum_{\mathbf{k}} G^{\text{KS}}(\bar{\mathbf{r}}_2\bar{\mathbf{r}}_1\mathbf{k} - \mathbf{q}\nu - \omega) G^{\text{KS}}(\bar{\mathbf{r}}_1\bar{\mathbf{r}}_2\mathbf{k}\nu).$$

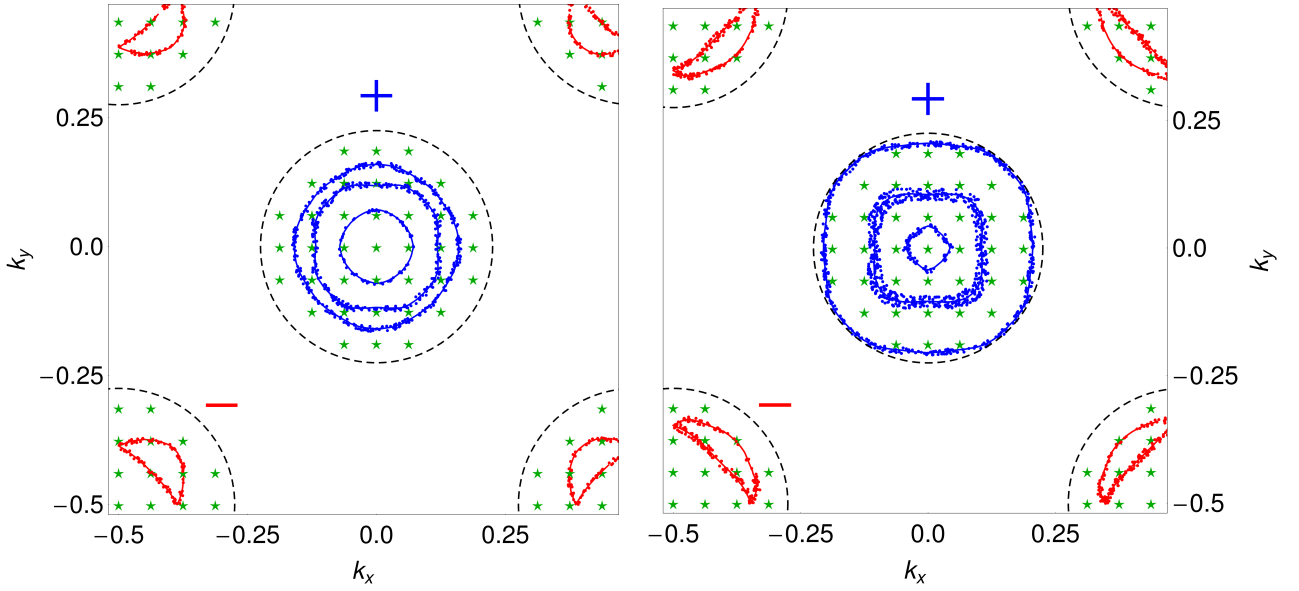
The Fourier transformation (FT) are given in Sec. B.1.2 and B.1.1 for the inverse space and time independent Hamiltonian, respectively. The response function is evaluated on a \mathbf{q} mesh of $20 \times 20 \times 1$ points. The energy points on the nearly real axis are sampled by a logarithmic mesh with 25 energy points ranging from an energy of 10^{-6} Ryd to 0.05 Ryd. The distance to the real axis is set to 0.008 Ryd and a Padé polynomial is used for the analytic continuation to the real axis. The dispersion along the z direction has been neglected due to the two-dimensional structure of the Fermi surface and additionally only \mathbf{q} with $|\mathbf{q} - \mathbf{q}_{\Gamma}| < r$ and $|\mathbf{q} - \mathbf{q}_{\text{M}}| < r$ are considered because this is the area where the bands close to the Fermi energy are located (Fig. 7.2). The radius r is shown in Fig. 7.11a as a dashed line and in Fig. 7.12a for the path along the Brillouin zone (BZ).

In Fig. 7.11a the regular \mathbf{q} grid and the random grid used in the calculation of the isotropic interaction is shown. The bands around the Γ point are larger in LiFeAs compared to FeSe, but all lie within the considered radius r indicated by the dashed black line. For the figure only random grid points with $|\epsilon(\mathbf{k}) - \mu| < 10^{-3}$ Ryd are included and a broad set of points around one band indicates a flat dispersion around the Fermi level. A thin line on the other hand indicates a strong dispersion. Especially the center band around the Γ point and the inner band around the M point in LiFeAs show a flat dispersion which indicates a large effective mass. The smallest effective mass is found for the inner band around Γ in FeSe.

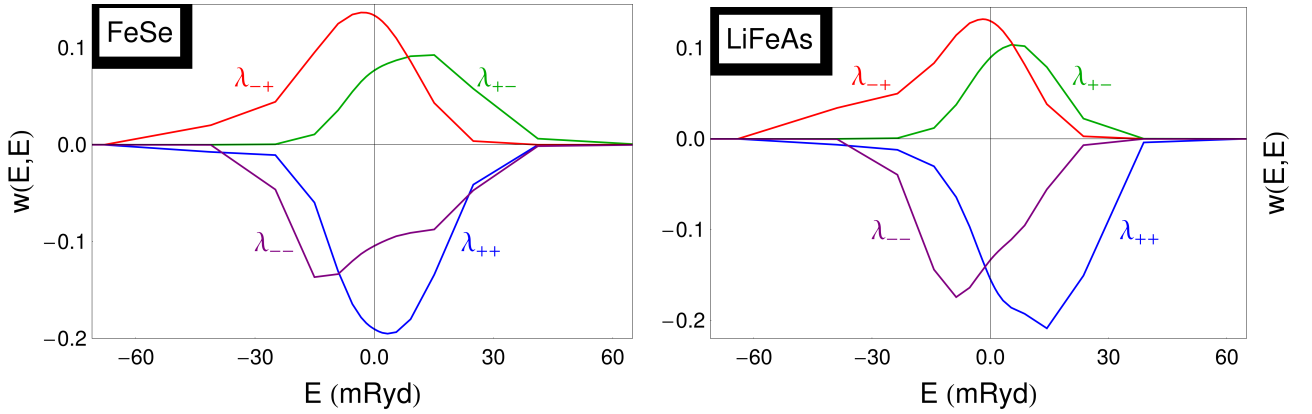
It is not expected that quasi particles corresponding to charge fluctuation (plasmons) are important and provide a coupling. The theory for a plasmon coupling works in an analogous way like the framework for the paramagnons. If the plasmonic excitations are strong for vectors connecting the two parts with altering sign of the gap function this could lead to a coupling (see Sec. 6.2 for a discussion on the paramagnon case). However, the excitation energies for 3D systems of the plasmons are very high (eV range) and there is no experimental evidence for charge fluctuations at $\mathbf{q} \approx \mathbf{q}_{\text{M}}$. Hence the dependence with respect to ω is neglected and the static RPA is used for the screened Coulomb interaction [Eq. (E.13)].

Since, the Phonon contributions are small, the gap must involve a sign change. From the model calculation in Sec. 6.3.2 it is known that the long Coulomb tail is not important for a two band system with a sign changing gap. Relevant are only the Coulomb contribution at the Fermi level which are given by the two bands $\{+\}$ and $\{-\}$ shown in Fig. 7.2. Hence, higher bands and \mathbf{k} points outside the random grid sets (Fig. 7.11a) are not considered for the Coulomb interaction and only a small energy window given by the dispersion of the bands at the Fermi level is used. Remember that this is only possible in a two band system with s_{\pm} symmetry, where the long isotropic Coulomb tail cancels between the bands with different sign. The results for the Coulomb contribution are shown in Fig. 7.11. For an interaction limited to this small energy window it is reasonable to consider also an average coupling at the Fermi level introduced for the phonon contribution in Eq. 7.1.

The Coulomb contribution are a bit larger, than the phononic ones. The values for scattering within one band are larger compared to intraband scattering: $\omega_{\pm\pm} > w_{\mp\pm}$. This difference is induced by



(a) Grids for the calculation of the response function and averaging of the effective interaction. The left panel is FeSe and the right LiFeAs at ambient pressure. The response is only calculated on a rough grid represented by the green stars, but the summation with respect to \mathbf{k} runs over the dense random grid (little dots for the two sets). In the picture only random points within a small energy interval around the Fermi surface are shown.



(b) Static screened Coulomb interaction $w_{IJ}(E, E')$ for $E = E'$. Also here the same sign convention like in Fig. 7.10 is made, but the screened Coulomb interaction is repulsive.

FeSe					LiFeAs				
	0 GPa	6 GPa	12 GPa	18 GPa	0 GPa	1 GPa	3 GPa	6 GPa	9GPa
w_{++}	-0.182	-0.175	-0.177	-0.171	-0.162	-0.155	-0.138	-0.116	-0.110
w_{+-}	0.077	0.069	0.068	0.076	0.093	0.094	0.086	0.090	0.097
w_{-+}	0.133	0.143	0.153	0.155	0.135	0.132	0.130	0.115	0.113
w_{--}	-0.108	-0.093	-0.122	-0.144	-0.138	-0.144	-0.130	-0.144	-0.161
\bar{w}	-0.048	-0.036	-0.038	-0.032	-0.037	-0.036	-0.032	-0.025	-0.029

(c) Table giving the value of w_{IJ} at the Fermi level and \bar{w} is the average with respect to the bands.

Figure 7.11.: Overview of the grids in inverse space for the linear response calculation for the screened Coulomb contributions.

the larger momentum transfer necessary for scattering between the two bands [see Eq. (6.14)]. This means the negative contribution induced by the Coulomb contribution ($\mathcal{C}_{++}^{\text{Coul}}\Delta_+$) in the gap equation are larger than the positive ones ($\mathcal{C}_{+-}^c\Delta_-$). The average Coulomb contribution taking the sign of the bands into account becomes negative and a reduction of the critical temperature by the Coulomb contribution is expected (Sec. 6.2). For both materials there is no strong change in the Coulomb term with respect to pressure. Therefore, like the phonon contribution also the Coulomb terms cannot be the reason for the experimentally observed trends of the critical temperature (Fig. 7.3).

From the three contributions **only** the SF remains to explain the high critical temperatures and the dependence with respect to pressure found in the materials. The Phonon and Coulomb contributions have been ruled out, due to the weak coupling strength and no dependence on pressure. Before the isotropic interactions related to the magnetic fluctuations are presented and discussed an additional approximation is made. In Fig. 7.12a the **spectral function** for FeSe and LiFeAs along a path in the BZ is shown. The spectrum features strong low energy fluctuations for the vector \mathbf{q}_M . The fluctuations are introduced by the **stripe** structure which is the ground state in these materials (see Sec. 7.1 for the ground state results). Also for the other high symmetry points like $\mathbf{q}_X = (\frac{\pi}{2a}, 0, 0)$ and $\mathbf{q}_\Gamma = (0, 0, 0)$ some (small) excitations are observed. The vector \mathbf{q}_Γ corresponds to a ferro magnetic structure and $2\mathbf{q}_X$ to the CB structure. The fluctuations at Γ are stronger in FeSe compared to LiFeAs where more excitations around the X point are found. For larger pressure the fluctuation for $\mathbf{q} \neq \mathbf{q}_M$ are suppressed, and the \mathbf{q}_M dominates because the systems are closer to the critical point for higher pressures.

The excitation with small momentum create the intraband ($\pm \rightarrow \pm$) coupling and the fluctuation around \mathbf{q}_M are responsible for the interband scattering between the two bands ($\mp \rightarrow \pm$). For the Coulomb interaction the intraband contribution were larger than the interband one. This is not the case for the SF: The intensity of the fluctuation is weaker for \mathbf{q}_Γ than for \mathbf{q}_M in LiFeAs and the energies of the excitations for $\mathbf{q} \neq \mathbf{q}_M$ are much higher. Especially the high energies lead to an effective coupling given in Eq. (6.17) which is more than 10 times larger for the interband scattering ($\mathbf{q} \approx \mathbf{q}_M$) than for the intraband one ($\mathbf{q} \approx \mathbf{q}_\Gamma$). Hence, the diagonal elements of the effective interaction related to the SF are neglected:

$$\Lambda_{zz}^{IJ}(EE'\omega) = \begin{pmatrix} \Lambda_{zz}^{++}(EE'\omega) & \Lambda_{zz}^{+-}(EE'\omega) \\ \Lambda_{zz}^{-+}(EE'\omega) & \Lambda_{zz}^{--}(EE'\omega) \end{pmatrix} \approx \begin{pmatrix} 0 & \Lambda_{zz}^{+-}(EE'\omega) \\ \Lambda_{zz}^{-+}(EE'\omega) & 0 \end{pmatrix}.$$

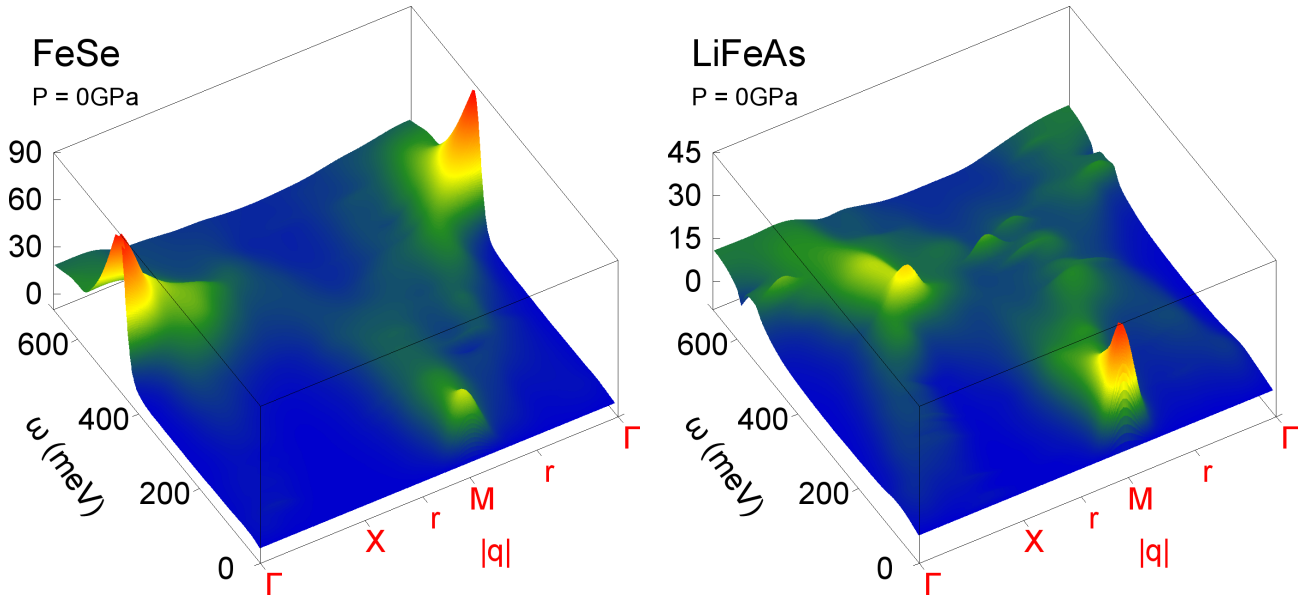
In Fig. 7.12a two ticks with a label r are shown. These indicate the range of possible vectors around M for interband scattering, given by the two spherical sets indicated by the dashed line in Fig. 7.11a. The radius r of the sets is large enough to include all the low lying excitations around the M point. The averaging process for the isotropic interaction involves the same steps already discussed for the Coulomb interaction and the same framework is used for the magnetic contributions. The results are shown in Fig. 7.12b.

The shape of the interaction is different for the two materials. The difference between the considered systems is created by the form of the magnetic response function. The adiabatic kernel is almost constant and does not change the form of the effective interaction given by $f_{zz}^{\text{xc}}\chi_{zz}f_{zz}^{\text{xc}}$ [Eq. (5.41)]. As in all the previous plots the terminus spectral function is used for the largest eigenvalue of the loss tensor introduced in Eq. B.13. The spectral function at \mathbf{q}_M is larger for LiFeAs than for FeSe and shows a clear peak. This is also seen in the effective interaction: For LiFeAs a low energy peak is present, whereas the contribution for FeSe is rather flat. This situation changes if pressure is applied.

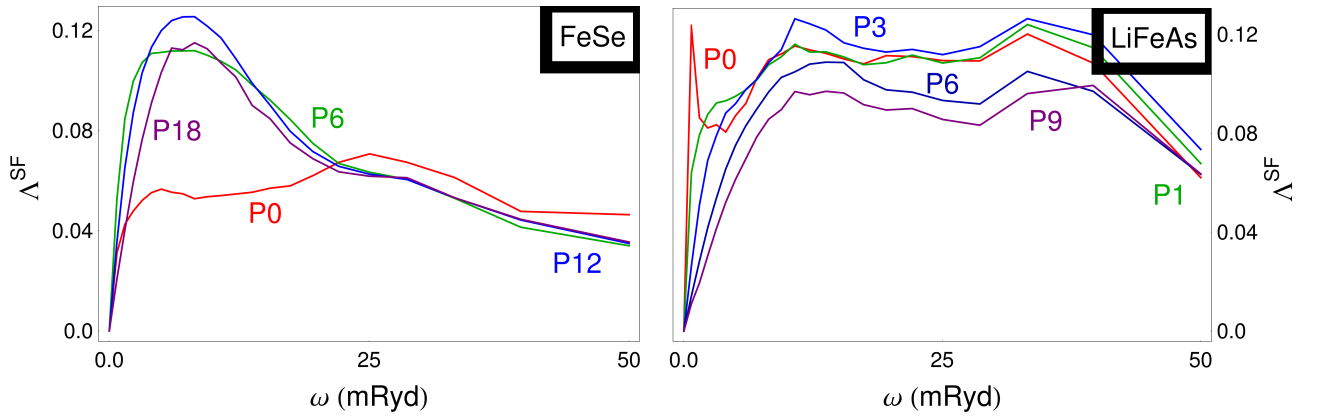
The tendency to magnetism is suppressed by pressure and the critical value α_{crit} is rising. All the values of the critical and used scaling values for each pressure and material are summarized in Tab. 7.2. For the LiFeAs compound the used values for the scaling are not increasing with pressure and are almost constant (~ 0.9). This means the distance between the critical and the used value increases as a function of pressure. This leads to a **decay** of the fluctuations with respect to pressure in LiFeAs and only for ambient pressure a low energy peak is visible in the effective interaction due to strong fluctuations at the M point. The characteristic frequency $\bar{\omega}$ (neglecting the log weight in Eq. (6.18)) is increasing with pressure because the main peak at \mathbf{q}_M is moving to larger values since $|\alpha - \alpha_{\text{crit}}|$ is increasing (Fig. 7.8)

This is different in FeSe. In this material the scaling values are adjusted with pressure. In particular the chosen values lead to a smaller difference $|\alpha - \alpha_{\text{crit}}|$ and stronger fluctuation for intermediate pressures of 6 and 12 GPa. The enhanced fluctuations due to the smaller difference to the critical value of the control parameter create a peak in the effective interaction. Since multiple \mathbf{q} close to \mathbf{q}_M are averaged in the isotropic interaction the peak is broad and at higher energy than the excitation shown in Fig. 7.6b at precisely $\mathbf{q} = \mathbf{q}_M$. A broad response function is also observed in experiment in the non-superconducting regime [102]. For pressures above 12 GPa the scaling is not increased anymore and as a consequence the fluctuations start to decrease due to a larger $|\alpha - \alpha_{\text{crit}}|$ compared to the intermediate pressures. This introduces the **dome** like structure in fluctuation strength with respect to pressure. It should be emphasized again that the scaling function is chosen in such a way to create the dome and decaying form of the response function in FeSe and LiFeAs, respectively.

In the Tab. 7.12c the effective coupling and logarithmic frequencies for the magnetic fluctuations are presented. It becomes immediately clear, that the fluctuation are the key in the description of the FeSC. The effective coupling strength $\bar{\lambda}^{\text{SF}}$ are ~ 10 times larger than the phonon contribution and the Coulomb terms. Also the trends implied for the critical temperature can be captured by the SF coupling. The strength is still in the **weak coupling** regime, but the characteristic frequencies are higher than the phonon ones (like predicted by the **model calculation** in Sec. 6.3.1). The obtained effective coupling and characteristic frequency, put the iron based superconductors in the central region (within the green iso lines) of the $T_c(\bar{\lambda}^{\text{SF}}, \bar{\omega})$ plot derived for the model interaction (Fig. 6.3). Since the iso lines indicate the experimentally observed critical temperatures, the coupling strength provided by the paramagnons will be strong enough to explain the experimentally observed critical temperatures. In the next section **SCDFT** calculations are performed to verify this statement.



(a) spectral function for FeSe and LiFeAs at ambient pressure for a path along the BZ. A dominant peak at the M point is present and some smaller fluctuation at higher energy around the Γ point. In the plot a Gaussian smearing has been used.



(b) Isotropic interaction related to the SF in FeSe and LiFeAs as a function of pressure in GPa. Shown is always the $\Lambda_{zz}^{+-}(E, E', \omega)$ element for $E = E' = 0$.

FeSe					LiFeAs				
	0 GPa	6 GPa	12 GPa	18 GPa	0 GPa	1 GPa	3 GPa	6 GPa	9 GPa
λ_{+-}^{SF}	-0.225	-0.375	-0.354	-0.291	-0.323	-0.294	-0.242	-0.224	-0.209
ω_{Log}	12.35	9.18	9.87	11.20	10.79	12.31	14.38	15.38	15.51
λ_{-+}^{SF}	-0.401	-0.785	-0.818	-0.598	-0.473	-0.423	-0.370	-0.289	-0.251
ω_{Log}	12.39	9.20	9.89	11.23	10.87	12.34	14.44	15.44	16.48
$\bar{\lambda}^{\text{SF}}$	0.289	0.509	0.494	0.392	0.384	0.348	0.293	0.253	0.228

(c) Table showing the relevant effective coupling strength and logarithmic frequency defined in Eq. (6.18). The ω_{Log} is given in (mRyd) and $\bar{\lambda}^{\text{SF}}$ is the arithmetic mean over the four sets.

Figure 7.12.: Overview of the SF contributions.

7.4. SCDFE Calculation

Now that all necessary ingredients for a SCDFE calculation have been computed and discussed, it is time to solve the [gap equation](#) and obtain critical temperatures. All contribution in the gap equation (phonon, Coulomb, SF) are just separate additive terms and it is trivial to include them in a calculation or set them to zero [Eq. (6.9)]. As a first step, the spin contribution are set to zero and the fully linearized gap equation given in Sec. E.3.2 is solved. There are now three possible combinations: Only Coulomb, only phonon and both. All have in common that the T_c is **zero** or to be more precise below the threshold of 0.1 K where the iterations are stopped. This was already expected from the discussion in the previous section, in which very small coupling strengths were found for the Coulomb and phonon terms.

Now the SF are added and three combinations are considered: Only SF, SF and Coulomb and all three contribution. The first setup is often used in model calculation, with the argument that the phonon and Coulomb contribution cancel [16]. In Fig. 7.13 the results for the critical temperatures as a function of pressure are shown together with the experimental data.

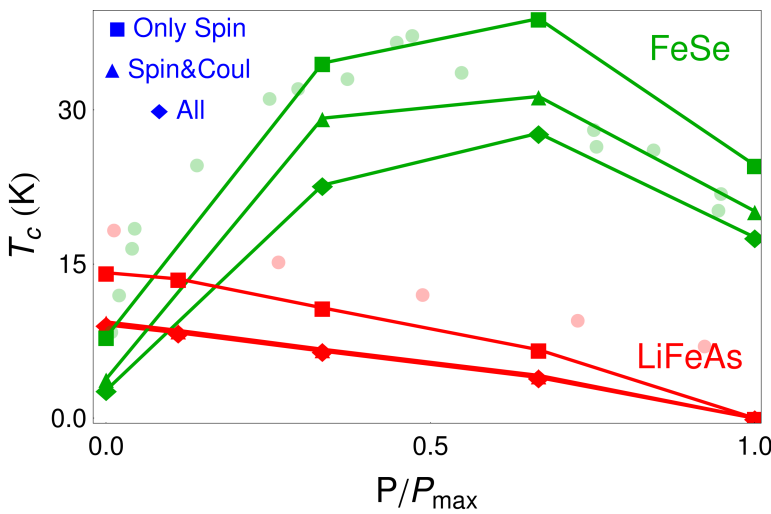


Figure 7.13.: T_c as function of pressure together with the experimental data [9, 126] as light green and red dots.

The message of the calculation is, that it is possible to obtain the correct trends in the T_c and that the trends are related to changes in the magnetic fluctuation with respect to pressure. However, it should be emphasized once more, that the calculations contain the phenomenological scaling of the kernel, and the trends in the T_c are not a result of an *ab-initio* calculation.

But not only the trends in the critical temperature are well reproduced by the calculation. Also the overall size of T_c is in reasonable agreement with experiments, with a tendency of underestimating the experimental values. However, since the materials are located in the weak coupling regime, where an exponential dependence of the critical temperature on the coupling strength is found (Sec. 6.3.1), it is possible to adjust the control parameter for each interaction in order to achieve perfect agreement with experiment. However, it was **not** the aim of this work, to achieve perfect agreement with experiment but to give a first estimation of the coupling strength related to SF in the FeSC.

The results for the critical temperature prove, that the pairing in the FeSe and LiFeAs is unconventional and that magnetic fluctuations are capable of explaining the trends and the magnitude of the critical temperature. The largest values for T_c are found, if only the SF are considered and the smallest if all contribution are included. The case where only repulsive electronic contribution are considered (spin and Coulomb) lies in between the two limiting cases. The reduction of the critical temperature by the phonon term is larger in FeSe compared to LiFeAs. The argument that the Coulomb and phonon contribution cancel, is not supported by our calculation in a two band system. The reason for this lies in the isotropy of the phonon terms with respect to the bands (Fig. 7.10c). For a compensation between

The coupling strength provided by the SF depends strongly on the rescaling of the XC-kernel which was necessary to overcome the problem of the wrongly predicted ground state (Sec. 7.2). The values for the rescaling of the kernel for each pressure are listed in Tab. 7.2. The values have been **chosen** in such a way to reproduce the experimental trends of the critical temperature with respect to pressure:

- LiFeAs has a higher T_c than FeSe at ambient pressure
- The T_c in FeSe shows a dome like dependence on pressure and a decaying one in LiFeAs.

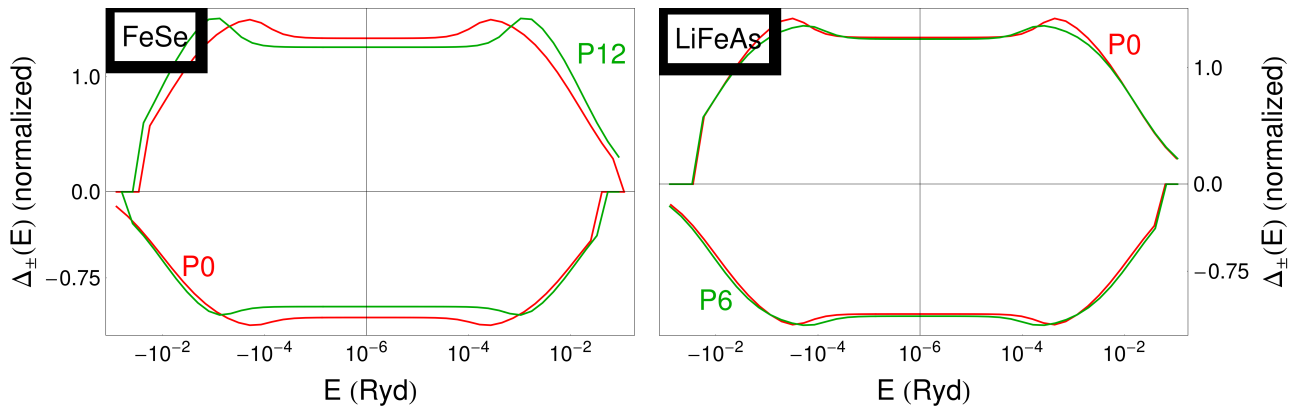


Figure 7.14.: Gap function $\Delta_{\pm}(E)$ close to the phase transition $T \approx T_c$ for FeSe and LiFeAs.

the two, the $\bar{\lambda}_{\pm\pm}^{\text{Ph}}$ should be substantially larger than the off diagonal contribution $\bar{\lambda}_{\pm\mp}^{\text{Ph}}$ in order to compensate the phononic *D-term* [Eq. (6.10)] and the overage of intraband Coulomb repulsion part.

The fact that the purely repulsive contribution (spin and Coulomb) lead to solid transition temperatures, makes a sign change of the gap function mandatory. In Fig. 7.14 the gap function $\Delta_{\pm}(E)$ is shown for the calculation considering only the spin contribution. Since the fully linearized equation is solved the function is normalized to one for each calculation. The form of the gap function is comparable to the results found for the model calculation in Sec. 6.3.2. The system is clearly in the s_{\pm} symmetry. The maximum of the gap is related to the critical temperature. This is already known from the model calculation (Sec. 6.3.2) and is now found for the two materials: For FeSe the maximum position is increasing with pressure as T_c and for LiFeAs it is the other way around. The ratio of the gap $\frac{|\Delta_{+}(E=\epsilon_F)|}{|\Delta_{-}(E=\epsilon_F)|}$ is $\sim \frac{3}{4}$ for both materials which is given by the ratio of the DOS at the Fermi energy (Fig. 7.10a). If the Coulomb contributions are added to the kernel [Eq. 6.11], the gap functions start to show little dips. These dips are well known from the model calculation in Sec. 6.3.2 and indicate the energy region where the Coulomb contributions start to compete with the SF ones. However, a proper *Coulomb renormalization* with a sign change of the gap is not observed. This is related to the small energy cutoff of the Coulomb contribution.

7.5. Summary

In this chapter a full *SCDFT* calculation for FeSe and LiFeAs has been presented. All contributions to the gap equation: screened Coulomb, phonon and magnetic fluctuations have been calculated from first principles and are discussed in Sec. 7.3. Due to the wrongly predicted magnetic ground state (7.2), a scaling parameter of the *XC*-kernel has been introduced. The results show that the Coulomb and phonon contribution are not able to explain the high T_c in this class of materials. The contribution related to the magnetic fluctuations depends strongly on the value of the scaling parameter. It is possible to choose a scaling for each material and at each pressure, such that the coupling provided by the magnetic fluctuations is sufficient to explain the critical temperature in the two compounds (Fig. 7.13).

8. Summary, Conclusion and Outlook

In the current work a theoretical method to include the effects of paramagnetic spin-fluctuations in an *ab-initio* theory of superconductivity has been proposed. The three main results of this work may be summarized as:

1. The construction of a simple expression for the electronic self-energy containing the spin-fluctuations (chapter 5).
2. The inclusion of this self-energy in the existing **SCDFT** framework using the Sham-Schlüter connection (chapter 6).
3. The application of the new functional containing phonon, Coulomb and magnetic contribution to the **FeSC** (chapter 7).

The derivation of the self-energy in chapter 5 is the main **theoretical** result of this work. The starting point for the derivation is the **SC** version of the Hedin equations (chapter 4). The construction involves various steps, but in the end a term with the same form as the well established *Gw* approximation related to the magnetic fluctuations is found (Fig. 6.1). Instead of the screened Coulomb interaction an effective interaction appears which can be viewed as a two-point *T*-matrix or, more abstractly, a correction due to the **vertex function**. This is not surprising since the vertex has been neglected in the *Gw* approximation which was the only Coulomb contribution in the theory before.

Once the equation for the self-energy is fixed, the construction of a **SCDFT** functional follows the same steps as in the existing approximation including the phonon and Coulomb contributions [110]. However, the use of the derived self-energy is not limited to **SCDFT**. It may be equally used in Green's function based methods for **SC** as **Eliashberg theory** or in the renormalization of quasi-particle energies in a non-**SC** context. For the latter application it may be useful that the expression have been derived not only for a non-magnetic state, but also for a collinear magnetic system.

The other main part of this work is **numerical** and evolves around the application of the new functional. This is done on the level of **model calculations** but also for real materials in chapter 6.1 and 7, respectively. Trends with respect to the effective coupling and characteristic frequency imposed by the **Eliashberg theory** are well reproduced by the new contribution related to spin fluctuations. However, the model calculations reveal conceptual differences between the conventional phonon based superconductors with one band and the unconventional case in which a purely electronic interaction is responsible for the pairing. The repulsive nature of the interaction requires a sign change of the gap function and a system with at least two bands or a highly anisotropic gap at the Fermi level. In contrast to the one band case, the long range Coulomb contribution turns out to be not essential for two bands and a sign changing gap.

In chapter 7 the field of model calculations is left and the universal functional is applied to FeSe and LiFeAs which are representatives of the 11 and 111 family of the **FeSC**. The main results of the calculation is that the new contribution related to the magnetic fluctuations are the essential contribution in the gap equation. Without them the critical temperature is unavoidably zero. Also the trends of the critical temperature with respect to pressure can be reproduced by the presented theory and the calculations show that the trends are due to changes in the pairing strength of the magnetic fluctuations. The pairing strength induced by the fluctuations lies in the weak coupling regime, but the involved frequencies are higher than in the usual phonon case. From an application to two materials it does not follow that every unconventional superconductor is captured by this theoretical approach. However, all the iron based superconductors have a similar Fermi surface and magnetic fluctuations nesting the two sheets of the Fermi surface are present in all of them (Tab. 1.1 and Fig. 7.2). Hence,

it is fair to say that the pairing in the **FeSC** is well captured by the **magnetic fluctuations** and it has been shown that this pairing can be included in the **SCDFT** framework.

The biggest obstacle for the systematic application of this work is the wrongly predicted ground state in the investigated materials. A large part of the community is working on this problem. Hence, the problem was circumvented by the inclusion of an empirical parameter α , which gives the rescaling of the **XC**-kernel. The value has been chosen to get a reasonable agreement with the experimental situation for each material at each pressure. This means the presented results are not *ab-initio* anymore. The invention of a simple ground state functional that accounts for the fluctuations (and strong correlation in the cuprates) would solve this problem. However, a functional like this would mark a milestone and change the world of solid state physics in a way only the **LDA** did before. A more straight forward, but less revolutionary road lies in the self-consistent feedback of the fluctuations to the ground-state function. This could be a promising approach to fix the problem of the wrongly predicted ground state and should be tried in the future.

Another project for the future are calculations using a fully **k** resolved gap equation. This would allow to predict properly the gap symmetry as a function of pressure and doping. In this work only the effects of pressure have been considered. However, the applied **KKR** method allows to model doping in terms of the **coherent potential approximation (CPA)**. This method is much more realistic than the rigid band doping used in **DFT** codes. It would be nice to investigate the changes of the gap structure and critical temperature including the effects of doping using the **CPA** properly. In the presented calculation a **NM** ground state has been used as a starting point for the **LRDFT** calculations. Most likely a **DLM** state gives a much more realistic description of the **PM** ground state in the materials. To investigate the difference in the response function with respect to the two ground states (**NM** and **DLM**) is also an interesting topic.

Finally, it can be said that there are many tasks left to do: Difficult ones like the solution of the ground state problem and simpler ones like fully **k** resolved calculations. However, the first results reported in this work are promising and hopefully they encourage other researchers to keep on developing an *ab-initio* theory for the **unconventional SC**.

A. Transformations

A.1. Fourier Transformation – No Boundary Conditions

A.1.1. Space

If the (infinite) real space is not limited by boundary conditions, the [Fourier transformation \(FT\)](#) becomes continuous and the transformation relations between real and inverse space read:

$$f(\mathbf{k}) = \Delta d^3 r f(\mathbf{r}) e^{-i\mathbf{k}\mathbf{r}} \quad f(\mathbf{r}) = \frac{1}{(2\pi)^3} \Delta d^3 k f(\mathbf{k}) e^{i\mathbf{k}\mathbf{r}}. \quad (\text{A.1})$$

Mathematicians tend to distribute a factor of $1/(2\pi)^{\frac{3}{2}}$ on both sides of the transformation, but this is a matter of taste. The only condition is that a double transformation must give back the initial function. This is the case since the delta distribution in three dimensions is given by:

$$\frac{1}{(2\pi)^3} \Delta d^3 r e^{-i\mathbf{k}\mathbf{r}} = \delta(\mathbf{k}) \quad \frac{1}{(2\pi)^3} \Delta d^3 k e^{i\mathbf{k}\mathbf{r}} = \delta(\mathbf{r}).$$

A.1.2. Time

The [FT](#) with respect to time is the one dimensional variant of the transformation from real space to inverse space introduced above:

$$f(\omega) = \Delta d^3 t f(t) e^{-i\omega t} \quad f(t) = \frac{1}{2\pi} \Delta d^3 \omega f(\omega) e^{i\omega t}.$$

A.2. Fourier Transformation – Boundary Conditions

A.2.1. Space

Boundary conditions in a solid state denote that after N_i lattice translations the system is repeated ($P(\mathbf{T})^{N_i} = \mathbf{1}$). Due to this condition the domain of the [FT](#) is finite¹⁹

$$\begin{aligned} \bar{\mathbf{r}} &= \sum_{i=1}^3 \lambda_i \mathbf{a}_i \text{ with } \lambda_i \in [0, 1[& \mathbf{k}_n &= \sum_{i=1}^3 \frac{n_i}{N_i} \mathbf{b}_i \text{ with } n_i \in \{0, \dots, N_i - 1\} \\ \mathbf{T}_n &= \sum_{i=1}^3 n_i \mathbf{a}_i \text{ with } n_i \in \{0, \dots, N_i - 1\} & \mathbf{G}_n &= \sum_{i=1}^3 n_i \mathbf{b}_i \text{ with } n \in 0, 1, 2, \dots \end{aligned}$$

where \mathbf{a}_i are the primitive unit cell vectors describing the crystal structure and \mathbf{b}_i are the primitive reciprocal lattice vectors. The Fourier components become discrete:

$$f(\mathbf{k} + \mathbf{G}) = \sum_{\mathbf{T}} \Delta d^3 \bar{\mathbf{r}} e^{-i(\bar{\mathbf{r}} + \mathbf{T})(\mathbf{k} + \mathbf{G})} f(\bar{\mathbf{r}} + \mathbf{T}) \quad f(\bar{\mathbf{r}} + \mathbf{T}) = \frac{1}{N\Omega_{\text{ws}}} \sum_{\mathbf{k}} \sum_{\mathbf{G}} e^{i(\bar{\mathbf{r}} + \mathbf{T})(\mathbf{k} + \mathbf{G})} f(\mathbf{k} + \mathbf{G}),$$

where the same convention as in the continuous case is used for the prefactor and Ω_{ws} is the size of the Wigner Seitz cell. Any vector \mathbf{r} or \mathbf{q} is given by the sum $\mathbf{r} = \bar{\mathbf{r}} + \mathbf{T}$ and $\mathbf{q} = \mathbf{k} + \mathbf{G}$. Note that the

¹⁹The index n is a collective index $n = \{n_1, n_2, n_3\}$ and $n = 0$ denotes $n_1 = n_2 = n_3 = 0$. The total number of unit cells N is given by $N_1 N_2 N_3$.

function f is invariant under $f(\mathbf{r}) \rightarrow f(\mathbf{r} + N_i a_i)$ due to the definition of the Fourier components. The $e^{i\mathbf{k}_j \mathbf{T}_n}$ is the n -th class of the j -th representation of the translation group. The orthogonality between different representations, derived in [group theory](#) [142], leads to the following relations:

$$\frac{1}{N} \sum_{\mathbf{T}} e^{-i(\mathbf{k}_n + \mathbf{G}_m) \mathbf{T}} = \delta_{0n} \quad \frac{1}{N} \sum_{\mathbf{k}} e^{i\mathbf{k} \mathbf{T}_n} = \delta_{0n}$$

$$\frac{1}{\Omega_{\text{WS}}} \Delta d\bar{r} e^{i\mathbf{G}_n \bar{\mathbf{r}}} = \delta_{0n} \quad \sum_{\mathbf{G}} e^{i\mathbf{G} \bar{\mathbf{r}}} = \delta_{\bar{\mathbf{r}}0}.$$

If a function is invariant with respect to lattice translation *i.e.* $f(\bar{\mathbf{r}} + \mathbf{T}) = f(\bar{\mathbf{r}})$, it becomes very simple in inverse space:

$$f(\mathbf{k} + \mathbf{G}) = N \delta_{\mathbf{k}0} \Delta d^3 \bar{r} e^{-i\bar{\mathbf{r}} \mathbf{G}} f(\bar{\mathbf{r}}). \quad (\text{A.2})$$

The electronic density in a periodic crystal has this symmetry. The function depends only on one vector \mathbf{G} due to the translation symmetry. Let's look at the FT of a function of two spatial variables with translational symmetry. This function depends only on the difference between the two translation vectors ($\mathbf{T}_{12} := \mathbf{T}_1 - \mathbf{T}_2$):

$$f(\mathbf{r}_1, \mathbf{r}_2) = f(\mathbf{r}_1 + \mathbf{T}, \mathbf{r}_2 + \mathbf{T}) \Rightarrow f(\mathbf{r}_1, \mathbf{r}_2) = f(\bar{\mathbf{r}}_1, \bar{\mathbf{r}}_2, \mathbf{T}_{12}).$$

An important example of such a function is the Green's function introduced in chapter 2. Also here the symmetry simplifies the dependence with respect to \mathbf{k}_1 and \mathbf{k}_2 :

$$f(\mathbf{k}_1, \mathbf{G}_1, \mathbf{k}_2, \mathbf{G}_2) = \frac{1}{A_1} \sum_{\mathbf{T}_{12} \mathbf{T}_2} \Delta d\bar{r}_1 d\bar{r}_2 e^{-i(\mathbf{k}_1 + \mathbf{G}_1) \bar{\mathbf{r}}_1} f(\bar{\mathbf{r}}_1, \bar{\mathbf{r}}_2, \mathbf{T}_{12}) e^{+i(\mathbf{k}_2 + \mathbf{G}_2) \bar{\mathbf{r}}_2} e^{-i\mathbf{k}_1 \mathbf{T}_{12}} e^{i(\mathbf{k}_2 - \mathbf{k}_1) \mathbf{T}_2}. \quad (\text{A.3})$$

The vector $\mathbf{k}_1 - \mathbf{k}_2$ is rewritten as $\mathbf{q}_{\mathbf{k}_1 \mathbf{k}_2} + \mathbf{G}_{\mathbf{k}_1 \mathbf{k}_2}$ where $\mathbf{q}_{\mathbf{k}_1 \mathbf{k}_2}$ lies in the first Brillouin zone (BZ). The orthogonality requires a vanishing $\mathbf{q}_{\mathbf{k}_1 \mathbf{k}_2}$ *i.e.* $\delta_{\mathbf{q}_{\mathbf{k}_1 \mathbf{k}_2}, 0}$. Note that for a difference of two \mathbf{k} , the $\delta_{\mathbf{q}_{\mathbf{k}_1 \mathbf{k}_2}, 0}$ is equivalent to a $\delta_{\mathbf{k}_1 \mathbf{k}_2}$ because $|\mathbf{k}_1 - \mathbf{k}_2| < |\mathbf{G}|$ due to $\mathbf{k}_{x,y,z} \in [-\frac{\pi}{a}, \frac{\pi}{a}]$:

$$f(\mathbf{k}_1, \mathbf{G}_1, \mathbf{k}_2, \mathbf{G}_2) = \frac{N \delta_{\mathbf{k}_1 \mathbf{k}_2}}{A_1} \sum_{\mathbf{T}_{12}} \Delta d\bar{r}_1 d\bar{r}_2 e^{-i(\mathbf{k}_1 + \mathbf{G}_1) \bar{\mathbf{r}}_1} f(\bar{\mathbf{r}}_1, \bar{\mathbf{r}}_2, \mathbf{T}_{12}) e^{+i(\mathbf{k}_2 + \mathbf{G}_2) \bar{\mathbf{r}}_2} e^{-i\mathbf{k}_1 \mathbf{T}_{12}}$$

$$f(\bar{\mathbf{r}}_1, \bar{\mathbf{r}}_2, \mathbf{T}_{12}) = \frac{1}{A_2} \sum_{\mathbf{k}_1 \mathbf{k}_2} \sum_{\mathbf{G}_1 \mathbf{G}_2} e^{+i(\mathbf{k}_1 + \mathbf{G}_1) \mathbf{r}_1} f(\mathbf{k}_1, \mathbf{G}_1, \mathbf{k}_2, \mathbf{G}_2) e^{-i(\mathbf{k}_2 + \mathbf{G}_2) \mathbf{r}_2}.$$

The total norm is $A_1 \cdot A_2 = (N \Omega_{\text{WS}})^{-2}$ and it would be straight forward to transfer everything to the real space side as in the previous cases. However, another choice is made here. For uniform systems the function depends only on the difference between spatial arguments and becomes diagonal in inverse space:

$$f(\mathbf{r}_1, \mathbf{r}_2) = f(\mathbf{r}_1 - \mathbf{r}_2, 0) \xrightarrow{\text{FT}} f(\mathbf{k}_1, \mathbf{G}_1, \mathbf{k}_2, \mathbf{G}_2) = \frac{N \Omega_{\text{WS}}}{A_1} \delta_{\mathbf{k}_1 \mathbf{k}_2} \delta_{\mathbf{G}_1 \mathbf{G}_2} f(\mathbf{k}_1 + \mathbf{G}_1).$$

The A_1 and A_2 are chosen such that the uniform function becomes a diagonal matrix with no additional prefactors:

$$A_1 = N \Omega_{\text{WS}} \quad A_2 = N \Omega_{\text{WS}}.$$

A.2.2. Time

For the time argument it seems odd to have periodic boundary conditions. However, in the context of perturbation theory it is essential to introduce a complex time argument for the [Green's function \(GF\)](#). In this formalism the [GF](#) becomes periodic with respect to time. This concept is explained in more detail in [Sec. B.3](#).

A.3. Spin Space Transformation

The set of [Pauli matrices](#) $\sigma^x, \sigma^y, \sigma^z$ and σ^0 is a basis for a four dimensional vector space:

$$\sigma^x = \begin{pmatrix} 0 & 1 \\ 1 & 0 \end{pmatrix} \quad \sigma^y = \begin{pmatrix} 0 & -i \\ i & 0 \end{pmatrix} \quad \sigma^z = \begin{pmatrix} 1 & 0 \\ 0 & -1 \end{pmatrix} \quad \sigma^0 = \begin{pmatrix} 1 & 0 \\ 0 & 1 \end{pmatrix}. \quad (\text{A.4})$$

Each quantity in spin space, may also be written in components of the four Pauli matrices

$$\begin{aligned} B_{\beta\alpha} &= \frac{1}{2} \sum_i \sigma_{\alpha\beta}^i B_i & B_i &= \sum_{\alpha\beta} \sigma_{\alpha\beta}^i B_{\alpha\beta} & \sum_{i=1}^4 \sigma_{\alpha\beta}^i \sigma_{\gamma\delta}^i &= 2\delta_{\alpha\delta} \delta_{\beta\gamma} & (\text{A.5}) \\ A_{\alpha\beta\gamma\delta} &= \frac{1}{4} \sum_{ij} \sigma_{\alpha\beta}^i A_{ij} \sigma_{\gamma\delta}^j & A_{ij} &= \sum_{\alpha\beta\gamma\delta} \sigma_{\beta\alpha}^i A_{\alpha\beta\gamma\delta} \sigma_{\delta\gamma}^j. \end{aligned}$$

B. Normal State Green's and Response Functions

B.1. Properties of the Green's Function and Response Function

The Green's function becomes the central object for a perturbation expansion of an interacting system. The symmetries implied by a Hamiltonian lead to simplifications in the corresponding Green's function. Also the response function is simplified by symmetries in the underlying system. The most common symmetries are listed here. The relations are shown for a general function (R=retarded, A=advanced, T=Time-ordered and M=Matsubara):

$$\begin{aligned} F_{AB}^R(t, t') &= -i\theta(t - t') \left\langle \left[\hat{A}_H(t), \hat{B}_H(t') \right]_- \right\rangle & F^T(t, t') &= -i \left\langle \hat{T} \left[\hat{A}_H(t), \hat{B}_H(t') \right] \right\rangle \\ F_{AB}^A(t, t') &= -i\theta(t' - t) \left\langle \left[\hat{A}_H(t), \hat{B}_H(t') \right]_- \right\rangle & F^M(t, t') &= - \left\langle \hat{T} \left[\hat{A}_H(\tau), \hat{B}_H(\tau') \right] \right\rangle \end{aligned}$$

which is either a single particle GF ($\hat{A} = \hat{\Psi}_\sigma(\mathbf{r})$ and $\hat{B} = \hat{\Psi}_\sigma^\dagger(\mathbf{r}')$) defined in Sec. 2.1, or a response function ($\hat{A} = \Delta\hat{\rho}_i(\mathbf{r})$ and $\hat{B} = \Delta\hat{\rho}_{i'}(\mathbf{r}')$) introduced in Sec. 2.2.

B.1.1. Time Independent System

For real times and time independent systems the Heisenberg picture reads:

$$\hat{O}_H(t) = e^{i(\hat{H} - \mu\hat{N})t} \hat{O}_S e^{-i(\hat{H} - \mu\hat{N})t},$$

where \hat{H} is the Hamilton operator defined in Eq. (2.2) and $\hat{H} - \mu\hat{N}$ is called \hat{K} . The simple exponential form with respect to \hat{K} leads to a function which depends only on the time difference:

$$\begin{aligned} F_{AB}^T(t, t') &\propto \left\langle \hat{A}_H(t) \hat{B}_H(t') \right\rangle = \sum_n \left\langle n \left| \hat{T} \left[\frac{e^{-\beta\hat{K}}}{Z_G} e^{i\hat{K}t} \hat{A} e^{-i\hat{K}} e^{i\hat{K}t'} \hat{B} e^{-\hat{K}t'} \right] \right| n \right\rangle \\ &= \sum_n \frac{e^{-\beta E_n}}{Z_G} e^{iE_n(t-t')} \left\langle n \left| \hat{T} \left[\hat{A} e^{-i\hat{K}(t-t')} \hat{B} \right] \right| n \right\rangle = F_{AB}^T(t - t', 0), \end{aligned}$$

where \hat{A} and \hat{B} are arbitrary operators. Also the retarded and advanced functions depends only on the time difference

$$\begin{aligned} F_{AB}^{R,A}(t, t') &\propto \left\langle \left[\hat{A}_H(t), \hat{B}_H(t') \right]_- \right\rangle = \sum_n \left\langle n \left| \hat{\rho} \left[e^{i\hat{K}t} \hat{A} e^{-i\hat{K}} e^{i\hat{K}t'} \hat{B} e^{-\hat{K}t'} - e^{i\hat{K}t'} \hat{B} e^{-\hat{K}t'} e^{i\hat{K}t} \hat{A} e^{-i\hat{K}} \right] \right| n \right\rangle \\ &= \sum_n \frac{e^{-\beta E_n}}{Z_G} \left\langle n \left| e^{iE_n(t-t')} \hat{A} e^{-i\hat{K}(t-t')} \hat{B} - e^{-iE_n(t-t')} \hat{B} e^{\hat{K}(t-t')} \hat{A} \right| n \right\rangle = F_{AB}^{R,A}(t - t', 0), \end{aligned}$$

and the standard Fourier transformation for a continuous variable are applied [Eq. (A.1)]:

$$\begin{aligned} F_{AB}^{R,A,T}(\omega) &= \Delta_{-\infty}^{\infty} d(t - t') e^{i\omega(t-t')} F_{AB}^{R,A,T}(t - t') & (B.1) \\ F_{AB}^{R,A,T}(t - t') &= \frac{1}{2\pi} \Delta_{-\infty}^{\infty} d\omega t e^{-i\omega(t-t')} F_{AB}^{R,A,T}(\omega). \end{aligned}$$

Also the Matsubara objects [Eqs. (2.11) and (2.22)] are functions of the time difference *i.e.*

$$F_{AB}^M(\tau, \tau') = - \sum_n \langle n | \hat{T} \left[\hat{\rho} e^{\hat{H}\tau} \hat{A} e^{-\hat{H}\tau} e^{\hat{H}\tau'} \hat{B} e^{-\hat{H}\tau'} \right] | n \rangle = F_{AB}(\tau - \tau', 0).$$

If $\tau - \tau' \in [0, \beta]$ the relation:

$$F_{AB}^M(\tau - \tau' + \beta, 0) = -\text{tr} \left[\hat{A}_H(\tau - \tau') e^{-\beta \hat{H}} \hat{B}_H(0) \right] = -\text{tr} \left[e^{-\beta \hat{H}} \hat{B}_H(0) \hat{A}_H(\tau - \tau') \right] = \epsilon F_{AB}(\tau - \tau', 0)$$

is obtained. The factor ϵ is defined in Eq. (B.17). On the other hand for $\tau - \tau' \in [-\beta, 0]$, the following is found:

$$F_{AB}^M(\tau - \tau' - \beta, 0) = -\epsilon \text{tr} \left[e^{-\beta \hat{H}} \hat{B}_H(0) \hat{A}_H(\tau - \tau' - \beta) \right] = \epsilon F_{AB}(\tau - \tau', 0).$$

So the knowledge of $F_{AB}^M(\tau - \tau', 0)$ in the interval $\tau - \tau' \in [-\beta, \beta]$ determines the whole time dependence²⁰ *i.e.* the function is periodic with respect to τ and the FT becomes discrete:

$$\begin{aligned} F_{AB}^M(\omega_n, \omega_{n'}) &:= \Lambda_{-\beta}^{+\beta} d\tau d\tau' e^{i\omega_n \tau} e^{-i\omega_{n'} \tau'} F_{AB}^M(\tau, \tau') \quad \text{with } \omega_n = \frac{2\pi}{2\beta} n \\ &= \frac{\delta_{\omega_n \omega_{n'}}}{2\beta} \Delta_{-\beta}^{+\beta} d(\tau - \tau') e^{i\omega_n(\tau - \tau')} F_{AB}^M(\tau - \tau', 0) = \delta_{\omega_n \omega_{n'}} F_{AB}^M(\omega_n) \\ F_{AB}^M(\tau - \tau', 0) &= \sum_{n=-\infty}^{\infty} e^{-i\omega_n(\tau - \tau')} F_{AB}^M(\omega_n). \end{aligned}$$

The discrete frequencies ω_n are called ‘‘Matsubara frequencies’’ [51]. The transformation to frequency representation is further simplified ($\tau - \tau' = \tilde{\tau}$):

$$F_{AB}^M(\omega_n, \omega_{n'}) = \delta_{\omega_n \omega_{n'}} \Delta_0^{+\beta} d(\tau - \tau') e^{i\omega_n(\tau - \tau')} F_{AB}^M(\tau - \tau', 0) \quad (\text{B.2})$$

$$F_{AB}^M(\tau - \tau', 0) = \frac{1}{\beta} \sum_{n=-\infty}^{\infty} e^{-i\omega_n(\tau - \tau')} F_{AB}^M(\omega_n)$$

$$\omega_n = \begin{cases} \frac{2n\pi}{\beta} & \text{if } \epsilon = 1 \text{ (bosons)} \\ \frac{(2n+1)\pi}{\beta} & \text{if } \epsilon = -1 \text{ (fermions)}. \end{cases} \quad (\text{B.3})$$

B.1.2. Periodic Hamiltonian

In a crystal the nuclear Coulomb potential and hence the whole Hamiltonian [Eq. (2.3)] is periodic with respect to lattice translations \mathbf{T} . This symmetry is transferred also to the Green's function or response function *i.e.*:

$$F(\mathbf{r}_1, \mathbf{r}_2) = F(\mathbf{r}_1 + \mathbf{T}, \mathbf{r}_2 + \mathbf{T}) \Rightarrow F(\mathbf{r}_1, \mathbf{r}_2) = F(\bar{\mathbf{r}}_1, \bar{\mathbf{r}}_2, \mathbf{T}_1 - \mathbf{T}_2),$$

where the vectors $\bar{\mathbf{r}}_1, \bar{\mathbf{r}}_2$ are within the unit cell Ω_{WS} and the translation vector \mathbf{T} connects two unit cells. A transformation to reciprocal space is made which leads to a diagonal function with respect to the long wavelength periodicity given by the \mathbf{k} vector [Eq. (A.3)]:

$$F(\mathbf{k}_1 \mathbf{G}_1 \mathbf{k}_2 \mathbf{G}_2) = \frac{\delta_{\mathbf{k}_1 \mathbf{k}_2}}{\Omega_{\text{WS}}} \Lambda d^3 \bar{\mathbf{r}}_1 d^3 \bar{\mathbf{r}}_2 \sum_{\mathbf{T}_{12}} F(\bar{\mathbf{r}}_1 \bar{\mathbf{r}}_2 \mathbf{T}_{12}) e^{-i(\mathbf{k}_1 + \mathbf{G}_1) \bar{\mathbf{r}}_1} e^{i(\mathbf{k}_2 + \mathbf{G}_2) \bar{\mathbf{r}}_2} e^{-i\mathbf{k}_1 \mathbf{T}_{12}} \quad (\text{B.4})$$

$$F(\bar{\mathbf{r}}_1 \bar{\mathbf{r}}_2 \mathbf{T}_{12}) = \frac{1}{\Omega_{\text{WS}} N} \sum_{\mathbf{k}_1 \mathbf{k}_2} \sum_{\mathbf{G}_1 \mathbf{G}_2} F(\mathbf{k}_1 \mathbf{G}_1 \mathbf{k}_2 \mathbf{G}_2) e^{i(\mathbf{k}_1 + \mathbf{G}_1) \bar{\mathbf{r}}_1} e^{-i(\mathbf{k}_2 + \mathbf{G}_2) \bar{\mathbf{r}}_2} e^{i\mathbf{k}_1 \mathbf{T}_1} e^{i\mathbf{k}_2 \mathbf{T}_2}.$$

²⁰Simply use $F_{AB}^M(\tau - \tau' \pm n\beta, 0) = \epsilon^n F_{AB}^M(\tau - \tau', 0)$ with $n \in \mathbb{N}$.

B.1.3. Collinear Hamiltonian

If the Hamiltonian is **collinear** *i.e.* $[\sigma_z, \hat{H}_0]_- = 0$, it is possible to create an electron with either spin up or spin down: $\hat{\Psi}_\sigma^\dagger(\mathbf{x}) = \sum_k \varphi_{k\sigma}(\mathbf{x}) \hat{a}_{k\sigma}^\dagger$. In such a case also the Green's function becomes diagonal with respect to the spin coordinates:

$$G_0^M(12) = - \left\langle \hat{T} \left[\hat{\Psi}_{\sigma_1}(\mathbf{x}_1) \hat{\Psi}_{\sigma_2}^\dagger(\mathbf{x}_2) \right] \right\rangle_0 = - \sum_{k_1 k_2} \varphi_{k_1 \sigma_1}(\mathbf{x}_1) \varphi_{k_2 \sigma_2}^*(\mathbf{x}_2) \underbrace{\left\langle \hat{T} \left[\hat{a}_{k\sigma_1} \hat{a}_{k'\sigma_2}^\dagger \right] \right\rangle_0}_{=\delta_{\sigma_1 \sigma_2} \delta_{k_1 k_2}}.$$

The full Green's function also becomes diagonal in spin because all parts (Coulomb interaction and G_0) in the expansion given in Eq. (2.29) are spin conserving. The diagonal **GF** leads to a sparse response:

$$\chi_{ij}^M = \begin{pmatrix} \chi_{xx}^M & \chi_{xy}^M & 0 & 0 \\ \chi_{yx}^M & \chi_{yy}^M & 0 & 0 \\ 0 & 0 & \chi_{zz}^M & \chi_{z0}^M \\ 0 & 0 & \chi_{0z}^M & \chi_{00}^M \end{pmatrix}. \quad (\text{B.5})$$

In the next section connections between the retarded, advanced and Matsubara functions are derived. The connections use the spectral representation and conserve the structure in spin space. This means the retarded and advanced **GF** are also diagonal in spin space if $[\sigma_z, \hat{H}_0]_- = 0$ and the $\chi_{ij}^{R,A}$ take the same form as χ_{ij}^M given in Eq. (B.5).

B.1.4. The Spectral Representation

Matsubara Function

The spectral representations is derived in frequency space. The Matsubara Green's function or response function in frequency space reads [Eq. (B.2)]:

$$F_{AB}^M(\omega_n) := - \Delta_0^{+\beta} d\tau e^{i\omega_n \tau} \left[\theta(\tau) \left\langle \hat{A}(\tau) \hat{B}(0) \right\rangle + \epsilon \theta(-\tau) \left\langle \hat{B}(0) \hat{A}(\tau) \right\rangle \right].$$

The Fourier transformation ensures $\tau > 0$ and hence only the first term gives a contribution. The trace in the thermal average [Eq. (2.5)] is evaluated with a set of eigenstates with respect to $\hat{K} = \hat{H} - \mu \hat{N}$, leading to:

$$\begin{aligned} \left\langle \hat{A}(\tau) \hat{B}(0) \right\rangle &= \sum_{nm} \frac{e^{-\beta E_n}}{Z_G} \left\langle n \left| \hat{A}(\tau) \right| m \right\rangle \left\langle m \left| \hat{B}(0) \right| n \right\rangle \\ &= \sum_{nm} \frac{e^{-\beta E_n}}{Z_G} e^{(E_n - E_m)\tau} \left\langle n \left| \hat{A} \right| m \right\rangle \left\langle m \left| \hat{B} \right| n \right\rangle = \sum_{nm} e^{-\beta E_n} e^{(E_n - E_m)\tau} A_{nm} B_{mn} \end{aligned}$$

$$\begin{aligned} \left\langle \hat{B}(0) \hat{A}(\tau) \right\rangle &= \sum_{nm} \frac{e^{-\beta E_n}}{Z_G} \left\langle m \left| \hat{B}(0) \right| n \right\rangle \left\langle n \left| \hat{A}(\tau) \right| m \right\rangle \\ &= \sum_{nm} \frac{e^{-\beta E_n}}{Z_G} e^{(E_n - E_m)\tau} \left\langle n \left| \hat{A} \right| m \right\rangle \left\langle m \left| \hat{B} \right| n \right\rangle = \sum_{nm} e^{-\beta E_m} e^{(E_n - E_m)\tau} A_{nm} B_{mn}. \end{aligned}$$

A shorter name for the matrix elements $A_{nm} := \left\langle n \left| \hat{A} \right| m \right\rangle$ is used and some rearranging is done:

$$F_{AB}^M(\omega_n) = \frac{1}{Z_G} \Delta_{-\infty}^{\infty} dE \sum_{nm} A_{nm} B_{mn} e^{-\beta E_n} \frac{1 - \epsilon e^{-\beta E}}{i\omega_n - E} \delta(E + (E_n - E_m)).$$

The **spectral function** S_{AB} is defined by everything besides the energy denominator:

$$S_{AB}(E) := \frac{1}{Z_G} \sum_{nm} \delta(E + (E_n - E_m)) A_{nm} B_{mn} e^{-\beta E_n} [1 - \epsilon e^{-\beta E}] \quad (\text{B.6})$$

$$F_{AB}^M(\omega_n) = \Delta_{-\infty}^{\infty} dE \frac{S_{AB}(E)}{i\omega_n - E}. \quad (\text{B.7})$$

The function has δ -peaks at the excitation energy $\Delta E_{mn} = E_m - E_n$. Hence the spectral function measures the excitations created in the system at energy E due to the operators \hat{A} and \hat{B} . For the spectral function the following symmetry relations hold:

$$\begin{aligned} S_{AB}(E) &= S_{BA}^*(E) \text{ only for hermitian operators } \hat{A} \text{ and } \hat{B} \\ S_{AB}(E) &= -\epsilon S_{BA}(-E). \end{aligned} \quad (\text{B.8})$$

Retarded and Advanced Function

The spectral representation of the Green's or the response function is obtained in complete analogy to the derivation of the [Matsubara](#) function:

$$F_{AB}^R(\omega) = \Delta_{-\infty}^{+\infty} dE \frac{S_{AB}(E)}{\omega - E + i0^+} \quad G_{AB}^A(\omega) = \Delta_{-\infty}^{+\infty} dE \frac{S_{AB}(E)}{\omega - E - i0^+}, \quad (\text{B.9})$$

where the spectral function S is defined in Eq. (B.6).

Connection R \leftrightarrow M and A \leftrightarrow M

By comparison of Eqs. (B.7) and (B.9) connections between the three functions are found:

$$\begin{aligned} F_{AB}^M(-i\omega + 0^+) &= F_{AB}^R(\omega) & F_{AB}^R(i\omega_n - i0^+) &= F_{AB}^M(\omega_n) \\ F_{AB}^M(-i\omega - 0^+) &= F_{AB}^A(\omega) & F_{AB}^A(i\omega_n + i0^+) &= F_{AB}^M(\omega_n). \end{aligned}$$

A general function with a complex frequency argument $x \in \mathbb{C}$ is defined ($\omega, \omega_n \in \mathbb{R}$):

$$F_{AB}(x) = \Delta_{-\infty}^{+\infty} \frac{S_{AB}(E)}{x - E} = \begin{cases} F_{AB}^R(\omega) & \text{if } x = \omega + i0^+ \\ F_{AB}^A(\omega) & \text{if } x = \omega - i0^+ \\ F_{AB}^M(\omega_n) & \text{if } x = i\omega_n. \end{cases} \quad (\text{B.10})$$

This function determines the retarded, advanced and Matsubara version of the [GF](#) or response function, depending where $F_{AB}(x)$ is evaluated. In general, the function is only known numerically on certain frequency points, and it is not possible to evaluate the function at some frequencies in the complex plane. An analytic continuation using a polynom is possible for short distances. In particular an [analytic continuation](#) from the real frequencies (retarded) to the complex (Matsubara) axis or *vice versa* is not working and a different connection is derived [54]. For this connection the Hermitian (\Re) and anti Hermitian (\Im) part are defined:

$$\Re[F_{AB}(\omega)] := \frac{1}{2} [F_{AB}(\omega) + F_{BA}^*(\omega)] \quad \Im[F_{AB}(\omega)] := \frac{1}{2i} [F_{AB}(\omega) - F_{BA}^*(\omega)].$$

For a diagonal function the definitions reduce to the real and imaginary part. The anti Hermitian part of the retarded or advanced function is [Eq. (B.8)]:

$$\begin{aligned} \Im[G_{AB}^{\text{R,A}}(\omega)] &= \frac{1}{2i} \left[\Delta_{-\infty}^{+\infty} dE \frac{S_{AB}(E)}{\omega - E \pm i0^+} - \Delta_{-\infty}^{+\infty} dE \frac{S_{BA}^*(E)}{\omega - E \mp i0^+} \right] \\ &= \frac{1}{2i} \Delta_{-\infty}^{+\infty} dE \left[\frac{S_{AB}(E)}{\omega - E \pm i0^+} - \frac{S_{AB}(E)}{\omega - E \mp i0^+} \right]. \end{aligned}$$

An expression like $\frac{1}{w-E\pm i0^+}$ leads to following two contributions:

$$\lim_{\eta \rightarrow 0} \frac{1}{w-E \pm i\eta} = \underbrace{\lim_{\eta \rightarrow 0} \frac{w-E}{(w-E)^2 + \eta^2}}_{\begin{cases} \frac{1}{w-E} & \text{for } w-E \neq 0 \\ 0 & \text{for } w-E=0 \end{cases}} \mp \underbrace{\lim_{\eta \rightarrow 0} \frac{i\eta}{(w-E)^2 + \eta^2}}_{\begin{matrix} \text{Lorentz peak with width } \eta \\ \rightarrow \pi i \delta(\omega - E) \end{matrix}}.$$

The first terms together with the integral is the principle value denoted by $\hat{\mathcal{P}}$:

$$\Im F_{AB}^{\text{R},\Lambda}(\omega) = \frac{1}{2i} \left(\hat{\mathcal{P}} \left[\frac{S_{AB}(E)}{\omega - E} \right] - \hat{\mathcal{P}} \left[\frac{S_{AB}(E)}{\omega - E} \right] \right) - \pi \Delta_{-\infty}^{+\infty} dE \delta(\omega - E) S_{AB}(E).$$

The principle value vanishes and the retarded or advanced function are directly related to the spectral function: $\Im [F_{AB}^{\text{R},\Lambda}(\omega)] = \mp \pi S_{AB}(\omega)$ and the Matsubara in terms of the retarded function reads:

$$F_{AB}^{\text{M}}(\omega_n) = \Delta_{-\infty}^{\infty} dE \frac{S_{AB}(E)}{i\omega_n - E} = -\frac{1}{\pi} \Delta_{-\infty}^{\infty} dE \frac{\Im [F_{AB}^{\text{R}}(E)]}{i\omega_n - E} = \frac{2}{\pi} \Delta_0^{\infty} dE \frac{\Im [F_{AB}^{\text{R}}(E)] E}{(\omega_n^2 + E^2)}. \quad (\text{B.11})$$

As discussed above, the spectral function is peaked at the excitation energies of the system. In particular Callen and Welton have shown [143] that the power absorbed by the system exposed to a magnetic field of the form $\mathbf{B}(\mathbf{r}) \sin(\omega t)$ is given by

$$P = -\frac{\omega}{2} \sum_{ij} \Lambda d^3 r_1 d^2 r_2 B_i(\mathbf{r}) \chi_{ij}^{\text{L}}(\mathbf{r}\mathbf{r}'\omega) B_j(\mathbf{r}'). \quad (\text{B.12})$$

This theorem is known as [fluctuation dissipation theorem](#) in literature and in Ph.D. thesis of P. Buczek a longer derivation of the concepts is given [141]. The object χ^{L} is called loss tensor and is given by the anti Hermitian part of the response function:

$$\chi_{ij}^{\text{L}}(\mathbf{r}\mathbf{r}'\omega) := -\frac{1}{2i} [\chi_{ij}(\mathbf{r}\mathbf{r}'\omega) - \chi_{ji}(\mathbf{r}'\mathbf{r}\omega)] = \pi S_{ij}(\mathbf{r}\mathbf{r}'\omega). \quad (\text{B.13})$$

Motivated by Eq. (B.12) the largest eigenvalue of the loss tensor or the spectral function largely determines the absorption strength in the system. This is a very convenient result because a scalar eigenvalue is much easier to analyze, then a complete matrix. Hence, unless mentioned **otherwise** the largest eigenvalue of the matrix $\chi_{ij}^{\text{L}}(\mathbf{r}\mathbf{r}'\omega)$ for each ω is called [spectral function](#) of an response function.

B.2. Coupling Constant Integration

For the [coupling constant](#) integration the full Hamiltonian [Eq. (2.2)] is split in two parts:

$$\hat{H}_\lambda = \hat{H}_0 + \lambda \hat{W}.$$

The parameter λ is zero for a non-interacting system and one for the fully interacting one. The partition function [Eq. (2.6)] and hence also the grand canonical potential [Eq. (2.32)] depends on the parameter λ : $\Omega_\lambda = -\frac{1}{\beta} \ln [Z_{G\lambda}]$. The derivative with respect to λ of the grand canonical potential reads:

$$\frac{d\Omega_\lambda}{d\lambda} = \frac{1}{\beta Z_{G\lambda}} \frac{dZ_{G\lambda}}{d\lambda} = \frac{1}{\beta Z_{G\lambda}} \frac{d}{d\lambda} \text{tr} [e^{\beta \hat{K}_\lambda}] = \text{tr} \left[\frac{e^{\beta \hat{K}_\lambda}}{Z_{G\lambda}} \hat{W} \right] = \text{tr} [\hat{\rho}_\beta^\lambda \hat{W}] = \langle \hat{W} \rangle_\lambda.$$

Integration with respect to λ from 0 to 1 leads to the standard equation connecting the full [grand canonical potential](#) with the non-interacting one[52]:

$$\Omega_{\lambda=1} = \Omega_{\lambda=0} + \Delta_0^1 d\lambda \langle \hat{W} \rangle_\lambda.$$

The expectation value on the right hand side may be connected to a one particle expectation value, later identified as the Green's function. The [equation of motion](#) for the electronic annihilation operator in the Heisenberg picture using the operator \hat{H}_λ reads:

$$\partial_{\tau_1} \hat{\Psi}_\lambda(1) = [\hat{K}, \hat{\Psi}_\lambda(1)] = [\hat{K}_0, \hat{\Psi}_\lambda(1)] + [\hat{W}, \hat{\Psi}_\lambda(1)]. \quad (\text{B.14})$$

The commutators are worked out and the operator $-\hat{\Psi}_\lambda^\dagger(2)$ is multiplied to the equation:

$$-\partial_{\tau_1} \hat{\Psi}_\lambda^\dagger(2) \hat{\Psi}_\lambda(1) = \hat{\Psi}_\lambda^\dagger(2) \left[K_0(\mathbf{r}_1) \hat{\Psi}_\lambda(1) + \Delta d^3v(31) \hat{\Psi}_\lambda^\dagger(3) \hat{\Psi}_\lambda(3) \hat{\Psi}(1) \right].$$

The thermal average [Eq. (2.5)] of the equation is taken and the integral with respect to \mathbf{r}_1 is performed in order to obtain the expectation value of \hat{W} :

$$2 \langle \hat{W} \rangle_\lambda = \sum_{\sigma_1} \Delta d^3r_1 \lim_{\substack{\mathbf{r}_2 \rightarrow \mathbf{r}_1 \\ \sigma_2 \rightarrow \sigma_1}} \lim_{\tau_2 \searrow \tau_1} [-\partial_{\tau_1} - K_0(\mathbf{r}_1)] \text{tr} \left[\hat{\rho}_\beta^\lambda \hat{\Psi}_\lambda^\dagger(2) \hat{\Psi}_\lambda(1) \right]. \quad (\text{B.15})$$

The function on the right hand side leads to the definition of the single particle [Matsubara GF](#) $G^M(12)$:

$$G_\lambda^M(12) := -\langle \hat{T} [\hat{\Psi}_\lambda(1) \hat{\Psi}_\lambda^\dagger(2)] \rangle = -\text{tr} \left[\hat{\rho}_\beta^\lambda \hat{T} [\hat{\Psi}_\lambda(1) \hat{\Psi}_\lambda^\dagger(2)] \right].$$

The operator \hat{T} is the [time ordering operator](#) which acts on two operators in the Heisenberg picture in the following way:

$$\hat{T} [\hat{A}(\tau_1) \hat{B}(\tau_2)] := \begin{cases} \hat{A}(\tau_1) \hat{B}(\tau_2) & \tau_1 > \tau_2 \\ \epsilon \hat{B}(\tau_2) \hat{A}(\tau_1) & \tau_2 > \tau_1 \end{cases} \quad (\text{B.16})$$

$$\epsilon = \begin{cases} -1 & \text{if } \hat{A} \text{ and } \hat{B} \text{ contain both an odd number of fermionic operators} \\ +1 & \text{otherwise.} \end{cases} \quad (\text{B.17})$$

The average of $\langle \hat{W} \rangle$ in terms of the electronic Green's function reads:

$$2 \langle \hat{W} \rangle_\lambda = \sum_{\sigma_1} \Delta d^3r_1 \lim_{\substack{\mathbf{r}_2 \rightarrow \mathbf{r}_1 \\ \sigma_2 \rightarrow \sigma_1}} \lim_{\tau_2 \searrow \tau_1} [-\partial_{\tau_1} - K_0(\mathbf{r}_1)] G_\lambda^M(12).$$

B.3. Non-SC Response Function

The review article [144] by Onida *et. al.* gives a nice comparison between the [GF](#) and [density functional theory \(DFT\)](#) approach for the response function.

B.3.1. χ^M – Many-Body Approach

In Sec. D.1.4 only one external field φ_0 coupling to the total charge density has been considered. In order to access also the magnetic degrees of freedom three additional fields coupling to the magnetic density are necessary:

$$\hat{\Phi}(\tau) = \sum_{i=0}^3 \Delta d^3r \varphi_i(\mathbf{x}) \hat{\rho}_i(\mathbf{r}) = \sum_{i=0}^3 \Delta d^3r \varphi_i(\mathbf{x}) \left[\sigma_{\alpha\beta}^i \hat{\Psi}_\alpha^\dagger(\mathbf{r}) \hat{\Psi}_\beta(\mathbf{r}) \right].$$

The generalization of Eq. (D.5) for four fields reads:

$$\begin{aligned} \frac{\delta G(12)}{\delta \varphi_i(\mathbf{x}_3)} &= \rho_i(\mathbf{r}_3) G(12) + \sum \sigma_{\alpha\beta}^i \left\langle \hat{T} \left[\hat{\Psi}_\alpha^\dagger(\mathbf{x}_3) \hat{\Psi}_\beta(\mathbf{x}_3) \Psi_{\sigma_1}(\mathbf{x}_1) \hat{\Psi}_{\sigma_2}^\dagger(\mathbf{x}_2) \right] \right\rangle \\ &= \rho_i(\mathbf{r}_3) G(12) - \sum \sigma_{\alpha\beta}^i \left\langle \hat{T} \left[\hat{\Psi}_\alpha^\dagger(\mathbf{x}_3) \hat{\Psi}_\beta(\mathbf{x}_3) \hat{\Psi}_{\sigma_2}^\dagger(\mathbf{x}_2) \Psi_{\sigma_1}(\mathbf{x}_1) \right] \right\rangle. \end{aligned}$$

By performing the equal time limit $\tau_2 \rightarrow \tau_2$ and $\mathbf{r}_2 = \mathbf{r}_1$ the GF $\bar{G}_{\sigma_1\sigma_2}(\mathbf{x}_1\mathbf{x}_2)$ becomes the expectation value $\langle \hat{\Psi}_{\sigma_2}^\dagger(\mathbf{r}_1) \hat{\Psi}_{\sigma_1}(\mathbf{r}_1) \rangle$ and the response function is defined in analogy to the proper part [Eq. (4.18)] using a functional derivative

$$\begin{aligned} \chi_{ji}^M(\mathbf{x}_1\mathbf{x}_3) &:= -\frac{\delta\rho_j(\mathbf{x}_1)}{\delta\varphi_i(\mathbf{x}_3)} = -\sigma_{\sigma_2\sigma_1}^j \frac{\delta G_{\sigma_1\sigma_2}(\mathbf{x}_1\mathbf{x}_1^+)}{\delta\varphi_i(\mathbf{x}_3)} \\ &= \langle \hat{\rho}_j(\mathbf{x}_1) \hat{\rho}_i(\mathbf{x}_3) \rangle + \rho_j(\mathbf{x}_1) \rho_i(\mathbf{x}_3) = \left\langle \hat{T} [\hat{\rho}_j(\mathbf{x}_1) - \rho_j(\mathbf{x}_1)] [\hat{\rho}_i(\mathbf{x}_3) - \rho_i(\mathbf{x}_3)] \right\rangle. \end{aligned} \quad (\text{B.18})$$

Note that the expression is identical to the retarded response function given in Eq. (2.21) derived using linear response (LR) theory, but the time ordered object is given here. Using the chain rule a Dyson equation is found:

$$\chi_{ij}^M(\mathbf{x}_1\mathbf{x}_2) = -\frac{\delta\rho_i(\mathbf{x}_1)}{\delta\varphi_j(\mathbf{x}_2)} = P_{ij}(\mathbf{x}_1\mathbf{x}_2) - \Lambda dx dx' P_{i0}(\mathbf{x}_1\mathbf{x}) v(\mathbf{x}\mathbf{x}') \chi_{0j}(\mathbf{x}'\mathbf{x}_2). \quad (\text{B.19})$$

B.3.2. χ^M – DFT Approach

An alternative way to calculate the response function is provided using the Kohn-Sham (KS) Green's function [Eq. (D.9)]. For the exact exchange-correlation (XC)-potential the exact density is reproduced by the KS system. With this relation the Matsubara response function is expressed using the G_{KS} :

$$\chi_{ij}^M(\mathbf{x}_1\mathbf{x}_2) = -\frac{\delta\rho_i(\mathbf{x}_1)}{\delta\varphi_j(\mathbf{x}_2)} = \sum_{\alpha\beta\sigma\sigma'} \Lambda dx dx' \sigma_{\beta\alpha}^i G_{\alpha\sigma}^{\text{KS}}(\mathbf{x}_1\mathbf{x}) \frac{\delta(G_{\sigma\sigma'}^{\text{KS}})^{-1}(\mathbf{x}\mathbf{x}')}{\delta\varphi_j(\mathbf{x}_2)} G_{\sigma'\beta}^{\text{KS}}(\mathbf{x}'\mathbf{x}_1^+).$$

The derivative of the inverse G^{KS} is [cf. Eqs. (D.9) or (D.2)]:

$$-\frac{\delta(G_{\sigma\sigma'}^{\text{KS}})^{-1}(\mathbf{x}\mathbf{x}')}{\delta\varphi_j(\mathbf{x}_2)} = \delta_{\mathbf{x}\mathbf{x}'} \left[\sigma_{\sigma\sigma'}^j \delta_{\mathbf{x}\mathbf{x}_2} + \sum_{lk} \sigma_{\sigma\sigma'}^l \Delta dx'' \frac{\delta[v^{\text{H}}(\mathbf{x}) \delta_{k0} \delta_{l0} + v_l^{\text{xc}}[\rho](\mathbf{x})] \delta\rho_k(\mathbf{x}'')}{\delta\rho_k(\mathbf{x}'')} \frac{\delta\rho_k(\mathbf{x}'')}{\delta\varphi_j(\mathbf{x}_2)} \right].$$

The expression for $\frac{\delta(G^{\text{KS}})^{-1}}{\delta\varphi}$ is plugged into the equation for the susceptibility:

$$\begin{aligned} \chi_{ij}^M(\mathbf{x}_1\mathbf{x}_2) &= - \sum_{\alpha\beta\sigma\sigma'} \Lambda dx dx' \sigma_{\beta\alpha}^i G_{\alpha\sigma}^{\text{KS}}(\mathbf{x}_1\mathbf{x}) \delta_{\mathbf{x}\mathbf{x}'} \left[\sigma_{\sigma\sigma'}^j \delta_{\mathbf{x}\mathbf{x}_2} + \right. \\ &\quad \left. \sum_{lk} \sigma_{\sigma\sigma'}^l \Delta dx'' \frac{\delta[v^{\text{H}}(\mathbf{x}) \delta_{k0} \delta_{l0} + v_l^{\text{xc}}[\rho](\mathbf{x})] \delta\rho_k(\mathbf{x}'')}{\delta\rho_k(\mathbf{x}'')} \underbrace{\frac{\delta\rho_k(\mathbf{x}'')}{\delta\varphi_j(\mathbf{x}_2)}}_{=-\chi_{kj}^M} \right] G_{\sigma'\beta}^{\text{KS}}(\mathbf{x}'\mathbf{x}_1^+) \\ \chi_{ij}^M(\mathbf{x}_1\mathbf{x}_2) &= - \sum_{\alpha\beta\sigma\sigma'} \Delta dx \sigma_{\beta\alpha}^i G_{\alpha\sigma}^{\text{KS}}(\mathbf{x}_1\mathbf{x}_2) \sigma_{\sigma\sigma'}^j G_{\sigma'\beta}^{\text{KS}}(\mathbf{x}_2\mathbf{x}_1^+) + \sum_{\alpha\beta\sigma\sigma'} \sum_{lk} \Lambda dx dx'' \times \\ &\quad \sigma_{\beta\alpha}^i G_{\alpha\sigma}^{\text{KS}}(\mathbf{x}_1\mathbf{x}) G_{\sigma'\beta}^{\text{KS}}(\mathbf{x}\mathbf{x}_1^+) \sigma_{\sigma\sigma'}^l [\delta_{k0} \delta_{l0} v(\mathbf{x}\mathbf{x}'') + f_{lk}^{\text{xc}}(\mathbf{x}\mathbf{x}'')] \chi_{kj}^M(\mathbf{x}''\mathbf{x}_2). \end{aligned}$$

The definition of the KS response function χ_{ij}^{KS} and the XC-kernel f_{lk}^{xc} [145]:

$$\begin{aligned} \chi_{ij}^{\text{KS}}(\mathbf{x}_1\mathbf{x}_2) &:= - \sum_{\alpha\beta\sigma\sigma'} \sigma_{\beta\alpha}^i G_{\alpha\sigma}^{\text{KS}}(\mathbf{x}_1\mathbf{x}_2) G_{\sigma'\beta}^{\text{KS}}(\mathbf{x}_2\mathbf{x}_1^+) \sigma_{\sigma\sigma'}^j \\ f_{lk}^{\text{xc}}(\mathbf{x}_1\mathbf{x}_2) &:= \frac{\delta v_l^{\text{xc}}[\rho](\mathbf{x}_1)}{\delta\rho_k(\mathbf{x}_2)} = \frac{\delta^2 E_{\text{xc}}}{\delta\rho_l(\mathbf{x}_1) \delta\rho_k(\mathbf{x}_2)} \end{aligned}$$

lead to the ‘‘DFT Dyson equation’’ for the response function [145]:

$$\chi_{ij}^M(\mathbf{x}_1\mathbf{x}_2) = \chi_{ij}^{\text{KS}}(\mathbf{x}_1\mathbf{x}_2) - \sum_{lk} \Lambda d\mathbf{x}d\mathbf{x}' \chi_{il}^{\text{KS}}(\mathbf{x}_1\mathbf{x}) [\delta_{k0}\delta_{0l}v(\mathbf{x}\mathbf{x}') + f_{lk}^{\text{xc}}(\mathbf{x}\mathbf{x}')] \chi_{kj}^M(\mathbf{x}'\mathbf{x}_2).$$

Note that at this point the XC-potential and density are time dependent. The reason for the time dependence lies in the probing field. However, the derivative is evaluated in the end at $\varphi_i = 0$ (as discussed in Sec. D.1.4) and the Hamiltonian becomes static and the response and kernel depend only on time differences. For the analysis in Sec. 5 it is convenient to split the Dyson equation for χ^M in two parts. Assume a general Dyson equation $c = a_0 + a_0 C c$ and split the operator $C = A + B$ in two contributions:

$$c = a_0 + a_0 (A + B) c = \frac{a_0}{1 - a_0 (A + B)}.$$

It is possible to iterate two separate Dyson equations containing the operators A and B to obtain c :

$$a = a_0 + a_0 A a = \frac{a_0}{1 - a_0 A} \quad \text{and} \quad c = a + a B c = \frac{a}{1 - a B},$$

which is seen by simply inserting the two equations in each other:

$$c = \frac{\frac{a_0}{1 - a_0 A}}{1 - \frac{a_0}{1 - a_0 A} B} = \frac{a_0}{1 - a_0 (A + B)}.$$

For the response function a separation in the proper part containing no Coulomb contribution and the rest is natural:

$$P = \chi^{\text{KS}} - \chi^{\text{KS}} f^{\text{xc}} P \quad \text{and} \quad \chi^M = P - P v \chi^M. \quad (\text{B.20})$$

B.4. Adiabatic Local Density Approximation

The XC-energy of the static, homogenous electron gas (HEG) is a functional of the constant density ρ and magnetization $|\mathbf{m}|$. The XC-kernel for the HEG reads:

$$f_{ij}^{\text{HEG}} = \frac{\delta^2 E^{\text{HEG}}[\rho, |\mathbf{m}|]}{\delta \rho_i \delta \rho_j}.$$

In the adiabatic local density approximation (ALDA) the functional for the HEG is evaluated at each point in space-time with the varying density of the interacting system:

$$f_{ij}^{\text{xc}}(\mathbf{x}\mathbf{x}') = \frac{\delta^2 E}{\delta \rho_i(\mathbf{x}) \delta \rho_j(\mathbf{x}')} \approx \delta_{\mathbf{x}\mathbf{x}'} f_{ij}^{\text{ALDA}}(\mathbf{x})$$

$$f_{ij}^{\text{ALDA}}(\mathbf{x}) = f_{ij}^{\text{HEG}}[\rho, |\mathbf{m}|]_{\rho_i=\rho_i(\mathbf{x})} = \left. \frac{\delta^2 E^{\text{HEG}}[\rho, |\mathbf{m}|]}{\delta \rho_i \delta \rho_j} \right|_{\rho_i=\rho_i(\mathbf{x})}.$$

For a lattice periodic and static density, the exact kernel depends only on the time difference $t_1 - t_2$, the position within the unit cell $\{\bar{\mathbf{r}}_1, \bar{\mathbf{r}}_2\}$ and the distance of the two unit cells $\mathbf{T}_1 - \mathbf{T}_2$. In the ALDA this symmetry leads to a static and local kernel *i.e.*:

$$f_{ij}^{\text{xc}}(\bar{\mathbf{r}}_1, \bar{\mathbf{r}}_2, \mathbf{T}_1 - \mathbf{T}_2, t_1 - t_2) \approx \delta_{t_1 t_2} \delta_{\mathbf{r}_1 \mathbf{r}_2} f_{ij}^{\text{ALDA}}(\bar{\mathbf{r}}_1).$$

and in reciprocal space the ALDA kernel depends only on a single \mathbf{G} vector [Eq. (A.2)].

C. DFT for Superconductors

C.1. The Pairing Potential

The **pairing potential** couples to the **anomalous density** χ . The most general contribution in the Hamiltonian corresponding to the anomalous density is:

$$\hat{H}_{\text{SC}} = \sum_{\sigma\sigma'} \Lambda d^3r d^3r' \Delta_{\sigma\sigma'}^{\text{ext}}(\mathbf{r}\mathbf{r}') \hat{\Psi}_{\sigma}(\mathbf{r}) \hat{\Psi}_{\sigma'}(\mathbf{r}') + h.c. .$$

The sum over spin is rewritten in terms of the one singlet and three triplet channels [Eq. (A.5)]:

$$\hat{H}_{\text{SC}} = \sum_{i=1}^4 \Lambda d^3r d^3r' \Delta_i^{\text{ext}}(\mathbf{r}\mathbf{r}') \chi_i(\mathbf{r}\mathbf{r}') + h.c. ,$$

where the densities are given by:

$$\hat{\chi}_i(\mathbf{r}, \mathbf{r}') = \sum_{\alpha\beta} \hat{\Psi}_{\alpha}(\mathbf{r}) \tau_{\alpha\beta}^i \hat{\Psi}_{\beta}(\mathbf{r}') = \begin{pmatrix} \hat{\Psi}_{\uparrow}(\mathbf{r}) \hat{\Psi}_{\downarrow}(\mathbf{r}') - \hat{\Psi}_{\downarrow}(\mathbf{r}) \hat{\Psi}_{\uparrow}(\mathbf{r}') \\ \hat{\Psi}_{\downarrow}(\mathbf{r}) \hat{\Psi}_{\downarrow}(\mathbf{r}') - \hat{\Psi}_{\uparrow}(\mathbf{r}) \hat{\Psi}_{\uparrow}(\mathbf{r}') \\ \hat{\Psi}_{\downarrow}(\mathbf{r}) \hat{\Psi}_{\downarrow}(\mathbf{r}') + \hat{\Psi}_{\uparrow}(\mathbf{r}) \hat{\Psi}_{\uparrow}(\mathbf{r}') \\ \hat{\Psi}_{\uparrow}(\mathbf{r}) \hat{\Psi}_{\downarrow}(\mathbf{r}') + \hat{\Psi}_{\downarrow}(\mathbf{r}) \hat{\Psi}_{\uparrow}(\mathbf{r}') \end{pmatrix} \quad (\text{C.1})$$

$$\tilde{\Delta}^i(\mathbf{r}, \mathbf{r}') = \begin{pmatrix} \tilde{\Delta}_s(\mathbf{r}, \mathbf{r}') \\ \tilde{\Delta}_{tx}(\mathbf{r}, \mathbf{r}') \\ \tilde{\Delta}_{ty}(\mathbf{r}, \mathbf{r}') \\ \tilde{\Delta}_{tz}(\mathbf{r}, \mathbf{r}') \end{pmatrix} = \frac{1}{2} \begin{pmatrix} (\Delta_{\uparrow\downarrow}^{\text{ext}}(\mathbf{r}, \mathbf{r}') - \Delta_{\downarrow\uparrow}^{\text{ext}}(\mathbf{r}, \mathbf{r}')) \\ (\Delta_{\downarrow\downarrow}^{\text{ext}}(\mathbf{r}, \mathbf{r}') - \Delta_{\uparrow\uparrow}^{\text{ext}}(\mathbf{r}, \mathbf{r}')) \\ (\Delta_{\downarrow\downarrow}^{\text{ext}}(\mathbf{r}, \mathbf{r}') + \Delta_{\uparrow\uparrow}^{\text{ext}}(\mathbf{r}, \mathbf{r}')) \\ (\Delta_{\uparrow\downarrow}^{\text{ext}}(\mathbf{r}, \mathbf{r}') + \Delta_{\downarrow\uparrow}^{\text{ext}}(\mathbf{r}, \mathbf{r}')) \end{pmatrix} \quad \vec{\tau} = (i\sigma^y - \sigma^z \sigma^0 \sigma^x). \quad (\text{C.2})$$

This notation is copied from the **Ph.D.** thesis of A. Linscheid, where an investigation of superconductivity beyond **singlet pairing** is given [146]. The $\sigma^{x,y,z,0}$ are the usual **Pauli matrices** defined in Eq. (A.4). If $\Delta_{\sigma\sigma'}^{\text{ext}}(\mathbf{r}, \mathbf{r}')$ has a totally symmetric part it has to drop out of the Hamiltonian:

$$\begin{aligned} \hat{H}_{\text{SC}}^{\text{sym}} &= \Lambda d^3r d^3r' \tilde{\Delta}_{\sigma\sigma'}^{\text{ext-sym}}(\mathbf{r}, \mathbf{r}') \hat{\Psi}_{\sigma}(\mathbf{r}) \hat{\Psi}_{\sigma'}(\mathbf{r}') = \Lambda d^3r d^3r' \tilde{\Delta}_{\sigma'\sigma}^{\text{ext-sym}}(\mathbf{r}', \mathbf{r}) \hat{\Psi}_{\sigma}(\mathbf{r}) \hat{\Psi}_{\sigma'}(\mathbf{r}') \\ &= -\Lambda d^3r d^3r' \tilde{\Delta}_{\sigma'\sigma}^{\text{ext-sym}}(\mathbf{r}', \mathbf{r}) \hat{\Psi}_{\sigma'}(\mathbf{r}') \hat{\Psi}_{\sigma}(\mathbf{r}) = -\hat{H}_{\text{SC}}^{\text{ext-sym}}. \end{aligned} \quad (\text{C.3})$$

As a consequence $\Delta_{\sigma\sigma'}^{\text{ext}}(\mathbf{r}, \mathbf{r}')$ is taken to be antisymmetric under particle exchange ($\mathbf{r}\sigma \leftrightarrow \mathbf{r}'\sigma'$). The singlet part of the pairing potential is symmetric:

$$2\tilde{\Delta}_s^{\text{ext}}(\mathbf{r}', \mathbf{r}) = \Delta_{\uparrow\downarrow}^{\text{ext}}(\mathbf{r}', \mathbf{r}) - \Delta_{\downarrow\uparrow}^{\text{ext}}(\mathbf{r}', \mathbf{r}) = -\Delta_{\downarrow\uparrow}^{\text{ext}}(\mathbf{r}, \mathbf{r}') + \Delta_{\uparrow\downarrow}^{\text{ext}}(\mathbf{r}, \mathbf{r}') = 2\tilde{\Delta}_s^{\text{ext}}(\mathbf{r}, \mathbf{r}') \quad (\text{C.4})$$

and the contribution in the Hamiltonian for the singlet pairing are:

$$\Lambda d^3r d^3r' \tilde{\Delta}_s(\mathbf{r}, \mathbf{r}') \hat{\chi}_s(\mathbf{r}, \mathbf{r}') = 2 \Lambda d^3r d^3r' \tilde{\Delta}_s(\mathbf{r}, \mathbf{r}') \hat{\Psi}_{\uparrow}(\mathbf{r}) \hat{\Psi}_{\downarrow}(\mathbf{r}').$$

The factor of 2 is included in the pairing potential and the tilde is left *i.e.* $2\tilde{\Delta}_s^{\text{ext}} = \Delta_s^{\text{ext}}$. The Δ_s^{ext} is the potential coupling to the anomalous density $\chi := \hat{\Psi}_{\uparrow}\hat{\Psi}_{\downarrow}$ which is the part included in the SCDFE equations [Eq. (3.6)].

C.2. KS-Bogoliubov-de Gennes Transformation

C.2.1. Introduction of the Bogoliubons

The Hamilton operator of the **superconductivity (SC)** Kohn-Sham system is given in Eq. (3.6):

$$\hat{K}_{\text{KS}} = \sum_{\alpha} \Delta d^3 \mathbf{r} (h_{\alpha}^{\text{KS}}(\mathbf{r}) - \mu) \hat{\Psi}_{\alpha}^{\dagger}(\mathbf{r}) \hat{\Psi}_{\alpha}(\mathbf{r}) + \Lambda d^3 r d^3 r' \left[\Delta_s^{\text{KS}}(\mathbf{r}, \mathbf{r}') \hat{\Psi}_{\uparrow}(\mathbf{r}) \hat{\Psi}_{\downarrow}(\mathbf{r}') - h.c. \right].$$

An elegant way to diagonalize such a Hamiltonian is to use a Bogoliubov-Valatin transformation²¹. Therefore new operators are defined:

$$\hat{\Psi}_{\sigma}(\mathbf{r}) = \sum_l \left(u_l(\mathbf{r}) \hat{\gamma}_{l\sigma} - z_{\sigma} v_l^*(\mathbf{r}) \hat{\gamma}_{l-\sigma}^{\dagger} \right) \quad \hat{\gamma}_{l\sigma} = \Delta d^3 r \left(u_l^*(\mathbf{r}) \hat{\Psi}_{\sigma}(\mathbf{r}) - z_{-\sigma} v_l^*(\mathbf{r}) \hat{\Psi}_{-\sigma}^{\dagger}(\mathbf{r}) \right).$$

The transformation matrix $u_k(\mathbf{r})$ and $v_k(\mathbf{r})$ are chosen in such a way that the initial Hamilton operator becomes diagonal in terms of the $\hat{\gamma}$ operators, *i.e.*: $\hat{H}^{\text{KS}} = \sum_k E_k \gamma_k^{\dagger} \gamma_k$. An equation for determining the transformation is found by calculating the anti-commutator $A = \left[\hat{\Psi}_{\sigma_1}(\mathbf{r}_1), \hat{K}_{\text{KS}} \right]_{-}$ starting from the field operators on the one hand:

$$\begin{aligned} A = \left[\hat{\Psi}_{\sigma_1}(\mathbf{r}_1), \hat{K}_{\text{KS}} \right] &= (h_{\sigma_1}^{\text{KS}}(\mathbf{r}_1) - \mu) \sum_l \left(u_l(\mathbf{r}_1) \hat{\gamma}_{l\sigma_1} - z_{\sigma_1} v_l^*(\mathbf{r}_1) \hat{\gamma}_{l-\sigma_1}^{\dagger} \right) \\ &\quad - \sum_l \Delta d^3 r \Delta_s^{\text{KS}*}(\mathbf{r}_1 \mathbf{r}) \sum_{\sigma} \delta_{\sigma_1-\sigma} \left(u_l^*(\mathbf{r}) \hat{\gamma}_{l\sigma}^{\dagger} - z_{\sigma} v_l(\mathbf{r}) \hat{\gamma}_{l-\sigma} \right). \end{aligned} \quad (\text{C.5})$$

and from the $\hat{\gamma}$ operators on the other hand:

$$\begin{aligned} A &= \left[\sum_l \left(u_l(\mathbf{r}_1) \hat{\gamma}_{l\sigma_1} - z_{\sigma_1} v_l^*(\mathbf{r}_1) \hat{\gamma}_{l-\sigma_1}^{\dagger} \right), \sum_{k\sigma} E_k \gamma_{k\sigma}^{\dagger} \gamma_{k\sigma} \right]_{-} \\ &= \sum_k E_k \left[u_k(\mathbf{r}_1) \gamma_{k\sigma_1} + z_{\sigma_1} v_k^*(\mathbf{r}_1) \gamma_{k-\sigma_1}^{\dagger} \right]. \end{aligned} \quad (\text{C.6})$$

By combining the two results an eigenvalue problem determining the transformation matrix $u_k(\mathbf{r})$ and $v_k(\mathbf{r})$ is found

$$\Delta d^3 r \begin{pmatrix} \left[-\frac{\Delta}{2} + v^{\text{KS}}(\mathbf{r}) - \mu \right] \delta_{\mathbf{r}_1 \mathbf{r}} & \Delta^{\text{KS}*}(\mathbf{r}_1 \mathbf{r}) \\ \Delta^{\text{KS}}(\mathbf{r}_1 \mathbf{r}) & -\left[-\frac{\Delta}{2} + v^{\text{KS}}(\mathbf{r}) - \mu \right] \delta_{\mathbf{r}_1 \mathbf{r}} \end{pmatrix} \begin{pmatrix} u_k(\mathbf{r}) \\ v_k(\mathbf{r}) \end{pmatrix} = E_k \begin{pmatrix} u_k(\mathbf{r}_1) \\ v_k(\mathbf{r}_1) \end{pmatrix}.$$

C.2.2. Commutator Relations for the Bogoliubons

For the calculation of the Green's functions corresponding to the operators $\hat{\gamma}$ (Sec. C.4) it is essential that the new operators $\hat{\gamma}$ and $\hat{\gamma}^{\dagger}$ are Fermionic operators. The transformations given in Eq. (3.9) are for a discrete basis:

$$\begin{aligned} \hat{c}_{m\sigma} &= \sum_k u_{mk} \hat{\gamma}_{k\sigma} - z_{\sigma} v_{mk}^* \hat{\gamma}_{k-\sigma}^{\dagger} & \hat{\gamma}_{m\sigma} &= \sum_k u_{km}^* \hat{c}_{k\sigma} - z_{-\sigma} \sum_k v_{km}^* \hat{c}_{k-\sigma}^{\dagger} \\ \hat{c}_{m-\sigma}^{\dagger} &= \sum_k u_{mk}^* \hat{\gamma}_{k-\sigma}^{\dagger} - z_{-\sigma} v_{mk} \hat{\gamma}_{k\sigma} & \hat{\gamma}_{m-\sigma}^{\dagger} &= \sum_k u_{km} \hat{c}_{k-\sigma}^{\dagger} - z_{\sigma} \sum_k v_{km} \hat{c}_{k\sigma}. \end{aligned}$$

With these definitions in hand it is straight forward to check the anti-commutator relations:

$$\begin{aligned} [\hat{\gamma}_{l\sigma}, \hat{\gamma}_{l'\sigma'}]_{+} &= \sum_{kk'} \left[u_{kl}^* \hat{c}_{k\sigma} - z_{-\sigma} v_{kl}^* \hat{c}_{k-\sigma}^{\dagger}, u_{k'l'}^* \hat{c}_{k'\sigma'} - z_{-\sigma'} v_{k'l'}^* \hat{c}_{k'-\sigma'}^{\dagger} \right]_{+} = -\delta_{\sigma\sigma'} \sum_k [z_{\sigma} u_{kl}^* v_{k'l'} + z_{-\sigma} v_{kl}^* u_{k'l'}] \\ [\hat{\gamma}_{l\sigma}, \hat{\gamma}_{l'\sigma'}^{\dagger}]_{+} &= \sum_{kk'} \left[u_{kl}^* \hat{c}_{k\sigma} - z_{-\sigma} v_{kl}^* \hat{c}_{k-\sigma}^{\dagger}, u_{k'l'} \hat{c}_{k'\sigma'}^{\dagger} - z_{-\sigma} v_{k'l'} \hat{c}_{k'-\sigma} \right]_{+} = \delta_{\sigma\sigma'} \sum_k [u_{kl}^* u_{k'l'} + v_{kl}^* v_{k'l'}]. \end{aligned}$$

²¹We denote the elementary excitations associated with the (Fermionic) $\hat{\gamma}$ and $\hat{\gamma}^{\dagger}$ as ‘‘Bogoliubons’’.

The Bogoliubov-Valatin transformation have to be unitary *i.e.*:

$$\sum_m (u_{ml}^* u_{mk} + v_{ml}^* v_{mk}) = \delta_{lk} \quad \sum_m (v_{ml} u_{mk} - u_{ml} v_{mk}) = 0 \quad (\text{C.7})$$

in order to ensure the Fermionic anti-commutator relations for the $\hat{\gamma}$ and $\hat{\gamma}^\dagger$.

C.2.3. Decoupling Approximation

Since the pairing potential is invariant under inversion [Eq. (3.20)] the minus sign in the argument of $\Delta^{\text{KS}*}$ can be dropped. The set of equations given in Eqs. (3.21) and (3.22) are written in $2N \times 2N$ matrix form:

$$\left(\begin{array}{ccc|ccc} \epsilon_1 - \mu & 0 & \cdots & \Delta_{-1-1}^{\text{KS}*} & \Delta_{-1-2}^{\text{KS}*} & \cdots \\ 0 & \epsilon_2 - \mu & \ddots & \Delta_{-2-1}^{\text{KS}*} & \Delta_{-2-2}^{\text{KS}*} & \cdots \\ \vdots & \ddots & \ddots & \vdots & \vdots & \ddots \\ \hline \Delta_{11}^{\text{KS}} & \Delta_{12}^{\text{KS}} & \cdots & \mu - \epsilon_1 & 0 & \cdots \\ \Delta_{21}^{\text{KS}} & \Delta_{22}^{\text{KS}} & \cdots & 0 & \mu - \epsilon_2 & \ddots \\ \vdots & \vdots & \ddots & \vdots & \ddots & \ddots \end{array} \right) \begin{pmatrix} u_{l1} \\ u_{l2} \\ \vdots \\ v_{l1} \\ v_{l2} \\ \vdots \end{pmatrix} = E_l \begin{pmatrix} u_{l1} \\ u_{l2} \\ \vdots \\ v_{l1} \\ v_{l2} \\ \vdots \end{pmatrix}. \quad (\text{C.8})$$

Within the [decoupling approximation](#) the off-diagonal parts of the pairing potential are assumed to be diagonal which leads to [Eqs. (3.23) and (3.20)]:

$$\left(\begin{array}{ccc|ccc} \epsilon_1 - \mu & 0 & \cdots & -\Delta_1^{\text{KS}*} & 0 & \cdots \\ 0 & \epsilon_2 - \mu & \ddots & 0 & -\Delta_2^{\text{KS}*} & \cdots \\ \vdots & \ddots & \ddots & \vdots & \vdots & \ddots \\ \hline \Delta_1^{\text{KS}} & 0 & \cdots & \mu - \epsilon_1 & 0 & \cdots \\ 0 & \Delta_2^{\text{KS}} & \cdots & 0 & \mu - \epsilon_2 & \ddots \\ \vdots & \vdots & \ddots & \vdots & \ddots & \ddots \end{array} \right) \begin{pmatrix} u_{l1} \\ u_{l2} \\ \vdots \\ v_{l1} \\ v_{l2} \\ \vdots \end{pmatrix} = E_l \begin{pmatrix} u_{l1} \\ u_{l2} \\ \vdots \\ v_{l1} \\ v_{l2} \\ \vdots \end{pmatrix}.$$

Note that for a uniform system this approximation becomes exact. The matrix is transformed by column-row permutations to:

$$\left(\begin{array}{cccccc} \epsilon_1 - \mu & \Delta_1^{\text{KS}*} & 0 & 0 & 0 & \cdots \\ \Delta_1^{\text{KS}} & \mu - \epsilon_1 & 0 & 0 & 0 & \cdots \\ 0 & 0 & \epsilon_2 - \mu & \Delta_2^{\text{KS}*} & 0 & \cdots \\ 0 & 0 & \Delta_2^{\text{KS}} & \mu - \epsilon_2 & 0 & \cdots \\ 0 & 0 & 0 & 0 & \ddots & \ddots \\ \vdots & \vdots & \vdots & \vdots & \ddots & \ddots \end{array} \right) \begin{pmatrix} u_{l1} \\ v_{l1} \\ u_{l2} \\ v_{l2} \\ \vdots \end{pmatrix} = E_l \begin{pmatrix} u_{l1} \\ v_{l1} \\ u_{l2} \\ v_{l2} \\ \vdots \end{pmatrix} \quad (\text{C.9})$$

$$\bar{M} \mathbf{b}_l = E_l \mathbf{b}_l.$$

The Hamiltonian in Eq. (3.6) is diagonalized by the operators $\hat{\gamma}$, if the vectors \mathbf{b}_l solve the eigenvalue problem in Eq. (C.9) for every l . Since the matrix \bar{M} is block diagonal, the problem is split in N decoupled two-dimensional eigenvalue problems with a different labeling of the eigenvalues ($E_l^\pm = \{E_l^+, E_l^-\}$) and eigenfunctions $(u_l, v_l)_\pm$:

$$\begin{pmatrix} \epsilon_l - \mu & \Delta_l^{\text{KS}*} \\ \Delta_l^{\text{KS}} & \mu - \epsilon_l \end{pmatrix} \begin{pmatrix} u_l \\ v_l \end{pmatrix}_\pm = E_l^\pm \begin{pmatrix} u_l \\ v_l \end{pmatrix}_\pm.$$

In order to link the eigenvectors and values of the 2×2 equations with the initial problem, the vectors $\{\mathbf{b}_l\}$ are expressed in terms of the new eigenvectors $(u_l v_l)_\pm$:

$$\{\mathbf{b}_1^\pm, \mathbf{b}_2^\pm, \dots\} = \left(\begin{pmatrix} u_1 \\ v_1 \\ 0 \\ \vdots \end{pmatrix}^\pm \right), \left(\begin{pmatrix} 0 \\ 0 \\ u_2 \\ v_2 \\ 0 \\ \vdots \end{pmatrix}^\pm \right), \dots \quad \bar{M}\mathbf{b}_l^\pm = E_l^\pm \mathbf{b}_l^\pm.$$

A comparison between \mathbf{b}_l^\pm and the initial definition of the \mathbf{b}_l leads to diagonal eigenvectors with respect to l and m :

$$(u_{lm}, v_{lm}) = \delta_{lm} (u_l^\pm, v_l^\pm).$$

.

C.2.4. Eigenvalues and Vectors of the KS-BdG Equations

The eigenvalue equations obtained after the Bogoliubov-Valatin transformation [Eq. (3.25)] read:

$$\begin{pmatrix} \varepsilon_l - \mu & \Delta_l^{\text{KS}*} \\ \Delta_l^{\text{KS}} & \mu - \varepsilon_l \end{pmatrix} \begin{pmatrix} u_l \\ v_l \end{pmatrix} = E_l \begin{pmatrix} u_l \\ v_l \end{pmatrix}.$$

The energy difference $\varepsilon_l - \mu$ is called ζ_l . The eigenvalues of the 2×2 matrix are given by:

$$E_{l\pm} = \pm \sqrt{\zeta_l^2 + |\Delta_l^{\text{KS}}|^2} = \pm R_l.$$

The eigenvectors are the kernel of the matrix $\begin{pmatrix} \varepsilon_l - \mu & \Delta_l^{\text{KS}*} \\ \Delta_l^{\text{KS}} & \mu - \varepsilon_l \end{pmatrix} - \mathbf{1}_{2 \times 2} E_{l\pm}$ and are given up within a scaling factor by:

$$\begin{pmatrix} u_l \\ v_l \end{pmatrix} = \alpha \begin{pmatrix} \frac{(-\zeta_l \mp R_l)}{\Delta_l^{\text{KS}}} \\ 1 \end{pmatrix} = \alpha \begin{pmatrix} -\frac{(\zeta_l \pm R_l)}{\Delta_l^{\text{KS}}} \\ 1 \end{pmatrix}.$$

In order to make the $\hat{\gamma}$'s Fermionic operators, the [Bogoliubov-de Gennes \(BdG\)](#) transformation has to be unitary (see previous section). In the decoupling approximation unitarity is given by $|u_l|^2 + |v_l|^2 = 1$ and the factor α is fixed:

$$u_l = \mp \frac{\Delta_l^{\text{KS}*}}{\sqrt{2} |\Delta_l^{\text{KS}}|} \sqrt{1 \pm \frac{\zeta_l}{R_l}} \quad v_l = \alpha = \sqrt{\frac{1}{2} \left(1 \mp \frac{\zeta_l}{R_l} \right)}.$$

C.3. Group Theory for the Gap

In this section the [gap function](#) $\Delta_{\mathbf{k}}$ is investigated with the tools provided by [group theory](#). The gap is found by solving an eigenvalue problem [Eq. (6.9)]. The symmetry group of the matrix determines also the symmetry of the eigenvector. To be more precise: The set of eigenfunction(s) corresponding to one eigenvalue forms a basis of the irreducible representation of the underlying symmetry group [147, 142]. With group theory:

- It is possible to predict the symmetry of these basis functions and hence the possible symmetries of the gap function. This analysis is based on the point group of the system, and does not involve an explicit knowledge of the interaction or [Fermi surface](#).
- It is **not** possible to predict the values or energetic order of the eigenvalues. In general there will be multiple representations and the one with the largest eigenvalue is the most stable solution and gives the experimentally observed gap structure.

The m basis functions φ_m^r of a representation r are computed using a projection operator \mathcal{P}_{mm}^r :

$$a_m^r \varphi_m^r = \mathcal{P}_{mm}^r \phi = \sum_T \Gamma_{mm}^r(T) P(T) \phi \quad (\text{C.10})$$

acting on a function ϕ . Γ_{mn}^r is the mn element of the representation r and $P(T)$ is the transformation operator corresponding to the symmetry operation T . In our case the symmetry operators are elements of the point-group G of the crystal. A transformation T corresponding to the crystal point group leads to a change in the spatial and spin coordinate of the gap. The transformation to the new coordinates is done in the following way:

$$\begin{aligned} \vec{\alpha}' &= \Gamma^{SU(2)} \vec{\alpha} \quad \mathbf{r}'_1 = \Gamma^{\mathbb{R}}(T) \mathbf{r}_1 \\ P(T) \Delta_{\sigma_1 \sigma_2}(\mathbf{r}_1, \mathbf{r}_2) &= \Delta_{\sigma'_1 \sigma'_2}(\mathbf{r}'_1, \mathbf{r}'_2) = \sum_{\sigma_1 \sigma_2} \Gamma_{\sigma'_1 \sigma_1}^{SU(2)} \Delta_{\sigma_1 \sigma_2}(\Gamma^{\mathbb{R}}(T) \mathbf{r}_1, \Gamma^{\mathbb{R}}(T) \mathbf{r}_2) \Gamma_{\sigma'_2 \sigma_2}^{SU(2)}. \end{aligned} \quad (\text{C.11})$$

Many of the [iron based superconductors \(FeSC\)](#) appear in the tetragonal crystal structure. From now on this group will be investigated. In the tetragonal lattice 16 symmetry operators are present. The nomenclature for the symmetry operation is as follows:

- $C_{n\nu}$ are proper rotations with an angle $\frac{2\pi}{n}$ around the axis ν .
- $S_{n\nu}$ are improper rotations with an angle $\frac{2\pi}{n}$ around the axis ν .
- σ_n are reflections on the plane with a normal vector n .
- E is the identity operator and I the inversion.

The symmetry operations in real and spin space are shown in Tab. C.1a. For a tetragonal lattice the coordinate transformation in real space are identical to the transformations in inverse space. With the explicit form of the symmetry operations, it is easy to work out the effect of a transformation operator $P(T)$ on an anti-symmetric function: $\phi = \Delta_{\sigma_1 \sigma_2}(\mathbf{r}_1, \mathbf{r}_2)$ defined in Eq. (C.11).

However, for the construction of the projection operator \mathcal{P}_{mm}^r given in Eq. (C.10) the irreducible representations Γ_{mn}^r are needed. These are shown in Tab. C.1b and are either taken from any standard group theory textbook or derived using orthogonality relations between the irreducible representations. Note that the three dimensional representation $\Gamma^{\mathbb{R}}$ is reducible. The number of times n_{ij} a representation Γ^j contains the irreducible representation Γ^i is given by the expression [142]:

$$n_{ji} = \frac{1}{g} \sum_T \chi_j(T) \chi_i^*(T),$$

where χ denotes the trace of the representation *i.e.* $\chi^r(T) = \sum_n \Gamma_{nn}^r(T)$ and g is the number of symmetry operations in our case 16. The $\Gamma^{\mathbb{R}}$ is decomposed in the following way:

$$\Gamma^{\mathbb{R}} = \Gamma^{10} \oplus \Gamma^5.$$

If the system would feature strong spin-orbit coupling, the transformation in real and spin space would couple and the picture would become much more complicated. As a last step, the domain for the operator $P(T)$ has to be specified: The gap is an antisymmetric function, due to the Fermionic commutation relations *i.e.* $\Delta_{\sigma\sigma'}(\mathbf{r}, \mathbf{r}') = -\Delta_{\sigma'\sigma}(\mathbf{r}', \mathbf{r})$ [Eq. (C.3)]. So any square integrable, anti-symmetric function is allowed for ϕ . For practical calculations the symmetry in inverse space is more relevant and the gap in the decoupling approximation reads:

$$\Delta_{\sigma\sigma'}^{\text{KS}}(\mathbf{k}) = \Lambda d^3 r d^3 r' \psi_{\mathbf{k}}^*(\mathbf{r}) \Delta_{\sigma\sigma'}^{\text{KS}}(\mathbf{r}\mathbf{r}') \psi_{\mathbf{k}}^{\text{KS}}(\mathbf{r}'),$$

which leads to a totally anti-symmetric function also in inverse space:

$$\begin{aligned} \Delta_{\sigma\sigma'}^{\text{KS}}(-\mathbf{k}) &= \Lambda d^3 r d^3 r' \psi_{-\mathbf{k}}^*(\mathbf{r}) \Delta_{\sigma\sigma'}^{\text{KS}}(\mathbf{r}\mathbf{r}') \psi_{-\mathbf{k}}(\mathbf{r}') \\ &= -\Lambda d^3 r d^3 r' \psi_{\mathbf{k}}^*(\mathbf{r}) \Delta_{\sigma'\sigma}^{\text{KS}}(\mathbf{r}'\mathbf{r}) \psi_{\mathbf{k}}^*(\mathbf{r}') \\ &= \Lambda d^3 r d^3 r' \psi_{\mathbf{k}}^*(\mathbf{r}) [-\Delta_{\sigma'\sigma}^{\text{KS}}(\mathbf{r}\mathbf{r}')] \psi_{\mathbf{k}}(\mathbf{r}') = -\Delta_{\sigma'\sigma}^{\text{KS}}(\mathbf{k}). \end{aligned}$$

Note that for the tetragonal point group the representation in real and inverse space are identical and the transformation $P(T)$ acts on $\Delta_{\sigma'\sigma}^{\text{KS}}$ as:

$$P(T) \Delta_{\sigma_1\sigma_2}^{\text{KS}}(\mathbf{k}) = \Delta_{\sigma'_1\sigma'_2}^{\text{KS}}(\mathbf{k}') = \sum_{\sigma_1\sigma_2} \Gamma_{\sigma'_1\sigma_1}^{SU(2)} \Delta_{\sigma_1\sigma_2}^{\text{KS}}(\Gamma^{\mathbb{R}}(T)\mathbf{k}) \Gamma_{\sigma'_2\sigma_2}^{SU(2)}.$$

Now all the necessary ingredients are collected to start projecting test functions $\phi_{\alpha\beta}(\mathbf{k})$. If the \mathbf{k} part of the basis function is even $f(-\mathbf{k}) = f(\mathbf{k})$ the spin part has to be anti-symmetric in other words being proportional to σ^y . If the \mathbf{k} part is odd on the other hand the spin part has to be even in spin (proportional to σ^0, σ^x or σ^z). The guessing is a non-unique process, as a first choice $\phi_{\alpha\beta}^1(\mathbf{k}) = \sum_i k_i \sigma_{\alpha\beta}^x$ is used. This function is odd with respect to \mathbf{k} and even in spin space so that the product is anti-symmetric. Very often a symmetry invariant function $f(|\mathbf{k}|) = e^{-|\mathbf{k}|}$ is multiplied in order to make the function ϕ^1 square integrable which is left out here for simplicity. The projection $\mathcal{P}_{mm}^r \phi_{\alpha\beta}^1(\mathbf{k})$ is zero for most of the representation except for Γ^6 and Γ^{10} :

$$\mathcal{P}_{11}^6 \phi_{\alpha\beta}^1(\mathbf{k}) = \sigma_{\alpha\beta}^x k_z \quad \mathcal{P}_{11}^{10} \phi_{\alpha\beta}^1(\mathbf{k}) = \sigma_{\alpha\beta}^x k_x \quad \mathcal{P}_{22}^{10} \phi_{\alpha\beta}^1(\mathbf{k}) = \sigma_{\alpha\beta}^x (k_x + k_y).$$

So the first basis functions are found. A second choice could be a function like: $\phi_{\alpha\beta}^2(\mathbf{k}) = \sum_{ij} k_i k_j \sigma_{\alpha\beta}^y$. This one is even with respect to \mathbf{k} and odd in spin space. The projection leads to:

$$\mathcal{P}_{11}^8 \phi_{\alpha\beta}^1(\mathbf{k}) = \sigma_{\alpha\beta}^y (k_x^2 + k_y^2 + k_z^2) \quad \mathcal{P}_{11}^9 \phi_{\alpha\beta}^1(\mathbf{k}) = \sigma_{\alpha\beta}^y (k_x + k_y) k_z.$$

After some attempts of guessing the first orders in k_x, k_y and k_z , the table C.1b is filled with basis functions. Experimentally clear indications are found that the pairing takes place in the singlet channel in the FeSC [67, 13, 12]. In order to have an anti-symmetric gap function for singlet pairing, the behavior with respect to \mathbf{k} has to be even and the five odd representation in \mathbf{k} space are ruled out as a possible pairing symmetry. The five remaining even representations are: $A_{1g}, B_{1g}, B_{2g}, A_{2g}$ and the two-dimensional E_g . The symmetry of the basis functions corresponding to these representations is illustrated in Fig. 7.9. The names s, d and g wave are related to the angular momentum quantum number of the $SO(3)$ group. For the thermodynamical properties like thermal conductivity it is important, whether the gap has nodes or the excitation spectrum is fully gaped. The d wave symmetries require nodes of the order parameter. However, nodes are not excluded for the s -wave state.

Accidental nodes are nodes that are not required by symmetry. For example the appearance of nodes in an A_{1g} (s wave) would be accidental.

Note that the s and s_{\pm} symmetry discussed in Sec. 6.2 are identical from a group theoretical point of view. For the pairing symmetry in \mathbf{k} space, the experimental situation is less clear compared to the spin part. There are experiments as [angle resolved photon emission spectroscopy \(ARPES\)](#), [superconducting quantum interference device \(SQUID\)](#) and tunneling in favor of an s wave symmetry without nodes. However, the thermal conductivity experiments indicate a structure with nodes at least for some materials in the 122 family. Whether this means a d wave or s wave with accidental nodes only \mathbf{k} resolved experiments could tell.

Model calculations using a ‘‘one iron atom five band’’ model predict a change from a s_{\pm} to a structure with nodes as a function of doping [148]. Most likely, the energies corresponding to the different symmetries are very close together and the energetic order changes as a function of an external parameter like doping or pressure. For a detailed discussion of the experimental and theoretical situation the review article [13] is a very good starting point.

In some iron based superconductors, a distortion from the tetragonal symmetry (D_{4h}) to the orthorhombic symmetry (D_{2h}) is found [9, 149, 150]. The change in symmetry is related to a reduction of the possible basis functions: The two-dimensional irreducible representation E_g disappears in the lower D_{2h} symmetry (red color in Tabs. C.1a and C.1b). So the corresponding symmetries $k_x k_z$ and $k_y k_z$ with nodes along the z direction are ruled out as a pairing symmetry because SC is observed also

Label	Real Space $\Gamma^{\mathbb{R}}$	Spinor $\Gamma^{SU(2)}$	Label	Real Space $\Gamma^{\mathbb{R}}$	Spinor $\Gamma^{SU(2)}$
E	$\begin{pmatrix} 1 & 0 & 0 \\ 0 & 1 & 0 \\ 0 & 0 & 1 \end{pmatrix}$	$\begin{pmatrix} 1 & 0 \\ 0 & 1 \end{pmatrix}$	I	$\begin{pmatrix} -1 & 0 & 0 \\ 0 & -1 & 0 \\ 0 & 0 & -1 \end{pmatrix}$	$\begin{pmatrix} 1 & 0 \\ 0 & 1 \end{pmatrix}$
C_{2z}	$\begin{pmatrix} -1 & 0 & 0 \\ 0 & -1 & 0 \\ 0 & 0 & 1 \end{pmatrix}$	$\begin{pmatrix} i & 0 \\ 0 & -i \end{pmatrix}$	σ_z	$\begin{pmatrix} 1 & 0 & 0 \\ 0 & 1 & 0 \\ 0 & 0 & -1 \end{pmatrix}$	$\begin{pmatrix} i & 0 \\ 0 & -i \end{pmatrix}$
C_{4z}^{-1}	$\begin{pmatrix} 0 & -1 & 0 \\ 1 & 0 & 0 \\ 0 & 0 & 1 \end{pmatrix}$	$\begin{pmatrix} \omega & 0 \\ 0 & \omega^* \end{pmatrix}$	S_{4z}	$\begin{pmatrix} 0 & -1 & 0 \\ 1 & 0 & 0 \\ 0 & 0 & -1 \end{pmatrix}$	$\begin{pmatrix} \omega^* & 0 \\ 0 & \omega \end{pmatrix}$
C_{4z}	$\begin{pmatrix} 0 & 1 & 0 \\ -1 & 0 & 0 \\ 0 & 0 & 1 \end{pmatrix}$	$\begin{pmatrix} \omega^* & 0 \\ 0 & \omega \end{pmatrix}$	S_{4z}^{-1}	$\begin{pmatrix} 0 & 1 & 0 \\ -1 & 0 & 0 \\ 0 & 0 & -1 \end{pmatrix}$	$\begin{pmatrix} \omega & 0 \\ 0 & \omega^* \end{pmatrix}$
C_{2x}	$\begin{pmatrix} 1 & 0 & 0 \\ 0 & -1 & 0 \\ 0 & 0 & -1 \end{pmatrix}$	$\begin{pmatrix} 0 & i \\ i & 0 \end{pmatrix}$	σ_x	$\begin{pmatrix} -1 & 0 & 0 \\ 0 & 1 & 0 \\ 0 & 0 & 1 \end{pmatrix}$	$\begin{pmatrix} 0 & i \\ i & 0 \end{pmatrix}$
C_{2y}	$\begin{pmatrix} -1 & 0 & 0 \\ 0 & 1 & 0 \\ 0 & 0 & -1 \end{pmatrix}$	$\begin{pmatrix} 0 & -1 \\ 1 & 0 \end{pmatrix}$	σ_y	$\begin{pmatrix} 1 & 0 & 0 \\ 0 & -1 & 0 \\ 0 & 0 & 1 \end{pmatrix}$	$\begin{pmatrix} 0 & -1 \\ 1 & 0 \end{pmatrix}$
C_{2a}	$\begin{pmatrix} 0 & 1 & 0 \\ 1 & 0 & 0 \\ 0 & 0 & -1 \end{pmatrix}$	$\begin{pmatrix} 0 & -\omega^* \\ \omega & 0 \end{pmatrix}$	σ_{x+y}	$\begin{pmatrix} 0 & -1 & 0 \\ -1 & 0 & 0 \\ 0 & 0 & -1 \end{pmatrix}$	$\begin{pmatrix} 0 & -\omega^* \\ \omega & 0 \end{pmatrix}$
C_{2b}	$\begin{pmatrix} 0 & -1 & 0 \\ -1 & 0 & 0 \\ 0 & 0 & -1 \end{pmatrix}$	$\begin{pmatrix} 0 & -\omega \\ \omega^* & 0 \end{pmatrix}$	σ_{x-y}	$\begin{pmatrix} 0 & 1 & 0 \\ 1 & 0 & 0 \\ 0 & 0 & 1 \end{pmatrix}$	$\begin{pmatrix} 0 & -\omega \\ \omega^* & 0 \end{pmatrix}$

(a) Representation of the point group D_{4h} where the axis a and b are in the xy plane and point in $(1, 1, 0)$ and $(1, -1, 0)$ direction, respectively. The ω determines the rotation in spin space $\omega = e^{i\frac{\pi}{4}}$. The symmetry operations in red are removed in case of an orthorhombic distortion (D_{2h} symmetry).

	Name	dim	parity \mathbf{k}	parity σ	Basis functions
Γ^1	B_{2g}	1	even	odd	$\sigma^x k_x k_y$
Γ^2	B_{1g}	1	even	odd	$\sigma^x (k_x^2 - k_y^2)$
Γ^3	B_{2u}	1	odd	even	$\sigma^z k_y - i\sigma^0 k_x$
Γ^4	B_{1u}	1	odd	even	$i\sigma^0 k_y - \sigma^z k_x$
Γ^5	A_{2u}	1	odd	even	$\sigma^0 k_x - \sigma^z i k_y$
Γ^6	A_{1u}	1	odd	even	$\sigma^x k_z, \sigma^z k_x - i\sigma_0 k_y$
Γ^7	A_{2g}	1	even	odd	$\sigma^y k_x k_y (k_x^2 - k_y^2)$
Γ^8	A_{1g}	1	even	odd	$\sigma^y, \sigma^y (k_x^2 + k_y^2), \sigma^y k_z^2$
Γ^9	E_g	2	even	odd	$\sigma^y k_x k_z, \sigma^y k_y k_z$
Γ^{10}	E_u	2	odd	even	$\sigma^x k_x, \sigma^x k_y$

(b) Basis function for the ten irreducible representations. Half of the representations are even and the other half are odd with respect to \mathbf{k} parity. For singlet pairing only the even functions are relevant. In the column ‘‘Name’’ the common labels of the representation are given [142]. The representations in red become reducible if the symmetry becomes lowered to orthorhombic.

Table C.1.: Representations and basis functions of the tetragonal point group.

in the orthorhombic phase. The other irreducible symmetries A_{1g} , B_{1g} , B_{2g} and A_{2g} remain in the D_{2h} symmetry.

However, this investigation shows that a reduction of symmetry will reduce the number of possible pairing symmetries. Only the trivial representation A_{1g} will **always** remain even for additional distortion and keep the channel for s_{\pm} superconductivity open.

C.4. The Kohn-Sham Green's function

C.4.1. The Kohn-Sham Green's function – Real Space

The statistical operator corresponding to the KS system reads:

$$\hat{\rho}_{\beta}^{\text{KS}} = \frac{1}{Z_{\text{G}}^{\text{KS}}} e^{-\beta \hat{K}_{\text{KS}}} \quad \text{with } Z_{\text{G}}^{\text{KS}} := \text{tr} \left[e^{-\beta \hat{K}_{\text{KS}}} \right].$$

The 11 element of the Nambu Green's function defined in Eq. (4.4) is evaluated:

$$\begin{aligned} G_{\sigma_1 \sigma_2}^{\text{KS}}(\mathbf{r}_1 \mathbf{r}_2 \omega_n) &= -\Delta_0^{+\beta} d(\tau_1 - \tau_2) e^{i\omega_n(\tau_1 - \tau_2)} \text{tr} \left[\hat{\rho}_{\beta}^{\text{KS}} \hat{T} \left[\hat{\Psi}_{\sigma_1}(\mathbf{x}_1) \hat{\Psi}_{\sigma_2}^{\dagger}(\mathbf{x}_2) \right] \right] \\ &:= -\left\langle \hat{T} \left[\hat{\Psi}_{\sigma_1}(\mathbf{x}_1) \hat{\Psi}_{\sigma_2}^{\dagger}(\mathbf{x}_2) \right] \right\rangle_{\text{KS}}^{\omega_n}. \end{aligned}$$

The definition of the field operators $\hat{\Psi}(\mathbf{r})$ in terms of the $\hat{\gamma}$'s is given in Eq. (3.9).

$$\begin{aligned} G_{\sigma_1 \sigma_2}^{\text{KS}}(\mathbf{r}_1 \mathbf{r}_2 \omega_n) &:= -\left\langle \hat{T} \left[\hat{\Psi}_{\sigma_1}(\mathbf{x}_1) \hat{\Psi}_{\sigma_2}^{\dagger}(\mathbf{x}_2) \right] \right\rangle_{\text{KS}}^{\omega_n} \\ &= -\sum_{kk'} \left\langle \hat{T} \left[\left(u_k(\mathbf{r}_1) \hat{\gamma}_{k\sigma_1}(\tau_1) - z_{\sigma_1} v_k^*(\mathbf{r}_1) \hat{\gamma}_{k-\sigma_1}^{\dagger}(\tau_1) \right) \times \right. \right. \\ &\quad \left. \left. \left(u_{k'}^*(\mathbf{r}_2) \hat{\gamma}_{k'\sigma_2}^{\dagger}(\tau_2) - z_{\sigma_2} v_{k'}(\mathbf{r}_2) \hat{\gamma}_{k'-\sigma_2}(\tau_2) \right) \right] \right\rangle_{\text{KS}}^{\omega_n} \\ &= -\sum_{kk'} u_k(\mathbf{r}_1) u_{k'}^*(\mathbf{r}_2) \left\langle \hat{T} \left[\hat{\gamma}_{k\sigma_1}(\tau_1) \hat{\gamma}_{k'\sigma_2}^{\dagger}(\tau_2) \right] \right\rangle_{\text{KS}}^{\omega_n} \\ &\quad - \sum_{kk'} z_{\sigma_1} z_{\sigma_2} v_k^*(\mathbf{r}_1) v_{k'}(\mathbf{r}_2) \left\langle \hat{T} \left[\hat{\gamma}_{k-\sigma_1}^{\dagger}(\tau_1) \hat{\gamma}_{k'-\sigma_2}(\tau_2) \right] \right\rangle_{\text{KS}}^{\omega_n}. \end{aligned}$$

The terms $A = \left\langle \hat{T} \left[\hat{\gamma}_{\sigma_1 k_1} \hat{\gamma}_{\sigma_2 k_2}^{\dagger} \right] \right\rangle$ and $B = \left\langle \hat{T} \left[\hat{\gamma}_{\sigma_1 k_1}^{\dagger} \hat{\gamma}_{\sigma_2 k_2} \right] \right\rangle$ appear also for the other elements of the Nambu GF and are evaluated separately. In Sec. C.2.2 it has been shown that the $\hat{\gamma}$ operators are Fermionic operators and the trace is evaluated using N particle Slater determinants composed of single particle states corresponding to the γ 's. For such states the time dependence of the operators is simple:

$$\begin{aligned} \hat{\gamma}_{\sigma k}(\tau) |Q\rangle &= e^{\hat{K}_{\text{KS}} \tau} \hat{\gamma}_{\sigma k} e^{-\hat{K}_{\text{KS}} \tau} |Q\rangle = e^{\hat{K}_{\text{KS}} \tau} e^{-E_Q \tau} |Q n_{\sigma k} = 0\rangle = e^{-E_k \tau} |Q n_{\sigma k} = 0\rangle = e^{-E_k \tau} \hat{\gamma}_{\sigma k} |Q\rangle \\ \hat{\gamma}_{\sigma k}^{\dagger}(\tau) |Q\rangle &= e^{+E_k \tau} \hat{\gamma}_{\sigma k}^{\dagger} |Q\rangle. \end{aligned}$$

The Fourier transformation given in Eq. (B.2) ensures $\tau_1 - \tau_2 > 0$ and the time ordering is trivial:

$$\begin{aligned}
 A(\tau - \tau') &= \left\langle \hat{\gamma}_{\sigma_1 k_1}(\tau_1) \hat{\gamma}_{\sigma_2 k_2}^\dagger(\tau_2) \right\rangle_{\text{KS}} = e^{-E_k(\tau_1 - \tau_2)} \left\langle \hat{\gamma}_{\sigma_1 k_1} \hat{\gamma}_{\sigma_2 k_2}^\dagger \right\rangle_{\text{KS}} \\
 &= e^{-E_k(\tau_1 - \tau_2)} [1 - f_\beta(E_{k_1})] \delta_{k_1 k_2} \delta_{\sigma_1 \sigma_2} = e^{-E_k(\tau_1 - \tau_2)} f_\beta(-E_{k_1}) \delta_{k_1 k_2} \delta_{\sigma_1 \sigma_2} \\
 A(\omega_n) &= \Delta_0^\beta \int d\tau e^{(i\omega_n - E_k)\tau} f_\beta(-E_{k_1}) \delta_{k_1 k_2} \delta_{\sigma_1 \sigma_2} = -f_\beta(-E_{k_1}) \delta_{k_1 k_2} \delta_{\sigma_1 \sigma_2} \frac{e^{-\beta E_k} + 1}{i\omega_n - E_k} \\
 &= -\frac{\delta_{k_1 k_2} \delta_{\sigma_1 \sigma_2}}{i\omega_n - E_k}
 \end{aligned} \tag{C.12}$$

$$\begin{aligned}
 B(\tau - \tau') &= \delta_{k_1 k_2} \delta_{\sigma_1 \sigma_2} \theta(\tau_1 - \tau_2) e^{E_{k_1}(\tau_1 - \tau_2)} f_\beta(E_{k_1}) \\
 B(\omega_n) &= \Delta_0^\beta \int d\tau e^{(i\omega_n + E_k)\tau} f_\beta(E_{k_1}) \delta_{k_1 k_2} \delta_{\sigma_1 \sigma_2} = f_\beta(E_{k_1}) \delta_{k_1 k_2} \delta_{\sigma_1 \sigma_2} \frac{e^{\beta E_k} + 1}{i\omega_n + E_k} \\
 &= -\frac{\delta_{k_1 k_2} \delta_{\sigma_1 \sigma_2}}{i\omega_n + E_k}.
 \end{aligned} \tag{C.13}$$

The expectation values in Eqs. (C.12) and (C.13) are inserted in the 11 element of the GF:

$$G_{\sigma_1 \sigma_2}^{\text{KS}}(\mathbf{r}_1 \mathbf{r}_2 \omega_n) = \delta_{\sigma_1 \sigma_2} \sum_k \left[\frac{u_k(\mathbf{r}_1) u_k^*(\mathbf{r}_2)}{i\omega_n - E_k} + \frac{v_k^*(\mathbf{r}_1) v_k(\mathbf{r}_2)}{i\omega_n + E_k} \right].$$

In an analogous way, the remaining normal and anomalous GF are found:

$$\begin{aligned}
 F_{\sigma_1 \sigma_2}^{\text{KS}}(\mathbf{r}_1 \mathbf{r}_2 \omega_n) &= \delta_{\sigma_1 - \sigma_2} \sum_k \left[\frac{v_k^*(\mathbf{r}_1) u_k(\mathbf{r}_2)}{i\omega_n + E_k} - \frac{u_k(\mathbf{r}_1) v_k^*(\mathbf{r}_2)}{i\omega_n - E_k} \right] \\
 G_{\sigma_1 \sigma_2}^{\text{KS}\dagger}(\mathbf{r}_1 \mathbf{r}_2 \omega_n) &= \delta_{\sigma_1 \sigma_2} \sum_k \left[\frac{u_k^*(\mathbf{r}_1) u_k(\mathbf{r}_2)}{i\omega_n + E_k} + \frac{v_k(\mathbf{r}_1) v_k^*(\mathbf{r}_2)}{i\omega_n - E_k} \right] \\
 F_{\sigma_1 \sigma_2}^{\text{KS}\dagger}(\mathbf{r}_1 \mathbf{r}_2 \omega_n) &= \delta_{\sigma_1 - \sigma_2} \sum_k \left[\frac{u_k^*(\mathbf{r}_1) v_k(\mathbf{r}_2)}{i\omega_n + E_k} - \frac{v_k(\mathbf{r}_1) u_k^*(\mathbf{r}_2)}{i\omega_n - E_k} \right].
 \end{aligned}$$

C.4.2. The Kohn-Sham Green's Function – Bloch Representation

First the spatial representation of the Green's function is rewritten using the expansion of $u_{n\mathbf{q}}(\mathbf{r})$ and $v_{n\mathbf{q}}(\mathbf{r})$ in terms of the Bloch states with respect to the non-SC system defined in Eqs. (3.16) and (3.17). In the decoupling approximation the coefficients are diagonal and the invariance of E_k^\pm with respect to $k \rightarrow -k$ leads to [Eqs. (3.24) and (3.27)]:

$$G_{\sigma_1 \sigma_2}^{\text{KS}}(\mathbf{r}_1 \mathbf{r}_2 \omega_n) = \delta_{\sigma_1 \sigma_2} \sum_k \hat{\psi}_k(\mathbf{r}_1) \psi_k^*(\mathbf{r}_2) \left[\frac{|u_k^\pm|^2}{i\omega_n - E_k^\pm} + \frac{|v_k^\pm|^2}{i\omega_n + E_k^\pm} \right].$$

The Bloch representation is the k dependent part of the real space function. Using the orthogonality of the non-superconducting Bloch states [Eq. (3.15)] the GF in Bloch representation is found:

$$\begin{aligned}
 \Rightarrow G_{\sigma_1 \sigma_2}^{\text{KS}}(kk' \omega_n \pm) &:= \delta_{\sigma_1 \sigma_2} \delta_{kk'} \Lambda d^3 r_1 d^3 r_2 \psi_k(\mathbf{r}_1) G_{\sigma_1 \sigma_2}^{\text{KS}}(\mathbf{r}_1 \mathbf{r}_2 \omega_n) \psi_{k'}^*(\mathbf{r}_2) \\
 &= \delta_{\sigma_1 \sigma_2} \delta_{kk'} \left[\frac{|u_k^\pm|^2}{i\omega_n - E_k^\pm} + \frac{|v_k^\pm|^2}{i\omega_n + E_k^\pm} \right].
 \end{aligned} \tag{C.14}$$

Every sum with respect to the quantum number k , is evaluated with the rule presented in Eq. (3.28) and for the other components of the GF it is found:

$$G_{\sigma_1\sigma_2}^{\text{KS}\dagger}(k_1k_2\omega_n\pm) = \delta_{\sigma_1\sigma_2}\delta_{k_1k_2} \left[\frac{|u_{k_1}^\pm|^2}{i\omega_n + E_{k_1}^\pm} + \frac{|v_{k_1}^\pm|^2}{i\omega_n - E_{k_1}^\pm} \right] \quad (\text{C.15})$$

$$F_{\sigma_1\sigma_2}^{\text{KS}}(k_1k_2\omega_n\pm) = \delta_{\sigma_1-\sigma_2}\delta_{k_1k_2} \left[\frac{v_{k_1}^{\pm*}u_{k_1}^\pm}{i\omega_n + E_{k_1}^\pm} - \frac{v_{k_1}^{\pm*}u_{k_1}^\pm}{i\omega_n - E_{k_1}^\pm} \right] \quad (\text{C.16})$$

$$F_{\sigma_1\sigma_2}^{\text{KS}\dagger}(k_1k_2\omega_n\pm) = \delta_{\sigma_1-\sigma_2}\delta_{k-k'} \left[\frac{u_{k_1}^{\pm*}v_{k_1}^\pm}{i\omega_n + E_{k_1}^\pm} - \frac{u_{k_1}^{\pm*}v_{k_1}^\pm}{i\omega_n - E_{k_1}^\pm} \right]. \quad (\text{C.17})$$

Note that some authors [69, 110] define the transformation of the anomalous terms via

$$\Lambda d^3r_1 d^3r_2 \psi_{k_1}^*(\mathbf{r}_1) F_{\sigma_1\sigma_2}^{\text{KS}}(\mathbf{r}_1\mathbf{r}_2\omega_n) \psi_{k_2}^*(\mathbf{r}_2)$$

leading to a $\delta_{k_1-k_2}$ instead of the $\delta_{k_1k_2}$. The transformation for all components reads (the spin conditions $\delta_{\sigma_1\sigma_1}$ for G and G^\dagger and $\delta_{\sigma_1-\sigma_2}$ for F and F^\dagger are left for simplicity):

$$\begin{aligned} \bar{G}^{\text{KS}}(kk'\omega_n\pm) &= \Lambda d^3r_1 d^3r_2 \psi_k^*(\mathbf{r}_1) \bar{G}^{\text{KS}}(\mathbf{r}_1\mathbf{r}_2\omega_n) \psi_{k'}(\mathbf{r}_2) \\ &= \delta_{kk'}\tau_3 \begin{pmatrix} \frac{|u_k^\pm|^2}{i\omega_n - E_k^\pm} + \frac{|v_k^\pm|^2}{i\omega_n + E_k^\pm} & \frac{v_k^{\pm*}u_k^\pm}{i\omega_n + E_k^\pm} - \frac{v_k^{\pm*}u_k^\pm}{i\omega_n - E_k^\pm} \\ \frac{u_k^{\pm*}v_k^\pm}{i\omega_n + E_k^\pm} - \frac{u_k^{\pm*}v_k^\pm}{i\omega_n - E_k^\pm} & \frac{|u_k^\pm|^2}{i\omega_n + E_k^\pm} + \frac{|v_k^\pm|^2}{i\omega_n - E_k^\pm} \end{pmatrix} \end{aligned} \quad (\text{C.18})$$

$$\bar{G}^{\text{KS}}(\mathbf{r}_1\mathbf{r}_2\omega_n) = \sum_{kk'} \psi_k(\mathbf{r}_1) \bar{G}^{\text{KS}}(kk'\omega_n) \psi_{k'}^*(\mathbf{r}_2). \quad (\text{C.19})$$

The transformation relation for the GF [Eq. (C.19)] together with the Dyson equation [Eq. (D.9)] lead to the following relations for the self-energy and XC-potential:

$$\bar{\Sigma}(kk'\omega_n) := \Lambda d^3r_1 d^3r_2 \psi_k^*(\mathbf{r}_1) \bar{\Sigma}(\mathbf{r}_1\mathbf{r}_2\omega_n) \psi_{k'}(\mathbf{r}_2) \quad (\text{C.20})$$

$$\bar{v}^{\text{xc}}(kk') := \Lambda d^3r_1 d^3r_2 \psi_k^*(\mathbf{r}_1) \bar{v}^{\text{xc}}(\mathbf{r}_1\mathbf{r}_2) \psi_{k'}(\mathbf{r}_2). \quad (\text{C.21})$$

Note that the definition given in Eq. (C.21) is in line with the definition used in the SCDFt introduction [Eq. (3.19)]. In some situation it is advantageous to write the Green's function in terms of the gap $\Delta_s^{\text{KS}}(k)$ and eigenvalue E_k . This is done by using the explicit equation for the eigenvectors given in Eq. (3.26):

$$\bar{G}^{\text{KS}}(kk'\omega_n\pm) = \frac{\delta_{kk'}}{2}\tau_3 \begin{pmatrix} \frac{1 + \frac{\zeta_k}{E_k^\pm}}{i\omega_n - E_k^\pm} + \frac{1 - \frac{\zeta_k}{E_k^\pm}}{i\omega_n + E_k^\pm} & \frac{\Delta_k^{\text{KS}*}}{E_k^\pm} \left[\frac{1}{i\omega_n + E_k^\pm} - \frac{1}{i\omega_n - E_k^\pm} \right] \\ \frac{\Delta_k^{\text{KS}}}{E_k^\pm} \left[\frac{1}{i\omega_n + E_k^\pm} - \frac{1}{i\omega_n - E_k^\pm} \right] & \frac{1 + \frac{\zeta_k}{E_k^\pm}}{i\omega_n + E_k^\pm} + \frac{1 - \frac{\zeta_k}{E_k^\pm}}{i\omega_n - E_k^\pm} \end{pmatrix}. \quad (\text{C.22})$$

In this form it is obvious that the $\bar{G}^{\text{KS}}(kk\omega_n+)$ is identical to the $\bar{G}^{\text{KS}}(kk\omega_n-)$ and hence it does not matter which function is chosen in the evaluation of the sum with respect to k (Fig. 3.1). From now on the index \pm is left out for simplicity. Using the expressions for $\bar{G}^{\text{KS}}(kk'\omega_n)$, relations for the substitution of the frequency $\omega_n \rightarrow -\omega_n$ are obtained:

$$F^{\text{KS}}(k - \omega_n) = \frac{v_k^* u_k}{-i\omega_n + E_k} - \frac{v_k^* u_k}{-i\omega_n - E_k} = \frac{v_k^* u_k}{i\omega_n + E_k} - \frac{v_k^* u_k}{i\omega_n - E_k} = F^{\text{KS}}(k\omega_n) \quad (\text{C.23})$$

$$G^{\text{KS}}(k - \omega_n) = \frac{|u_k|^2}{-i\omega_n - E_k} + \frac{|v_k|^2}{-i\omega_n + E_k} = -\frac{|u_k|^2}{i\omega_n + E_k} - \frac{|v_k|^2}{i\omega_n - E_k} = -G^{\text{KS}\dagger}(k\omega_n). \quad (\text{C.24})$$

D. Hedin Equations for Superconductors

D.1. Nambu Green's Function

D.1.1. Equation of Motion

The equation of motion for the Nambu GF given in Eq. (4.4) reads:

$$\begin{aligned} \partial_{\tau_1} \bar{G}(12) = & -\tau^z \begin{pmatrix} [\Psi(1), \Psi^\dagger(2)]_+ & [\Psi(1), z_{\sigma_2} \Psi(2)]_+ \\ [z_{\sigma_1} \Psi^\dagger(1), \Psi^\dagger(2)]_+ & [z_{\sigma_1} \Psi^\dagger(1), z_{\sigma_2} \Psi(2)]_+ \end{pmatrix} \\ & - \tau^z \begin{pmatrix} \left\langle \hat{T} [\hat{K}, \Psi_{\sigma_1}(\mathbf{r}_1)]_-(\tau_1) \Psi^\dagger(2) \right\rangle & \left\langle \hat{T} [\hat{K}, \Psi_{\sigma_1}(\mathbf{r}_1)]_-(\tau_1) z_{\sigma_2} \Psi(2) \right\rangle \\ \left\langle \hat{T} [\hat{K}, z_{\sigma_1} \Psi_{\sigma_1}^\dagger(\mathbf{r}_1)]_-(\tau_1) \Psi^\dagger(2) \right\rangle & \left\langle \hat{T} [\hat{K}, z_{\sigma_1} \Psi_{\sigma_1}^\dagger(\mathbf{r}_1)]_-(\tau_1) z_{\sigma_2} \Psi(2) \right\rangle \end{pmatrix}. \end{aligned}$$

The commutator leads to the unity and the τ^z is brought to the left hand side of the equation:

$$\begin{aligned} -\tau^z \partial_{\tau_1} \bar{G}(12) = & \delta_{12} \tau^0 + \\ & \begin{pmatrix} \left\langle \hat{T} [\hat{K}, \Psi_{\sigma_1}(\mathbf{r}_1)](\tau_1) \Psi^\dagger(2) \right\rangle & \left\langle z_{\sigma_2} \hat{T} [\hat{K}, \Psi_{\sigma_1}(\mathbf{r}_1)](\tau_1) \Psi(2) \right\rangle \\ \left\langle z_{\sigma_1} \hat{T} [\hat{K}, \Psi_{\sigma_1}^\dagger(\mathbf{r}_1)](\tau_1) \Psi^\dagger(2) \right\rangle & \left\langle z_{\sigma_1} z_{\sigma_2} \hat{T} [\hat{K}, \Psi_{\sigma_1}^\dagger(\mathbf{r}_1)](\tau_1) \Psi(2) \right\rangle \end{pmatrix}. \end{aligned} \quad (\text{D.1})$$

The Hamilton operator determining the time evolution contains single and two-particle contributions which are defined in Eqs. (4.1) and (4.3). The single-particle operator terms are unproblematic. The complications are created by the two-particle operator \hat{W} .

D.1.2. Single-Particle Contributions

For the single particle parts of the Hamiltonian the commutators give the following contribution:

$$\begin{aligned} [\hat{K}_0, \hat{\Psi}_{\sigma_1}(\mathbf{r}_1)]_- &= - \sum_{\beta} \Delta d^3 r k_{\sigma_1 \beta}^0(\mathbf{r}_1 \mathbf{r}') \hat{\Psi}_{\beta}(\mathbf{r}') & [\hat{K}_0, \hat{\Psi}_{\sigma_1}^\dagger(\mathbf{r}_1)]_- &= - [\hat{K}_0, \hat{\Psi}_{\sigma_1}(\mathbf{r}_1)]_-^\dagger \\ [\hat{H}_{\text{SC}}, \hat{\Psi}_{\sigma_1}(\mathbf{r}_1)]_- &= z_{\sigma_1} \Delta d^3 r \Delta^{\text{ext}*}(\mathbf{r}_1 \mathbf{r}) \hat{\Psi}_{-\sigma_1}^\dagger(\mathbf{r}) & [\hat{H}_{\text{SC}}, \hat{\Psi}_{\sigma_1}^\dagger(\mathbf{r}_1)]_- &= - [\hat{H}_{\text{SC}}, \hat{\Psi}_{\sigma_1}(\mathbf{r}_1)]_-, \end{aligned}$$

where \hat{K}_0 is given by $\hat{H}_0 - \mu \hat{N}$. Inserting the single particle results in the equation of motion [Eq. (D.1)] leads to:

$$\begin{aligned} -\tau^z \partial_{\tau_1} \bar{G}(12)_{11} &= \delta_{12} \tau^0 + \left\langle \hat{T} \left(- \sum_{\beta} k_{\sigma_1 \beta}^0(\mathbf{r}_1 \mathbf{r}) \hat{\Psi}_{\beta}(\mathbf{r} \tau_1) + z_{\sigma_1} \Delta^{\text{ext}*}(\mathbf{r}_1 \mathbf{r}) \hat{\Psi}_{-\sigma_1}^\dagger(\mathbf{r} \tau_1) \right) \hat{\Psi}_{\sigma_2}^\dagger(\mathbf{x}_2) \right\rangle \\ -\tau^z \partial_{\tau_1} \bar{G}(12)_{12} &= \left\langle \hat{T} \left(- \sum_{\beta} k_{\sigma_1 \beta}^0(\mathbf{r}_1 \mathbf{r}) \hat{\Psi}_{\beta}(\mathbf{r} \tau_1) + z_{\sigma_1} \Delta d^3 r \Delta^{\text{ext}*}(\mathbf{r}_1 \mathbf{r}) \hat{\Psi}_{-\sigma_1}^\dagger(\mathbf{r} \tau_1) \right) z_{\sigma_2} \hat{\Psi}_{\sigma_2}(\mathbf{x}_2) \right\rangle \\ -\tau^z \partial_{\tau_1} \bar{G}(12)_{21} &= \left\langle \hat{T} \left(\sum_{\beta} k_{\sigma_1 \beta}^{0*}(\mathbf{r}_1 \mathbf{r}) z_{\sigma_1} \hat{\Psi}_{\beta}^\dagger(\mathbf{r} \tau_1) - \Delta d^3 r \Delta^{\text{ext}}(\mathbf{r}_1 \mathbf{r}) \hat{\Psi}_{-\sigma_1}(\mathbf{r} \tau_1) \right) \hat{\Psi}_{\sigma_2}^\dagger(\mathbf{x}_2) \right\rangle \\ -\tau^z \partial_{\tau_1} \bar{G}(12)_{22} &= \delta_{12} + \left\langle \hat{T} \left(\sum_{\beta} k_{\sigma_1 \beta}^{0*}(\mathbf{r}_1 \mathbf{r}) z_{\sigma_1} \hat{\Psi}_{\beta}^\dagger(\mathbf{r} \tau_1) - \Delta d^3 r \Delta^{\text{ext}}(\mathbf{r}_1 \mathbf{r}) \hat{\Psi}_{-\sigma_1}(\mathbf{r} \tau_1) \right) z_{\sigma_2} \hat{\Psi}_{\sigma_2}(\mathbf{x}_2) \right\rangle. \end{aligned}$$

The components of the Nambu Green's function defined in Eq. (4.4) are identified

$$\begin{aligned}
-\tau^z \partial_{\tau_1} \bar{G}(12)_{11} &= \delta_{12} \tau^0 + \left\langle \sum_{\beta} k_{\sigma_1 \beta}^0(\mathbf{r}_1 \mathbf{r}) G_{\beta \sigma_2}(\mathbf{r} \tau_1 \mathbf{x}_2) - \Delta^{\text{ext}*}(\mathbf{r}_1 \mathbf{r}) F_{-\sigma_1 \sigma_2}^{\dagger}(\mathbf{r} \tau_1 \mathbf{x}_2) \right\rangle \\
-\tau^z \partial_{\tau_1} \bar{G}(12)_{12} &= \left\langle \sum_{\beta} k_{\sigma_1 \beta}^0(\mathbf{r}_1 \mathbf{r}) F_{\beta \sigma_2}(\mathbf{r} \tau_1 \mathbf{x}_2) - \Delta d^3 r \Delta^{\text{ext}*}(\mathbf{r}_1 \mathbf{r}) G_{-\sigma_1 - \sigma_2}^{\dagger}(\mathbf{r} \tau_1 \mathbf{x}_2) \right\rangle \\
-\tau^z \partial_{\tau_1} \bar{G}(12)_{21} &= \left\langle - \sum_{\beta} z_{\sigma_1} k_{\sigma_1 \beta}^{0*}(\mathbf{r}_1 \mathbf{r}) z_{\beta} F_{\beta \sigma_2}^{\dagger}(\mathbf{x}_1 \mathbf{x}_2) + \Delta d^3 r \Delta^{\text{ext}}(\mathbf{r}_1 \mathbf{r}) G_{-\sigma_1 \sigma_2}(\mathbf{r} \tau_1 \mathbf{x}_2) \right\rangle \\
-\tau^z \partial_{\tau_1} \bar{G}(12)_{22} &= \delta_{12} \tau^0 + \left\langle - \sum_{\beta} z_{\sigma_1} k_{\sigma_1 \beta}^{0*}(\mathbf{r}_1 \mathbf{r}) z_{\beta} G_{\beta \sigma_2}^{\dagger}(\mathbf{r} \tau_1 \mathbf{x}_2) + \Delta^{\text{ext}}(\mathbf{r}_1 \mathbf{r}) F_{-\sigma_1 \sigma_2}(\mathbf{r} \tau_1 \mathbf{x}_2) \right\rangle
\end{aligned}$$

and written in compact matrix notation:

$$\begin{aligned}
-\tau^z \partial_{\tau_1} \bar{G}(12) &= \delta_{12} \tau^0 + \\
&\sum_{\sigma} \Delta d\mathbf{r} \begin{pmatrix} k_{\sigma_1 \sigma}^0(\mathbf{r}_1 \mathbf{r}) & \Delta^{\text{ext}*}(\mathbf{r}_1 \mathbf{r}) \delta_{-\sigma_1 \sigma} \\ \Delta^{\text{ext}}(\mathbf{r}_1 \mathbf{r}) \delta_{\sigma_1 - \sigma} & k_{\sigma_1 \sigma}^{0*}(\mathbf{r}_1 \mathbf{r}) z_{\sigma_1} z_{\sigma_2} \end{pmatrix} \begin{pmatrix} G_{\sigma \sigma_2}(\mathbf{r} \tau_1 \mathbf{x}_2) & F_{\sigma \sigma_2}(\mathbf{r} \tau_1 \mathbf{x}_2) \\ -F_{\sigma \sigma_2}^{\dagger}(\mathbf{r} \tau_1 \mathbf{x}_2) & -G_{\sigma \sigma_2}^{\dagger}(\mathbf{r} \tau_1 \mathbf{x}_2) \end{pmatrix} + \mathcal{O}[\hat{\Psi}^4].
\end{aligned} \tag{D.2}$$

The time dependent potentials are introduced to simplify the notation:

$$\begin{aligned}
-\tau^z \partial_{\tau_1} \bar{G}(12) &= \delta_{12} \tau^0 + \Delta d^3 \begin{pmatrix} k^0(13) & \Delta^{\text{ext}*}(13) \\ \Delta^{\text{ext}}(13) & k^{0*}(13) \end{pmatrix} \bar{G}(32) \\
&+ \underbrace{\left(\left\langle \hat{T} \left[\hat{W}, \Psi_{\sigma_1}(\mathbf{r}_1) \right] (\tau_1) \Psi^{\dagger}(2) \right\rangle \left\langle \hat{T} \left[\hat{W}, \Psi_{\sigma_1}(\mathbf{r}_1) \right] (\tau_1) \Psi(2) \right\rangle \right.} \\
&\quad \left. \left\langle \hat{T} \left[\hat{W}, \Psi_{\sigma_1}^{\dagger}(\mathbf{r}_1) \right] (\tau_1) \Psi^{\dagger}(2) \right\rangle \left\langle \hat{T} \left[\hat{W}, \Psi_{\sigma_1}^{\dagger}(\mathbf{r}_1) \right] (\tau_1) \Psi(2) \right\rangle \right) \\
&\quad \text{This part is done in the next section} \\
k^0(12) &= \delta_{\tau_1 \tau_2} k_{\sigma_1 \sigma_2}^0(\mathbf{r}_1 \mathbf{r}_2) \\
\Delta^{\text{ext}}(12) &= \delta_{\tau_1 \tau_2} \delta_{\sigma_1, -\sigma_2} \Delta^{\text{ext}}(\mathbf{r}_1 \mathbf{r}_2).
\end{aligned}$$

In a **non-magnetic (NM)** Kohn-Sham system considered in the **superconducting density functional theory (SCDFT)** chapter 3, the diagonal part A is given by the normal single particle contribution plus the **XC** and **Hartree potential**: $-\frac{\Delta}{2} + v_0 + v^{\text{H}} + v^{\text{xc}}$ and the Δ^{ext} is replaced by the sum of external pairing field Δ^{ext} and the **XC** part Δ^{xc} .

D.1.3. Two-Particle Contributions

The commutator for the two-particle term \hat{W} is evaluated:

$$\begin{aligned}
[\hat{W}, \hat{\Psi}_{\sigma_1}(\mathbf{r}_1)] &= -2 \sum_{\alpha} \Delta d^3 r \frac{v(\mathbf{r} \mathbf{r}_1)}{2} \hat{\Psi}_{\alpha}^{\dagger}(\mathbf{r}) \hat{\Psi}_{\alpha}(\mathbf{r}) \hat{\Psi}_{\sigma_1}(\mathbf{r}_1) \quad [\hat{W}, \hat{\Psi}_{\sigma_1}^{\dagger}(\mathbf{r}_1)] = -[\hat{W}, \hat{\Psi}_{\sigma_1}(\mathbf{r}_1)]^{\dagger}.
\end{aligned} \tag{D.3}$$

Inserting this on the right hand side of the equation of motion [Eq. (D.1)] leads to:

$$\begin{aligned}
\mathcal{O}[\hat{\Psi}^4] &= \sum_{\alpha} \Delta d^3 r v(\mathbf{r}_1 \mathbf{r}) \times \\
&\left(- \left\langle \hat{T} \hat{\Psi}_{\alpha}^{\dagger}(\mathbf{r} \tau_1) \hat{\Psi}_{\alpha}(\mathbf{r} \tau_1) \hat{\Psi}_{\sigma_1}(\mathbf{x}_1) \hat{\Psi}_{\sigma_2}^{\dagger}(\mathbf{x}_2) \right\rangle - \left\langle \hat{T} \hat{\Psi}_{\alpha}^{\dagger}(\mathbf{r} \tau_1) \hat{\Psi}_{\alpha}(\mathbf{r} \tau_1) \hat{\Psi}_{\sigma_1}(\mathbf{x}_1) z_{\sigma_2} \hat{\Psi}_{\sigma_2}(\mathbf{x}_2) \right\rangle \right) \\
&\left(\left\langle \hat{T} z_{\sigma_1} \hat{\Psi}_{\alpha}^{\dagger}(\mathbf{r} \tau_1) \hat{\Psi}_{\alpha}(\mathbf{r} \tau_1) \hat{\Psi}_{\sigma_1}^{\dagger}(\mathbf{x}_1) \hat{\Psi}_{\sigma_2}^{\dagger}(\mathbf{x}_2) \right\rangle \left\langle \hat{T} z_{\sigma_1} \hat{\Psi}_{\alpha}^{\dagger}(\mathbf{r} \tau_1) \hat{\Psi}_{\alpha}(\mathbf{r} \tau_1) \hat{\Psi}_{\sigma_1}^{\dagger}(\mathbf{x}_1) z_{\sigma_2} \hat{\Psi}_{\sigma_2}(\mathbf{x}_2) \right\rangle \right).
\end{aligned} \tag{D.4}$$

D.1.4. Schwinger's Functional Derivative Approach

The two-particle expectation values are too difficult to evaluate, but it is possible to connect the expectation value to a functional derivative with respect to an external probing field. This procedure is called Schwinger's functional derivative approach [83]. The probing field or perturbation φ_i is time dependent and couples to the densities:

$$\hat{\Phi}(\tau) = \sum_i \Delta d^3r \varphi_i(\mathbf{x}) \hat{\rho}_i(\mathbf{r}).$$

This field is used as a mathematical tool and it is set to zero after the derivative is calculated *i.e.*:

$$\frac{\delta A}{\delta \varphi_i} := \lim_{\varphi_i \rightarrow 0} \left. \frac{\delta A}{\delta \varphi_i} \right|_{e,v,H_0}.$$

The limit guarantees that the considered Hamiltonian remains time independent and all quantities depend only on the time difference. The new term in the Hamiltonian $\hat{\Phi}(\tau) = \Delta d^3r \varphi(\mathbf{x}) \hat{\rho}(\mathbf{r})$ is considered as the interaction in the Dirac picture. Note that in this way the fully interacting system takes the roles of the unperturbed system. In the standard definition of the **Dirac picture** the two-particle interaction is the perturbation. In order to highlight this difference the label \hat{S} is used for the time propagation operator, instead of the usual $\hat{U}(\beta, 0)$ [Eq. 2.25]. However, the perturbative expression [Eq. (2.29)] holds also for the $\hat{\Phi}$ related to the probing field:

$$\begin{aligned} \bar{G}(12) &= -\lim_{\Phi \rightarrow 0} \frac{\tau^z}{\langle \hat{S} \rangle} \left(\frac{\langle \hat{T} [\hat{S} \Psi_{\sigma_1}(\mathbf{x}_1)_D \Psi_{\sigma_2}^\dagger(\mathbf{x}_2)_D] \rangle}{\langle \hat{T} [\hat{S} z_{\sigma_1} \Psi_{\sigma_1}^\dagger(\mathbf{x}_1)_D \Psi_{\sigma_2}^\dagger(\mathbf{x}_2)_D] \rangle} \quad \frac{\langle \hat{T} [\hat{S} \Psi_{\sigma_1}(\mathbf{x}_1)_D z_{\sigma_2} \Psi_{\sigma_2}(\mathbf{x}_2)_D] \rangle}{\langle \hat{T} [\hat{S} z_{\sigma_1} \Psi_{\sigma_1}^\dagger(\mathbf{x}_1)_D z_{\sigma_2} \Psi_{\sigma_2}(\mathbf{x}_2)_D] \rangle} \right) \\ \hat{S}(\beta, 0) &= e^{-\Delta_0^\beta \int d\tau \hat{\Phi}(\tau)_D} \\ \frac{\delta \hat{S}}{\delta \varphi_i(\mathbf{x})} &= -\hat{S} \hat{\rho}_i(\mathbf{x})_D = -\hat{S} \sum_{\alpha\beta} \sigma_{\alpha\beta}^i \hat{\Psi}_\alpha^\dagger(\mathbf{x})_D \hat{\Psi}_\beta(\mathbf{x})_D. \end{aligned}$$

Fields coupling to the anomalous density are not needed because the Coulomb part creates no terms like $\langle \hat{\Psi} \hat{\Psi} \hat{\Psi} \hat{\Psi} \rangle$ or $\langle \hat{\Psi}^\dagger \hat{\Psi}^\dagger \hat{\Psi}^\dagger \hat{\Psi}^\dagger \rangle$. Evaluating the **functional derivative** leads to:

$$\begin{aligned} \frac{\delta \bar{G}(12)}{\delta \varphi_0(\mathbf{x}_3)} &= \hat{\rho}_i(\mathbf{x}_3)_D \bar{G}(12) + \sum_{\alpha\beta} \frac{\sigma_{\alpha\beta}^0 \tau^z}{\langle \hat{S} \rangle} \left(\frac{\langle \hat{T} [\hat{S} \hat{\Psi}_\alpha^\dagger(\mathbf{x}_3)_D \hat{\Psi}_\beta(\mathbf{x}_3)_D \Psi_{\sigma_1}(\mathbf{x}_1)_D \Psi_{\sigma_2}^\dagger(\mathbf{x}_2)_D] \rangle}{\langle \hat{T} [\hat{S} \hat{\Psi}_\alpha^\dagger(\mathbf{x}_3)_D \hat{\Psi}_\beta(\mathbf{x}_3)_D z_{\sigma_1} \Psi_{\sigma_1}^\dagger(\mathbf{x}_1)_D \Psi_{\sigma_2}^\dagger(\mathbf{x}_2)_D] \rangle} \quad 0 \right) \\ &\quad + \sum_{\alpha\beta} \frac{\sigma_{\alpha\beta}^0 \tau^z}{\langle \hat{S} \rangle} \left(0 \quad \frac{\langle \hat{T} [\hat{S} \hat{\Psi}_\alpha^\dagger(\mathbf{x}_3)_D \hat{\Psi}_\beta(\mathbf{x}_3)_D \Psi_{\sigma_1}(\mathbf{x}_1)_D z_{\sigma_2} \Psi_{\sigma_2}(\mathbf{x}_2)_D] \rangle}{\langle \hat{T} [\hat{S} \hat{\Psi}_\alpha^\dagger(\mathbf{x}_3)_D \hat{\Psi}_\beta(\mathbf{x}_3)_D z_{\sigma_1} \Psi_{\sigma_1}^\dagger(\mathbf{x}_1)_D z_{\sigma_2} \Psi_{\sigma_2}(\mathbf{x}_2)_D] \rangle} \right). \end{aligned}$$

The perturbation is set to zero after the derivative is performed. This means $\hat{S} = 1$ and the Dirac picture of this section reduces to the normal **Heisenberg picture**. The steps in this section are in complete analogy to the procedure in the **LR** theory in Sec. 2.2. The two-particle contributions are given in terms of the functional derivative of \bar{G} with respect to the external probing field and a comparison with Eq. (D.4) leads to:

$$\begin{aligned} \sum_\alpha \Delta d^3r v(\mathbf{r}_1 \mathbf{r}) \left[\rho_0(\mathbf{r} \tau_1) \bar{G}(12) - \frac{\delta \bar{G}(12)}{\delta \varphi_0(\mathbf{r} \tau_1)} \right] = \\ \left(\frac{\langle \hat{T} [\hat{W}, \hat{\Psi}_{\sigma_1}(\mathbf{r}_1)](\tau_1) \hat{\Psi}_{\sigma_2}^\dagger(\mathbf{x}_2) \rangle}{\langle \hat{T} [\hat{W}, z_{\sigma_1} \hat{\Psi}_{\sigma_1}^\dagger(\mathbf{r}_1)](\tau_1) \hat{\Psi}_{\sigma_2}^\dagger(\mathbf{x}_2) \rangle} \quad \frac{\langle \hat{T} [\hat{W}, \hat{\Psi}_{\sigma_1}(\mathbf{r}_1)](\tau_1) z_{\sigma_2} \hat{\Psi}_{\sigma_2}(\mathbf{x}_2) \rangle}{\langle \hat{T} [\hat{W}, z_{\sigma_1} \hat{\Psi}_{\sigma_1}^\dagger(\mathbf{r}_1)](\tau_1) z_{\sigma_2} \hat{\Psi}_{\sigma_2}(\mathbf{x}_2) \rangle} \right). \end{aligned} \quad (\text{D.5})$$

D.2. The Loop Rule

Within the perturbation expansion of the GF, the interaction enters in multiples of [Eq. 2.29]:

$$-v(12) \hat{\Psi}_D^\dagger(1) \hat{\Psi}_D^\dagger(2) \hat{\Psi}_D(2) \hat{\Psi}_D(1).$$

Assume now a fully contracted contribution, in which the GF is separated into two parts (see left side of Fig. D.1):

$$G(12) = \left\langle \hat{\Psi}_D(1) \dots \text{some contraction} \dots \hat{\Psi}_D^\dagger(2) \right\rangle \times \underbrace{\left\langle \hat{\Psi}_D^\dagger(4) \hat{\Psi}_D(4) \hat{\Psi}_D^\dagger(5) \hat{\Psi}_D^\dagger(6) \hat{\Psi}_D(6) \hat{\Psi}_D(5) \dots \hat{\Psi}_D^\dagger(N) \hat{\Psi}_D(N) \right\rangle v(34) v(56) \dots v(N-1N)}_{=\text{Part } A \text{ only connected via } v \text{ to the other term}}.$$

Within the separate Part A at least one **Fermionic loop** must appear. If there are multiple loops the part A is split in $A_1 \dots A_s$ separate parts, where each A_i contains only a single loop and from now on only parts with a single loop are considered. Since the product of the various interactions is always within the time ordering operator the terms are rearranged:

$$\left\langle \dots \hat{\Psi}_D^\dagger(3) \hat{\Psi}_D(3) \hat{\Psi}_D^\dagger(4) \hat{\Psi}_D(2) \dots \hat{\Psi}_D^\dagger(N) \hat{\Psi}_D(N) \dots \right\rangle_0.$$

With the help of Wick's theorem (Sec. 2.4), such expectation values are evaluated by the sum of all possible totally contracted contributions. The **contraction** is defined in Eq. (2.30) and a contraction with a single loop leads to:

$$\begin{aligned} & \hat{\Psi}_D^\dagger(1)_D \hat{\Psi}_D(1)_D \hat{\Psi}_D^\dagger(2)_D \hat{\Psi}_D(2)_D \dots \hat{\Psi}_D^\dagger(N)_D \hat{\Psi}_D(N)_D \\ & \hat{\Psi}_D^\dagger(1)_D G_0(12) \dots G_0(N-1N) \hat{\Psi}_D(N)_D = -G_0(N1) G_0(12) \dots G_0(N-1N). \end{aligned}$$

For each Part A_i containing a single loop of normal state Green's functions a (-1) appears. Up to now only loops with multiple Green's functions have been considered, but the most simple form of a loop is just the contraction between two operators with the same space-time argument:

$$\lim_{2 \nearrow 1} \hat{\Psi}_D^\dagger(1) \hat{\Psi}_D(2) = \lim_{2 \nearrow 1} \left\langle \hat{T} \left[\hat{\Psi}_D^\dagger(1) \hat{\Psi}_D(2) \right] \right\rangle_0 = -\lim_{2 \nearrow 1} G_0(21) = -G_0(11^+).$$

This means a factor of $(-1)^s$ is added, where s is the number of loops. Note that this rule is only necessary for purely normal GF loops. If SC contributions are present in the loop, no minus signs appear. For the **anomalous Green's function** a single Green's function loop like $F(11^+)$ is not possible because the Coulomb interaction contains always an incoming and an outgoing GF line. Hence, the first loops containing anomalous terms are

$$\begin{aligned} & \hat{\Psi}_D^\dagger(1)_D \hat{\Psi}_D^\dagger(2)_D \hat{\Psi}_D(2)_D \hat{\Psi}_D(1)_D = -\hat{\Psi}_D(2)_D \hat{\Psi}_D^\dagger(1)_D \hat{\Psi}_D(1)_D \hat{\Psi}_D^\dagger(2)_D = -G_0(21) G_0(12) \\ & \hat{\Psi}_D^\dagger(1)_D \hat{\Psi}_D^\dagger(2)_D \hat{\Psi}_D(2)_D \hat{\Psi}_D(1)_D = F_0^\dagger(12) F_0(21) \\ & \hat{\Psi}_D^\dagger(1)_D \hat{\Psi}_D(1)_D \hat{\Psi}_D^\dagger(2)_D \hat{\Psi}_D(2)_D \hat{\Psi}_D^\dagger(3)_D \hat{\Psi}_D(3)_D = -G_0(13) G_0(12) G_0(23) \\ & \hat{\Psi}_D^\dagger(1)_D \hat{\Psi}_D(1)_D \hat{\Psi}_D^\dagger(2)_D \hat{\Psi}_D(2)_D \hat{\Psi}_D^\dagger(3)_D \hat{\Psi}_D(3)_D = F_0^\dagger(12) G_0(13) F_0(23) \\ & \quad \vdots \end{aligned}$$

and no minus sign appears for loops with an anomalous term.

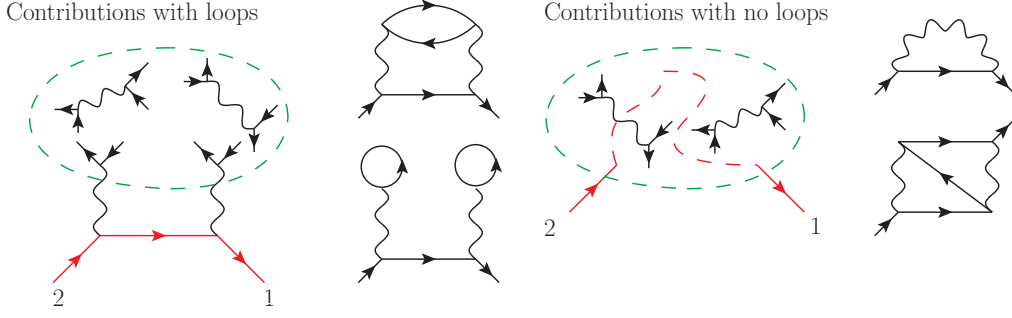


Figure D.1.: Contributions in the expansion of the Green's function containing at least one loop (left) and without loops (right).

D.3. Different Reference Systems

Two different [reference systems](#) have been used already in chapter 4: The \hat{h}^0 system related to a [self-energy](#) with Hartree terms and \hat{h}^H where the Hartree contribution are removed from the self-energy (Eqs. (2.33) and Eq. (4.10)). However, it is possible to add arbitrary single particle potentials \bar{v} on both sides of the [equation of motion](#) [Eq. (4.10)]:

$$-\left[\tau^z \partial_{\tau_1} + \sum_{\alpha} \Delta d^3 r \bar{h}_{\sigma_1 \alpha}^{H+\bar{v}}(\mathbf{r}_1 \mathbf{r})\right] \bar{G}_{\alpha \sigma_2}(\mathbf{r} \tau_1 \mathbf{x}_2) = \mathbf{1}_{2 \times 2} + \Delta d^3 [\bar{\Sigma}(13) - \bar{v}(13)] \bar{G} \quad (32)$$

$$\bar{h}_{\sigma_1 \sigma_2}^{H+\bar{v}}(\mathbf{r}_1 \mathbf{r}_2) = \bar{h}_{\sigma_1 \sigma_2}^H(\mathbf{r}_1 \mathbf{r}_2) + \bar{v}_{\sigma_1 \sigma_2}(\mathbf{r}_1 \mathbf{r}_2).$$

By adding a \bar{v} to the non-interacting system, the corresponding reference GF changes. The full \bar{G} is **independent** of the selected reference system because also the self-energy [Eq. (4.10)] in the Dyson equation for \bar{G} is changed *i.e.*:

$$\bar{G} = \bar{G}^{\text{ref}} + \bar{G}^{\text{ref}} \bar{\Sigma}^{\text{ref}} \bar{G} \quad \bar{\Sigma}^{\text{ref}} = \bar{\Sigma} - \bar{v} \quad \text{and} \quad -[\tau_3 \partial_{\tau} + \bar{h}^{H+\bar{v}}] \bar{G}^{\text{ref}} = \mathbf{1}.$$

All further steps in the Hedin cycle are independent of the reference system because the equations depend only on the full Green's function and Σ . For practical applications some choices for the reference system are a better starting point than others [151]. The standard reference systems in the literature are:

1. The “free Green's function”:

$$-\begin{pmatrix} \partial_{\tau_1} - \Delta_{\mathbf{r}_1} & 0 \\ 0 & -\partial_{\tau_1} - \Delta_{\mathbf{r}_1} \end{pmatrix} \bar{G}^{\text{HEG}} = \mathbf{1} \quad \bar{G} = \bar{G}^{\text{HEG}} + \bar{G}^{\text{HEG}} [\pm + v^H + v_0] \bar{G} \quad (D.6)$$

corresponding to the [HEG](#) and all system information must enter in the renormalization process.

2. The “non interacting Green's function”:

$$-[\tau^z \partial_{\tau_1} + \bar{h}_0] \bar{G}_0 = \mathbf{1} \quad \bar{G} = \bar{G}_0 + \bar{G}_0 [\bar{\Sigma} + \tau_0 v^H] \bar{G} \quad (D.7)$$

corresponding to non-interacting electrons in the background potential of the nuclei (Eq. (4.6) for the definition of \bar{h}_0). This means the structural information of the system is added to the reference system, but all interaction between the electrons enters in the Dyson equation.

3. The “Hartree Green's function”:

$$-\tau^z [\partial_{\tau_1} + \bar{h}^H] \bar{G}^H = \mathbf{1} \quad \bar{G} = \bar{G}^H + \bar{G}^H \bar{\Sigma} \bar{G}, \quad (D.8)$$

where the [Hartree potential](#) is added to the reference system. In this form the self-energy contains no local contributions [Eq. (4.9) for definition of \bar{h}^H].

4. The ‘‘Kohn-Sham Green’s function’’:

$$- \left[\tau^z \partial_{\tau_1} + \left[\bar{h}^H + \begin{pmatrix} v^{\text{xc}} + B^{\text{xc}} & \Delta_s^{\text{xc}*} \\ \Delta_s^{\text{xc}} & (v^{\text{xc}} + B_i^{\text{xc}})^* \end{pmatrix} \right] \right] \bar{G}^{\text{KS}} = \mathbf{1} \quad \bar{G} = \bar{G}^{\text{KS}} + \bar{G}^{\text{KS}} [\bar{\Sigma} - \bar{v}^{\text{xc}}] \bar{G} \quad (\text{D.9})$$

corresponding to the Hamiltonian given in Eq. (3.6). The **KS** system is obtained by adding the **XC-potential** and **Hartree potential** ($B_i^{\text{ext}} \rightarrow B_i^{\text{ext}} + B_i^{\text{xc}}$, $v_0 \rightarrow v_0 + v^H + v^{\text{xc}}$ and $\Delta_s^{\text{ext}} \rightarrow \Delta_s^{\text{ext}} + \Delta_s^{\text{xc}}$) to the non-interacting Hamiltonian [Eq. (4.6)]. The **KS** system has the special property that it reproduces (for the exact \bar{v}^{xc}) the density of the full system *i.e.* $\sum_{\alpha} G_{\alpha\alpha}^{\text{KS}} (11^+)_{11} = \rho(\mathbf{r}_1)$ and $\chi(\mathbf{r}_1\mathbf{r}_2) = \sum F_{\uparrow\downarrow}^{\text{KS}}(\mathbf{r}_1\tau_1\mathbf{r}_2\tau_1^+)$. In practice, the **XC-potential** is approximated by one of the countless approximations (**local density approximation (LDA)**, **generalized gradient approximation (GGA)**, ...) and the full **GF** will depend on the choice of the reference system [151].

The functions \bar{G}^{KS} or \bar{G}^H are much closer to the full Green’s function than \bar{G}^{HEG} and \bar{G}^0 because many-body effects like exchange for \bar{G}^H and **XC** for \bar{G}^{KS} are included. This is advantageous for a perturbation expansion.

E. Sham-Schlüter Equation

E.1. Frequency Sums – Residue Theorem

In the [Sham-Schlüter equation \(SSEq\)](#), summations with respect to the [Matsubara frequencies](#) are involved. Any Matsubara summation can be rewritten using the residue theorem and the Fermi (f_β) or Bose (b_β) distribution functions: The f_β or b_β have poles on the imaginary axis at either $\frac{2\pi n}{\beta}i$ or $\frac{(2n+1)\pi}{\beta}i$ (Fig. E.1) and the residue at every pole is simply $-\frac{1}{\beta}$. From now on only the Fermionic case is considered, but analogous equations hold also for bosonic Matsubara sums.

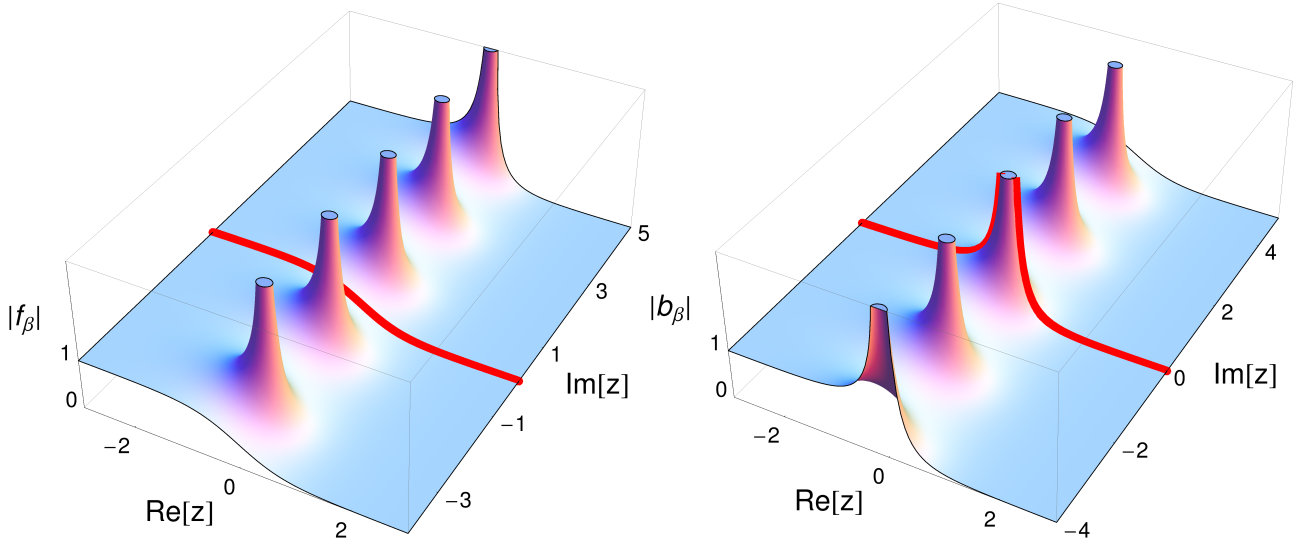


Figure E.1.: Absolute values of the Fermi function $f_\beta(z) = \frac{1}{e^{\beta z} + 1}$ and bosonic distribution function $b_\beta(z) = \frac{1}{e^{\beta z} - 1}$ in the complex plane. The red line is the function for $z \in \mathbb{R}$ which is shown in every many-body text book [52, 51].

Assume a function $A(z)$ which is analytic (has no poles) in the complex frequency plane. By multiplying this function with f_β a function is created with poles at every ω_n . The Cauchy integral formula or [residue theorem](#) connects such a sum to a contour integral:

$$-\frac{1}{2\pi i} \text{ff}_\gamma dz A(z) f_\beta(z) = \sum_{\substack{\text{Poles} \in \gamma \\ n}} \text{res}[f_\beta(z) A(z), z_n] = \frac{1}{\beta} \sum_{\omega_n} A(i\omega_n),$$

where $\text{res}[f(z), z_0]$ denotes the residue of the function f located at z_0 . Note that the residue theorem is unique only in one direction. If a function $f(z)$ is analytic on a region Γ and the values of the function are known on the contour γ surrounding that region all function values $z_0 \in \Gamma$ are determined via:

$$\text{ff}_\gamma dz \frac{f(z)}{z - z_0} = 2\pi i f(z_0)$$

and it is **not** possible to multiply an analytic function which is 1 on the contour and not identical to 1 (\Rightarrow). However, in this section the summation with respect to discrete Matsubara frequencies is rewritten. This means the function is known on only Matsubara points ($z_0 = \{\omega_1, \omega_2, \dots\}$) and not on a contour. In this case it is possible to add a function \tilde{f} which is 1 for $z = z_0$ and different elsewhere *i.e.* the [analytic continuation](#) from points to the complex plane is in general not unique (\nRightarrow). However,

for the GF it can be shown that the continuation is unique because a non-trivial \tilde{f} breaks the limit behavior: $\lim_{|z| \rightarrow 0} G(z) = 0$ [52]. It is assumed that such a condition is also valid for the considered functions $A(z)$ which will be a product of Green's functions and self-energy contributions. The contour γ is transformed to γ' (Fig. E.2):

$$\frac{1}{\beta} \sum_{\omega_n} A(i\omega_n) = -\frac{1}{2\pi i} \oint_{\gamma'} dz A(z) f_{\beta}(z).$$

In order to close the contour with the infinite cycle the function $A(z)$ must vanishes for $|z| \rightarrow \infty$ faster than $\frac{1}{|z|}$ (Jordan's lemma). The Fermi function has no poles besides the ones on the imaginary axis. Hence, the contour integral with respect to γ' is given by the residues of $A(z)$ in the complex plane (imaginary axis excluded):

$$\frac{1}{\beta} \sum_{\omega_n} A(i\omega_n) = \sum_n^{\text{Poles} \in \gamma'} \text{res} [f_{\beta}(z) A(z), z_n]. \quad (\text{E.1})$$

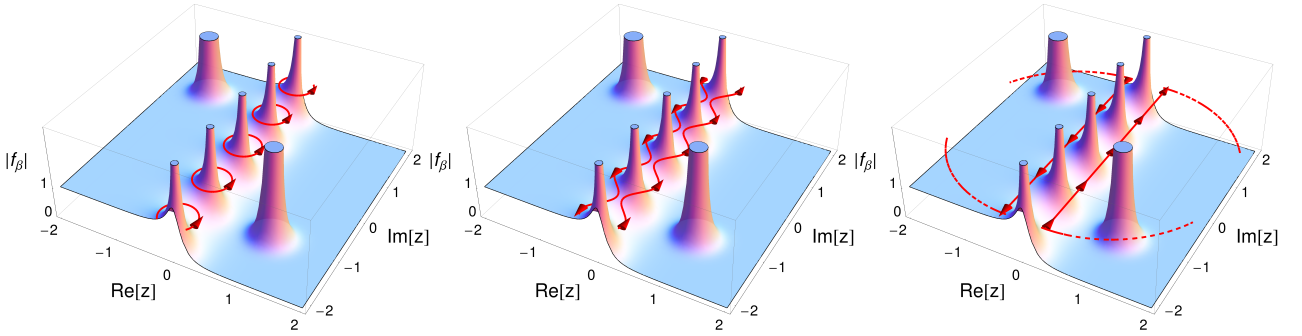


Figure E.2.: Fermi function with poles on the imaginary axis and some example function A with two poles in the complex plane. The initial contour γ (left) is changed in two steps to the contour γ' (right), where the poles of the function A lie inside the contour [Eq. (E.1)]. For closing the contour with the infinite circle (dashed line) it is assumed that the function $A(z)$ vanishes for $|z| \rightarrow \infty$ faster than $\frac{1}{|z|}$.

E.2. Various Terms in the Sham-Schlüter Equation

In this section the Matsubara summations appearing in the Sham-Schlüter equation [Eq. (6.2)] are worked out analytically.

E.2.1. The GG^\dagger Term

The first rather simple contribution in Eq. (6.2) is: $\sum_n G^{\text{KS}}(k\omega_n) G^{\text{KS}\dagger}(k\omega_n)$. The explicit expression for G^{KS} given in Eq. (C.18) is inserted:

$$\begin{aligned} G^{\text{KS}} G^{\text{KS}\dagger} &= \left(\frac{|u_k|^2}{i\omega_n - E_k} + \frac{|v_k|^2}{i\omega_n + E_k} \right) \left(\frac{|u_k|^2}{i\omega_n + E_k} + \frac{|v_k|^2}{i\omega_n - E_k} \right) \\ &= \frac{|u_k|^4 + |v_k|^4}{(i\omega_n - E_k)(i\omega_n + E_k)} + \frac{|u_k|^2 |v_k|^2}{(i\omega_n - E_k)^2} + \frac{|u_k|^2 |v_k|^2}{(i\omega_n + E_k)^2}. \end{aligned}$$

Note that $|u_k|^2 |v_k|^2$ contains only $|\Delta_k|^2$ and higher orders in Δ_k [Eq. (6.7)]. Since the equation is linearized in Δ_k the last two terms are neglected and $2|u_k|^2 |v_k|^2$ is added to the first term:

$$G^{\text{KS}} G^{\text{KS}\dagger} = \frac{|u_k|^4 + |v_k|^4 + 2|u_k|^2 |v_k|^2}{(i\omega_n - E_k)(i\omega_n + E_k)} = \frac{\left(|u_k|^2 + |v_k|^2 \right)^2}{(i\omega_n - E_k)(i\omega_n + E_k)}.$$

The coefficients are renormalized $|u_k|^2 + |v_k|^2 = 1$ and the KS Green's function reads:

$$\begin{aligned} \frac{1}{\beta} \sum_n e^{i\omega_n 0^+} G^{\text{KS}} G^{\text{KS}\dagger} &= \frac{1}{\beta} \sum_n \frac{e^{i\omega_n 0^+}}{(i\omega_n - E_k)(i\omega_n + E_k)} = \frac{1}{2E_k \beta} \sum_n e^{i\omega_n 0^+} \left[\frac{1}{i\omega_n + E_k} - \frac{1}{i\omega_n - E_k} \right] \\ &= \sum_n^{\text{Poles} \in \gamma'} \text{res} \left[\frac{f_\beta(z) e^{iz0^+}}{2E_k} \left[\frac{1}{z + E_k} - \frac{1}{z - E_k} \right], z_n \right]. \end{aligned} \quad (\text{E.2})$$

The two poles of $A(z) = \frac{1}{z+E_k} - \frac{1}{z-E_k}$ are at $\pm E_k$ and the residues are obviously $\frac{\pm f_\beta(E_k)}{\pm 2E_k}$, since the function f_β has no poles in the contour γ' (Fig. E.2). Inserting this in the Eq. (E.1) leads to:

$$\frac{1}{\beta} \sum_n e^{i\omega_n 0^+} G^{\text{KS}} G^{\text{KS}\dagger} = -\frac{1}{2E_k} [f_\beta(E_k) - f_\beta(-E_k)] = \frac{\tanh\left[\frac{\beta E_k}{2}\right]}{2E_k}. \quad (\text{E.3})$$

E.2.2. The I Term

In the contributions to the SSEq containing the self-energy *i.e.* $G^{\text{KS}} \bar{\Sigma}_{11} F^{\text{KS}}$ and $G^{\text{KS}} \bar{\Sigma}_{12} G^{\text{KS}\dagger}$ [Eq. (6.2)] a function depending on $E_k, E_{k'}$ and ω appears. The function contains all the Matsubara summations and is defined by:

$$I_\beta(E_k, E_{k'} \omega) := -\frac{1}{\beta^2} \sum_{nm} \frac{1}{i\omega_n + E_k} \frac{2\omega e^{i\omega_n 0^+}}{\omega^2 + (\omega_n - \omega_m)^2} \frac{1}{i\omega_m + E_{k'}}. \quad (\text{E.4})$$

The calculation of the residues is easier, if the fraction is split into two parts:

$$I_\beta(E_k, E_{k'} \omega) = \frac{1}{\beta^2} \sum_{nm} \underbrace{\frac{1}{i\omega_n + E_k} \frac{e^{i\omega_n 0^+}}{\omega + i(\omega_n - \omega_m)} \frac{1}{\omega_m + E_{k'}}}_{A(\omega\omega_n\omega_m E_k E_{k'})} + \frac{1}{\beta^2} \sum_{nm} \underbrace{\frac{1}{i\omega_n + E_k} \frac{e^{i\omega_n 0^+}}{\omega - i(\omega_n - \omega_m)} \frac{1}{\omega_m + E_{k'}}}_{B(\omega\omega_n\omega_m E_k E_{k'})}.$$

Mathematica helps with the determination of the residues. The final results from the term A and B , using the relations discussed in Sec. E.1, are

$$\begin{aligned} \sum_{nm} A(\omega\omega_n\omega_m E_k E_{k'}) &= \frac{f_\beta(E_{k'}) f_\beta(E_k) b_\beta(\omega)}{E_k - E_{k'} - \omega} [e^{E_k} - e^{E_{k'} + \omega}] \\ \sum_{nm} B(\omega\omega_n\omega_m E_k E_{k'}) &= \frac{f_\beta(E_k) f_\beta(E_{k'}) b_\beta(\omega)}{E_k - E_{k'} + \omega} [e^{E_k + \omega} - e^{E_{k'}}] \end{aligned}$$

and the function I , after the Matsubara frequencies have been summed analytically, reads:

$$I_\beta(E_k, E_{k'} \omega) = -f_\beta(E_k) f_\beta(E_{k'}) b_\beta(\omega) \left[\frac{e^{\beta E_k} - e^{\beta(E_{k'} + \omega)}}{E_k - E_{k'} - \omega} - \frac{e^{\beta E_{k'}} - e^{\beta(E_k + \omega)}}{E_k - E_{k'} + \omega} \right]. \quad (\text{E.5})$$

Note that this function diverges for $\omega \rightarrow 0$ as $b_\beta(\omega) \approx \frac{1}{\omega}$. This means the interaction has to behave like $a_1\omega + \frac{a_2}{2}\omega^2 + \dots$ for small frequencies in order to avoid divergences in the frequency integrals [Eq. (6.6)]. On the other hand, the Bose function goes to zero for $\omega \rightarrow \infty$ ensuring the convergence of the frequency integrals even if the retarded response decays slowly.

E.2.3. Preparation for the Self-Energy Terms

The structure of the self-energy contribution, required in the SSEq in real space reads [Eq. (6.1)]:

$$\bar{\Sigma}(\mathbf{r}_1 \mathbf{r}_2 \omega_n) = \frac{1}{\beta} \sum_{\omega_m} M(\mathbf{r}_1 \mathbf{r}_2 \omega_n - \omega_m) \bar{G}(\mathbf{r}_1 \mathbf{r}_2 \omega_m).$$

In principle, the interaction M varies for the different components of the GF [Eq. (6.1)], but for the discussion at this point this is irrelevant. The self-energy in Bloch representation [Eq. (C.20)] and the transformation of the GF [Eq. (C.19)] are inserted:

$$\begin{aligned}\bar{\Sigma}(k\omega_n) &= \frac{1}{\beta} \sum_{k'\omega_m} \Lambda d^3r_1 d^3r_2 \psi_k^*(\mathbf{r}_1) \psi_{k'}(\mathbf{r}_1) M(\mathbf{r}_1\mathbf{r}_2\omega_n - \omega_m) \bar{G}(k'\omega_m) \psi_{k'}^*(\mathbf{r}_2) \psi_k(\mathbf{r}_2) \\ \bar{\Sigma}(k\omega_n) &= \frac{1}{\beta} \sum_{k'\omega_m} M_{kk'}(\omega_n - \omega_m) \bar{G}(k'\omega_m)\end{aligned}\quad (\text{E.6})$$

$$M_{kk'}(\omega_n - \omega_m) := \Lambda d^3r_1 d^3r_2 \psi_k^*(\mathbf{r}_1) \psi_{k'}(\mathbf{r}_1) M(\mathbf{r}_1\mathbf{r}_2\omega_n - \omega_m) \psi_{k'}^*(\mathbf{r}_2) \psi_k(\mathbf{r}_2). \quad (\text{E.7})$$

In the analytic evaluation of the Matsubara sums, the frequency dependence of the interaction is crucial. The basic form of the interactions given in Eq. (5.41) is:

$$M(\mathbf{r}_1\mathbf{r}_2\omega_n) \propto \Lambda d^3r d^3r' f_{zz}^{\text{xc}}(\mathbf{r}_1\mathbf{r}\omega_n) \chi_{zz}^{\text{M}}(\mathbf{r}\mathbf{r}'\omega_n) f_{zz}^{\text{xc}}(\mathbf{r}'\mathbf{r}_2\omega_n).$$

A restriction to real, local and static kernels as the ALDA (Sec. B.4) is made:

$$M(\mathbf{r}_1\mathbf{r}_2\omega_n) \propto f_{zz}^{\text{xc}}(\mathbf{r}_1) \chi_{zz}^{\text{M}}(\mathbf{r}_1\mathbf{r}_2\omega_n) f_{zz}^{\text{xc}}(\mathbf{r}_2).$$

The connection between the retarded and Matsubara functions [Eq. (B.11)] is used and the interaction is transformed to Bloch representation:

$$M_{kk'}(\omega_n) \propto \Delta d\omega \frac{M_{kk'}^{\text{R}}(\omega) - M_{k'k}^{\text{R}*}(\omega)}{\omega_n^2 + \omega^2} = \Delta d\omega \frac{\Im[M_{kk'}^{\text{R}}(\omega)]\omega}{\omega_n^2 + \omega^2}. \quad (\text{E.8})$$

The adiabatic kernel leads to the convenient result that simply the anti-Hermitian part of the whole interaction is used in the expression. For frequency dependent kernels the situation becomes more complicated. The kernel is also defined implicitly by Eq. (5.17):

$$f_{zz}^{\text{xc}}(\omega) = \chi_{zz}^{\text{KS}-1}(\omega) - \chi_{zz}^{-1}(\omega),$$

where the $^{-1}$ denotes a matrix inversion in space: $\chi_{zz}(\mathbf{r}_1\mathbf{r}_2\omega)$. For the response functions the Eq. (B.11) holds:

$$f_{zz}^{\text{xc}}(\omega_n) = \frac{2}{\pi} \Delta_0^\infty dE \frac{\Im[\chi_{zz}^{\text{KS}-1}(E) - \chi_{zz}^{-1}(E)]E}{\omega_n^2 + E^2} =: \Delta dE \frac{A(E)}{\omega_n^2 + E^2},$$

and the matrix elements read:

$$M(\mathbf{r}_1\mathbf{r}_2\omega_n) \propto \Lambda d^3r d^3r' \Pi dE_1 \dots dE_3 \frac{A(\mathbf{r}_1\mathbf{r}E_1)E_1}{\omega_n^2 + E_1^2} \frac{\Im[\chi_{zz}(\mathbf{r}\mathbf{r}'E_2)]E_2}{\omega_n^2 + E_2^2} \frac{A(\mathbf{r}'\mathbf{r}_2E_3)E_3}{\omega_n^2 + E_3^2}. \quad (\text{E.9})$$

Also for this expression it is possible to evaluate the Matsubara summation analytically, but the poles have higher order compared to the adiabatic situation. This leads to more complicated expressions for the residues compared to Eq. (E.5).

Before the contributions to the SSEq containing the self-energy are evaluated, a helpful observation is made: The two contributions $G^{\text{KS}}\Sigma_{11}F^{\text{KS}}$ and $G^{\text{KS}\dagger}\Sigma_{22}F^{\text{KS}}$ in Eq. (6.2) are identical. This is shown by using the symmetry relations with respect to $\omega_n \rightarrow -\omega_n$ given in Eqs. (C.24) and (C.23):

$$\begin{aligned}\frac{1}{\beta} \sum_n G\Sigma_{11}F &\stackrel{n \rightarrow -n}{=} \frac{1}{\beta^2} \sum_{nm} \sum_{k'} G(k - \omega_n) M_{kk'}(\omega_n - \omega_m) G(k' - \omega_m) F(k - \omega_n) \\ &= \frac{1}{\beta^2} \sum_{nm} \sum_{k'} G^\dagger(k\omega_n) M_{kk'}(\omega_n - \omega_m) G^\dagger(k'\omega_m) F(k\omega_n) = -\frac{1}{\beta} \sum_n G^\dagger\Sigma_{22}F.\end{aligned}\quad (\text{E.10})$$

This reduces the work by 50% and only the $\sum_n G^{\text{KS}}\Sigma_{11}F^{\text{KS}}$ term is evaluated in Sec. E.2.5. But first the term containing the 12 elements of the self-energy *i.e.* $G^{\text{KS}}\Sigma_{12}G^{\text{KS}\dagger}$ is evaluated.

E.2.4. The $G^{\text{KS}}\Sigma_{12}G^{\text{KS}\dagger}$ Term

The Matsubara sums are evaluated first for the contribution with respect to the off diagonal element of the self-energy in Eq. (6.2). The expression for the self-energy is given in Eq. (E.7):

$$\begin{aligned} \underbrace{\frac{1}{\beta} \sum_n G^{\text{KS}}\Sigma_{12}G^{\text{KS}\dagger}}_{:=G\Sigma_{12}G^\dagger} &= \frac{1}{\beta} \sum_n G^{\text{KS}}(k\omega_n)\Sigma_{12}(k\omega_n)G^{\text{KS}\dagger}(k\omega_n) \\ &= \frac{1}{\beta^2} \sum_{nm} \sum_{k'} G^{\text{KS}}(k\omega_n)G^{\text{KS}\dagger}(k\omega_n)M_{kk'}(\omega_n - \omega_m)F^{\text{KS}}(k'\omega_m). \end{aligned}$$

As a first step the Green's functions are inserted and the simplified form for $G^{\text{KS}}G^{\text{KS}\dagger}$ [Eq. (E.2)] is used directly:

$$G\Sigma_{12}G^\dagger = \frac{1}{\beta^2} \sum_{nm} \sum_{k'} \frac{1}{(i\omega_n - E_k)(i\omega_n + E_k)} M_{kk'}(\omega_n - \omega_m) \left(\frac{1}{i\omega_m + E_{k'}} - \frac{1}{i\omega_m - E_{k'}} \right) v_{k'}^* u_{k'}.$$

The anomalous Green's function F^{KS} is written in terms of the gap [Eq. (C.22)]:

$$\begin{aligned} G\Sigma_{12}G^\dagger &= \frac{1}{\beta^2} \sum_{nm} \sum_{k'} \frac{1}{2E_k} \left(\frac{1}{i\omega_n - E_k} - \frac{1}{i\omega_n + E_k} \right) M_{kk'}(\omega_n - \omega_m) \times \\ &\quad \left(\frac{1}{i\omega_m + E_{k'}} - \frac{1}{i\omega_m - E_{k'}} \right) \frac{\Delta_{k'}^*}{2E_{k'}}. \end{aligned}$$

From Eq. (E.8) it is seen that the interaction $M(kk'\omega_n)$ is invariant with respect to $\{\omega_m, \omega_n\} \rightarrow -\{\omega_m, \omega_n\}$. This symmetry is used to merge the different contributions:

$$\begin{aligned} G\Sigma_{12}G^\dagger &= -\frac{1}{\beta^2} \sum_{k'} \Delta_0^\infty d\omega \frac{\Im [M_{kk'}(\omega)] \Delta_{k'}^*}{2\pi E_{k'} E_k} \times \\ &\quad \sum_{nm} \frac{1}{i\omega_n + E_k} \frac{2\omega}{\omega^2 + (\omega_n - \omega_m)^2} \left(\frac{1}{i\omega_m + E_{k'}} - \frac{1}{i\omega_m - E_{k'}} \right). \end{aligned}$$

The expression has been changed to a form, such that the function I given in Eq. (E.4) is found and inserted in the equation:

$$G\Sigma_{12}G^\dagger = \frac{1}{\pi} \sum_{k'} \Delta_0^\infty d\omega \frac{\Im [M_{kk'}(\omega)] \Delta_{k'}^*}{2E_{k'} E_k} [I_\beta(E_k E_{k'} \omega) - I_\beta(E_k - E_{k'} \omega)].$$

As a last step, the explicit contribution to the interaction $M_{kk'}(\omega)$ for the off diagonal element of the self-energy [Eq. (5.43)] is inserted:

$$\frac{1}{\beta} \sum_n G^{\text{KS}}\Sigma_{12}G^{\text{KS}\dagger} = \frac{1}{\pi} \sum_{k'} \Delta_0^\infty d\omega \frac{\Im [-w_{kk'}^F(\omega) - a_C \Lambda_{kk'}^{\text{SF}}(\omega)] \Delta_{k'}^*}{2E_{k'} E_k} [I_\beta(E_k E_{k'} \omega) - I_\beta(E_k - E_{k'} \omega)]. \quad (\text{E.11})$$

At this point it was assumed that the XC-kernel also fulfills Eq. (E.8). The expression contains the spin interaction $\Lambda_{kk'}^{\text{SF}}(\omega)$ and the screened Coulomb interaction w . For the Coulomb contribution and XC-kernel [Eq. (5.47)] the frequency dependence is neglected and a static approximation *i.e.* $w_{kk'}^F(\omega_n) \approx w_{kk'}^F$ is used in the final calculations. This approximation simplifies the equation significantly:

$$\begin{aligned} &\frac{1}{\beta} \sum_n G^{\text{KS}}\Sigma_{12}^{\text{C}}G^{\text{KS}\dagger} \\ &= \frac{1}{\beta^2} \sum_{nm} \sum_{k'} G^{\text{KS}}(k\omega_n) w_{kk'}^F F^{\text{KS}}(k'\omega_m) G^{\text{KS}\dagger}(k\omega_n) = \frac{1}{\beta^2} \sum_{nk'} G^{\text{KS}}(k\omega_n) G^{\text{KS}\dagger}(k\omega_n) w_{kk'}^F \sum_{k'm} F^{\text{KS}}(k'\omega_m) \\ &= \sum_{k'} \frac{\tanh\left[\frac{\beta E_k}{2}\right]}{2E_k} w_{kk'}^F \frac{\Delta_{k'}^*}{E_{k'}} [f_\beta(E_{k'}) - f_\beta(-E_{k'})] = -\sum_{k'} \frac{\tanh\left[\frac{\beta E_k}{2}\right] \tanh\left[\frac{\beta E_{k'}}{2}\right]}{4E_k E_{k'}} w_{kk'}^F \Delta_{k'}^*. \end{aligned}$$

A simple approximation for the static screened interaction is the [Thomas Fermi](#) screening:

$$v^{\text{Bare}}(\mathbf{r}_1\mathbf{r}_2) = \frac{1}{|\mathbf{r}_1 - \mathbf{r}_2|} \xrightarrow{\text{Screening}} \frac{e^{-\alpha|\mathbf{r}_{12}|}}{|\mathbf{r}_1 - \mathbf{r}_2|},$$

where α is a parameter describing the screening length. The translation invariance of the interaction leads to a diagonal form with respect to \mathbf{G} [Eq. (A.3)]:

$$v(\mathbf{q}\mathbf{G}\mathbf{G}') = v(\mathbf{q} + \mathbf{G}) \delta_{\mathbf{G}\mathbf{G}'} \quad v(\mathbf{q} + \mathbf{G}) = \frac{4\pi}{\alpha^2 + |\mathbf{q} + \mathbf{G}|^2}. \quad (\text{E.12})$$

An intermediate step between the phenomenological Thomas Fermi screening with a parameter α and the full screened Coulomb interaction [Eq. (4.17)] is to use the statically screened Coulomb interaction in the [random phase approximation \(RPA\)](#):

$$w^{\text{RPA}}(\mathbf{q}\mathbf{G}_1\mathbf{G}_2) = v(\mathbf{q}\mathbf{G}_1\mathbf{G}_2) - \sum_{\mathbf{G}\mathbf{G}'} \sum_{\sigma\sigma'} v(\mathbf{q}\mathbf{G}_1\mathbf{G}) \chi_{\sigma\sigma'\sigma'}^{\text{KS}}(\mathbf{q}\mathbf{G}\mathbf{G}'\omega = 0) w^{\text{RPA}}(\mathbf{q}\mathbf{G}'\mathbf{G}_2).$$

It is convenient to write the equation for w^{RPA} in terms of the [dielectric constant](#):

$$w^{\text{RPA}}(\mathbf{q}\mathbf{G}_1\mathbf{G}_2) = [\delta_{\mathbf{G}_1\mathbf{G}_2} + v(\mathbf{q} + \mathbf{G}_1) \chi_{00}^{\text{KS}}(\mathbf{q}\mathbf{G}_1\mathbf{G}_2)]^{-1} v(\mathbf{q} + \mathbf{G}_2) = \epsilon^{-1}(\mathbf{q}\mathbf{G}_1\mathbf{G}_2) v(\mathbf{q} + \mathbf{G}_2). \quad (\text{E.13})$$

E.2.5. The $G^{\text{KS}}\Sigma_{11}F^{\text{KS}}$ Term

Last but not least, the term containing the diagonal part of the self-energy in the [SSEq](#) is evaluated [Eq. (6.2)]. Using again some generic interaction M to keep the expression shorter, the term reads:

$$\underbrace{\frac{1}{\beta} \sum_n G^{\text{KS}}\Sigma_{11}F^{\text{KS}}}_{:=G\Sigma_{11}F} = \frac{1}{\beta^2} \sum_{nm} \sum_{k'} F^{\text{KS}}(k\omega_n) G^{\text{KS}}(k\omega_n) M_{kk'}(\omega_n - \omega_m) G^{\text{KS}}(k'\omega_m). \quad (\text{E.14})$$

Before the Matsubara summation is evaluated, some simple algebra is done for the part $F^{\text{KS}}(k\omega_n) G^{\text{KS}}(k\omega_n)$:

$$\begin{aligned} F^{\text{KS}}(k\omega_n) G^{\text{KS}}(k\omega_n) &= v_k^* u_k \left(\frac{1}{i\omega_n + E_k} - \frac{1}{i\omega_n - E_k} \right) \left(\frac{1}{2} \frac{1 + \frac{\zeta_k}{E_k}}{i\omega_n - E_k} + \frac{1}{2} \frac{1 - \frac{\zeta_k}{E_k}}{i\omega_n + E_k} \right) \\ &= -\frac{\Delta_k^*}{2E_k} \frac{2E_k(i\omega_n + \zeta_k)}{(\omega_n^2 + E_k^2)^2}. \end{aligned}$$

The second order pole is rewritten by a derivative with respect to E_k :

$$F^{\text{KS}}(k\omega_n) G^{\text{KS}}(k\omega_n) = \frac{\Delta_k^*}{2E_k} (i\omega_n + \zeta_k) \frac{d}{dE_k} \frac{1}{\omega_n^2 + E_k^2} = \frac{\Delta_k^*}{2E_k} \left(\frac{d}{dE_k} \frac{i\omega_n}{\omega_n^2 + E_k^2} + \zeta_k \frac{d}{dE_k} \frac{1}{\omega_n^2 + E_k^2} \right).$$

The simplified expression for $F^{\text{KS}}(k\omega_n) G^{\text{KS}}(k\omega_n)$ containing a first order pole and the derivative is inserted in Eq. (E.14):

$$\begin{aligned} G\Sigma_{11}F &= \frac{1}{\beta^2} \sum_{nm} \sum_{k'} \frac{\Delta_k^*}{2E_k} \left[\zeta_k \frac{d}{dE_k} \frac{1}{\omega_n^2 + E_k^2} + \frac{d}{dE_k} \frac{i\omega_n}{\omega_n^2 + E_k^2} \right] M_{kk'}(\omega_n - \omega_m) G(k'\omega_m) \\ &= \frac{1}{\beta^2} \sum_{nm} \sum_{k'} \frac{\Delta_k^*}{2E_k} \zeta_k \frac{d}{dE_k} \left(\frac{1}{2E_k} \left[\frac{1}{i\omega_n + E_k} - \frac{1}{i\omega_n - E_k} \right] \right) M_{kk'}(\omega_n - \omega_m) G(k'\omega_m) \\ &\quad - \frac{1}{\beta^2} \sum_{nm} \sum_{k'} \frac{\Delta_k^*}{2E_k} \frac{d}{dE_k} \left(\frac{1}{2} \left[\frac{1}{i\omega_n + E_k} + \frac{1}{i\omega_n - E_k} \right] \right) M_{kk'}(\omega_n - \omega_m) G(k'\omega_m). \end{aligned}$$

The invariance of the interaction $M(kk'\omega_n - \omega_m)$ with respect to $\{\omega_m, \omega_n\} \rightarrow -\{\omega_m, \omega_n\}$ is used again to merge the to parts $\frac{1}{i\omega_n + E_k} - \frac{1}{i\omega_n - E_k}$:

$$G\Sigma_{11}F = \frac{1}{\beta^2} \sum_{nm} \sum_{k'} \frac{\Delta_k^* \zeta_k}{4E_k} \frac{d}{dE_k} \left(\frac{1}{E_k} \frac{1}{i\omega_n + E_k} \right) M_{kk'}(\omega_n - \omega_m) [G(k'\omega_m) + G(k' - \omega_m)] \\ - \frac{1}{\beta^2} \sum_{nm} \sum_{k'} \frac{\Delta_k^*}{4E_k} \frac{d}{dE_k} \left(\frac{1}{i\omega_n + E_k} \right) M_{kk'}(\omega_n - \omega_m) [G(k'\omega_m) - G(k' - \omega_m)].$$

The $G^{\text{KS}}(k' - \omega_m)$ are rewritten using Eq. (C.24):

$$G\Sigma_{11}F = \frac{1}{\beta^2} \sum_{nm} \sum_{k'} \frac{\Delta_k^* \zeta_k}{4E_k} \frac{d}{dE_k} \left(\frac{1}{E_k} \frac{1}{i\omega_n + E_k} \right) M_{kk'}(\omega_n - \omega_m) [G^{\text{KS}}(k'\omega_m) - G^{\text{KS}\dagger}(k'\omega_m)] \\ - \frac{1}{\beta^2} \sum_{nm} \sum_{k'} \frac{\Delta_k^*}{4E_k} \frac{d}{dE_k} \left(\frac{1}{i\omega_n + E_k} \right) M_{kk'}(\omega_n - \omega_m) [G^{\text{KS}}(k'\omega_m) + G^{\text{KS}\dagger}(k'\omega_m)].$$

The sum of the two Green's functions is evaluated:

$$2(G^{\text{KS}} + G^{\text{KS}\dagger}) = \frac{1 + \frac{\zeta_{k'}}{E_{k'}}}{i\omega_m - E_{k'}} + \frac{1 - \frac{\zeta_{k'}}{E_{k'}}}{i\omega_m + E_{k'}} + \frac{1 + \frac{\zeta_{k'}}{E_{k'}}}{-i\omega_m - E_{k'}} + \frac{1 - \frac{\zeta_{k'}}{E_{k'}}}{-i\omega_m + E_{k'}} = \frac{-2\frac{\zeta_{k'}}{E_{k'}}}{i\omega_m + E_{k'}} + \frac{2\frac{\zeta_{k'}}{E_{k'}}}{i\omega_m - E_{k'}} \\ 2(G^{\text{KS}} - G^{\text{KS}\dagger}) = \frac{1 + \frac{\zeta_{k'}}{E_{k'}}}{i\omega_m - E_{k'}} + \frac{1 - \frac{\zeta_{k'}}{E_{k'}}}{i\omega_m + E_{k'}} - \frac{1 + \frac{\zeta_{k'}}{E_{k'}}}{-i\omega_m - E_{k'}} - \frac{1 - \frac{\zeta_{k'}}{E_{k'}}}{-i\omega_m + E_{k'}} = \frac{2}{i\omega_m + E_{k'}} + \frac{2}{i\omega_m - E_{k'}}.$$

The expression is further simplified and the interaction in terms of the retarded quantity given in Eq. (E.8) is inserted:

$$G\Sigma_{11}F = \frac{1}{\beta^2} \sum_{nm} \sum_{k'} \frac{\Delta_k^* \zeta_k}{4E_k} \frac{d}{dE_k} \left(\frac{1}{E_k} \frac{1}{i\omega_n + E_k} \right) \Delta_0^\infty d\omega \frac{2}{\pi} \frac{\omega \Im [M_{kk'}(\omega)]}{\omega^2 + (\omega_n - \omega_m)^2} \left[\frac{-1}{i\omega_m + E_{k'}} + \frac{1}{i\omega_m - E_{k'}} \right] \\ - \frac{1}{\beta^2} \sum_{nm} \sum_{k'} \frac{\Delta_k^* \zeta_{k'}}{4E_k E_{k'}} \frac{d}{dE_k} \left(\frac{1}{i\omega_n + E_k} \right) \Delta_0^\infty d\omega \frac{2}{\pi} \frac{\omega \Im [M_{kk'}(\omega)]}{\omega^2 + (\omega_n - \omega_m)^2} \left[\frac{1}{i\omega_m + E_{k'}} + \frac{1}{i\omega_m - E_{k'}} \right].$$

The function I [Eq. (E.4)] is used to express the Matsubara summations:

$$G\Sigma_{11}F = \sum_{k'} \frac{\Delta_k^* \zeta_k}{4\pi E_k} \Delta_0^\infty d\omega \Im [M_{kk'}(\omega)] \frac{d}{dE_k} \left(\frac{1}{E_k} I(E_k E_{k'} \omega) - \frac{1}{E_k} I(E_k - E_{k'} \omega) \right) \\ + \sum_{k'} \frac{\Delta_k^* \zeta_{k'}}{4\pi E_k E_{k'}} \Delta_0^\infty d\omega \Im [M_{kk'}(\omega)] \frac{d}{dE_k} (I(E_k E_{k'} \omega) + I(E_k - E_{k'} \omega)).$$

The derivatives are evaluated and M is replaced with the interaction on the diagonal part of the self-energy [Eq. (5.43)]:

$$\frac{1}{\beta} \sum_n G^{\text{KS}} \Sigma_{11} F^{\text{KS}} = \frac{\Delta_k^*}{4\pi E_k} \sum_{k'} \Delta_0^\infty d\omega \Im [a_{\mathcal{D}} \Lambda_{kk'}^{\text{SF}}(\omega)] \times \\ \left(\left[\frac{\zeta_k}{E_k} + \frac{\zeta_{k'}}{E_{k'}} \right] I'(E_k E_{k'} \omega) + \left[\frac{\zeta_k}{E_k} - \frac{\zeta_{k'}}{E_{k'}} \right] I'(E_k - E_{k'} \omega) - \zeta_k \frac{I(E_k E_{k'} \omega) - I(E_k - E_{k'} \omega)}{E_k^2} \right). \quad (\text{E.15})$$

E.3. Approximations to the Gap Equation

E.3.1. The Fully Linearized Gap Equation and Isotropic Approximation

The gap equation given in Eq. (6.6) is a non-linear eigenvalue problem due to the factor $\tanh\left(\frac{\beta E_{k'}}{2}\right)$. This non-linearity fixes the value of the gap and it is possible to obtain the gap as a function of

temperature *i.e.* $\Delta_k = \Delta_k(T)$. However, a self-consistent treatment of a non-linear eigenvalue problem is computationally demanding and the interaction matrix element in the kernels are calculated in the normal phase (Sec. 5.4.1). The equation is fully linearized ($\tanh\left(\frac{\beta E_{k'}}{2}\right) = \tanh\left(\frac{\beta \zeta_{k'}}{2}\right)$):

$$\Delta_k^{\text{xc}} = \sum_{k'} \left[\mathcal{Z}_k^D \delta_{kk'} + \mathcal{K}_{kk'}^C \frac{\tanh\left(\frac{\beta \zeta_{k'}}{2}\right)}{2\zeta_{k'}} \right] \Delta_{k'}^{\text{xc}}.$$

Since the gap equation has been fully linearized, the eigenvector (*i.e.* the [gap function](#)) is only determined up to a complex factor. This means the fully linearized gap equation determines T_c only and the shape of the gap close to the phase transition *i.e.* $\frac{\Delta_k(T \approx T_c)}{|\Delta_k(T \approx T_c)|}$, not its magnitude. The temperature where an eigenvalue $\lambda = 1$ appears, marks the phase transition.

Now a second approximation reducing the computational effort is made. The summation with respect to the momentum quantum number \mathbf{k} in the gap equation may be demanding. However, in many cases the gap depends only weakly on the vector \mathbf{k} , but strongly on the band index n . Such a situation has been assumed in the discussion of the gap equation in Sec. 6.2, where the gap was approximated by a positive number for all \mathbf{k} around the Γ -point and negative value for the band around the corners of the Brillouin zone (Fig. 6.2). In such a case it is possible to neglect the isotropy of the gap with respect to \mathbf{k} . Formally this is done by replacing the full \mathbf{k} dependent gap by its average with respect to \mathbf{k}

$$\Delta_k^{\text{xc}} \approx \Delta_n^{\text{xc}}(E) := \frac{1}{N_n(E)} \sum_{\mathbf{k}} \delta(\zeta_{n\mathbf{k}} - E) \Delta^{\text{xc}}(k) \quad N_n(E) = \sum_{\mathbf{k}} \delta(\zeta_{n\mathbf{k}} - E), \quad (\text{E.16})$$

where N_n is the density of states ([density of states \(DOS\)](#)) of the n -th band. Note that the $N_n(E)$ is the [DOS](#) per spin because in a non-magnetic system each eigenvalue is two-fold degenerate. Inserting this average in the linearized gap equation and multiplying from the left with the averaging operator $\sum_{\mathbf{k}} \frac{\delta(\zeta_{n\mathbf{k}} - E)}{N_n(E)}$, leads to the isotropic gap equation:

$$\Delta_n^{\text{xc}}(E) = -\mathcal{Z}_n^D(E) - \sum_n \Delta_n dE \mathcal{K}_{nn'}^C(EE') \frac{\tanh\left(\frac{\beta E'}{2}\right)}{2E'} \Delta_{n'}^{\text{xc}*}(E')$$

$$\mathcal{Z}_n^D(E) = \frac{1}{N_n(E)} \sum_{\mathbf{k}} \delta(\zeta_{n\mathbf{k}} - E) \mathcal{Z}_k^D \quad \mathcal{K}_{nn'}^C(EE') = \frac{1}{N_n(E)} \sum_{\mathbf{k}\mathbf{k}'} \delta(\zeta_{n\mathbf{k}} - E) \mathcal{K}_{kk'}^C \delta(\zeta_{n\mathbf{k}'} - E').$$

E.3.2. Alternative Gap Equation

Instead of using the [Bardeen, Cooper and Schrieffer \(BCS\)](#) like [gap equation](#) from the previous section, it is also possible to go one step back and investigate the linearized [SSEq](#) directly. This is equivalent to solving the gap equation, but the new equation is numerically easier to handle which was found by A. Linscheid and is discussed in his [Ph.D. thesis](#) [146]. The [SSEq](#) is an implicit expression for the gap [Eq. (6.2)]:

$$0 = \sum_{\omega_n} \left(G^{\text{KS}} G^{\text{KS}\dagger} \Delta_k^{\text{xc}*} + 2G^{\text{KS}}(k\omega_n) \bar{\Sigma}_{\uparrow\uparrow}^{11}(k\omega_n) F^{\text{KS}}(k\omega_n) \right) - \sum_{\omega_n} G^{\text{KS}}(k\omega_n) \bar{\Sigma}_{\uparrow\downarrow}^{12}(k\omega_n) G^{\text{KS}\dagger}(k\omega_n).$$

The three different contributions are evaluated in Eqs. (E.11), (E.15) and (E.3). The resulting equation is also fully linearized with respect to Δ_k and the symmetric part with respect to I' and the factor $\frac{1}{2}$ are used for the D -term [Eq. (6.9)]. Applying these steps lead to the following form of the [SSEq](#) :

$$0 = \sum_{k'} [\mathcal{D}_{kk'}^{GG} + \mathcal{D}_{kk'}^{11} + \mathcal{C}_{kk'}^{12}] \Delta_{k'}^{\text{xc}*} = \sum_{k'} M_{kk'}^\beta \Delta_{k'}^{\text{xc}*} \quad (\text{E.17})$$

$$\begin{aligned}
 \mathcal{D}_{kk'}^{GG} &= \delta_{kk'} \frac{\tanh\left[\frac{\beta\zeta_k}{2}\right]}{2\zeta_k} \\
 \mathcal{D}_{kk'}^{11} &= \delta_{kk'} \Delta_0^\infty d\omega \sum_{k_2} \frac{\Im\left[a_{\mathcal{D}}\Lambda_{kk_2}^{\text{SF}}(\omega)\right] - \Lambda_{kk_2}^{\text{Ph}}(\omega)}{4\pi\zeta_k} \frac{d}{d\zeta_k} J_\beta^+(\zeta_k, \zeta_{k_2}\omega) \\
 \mathcal{C}_{kk'}^{12} &= \Delta_0^\infty d\omega \frac{\Im\left[w_{kk'}^{\text{F}}(\omega) + a_{\mathcal{C}}\Lambda_{kk'}^{\text{SF}}(\omega)\right] + \Lambda_{kk'}^{\text{Ph}}(\omega)}{2\pi\zeta_{k'}\zeta_k} J_\beta^-(\zeta_k, \zeta_{k'}\omega).
 \end{aligned}$$

Instead of having an eigenvalue with the value 1 in the spectrum (linearized gap equation), the matrix $M_{kk'}^\beta$ becomes singular at the critical temperature. Like the fully linearized gap equation, also the linearized SSEq determines only the critical temperature and not the value of the gap. If the value of the gap is of interest, the non-linear eigenvalue problem has to be solved by rewriting the problem as an iterative scheme:

$$\begin{aligned}
 0 &= M^\beta[\Delta] \Delta = \left[M^\beta[\Delta] - A + A\right] \Delta \\
 \Delta^{i+1} &= A^{-1} \left(M^\beta[\Delta^i] + A\right) \Delta^i.
 \end{aligned}$$

The matrix A is referred to as **splitting matrix** and should make the fix point problem contractive [146]. In the standard gap equation the factor $\frac{\tanh\left[\frac{\beta E_k}{2}\right]}{2E_k}$ is the splitting matrix [Eq. (E.3)]. Also for this equation the full anisotropy in \mathbf{k} space is hard to handle and an isotropic approximation of Eq. (E.17) is introduced. The average value of the gap in Eq. (E.16) and the averaging operator $\sum_{\mathbf{k}} \frac{\delta(\zeta_{n\mathbf{k}} - E)}{N_n(E)}$ lead to:

$$\begin{aligned}
 0 &= \sum_{n'} \Delta dE' M_{nn'}^\beta(EE') \Delta_{n'}^{\text{xc}*}(n'E') \quad (\text{E.18}) \\
 M_{nn'}^\beta(EE') &:= \frac{1}{N_n(E)} \sum_{\mathbf{k}\mathbf{k}'} \delta(\zeta_{n\mathbf{k}} - E) \left[\mathcal{D}_{kk'}^{GG} + \mathcal{D}_{kk'}^{11} + \mathcal{C}_{kk'}^{12}\right] \delta(\zeta_{n'\mathbf{k}'} - E').
 \end{aligned}$$

The first diagonal term $\mathcal{D}_{kk'}^{GG}$ depends only on energy and the average is simple:

$$\mathcal{D}_{nn'}^{GG}(EE') = \frac{1}{N_n(E)} \sum_{\mathbf{k}} \delta(\zeta_{n\mathbf{k}} - E) \delta_{EE'} \delta_{nn'} \frac{\tanh\left[\frac{\beta E}{2}\right]}{2E} = \delta_{EE'} \delta_{nn'} \frac{\tanh\left[\frac{\beta E}{2}\right]}{2E}.$$

For the other contributions, the isotropy with respect to \mathbf{k} is located in the interaction matrix elements and an isotropic interaction is defined by:

$$\Lambda_{nn'}(EE'\omega) := \frac{1}{N_n(E)} \sum_{\mathbf{k}\mathbf{k}'} \delta(\zeta_{n\mathbf{k}} - E) \Lambda_{kk'}(\omega) \delta(\zeta_{n'\mathbf{k}'} - E'). \quad (\text{E.19})$$

Using this definition in $\mathcal{D}_{kk'}^{11}$ and $\mathcal{C}_{kk'}^{12}$ leads to isotropic variants of the \mathcal{D} and \mathcal{C} term:

$$\mathcal{D}_{nn'}^{11}(EE') = +\delta_{nn'} \delta_{EE'} \sum_{n_2} \Delta dE_2 \Delta_0^\infty d\omega \frac{\Im\left[a_{\mathcal{D}}\Lambda_{nn_2}^{\text{SF}}(EE_2\omega)\right] - \Lambda_{nn_2}^{\text{Ph}}(EE_2\omega)}{4\pi E} \frac{d}{d\zeta_k} J_\beta^+(E, E_2\omega) \quad (\text{E.20})$$

$$\mathcal{C}_{nn'}^{12}(EE') = \Delta_0^\infty d\omega \frac{\Im\left[w_{nn'}^{\text{F}}(EE'\omega) + a_{\mathcal{C}}\Lambda_{nn'}^{\text{SF}}(EE'\omega)\right] + \Lambda_{nn'}^{\text{Ph}}(EE'\omega)}{2\pi EE'} J_\beta^-(E, E'\omega). \quad (\text{E.21})$$

E.4. Details for the Implementation of the Matrix Elements

The matrix elements defined in Eq. (E.6) are calculated using the Bloch states of the non-superconducting KS system. The eigenstates are calculated with a plane wave (PW) code [131]. For the implementation it is useful to write the matrix elements in more detail. The eigenstates are expanded in terms of the plane waves:

$$\psi_{n\mathbf{k}}(\mathbf{r}) = \frac{1}{\sqrt{N}} e^{i\mathbf{k}\mathbf{T}} \psi_{n\mathbf{k}}(\bar{\mathbf{r}}) = \frac{1}{\sqrt{N\Omega_{\text{WS}}}} \sum_{\mathbf{T}} \sum_{\mathbf{G}} e^{i\mathbf{k}\mathbf{T}} c_{\mathbf{k}+\mathbf{G}}^n e^{i(\mathbf{k}+\mathbf{G})\bar{\mathbf{r}}}.$$

The matrix elements in terms of the Bloch states are given in Eq. (E.7):

$$M_{kk'}(\omega_n \nu_n) = \Lambda d^3 r_1 d^3 r_2 \psi_{n\mathbf{k}}^*(\mathbf{r}_1) \psi_{n'\mathbf{k}'}(\mathbf{r}_1) M(\mathbf{r}_1 \mathbf{r}_2 \omega_n - \nu_m) \psi_{n'\mathbf{k}'}^*(\mathbf{r}_2) \psi_{n\mathbf{k}}(\mathbf{r}_2).$$

The plane wave expansion is inserted for the wave functions:

$$M_{kk'}(\omega_n \nu_n) = \frac{1}{V^2} \sum_{\mathbf{G}_1 \dots \mathbf{G}_4} \Lambda d^3 r_1 d^3 r_2 (c_{\mathbf{k}+\mathbf{G}_1}^n)^* c_{\mathbf{k}'+\mathbf{G}_2}^{n'} (c_{\mathbf{k}'+\mathbf{G}_3}^{n'})^* c_{\mathbf{k}+\mathbf{G}_4}^n \times \\ e^{-i(\mathbf{k}-\mathbf{k}'+\mathbf{G}_1-\mathbf{G}_2)\bar{\mathbf{r}}_1} M(\mathbf{r}_1 \mathbf{r}_2 \omega_n - \nu_m) e^{i(\mathbf{k}-\mathbf{k}'+\mathbf{G}_4-\mathbf{G}_3)\bar{\mathbf{r}}_2} e^{i(\mathbf{k}'-\mathbf{k})(\mathbf{T}_1-\mathbf{T}_2)}.$$

The FT given in Eq. (A.3) requires $\mathbf{k}_1 = \mathbf{k}_2$ within the first BZ zone. Hence the difference is rewritten as $\mathbf{k} - \mathbf{k}' = \mathbf{q}_{\mathbf{k}\mathbf{k}'} + \mathbf{G}_{\mathbf{k}\mathbf{k}'}$, where $\mathbf{q}_{\mathbf{k}\mathbf{k}'}$ lies always in the BZ. With this rewriting the definition for the double transformation in Eq. (A.3) leads to:

$$M_{kk'}(\omega_n \nu_n) = \frac{1}{V} \sum_{\mathbf{G}_1 \dots \mathbf{G}_4} (c_{\mathbf{k}+\mathbf{G}_1}^n)^* c_{\mathbf{k}'+\mathbf{G}_2}^{n'} (c_{\mathbf{k}'+\mathbf{G}_3}^{n'})^* c_{\mathbf{k}+\mathbf{G}_4}^n \times \\ M(\mathbf{q}_{\mathbf{k}\mathbf{k}'}, \mathbf{G}_1 - \mathbf{G}_2 + \mathbf{G}_{\mathbf{k}\mathbf{k}'}, \mathbf{q}_{\mathbf{k}\mathbf{k}'}, \mathbf{G}_4 - \mathbf{G}_3 + \mathbf{G}_{\mathbf{k}\mathbf{k}'}, \omega_n - \nu_m).$$

With the substitutions

$$\mathbf{G} := \mathbf{G}_1 - \mathbf{G}_2 \quad \mathbf{G}' := \mathbf{G}_4 - \mathbf{G}_3$$

it is possible to separate two \mathbf{G} loops. The notation for the matrix elements is also simplified $M(\mathbf{q}, \mathbf{G}_1, \mathbf{q}, \mathbf{G}_2) = M(\mathbf{q}, \mathbf{G}_1, \mathbf{G}_2)$:

$$M_{kk'}(\omega_n \nu_n) = \frac{1}{N\Omega_{\text{WS}}} \sum_{\mathbf{G}\mathbf{G}'} \left[\sum_{\mathbf{G}_1} (c_{\mathbf{k}+\mathbf{G}_1}^n)^* c_{\mathbf{k}'+\mathbf{G}_1-\mathbf{G}}^{n'} \right] \left[\sum_{\mathbf{G}_4} c_{\mathbf{k}+\mathbf{G}_4}^n (c_{\mathbf{k}'+\mathbf{G}_4-\mathbf{G}'}^{n'})^* \right] \times \\ M(\mathbf{q}_{\mathbf{k}\mathbf{k}'}, \mathbf{G} + \mathbf{G}_{\mathbf{k}\mathbf{k}'}, \mathbf{G}' + \mathbf{G}_{\mathbf{k}\mathbf{k}'}, \omega_n - \nu_m).$$

An auxiliary function is defined:

$$b_{\mathbf{k}\mathbf{k}'}^{nn'}(\mathbf{G}) := \sum_{\mathbf{G}'} (c_{\mathbf{k}+\mathbf{G}'}^n)^* c_{\mathbf{k}'+\mathbf{G}'-\mathbf{G}}^{n'}. \quad (\text{E.22})$$

Inserting the auxiliary function, the expression for the matrix elements in Bloch representation becomes:

$$M_{kk'}(\omega_n \nu_n) = \frac{1}{N\Omega_{\text{WS}}} \sum_{\mathbf{G}\mathbf{G}'} b_{\mathbf{k}\mathbf{k}'}^{nn'}(\mathbf{G}) (b_{\mathbf{k}\mathbf{k}'}^{nn'}(\mathbf{G}'))^* M(\mathbf{q}_{\mathbf{k}\mathbf{k}'}, \mathbf{G} + \mathbf{G}_{\mathbf{k}\mathbf{k}'}, \mathbf{G}' + \mathbf{G}_{\mathbf{k}\mathbf{k}'}, \omega_n - \nu_m). \quad (\text{E.23})$$

For the different parts of the interaction, different cutoffs in the PW expansion are needed:

- The wave function $\psi_{n\mathbf{k}}(\mathbf{r})$ needs a very high cutoff and a value around ~ 100 Ryd is used in the ground state calculation.

- The product of the two plane wave coefficients converges faster and a value of ~ 40 Ryd is used for the summation in $b_{\mathbf{k}\mathbf{k}'}^{nn'}$ [Eq. (E.22)].
- The spin fluctuation interaction decays very fast with respect to \mathbf{G} and small values of ~ 10 Ryd are sufficient. In Fig. E.3 it is shown that only the first two or three plane wave coefficients give a relevant contribution. Also for the Coulomb contribution only the first coefficients are important due to the monotone decay in momentum space $\frac{1}{|\mathbf{q}+\mathbf{G}|^2}$.

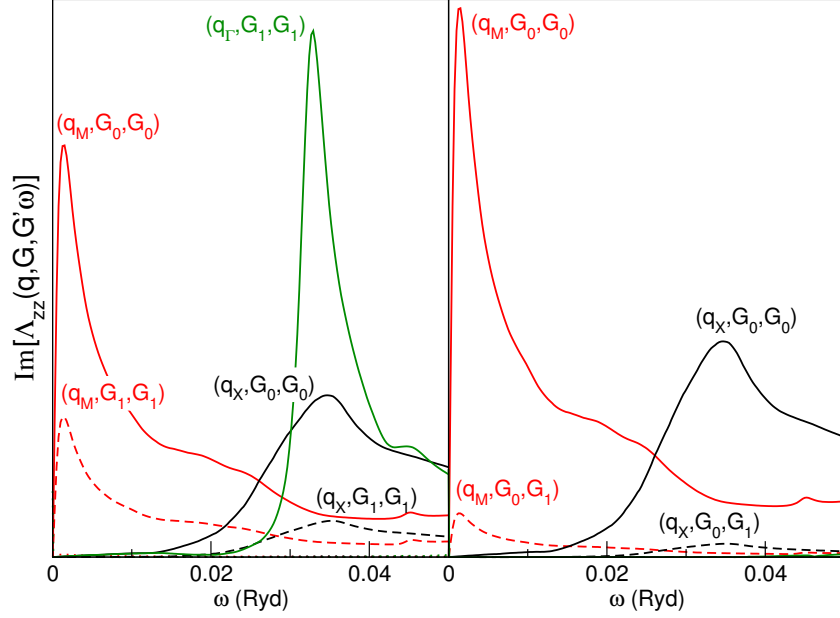


Figure E.3.: Anti-Hermitian part of the spin fluctuation interaction Λ_{zz} [Eq. (5.41)] for FeSe in PW representation. The vectors $\mathbf{q}_M, \mathbf{q}_X$ and \mathbf{q}_Γ are the usual high symmetry points given in chapter 7 and the plane wave in units of $\frac{2\pi}{a}$ is: $\mathbf{G}_0 = (0, 0, 0)$ and $\mathbf{G}_1 = (1, 0, 0)$ and $\mathbf{G}_2 = (2, 0, 0)$.

Index

A

accidental nodes	C-6
adiabatic	57, B-8
adiabatic local density approximation (ALDA) \rightarrow <i>LDA</i>	ix, B-8
analytic continuation	79, B-4 , E-1
anomalous density	17, 21, 25, 30, C-1
atomic sphere approximation (ASA)	ix

B

Bardeen, Cooper and Schrieffer (BCS)	ix, 57
Bloch states	20, 56, C-9 , E-9
Bogoliubov-de Gennes (BdG)	ix, 19
Brillouin zone (BZ)	ix, 70

C

codes	
ELK [125]	70
HUTSEPOT [56]	79
QuantumEspresso [131]	71, 76
coherent potential approximation (CPA)	ix
conventional SC	1, 60, 66
Coulomb renormalization	66, 85
coupling constant	6, B-5
critical temperature (T_c)	ix, 84
crossed contribution	35, 43, 52
<i>C</i> -term	57, 65

D

decoupling approximation	21, 56, C-3
density functional theory (DFT)	ix, 18
density of states (DOS)	ix, 78
diagram rules	14, 29
dielectric constant	27, E-6
Dirac picture	8, 10, D-3
direct contribution	35, 42, 43, 52
disordered local moments (DLM)	ix
double counting (DC)	ix
dressed \rightarrow <i>renormalized</i>	15
<i>D</i> -term	57, 59, 67, 85
dynamical mean field (DMF)	ix
Dyson equation	15, 28, 29, B-7

E

effective coupling	62
--------------------------	----

- effective interaction \rightarrow *interactions* 42
 Eliashberg function 62
 Eliashberg theory 34, 57, 63, 87
 equation of motion 25, B-6, D-1, D-5
 experimental techniques
 angle resolved photon emission spectroscopy (**ARPES**) ix
 nuclear magnetic resonance (**NMR**) ix
 superconducting quantum interference device (**SQUID**) ix
- F**
- Fermi surface 51, 60, 70, 76, C-4
 Fermionic loop 14, 29, D-4
 Feynman diagrams 14
 fluctuation dissipation theorem B-5
 Fourier transformation (**FT**) ix, A-1
 functional derivative 23, 26, 28, 35, D-3
 functionals
 generalized gradient approximation (**GGA**) ix
 local density approximation (**LDA**) ix
- G**
- gap equation 57, 58, 60, 76, 84, E-8
 gap function \rightarrow *pairing potential* 21, 55, 79, C-4, C-6, E-8
 grand canonical potential 6, 12, 18, B-5
 Green's function (**GF**) ix, 5
 Green's functions
 advanced **GF** 5, 10
 anomalous Green's function 25, D-4
 Matsubara **GF** 5, 7, B-4-B-6
 Nambu **GF** 25, 31, D-1
 retarded **GF** \rightarrow *response function* 5, 9, B-5
 group theory A-2, C-4
Gw approximation 30, 39, 87
- H**
- Hedin equations 25, 27, 33, 52
 homogenous electron gas (**HEG**) ix, B-8
- I**
- interactions
 effective interaction 34, 42, 45, 46, 49, 50
 screened Coulomb interaction 15, 27, 29, 42, 55
 iron based superconductors (**FeSC**) ix, 69
 irreducible particle-hole propagator 28, 29, 34, 50, 52
- K**
- XC**-kernel 52, B-7
 Kohn-Sham (**KS**) ix, 18
 Kohn-Sham Bogoliubov-de Gennes (**KS-BdG**) ix, 19
 Korringa-Kohn-Rostoker (**KKR**) ix, 79
- II**

L

linear response (LR)	ix, 9
linear response density functional theory (LRDFT)	ix, B-7
linked cluster theorem	11
local field factor \rightarrow <i>xc-kernel</i>	52
London equations	48

M

magnetic structures	
anti ferro magnetic (AFM)	ix, 72
checkerboard (CB)	ix, 72
collinear	46, B-3
ferro magnetic (FM)	ix, 33
non-magnetic (NM)	ix
paramagnetic (PM)	ix
stripe	71 , 81
many body perturbation theory (MBPT) \rightarrow <i>perturbation expansion</i>	ix, 11
mass operator	16
Matsubara frequencies	B-2 , E-1, E-3
Meissner-Ochsenfeld effect	48
model calculation	63 , 69, 79, 82, 87
Mott physics	1 , 69

O

operator pictures	
contraction	12 , D-4
Heisenberg picture	7 , 9, D-3
Schrödinger picture	7
optimized effective potential (OEP)	ix
order parameter	17

P

pairing symmetries	
<i>d</i> -wave	C-6
<i>s</i> _± -wave	61, 85, C-6
<i>s</i> -wave	61, 63, C-6
particle-hole propagator	37
particle-particle propagator	50
Pauli matrix	9, A-3 , C-1
perturbation expansion \rightarrow MBPT	10
phase transition	9, 62, 73
philosophiae doctor (Ph.D.)	ix
plane wave (PW)	ix, E-10
polarization propagator	15, 29 , 37
potentials	
Hartree potential	27 , 42, 48, D-2, D-5, D-6
pairing potential \rightarrow <i>function</i>	17, 21, 52, 62, C-1
XC -potential	19 , 55, 71, C-10, D-6
proper	14 , 42, B-7

Q

- quasi particle (**QP**) ix, **9**, 76
- QP excitations
- magnon **9**, 46
 - paramagnons \rightarrow *spin-fluctuations* **2**, 23, 55, 59, 79
 - phonons (**Ph**) ix, **9**, 23, 25, 48, 55, 59, 78
 - plasmons **9**, 59, 79
- R**
- random phase approximation (**RPA**) ix, **15**, 40
- reducible **14**
- reference system 27, 42, **D-5**
- renormalization \rightarrow *dressed* 15
- residue theorem 57, **E-1**
- response function \rightarrow *susceptibility* 5, 7, **9**, 43, 44, 50, 59, B-7
- S**
- screened Coulomb interaction \rightarrow *interactions* 15
- second order phase transition 74
- self-energy 15, 26, **27**, 47, 52, D-5
- Sham-Schlüter equation (**SSEq**) ix, 31
- singlet pairing 17, 19, 20, 25, **C-1**
- spectral function 74, 81, 83, B-3, **B-5**
- spin-fluctuations (**SF**) \rightarrow *paramagnons* ix, **23**, 59, 83
- splitting matrix E-9
- structural family 69
- superconducting density functional theory (**SCDFT**) ix, 18
- superconductivity, superconducting, superconductor *etc.* (**SC**) ix, 17
- susceptibility \rightarrow *response function* 9
- T**
- Thomas Fermi 62, **E-6**
- time evolution operator 10
- time ordering operator 7, **B-6**
- T*-matrix **33**, 48, 87
- U**
- unconventional **SC** 2, **60**, 66, 88
- V**
- vertex function 15, **27**, **28**, 37, 87
- W**
- weak coupling **64**, 82
- Wick's Theorem 11
- X**
- exchange-correlation (**XC**) ix, 18

Bibliography

- [1] P. F. Dahl, “Kamerlingh Onnes and the discovery of superconductivity: The Leyden years, 1911-1914,” *JSTOR: Historical Studies in the Physical Sciences*, vol. 15, no. 1, pp. 1–37, 1984. [Online]. Available: <http://www.jstor.org/stable/27757541>
- [2] J. Bardeen, L. N. Cooper, and J. R. Schrieffer, “Theory of superconductivity,” *Phys. Rev.*, vol. 108, pp. 1175–1204, Dec 1957. [Online]. Available: <http://link.aps.org/doi/10.1103/PhysRev.108.1175>
- [3] J. Bednorz and K. Müller, “Possible high T_c superconductivity in the Ba-La-Cu-O system,” *Zeitschrift für Physik B Condensed Matter*, vol. 64, pp. 189–193, 1986. [Online]. Available: <http://link.springer.com/article/10.1007%2FBF01303701>
- [4] A. Schilling, M. Cantoni, J. Guo, and H. Ott, “Superconductivity above 130 K in the Hg-Ba-Ca-Cu-O system,” *Nature*, vol. 363, pp. 56–58, 1993. [Online]. Available: <http://www.nature.com/nature/journal/v363/n6424/abs/363056a0.html>
- [5] L. Testardi, J. Wernick, and W. Royer, “Superconductivity with onset above 23 K in Nb_3Ge sputtered films,” *Elsevier*, vol. 15, pp. 1–4. [Online]. Available: [http://dx.doi.org/10.1016/0038-1098\(74\)90002-7](http://dx.doi.org/10.1016/0038-1098(74)90002-7)
- [6] G. Eliashberg, “Interactions between electrons and lattice vibrations in a superconductor,” *J. Exptl. Theoret. Phys (U.S.S.R.)*, vol. 11, pp. 696–702, 1960. [Online]. Available: <http://www.w2agz.com/Library/Classic%20Papers%20in%20Superconductivity/Eliashberg,%20e-p%20Interactions%20in%20SCs,%20Sov-Phys%20JETP%2011,%20696%20%281960%29.pdf>
- [7] S. Y. Savrasov and O. K. Andersen, “Linear-response calculation of the electron-phonon coupling in doped $CaCuO_2$,” *Phys. Rev. Lett.*, vol. 77, pp. 4430–4433, Nov 1996. [Online]. Available: <http://link.aps.org/doi/10.1103/PhysRevLett.77.4430>
- [8] Y. Kamihara, T. Watanabe, M. Hirano, and H. Hosono, “Iron-based layered superconductor $La[O_{1-x}F_x]FeAs$ ($x = 0.05-0.12$) with $T_c = 26$ K,” *Journal of the American Chemical Society*, vol. 130, pp. 3296–3297, 2008. [Online]. Available: <http://pubs.acs.org/doi/abs/10.1021/ja800073m>
- [9] S. Medvedev, T. McQueen, I. Troyan, T. Palasyuk, M. Eremets, R. Cava, S. Naghavi, F. Casper, V. Ksenofontov, G. Wortmann, and C. Felser, “Electronic and magnetic phase diagram of $\beta - Fe_{1.01}Se$ with superconductivity at 36.7 K under pressure,” *Nature Materials*, vol. 8, p. 630, 2009. [Online]. Available: <http://www.nature.com/nmat/journal/v8/n8/full/nmat2491.html>
- [10] E. Maxwell, “Isotope effect in the superconductivity of mercury,” *Phys. Rev.*, vol. 78, pp. 477–477, May 1950. [Online]. Available: <http://link.aps.org/doi/10.1103/PhysRev.78.477>
- [11] P. A. Lee, N. Nagaosa, and X.-G. Wen, “Doping a mott insulator: Physics of high-temperature superconductivity,” *Rev. Mod. Phys.*, vol. 78, pp. 17–85, Jan 2006. [Online]. Available: <http://link.aps.org/doi/10.1103/RevModPhys.78.17>
- [12] I. Mazin, “Superconductivity gets an iron boost,” *Nature*, vol. 464, pp. 183–186, Mar 2010. [Online]. Available: <http://www.nature.com/nature/journal/v464/n7286/full/nature08914.html>
- [13] P. J. Hirschfeld, M. M. Korshunov, and I. I. Mazin, “Gap symmetry and structure of fe-based superconductors,” *Reports on Progress in Physics*, vol. 74, no. 12, p. 124508, 2011. [Online]. Available: <http://stacks.iop.org/0034-4885/74/i=12/a=124508>

- [14] M. Vojta, “Magnetic fluctuations revealed,” *Nature Physics*, vol. 7, pp. 674–675, 2011. [Online]. Available: <http://www.nature.com/nphys/journal/v7/n9/full/nphys2077.html>
- [15] M. Le Tacon and B. e. Keimer, “Intense paramagnon excitations in large family of high-temperature superconductors,” *Nature Physics*, vol. 7, pp. 725–730, 2011. [Online]. Available: <http://www.nature.com/nphys/journal/v7/n9/full/nphys2041.html>
- [16] D. Manske, *Theory of Unconventional Superconductors, Cooper-Pairing Mediated by Spin Excitations*. Springer-Verlag Berlin Heidelberg, 2004.
- [17] A. S. Mishchenko and N. Nagaosa, “Electron-phonon coupling and a polaron in the t - j model: From the weak to the strong coupling regime,” *Phys. Rev. Lett.*, vol. 93, p. 036402, Jul 2004. [Online]. Available: <http://link.aps.org/doi/10.1103/PhysRevLett.93.036402>
- [18] T. Saito, S. Onari, and H. Kontani, “Orbital fluctuation theory in iron pnictides: Effects of as-fe-as bond angle, isotope substitution, and Z^2 -orbital pocket on superconductivity,” *Phys. Rev. B*, vol. 82, p. 144510, Oct 2010. [Online]. Available: <http://link.aps.org/doi/10.1103/PhysRevB.82.144510>
- [19] N. F. Berk and J. R. Schrieffer, “Effect of ferromagnetic spin correlations on superconductivity,” *Phys. Rev. Lett.*, vol. 17, pp. 433–435, Aug 1966. [Online]. Available: <http://link.aps.org/doi/10.1103/PhysRevLett.17.433>
- [20] S. Doniach and S. Engelsberg, “Low-temperature properties of nearly ferromagnetic fermi liquids,” *Phys. Rev. Lett.*, vol. 17, pp. 750–753, Oct 1966. [Online]. Available: <http://link.aps.org/doi/10.1103/PhysRevLett.17.750>
- [21] T. Imai, K. Ahilan, F. L. Ning, T. M. McQueen, and R. J. Cava, “Why does undoped FeSe become a high- T_c superconductor under pressure?” *Phys. Rev. Lett.*, vol. 102, p. 177005, Apr 2009. [Online]. Available: <http://link.aps.org/doi/10.1103/PhysRevLett.102.177005>
- [22] H. Fröhlich, “Theory of the superconducting state. i. the ground state at the absolute zero of temperature,” *Phys. Rev.*, vol. 79, pp. 845–856, Sep 1950. [Online]. Available: <http://link.aps.org/doi/10.1103/PhysRev.79.845>
- [23] L. N. Oliveira, E. K. U. Gross, and W. Kohn, “Density-functional theory for superconductors,” *Phys. Rev. Lett.*, vol. 60, pp. 2430–2433, Jun 1988. [Online]. Available: <http://link.aps.org/doi/10.1103/PhysRevLett.60.2430>
- [24] Y. Nambu, “Quasi-particles and gauge invariance in the theory of superconductivity,” *Phys. Rev.*, vol. 117, pp. 648–663, Feb 1960. [Online]. Available: <http://link.aps.org/doi/10.1103/PhysRev.117.648>
- [25] L. Hedin, “New method for calculating the one-particle green’s function with application to the electron-gas problem,” *Phys. Rev.*, vol. 139, pp. A796–A823, Aug 1965. [Online]. Available: <http://link.aps.org/doi/10.1103/PhysRev.139.A796>
- [26] L. J. Sham and M. Schlüter, “Density-functional theory of the energy gap,” *Phys. Rev. Lett.*, vol. 51, pp. 1888–1891, Nov 1983. [Online]. Available: <http://link.aps.org/doi/10.1103/PhysRevLett.51.1888>
- [27] M. Lüders, M. A. L. Marques, N. N. Lathiotakis, A. Floris, G. Profeta, L. Fast, A. Continenza, S. Massidda, and E. K. U. Gross, “*Ab initio* theory of superconductivity. i. density functional formalism and approximate functionals,” *Phys. Rev. B*, vol. 72, p. 024545, Jul 2005. [Online]. Available: <http://link.aps.org/doi/10.1103/PhysRevB.72.024545>
- [28] J. Rehr, “Lars hedin and the quest for a theory of excited states,” *Physica Scripta*, vol. T115, pp. 19–26, 2005. [Online]. Available: <http://iopscience.iop.org/1402-4896/2005/T115/001>

- [29] P. Alireza, Y. Chris, J. Gillet, C. Petrone, J. Cole, G. Lonzarich, and S. Sebastian, "Superconductivity up to 29 k in $SrFeAs_2$ and $BaFe_2As_2$ at high pressures," *Journal of Physics: Condensed Matter*, vol. 21, p. 012208, 2009. [Online]. Available: <http://iopscience.iop.org/0953-8984/21/1/012208/>
- [30] M. Rotter, M. Tegel, and D. Johrendt, "Superconductivity at 38 K in the iron arsenide $(Ba_{1-x}K_x)Fe_2As_2$," *Phys. Rev. Lett.*, vol. 101, p. 107006, Sep 2008. [Online]. Available: <http://link.aps.org/doi/10.1103/PhysRevLett.101.107006>
- [31] C. Gen-Fu, L. Zhend, L. Gang, H. Wan-Zheng, D. Jing, Z. Jun, Z. Xiao-Dong, Z. Ping, and W. Nan-Lin, "Superconductivity in hole-doped $(Sr_{1-x}K_x)Fe_2As_2$," *Chinese Physics Letters*, vol. 25, p. 3403, 2008. [Online]. Available: <http://iopscience.iop.org/0256-307X/25/9/083>
- [32] S. Zhang, X. Wang, Q. Liu, Y. Lv, X. Yu, Z. Lin, Y. Zhao, L. Wang, Y. Ding, H. Mao, and C. Jin, "Superconductivity at 31 K in the "111"-type iron arsenide superconductor $Na_{1-x}FeAs$ induced by pressure," *Europhysics Letters*, vol. 88, p. 47008, 2009. [Online]. Available: <http://iopscience.iop.org/0295-5075/88/4/47008>
- [33] G. Wu, H. Chen, T. Wu, Y. Xie, Y. Yan, R. Lui, X. Wang, J. Ying, and X. Chen, "Different resistivity response to spin-density wave and superconductivity at 20 K in $Ca_{1-x}Na_xFe_2As_2$," *Journal of Physics: Condensed Matter*, vol. 20, p. 422201, 2008. [Online]. Available: <http://iopscience.iop.org/0953-8984/20/42/422201>
- [34] T. Xia, J. He, D. Wang, and G. Chen, "Superconductivity at 33 k in "111" single crystals at ambient pressure," *arXiv 1001.3311*, 2010. [Online]. Available: <http://arxiv.org/abs/1001.3311>
- [35] Y. Mizuguchi, F. Tomioka, S. Tsuda, T. Yamaguchi, and Y. Takano, "Substitution effects on FeSe superconductor," *Journal of the Physical Society of Japan*, vol. 78, p. 074712, 2009. [Online]. Available: <http://jpsj.ipap.jp/link?JPSJ/78/074712/>
- [36] R. Hu, E. S. Bozin, J. B. Warren, and C. Petrovic, "Superconductivity, magnetism, and stoichiometry of single crystals of $Fe_{1+y}(Te_{1-x}S_x)_z$," *Phys. Rev. B*, vol. 80, p. 214514, Dec 2009. [Online]. Available: <http://link.aps.org/doi/10.1103/PhysRevB.80.214514>
- [37] M. Mito, M. Pitcher, W. Crichton, G. Garbarino, P. Baker, S. Blundell, P. Adamson, D. Parker, and S. Clarke, "Response of superconductivity and crystal syructure of LiFeAs to hydrostatic pressure," *J. Am. Chem. Soc.*, vol. 131, pp. 29 866–2992, 2009. [Online]. Available: <http://pubs.acs.org/doi/abs/10.1021/ja808914a>
- [38] S. O. Diallo, V. P. Antropov, T. G. Perring, C. Broholm, J. J. Pulikkotil, N. Ni, S. L. Bud'ko, P. C. Canfield, A. Kreyssig, A. I. Goldman, and R. J. McQueeney, "Itinerant magnetic excitations in antiferromagnetic $CaFe_2As_2$," *Phys. Rev. Lett.*, vol. 102, p. 187206, May 2009. [Online]. Available: <http://link.aps.org/doi/10.1103/PhysRevLett.102.187206>
- [39] H. Luetkens, H. Klauss, M. Kraken, F. Litterst, T. Dellmann, R. Klingeler, C. Hess, R. Khasanov, A. Amato, C. Baines, M. Kosmala, O. Schumann, M. Draden, J. Hamann-Borrero, N. Leps, A. Kondrat, G. Berh, J. Werner, and B. Büchner, "The electronic phase diagram of the $LaO_{1-x}F_xFeAs$ superconductor," *Nature Materials*, vol. 8, pp. 305–309, 2009. [Online]. Available: <http://www.nature.com/nmat/journal/v8/n4/abs/nmat2397.html>
- [40] J. Zhao, Q. Huang, C. de la Cruz, L. Shiliang, J. Lynn, Y. Chen, M. Greem, G. Chen, G. Li, Z. Li, J. Luo, N. Wang, and D. P., "Structural and magnetic phase diagram of $CeFeAsO_{1-x}F_x$ and its relation to high-temperature superconductivity," *Nature Materials*, vol. 7, pp. 953–959, 2008. [Online]. Available: <http://www.nature.com/nmat/journal/v7/n12/abs/nmat2315.html>
- [41] H. Takahashi, K. Igawa, K. Arii, Y. Kamihara, H. Masahiro, and H. Hosono, "Superconductivity at 43 k in an iron-based layered compound $LaO_{1-x}F_xFeAs$," *Nature*, vol. 453, pp. 376–378, 2008. [Online]. Available: <http://www.nature.com/nature/journal/v453/n7193/abs/nature06972.html>

- [42] R. Kumar, D. Antonio, M. Kanagaraj, S. Arumugam, J. Prakash, S. Sinogeikin, G. Thakur, A. Ganguli, A. Cornelius, and Y. Zhao, "Pressure induced structural transition and enhancement of superconductivity in Co doped CeFeAsO," *Applied Physics Letters*, vol. 98–101, p. 012511, 2011. [Online]. Available: <http://dx.doi.org/10.1063/1.3536521>
- [43] S. Li, D. Yao, Y. Qiu, H. Jung Kang, E. Carlson, J. Hu, G. Chen, N. Wang, and P. Dai, "Low-energy ce spin excitations in *cefeaso* and *cefeaso_{0.84}f_{0.16}*," *Frontiers of Physics in China*, vol. 5, pp. 161–165, 2010. [Online]. Available: <http://dx.doi.org/10.1007/s11467-009-0077-8>
- [44] J. Wen, G. Xu, Z. Xu, Z. W. Lin, Q. Li, Y. Chen, S. Chi, G. Gu, and J. M. Tranquada, "Effect of magnetic field on the spin resonance in FeTe_{0.5}Se_{0.5} as seen via inelastic neutron scattering," *Phys. Rev. B*, vol. 81, p. 100513, Mar 2010. [Online]. Available: <http://link.aps.org/doi/10.1103/PhysRevB.81.100513>
- [45] A. E. Taylor, M. J. Pitcher, R. A. Ewings, T. G. Perring, S. J. Clarke, and A. T. Boothroyd, "Antiferromagnetic spin fluctuations in LiFeAs observed by neutron scattering," *Phys. Rev. B*, vol. 83, p. 220514, Jun 2011. [Online]. Available: <http://link.aps.org/doi/10.1103/PhysRevB.83.220514>
- [46] M. Wang, H. Luo, M. Wang, S. Chi, J. A. Rodriguez-Rivera, D. Singh, S. Chang, J. W. Lynn, and P. Dai, "Magnetic field effect on static antiferromagnetic order and spin excitations in the underdoped iron arsenide superconductor BaFe_{1.92}Ni_{0.08}As₂," *Phys. Rev. B*, vol. 83, p. 094516, Mar 2011. [Online]. Available: <http://link.aps.org/doi/10.1103/PhysRevB.83.094516>
- [47] S. Wakimoto, K. Kodama, M. Ishikado, M. Matsuda, R. Kajimoto, M. Arai, K. Kakurai, F. Esaka, A. Iyo, H. Kito, H. Eisaki, and S. Shamoto, "Degradation of superconductivity and spin fluctuations by electron overdoping in *LaFeAsO_{1-x}F_x*," *Journal of the Physical Society of Japan*, vol. 79, pp. 074 715–074 719, 2010. [Online]. Available: <http://jpsj.ipap.jp/link?JPSJ/79/074715/>
- [48] Y. Kamihara, H. Hiramatsu, M. Hirano, R. Kawamura, H. Yanagi, T. Kamiya, and H. Hosono, "Iron-based layered superconductor: LaOFeP," *Journal of the American Chemical Society*, vol. 128, pp. 10 012–10 013, 2006. [Online]. Available: <http://pubs.acs.org/doi/abs/10.1021/ja063355c>
- [49] A. I. Coldea, J. D. Fletcher, A. Carrington, J. G. Analytis, A. F. Bangura, J.-H. Chu, A. S. Erickson, I. R. Fisher, N. E. Hussey, and R. D. McDonald, "Fermi surface of superconducting LaFePO determined from quantum oscillations," *Phys. Rev. Lett.*, vol. 101, p. 216402, Nov 2008. [Online]. Available: <http://link.aps.org/doi/10.1103/PhysRevLett.101.216402>
- [50] K. Igawa, H. Okada, K. Arii, H. Takahashi, Y. Kamihara, M. Hirano, H. H., S. Nakano, and T. Kikegawa, "Pressure study of superconducting oxypnictide lafepo," *Journal of the Physical Society of Japan*, vol. 78, pp. 03 701–023 705, 2009. [Online]. Available: <http://jpsj.ipap.jp/link?JPSJ/78/023701/>
- [51] W. Nolting, *Grundkurs Theoretische Physik 7: Viel-Teilchen-Theorie*, 7th ed. Springer Berlin Heidelberg, 2009.
- [52] A. Fetter and J. Walecka, *Quantum Theory of Many-Particle Systems*. Dover Publications, 2003.
- [53] S. Baroni, S. de Gironcoli, A. Dal Corso, and P. Giannozzi, "Phonons and related crystal properties from density-functional perturbation theory," *Rev. Mod. Phys.*, vol. 73, pp. 515–562, Jul 2001. [Online]. Available: <http://link.aps.org/doi/10.1103/RevModPhys.73.515>
- [54] P. Buczek, A. Ernst, and L. M. Sandratskii, "Different dimensionality trends in the landau damping of magnons in iron, cobalt, and nickel: Time-dependent density functional study," *Phys. Rev. B*, vol. 84, p. 174418, Nov 2011. [Online]. Available: <http://link.aps.org/doi/10.1103/PhysRevB.84.174418>

- [55] M. S. Hybertsen and S. G. Louie, “*Ab initio* static dielectric matrices from the density-functional approach. i. formulation and application to semiconductors and insulators,” *Phys. Rev. B*, vol. 35, pp. 5585–5601, Apr 1987. [Online]. Available: <http://link.aps.org/doi/10.1103/PhysRevB.35.5585>
- [56] P. Buczek, A. Ernst, P. Bruno, and L. M. Sandratskii, “Energies and lifetimes of magnons in complex ferromagnets: A first-principle study of heusler alloys,” *Phys. Rev. Lett.*, vol. 102, p. 247206, Jun 2009. [Online]. Available: <http://link.aps.org/doi/10.1103/PhysRevLett.102.247206>
- [57] R. Zhang and C. Deng, “Exact solutions of the schrödinger equation for some quantum-mechanical many-body systems,” *Phys. Rev. A*, vol. 47, pp. 71–77, Jan 1993. [Online]. Available: <http://link.aps.org/doi/10.1103/PhysRevA.47.71>
- [58] S. Kurth Ph.D. thesis, *Exchange-Correlation Functional for Inhomogenous Superconductors*. Bayerische Julius-Maximilians Universität Würzburg, 1992. [Online]. Available: <http://katalog.bibliothek.uni-wuerzburg.de/InfoGuideClient.ubwsis/start.do?Login=igubwww&Language=de&Query=10=%22BV010588953%22>
- [59] R. Mattuck, *A Guide to Feynman Diagrams in the Many-Body Problem*, 2nd ed. Dover Publications INC. New York, 1967.
- [60] F. Aryasetiawan and S. Biermann, “Generalized Hedin’s equations for quantum many-body systems with spin-dependent interactions,” *Phys. Rev. Lett.*, vol. 100, p. 116402, Mar 2008. [Online]. Available: <http://link.aps.org/doi/10.1103/PhysRevLett.100.116402>
- [61] R. Dreizler and E. Gross, *Density Functional Theory – An Approach to the Quantum Many–Body Problem*. Springer-Verlag Berlin Heidelberg, 1990.
- [62] P. Hohenberg and W. Kohn, “Inhomogeneous electron gas,” *Phys. Rev.*, vol. 136, pp. B864–B871, Nov 1964. [Online]. Available: <http://link.aps.org/doi/10.1103/PhysRev.136.B864>
- [63] C. J. Grayce and R. A. Harris, “Magnetic-field density-functional theory,” *Phys. Rev. A*, vol. 50, pp. 3089–3095, Oct 1994. [Online]. Available: <http://link.aps.org/doi/10.1103/PhysRevA.50.3089>
- [64] O. Gunnarsson and B. I. Lundqvist, “Exchange and correlation in atoms, molecules, and solids by the spin-density-functional formalism,” *Phys. Rev. B*, vol. 13, pp. 4274–4298, May 1976. [Online]. Available: <http://link.aps.org/doi/10.1103/PhysRevB.13.4274>
- [65] K. Capelle and G. Vignale, “Nonuniqueness of the potentials of spin-density-functional theory,” *Phys. Rev. Lett.*, vol. 86, pp. 5546–5549, Jun 2001. [Online]. Available: <http://link.aps.org/doi/10.1103/PhysRevLett.86.5546>
- [66] C. A. Ullrich, “Nonuniqueness in spin-density-functional theory on lattices,” *Phys. Rev. B*, vol. 72, p. 073102, Aug 2005. [Online]. Available: <http://link.aps.org/doi/10.1103/PhysRevB.72.073102>
- [67] C. C. Tsuei and J. R. Kirtley, “Pairing symmetry in cuprate superconductors,” *Rev. Mod. Phys.*, vol. 72, pp. 969–1016, Oct 2000. [Online]. Available: <http://link.aps.org/doi/10.1103/RevModPhys.72.969>
- [68] A. P. Mackenzie and Y. Maeno, “The superconductivity of Sr_2RuO_4 and the physics of spin-triplet pairing,” *Rev. Mod. Phys.*, vol. 75, pp. 657–712, May 2003. [Online]. Available: <http://link.aps.org/doi/10.1103/RevModPhys.75.657>
- [69] M. Lüders Ph.D. thesis, *Density Functional Theory for Superconductors, A first Principles Approach to the SC Phase*. Bayerische Julius-Maximilians Universität Würzburg, 1998. [Online]. Available: <http://katalog.bibliothek.uni-wuerzburg.de/InfoGuideClient.ubwsis/start.do?Login=igubwww&Language=de&Query=10=%22BV012665182%22>

- [70] N. D. Mermin, “Thermal properties of the inhomogeneous electron gas,” *Phys. Rev.*, vol. 137, pp. A1441–A1443, Mar 1965. [Online]. Available: <http://link.aps.org/doi/10.1103/PhysRev.137.A1441>
- [71] W. Kohn and L. J. Sham, “Self-consistent equations including exchange and correlation effects,” *Phys. Rev.*, vol. 140, pp. A1133–A1138, Nov 1965. [Online]. Available: <http://link.aps.org/doi/10.1103/PhysRev.140.A1133>
- [72] O. Lucas, E. Stoudenmire, K. Burke, and S. White, “Guaranteed convergence of the kohn-sham equations,” *arXiv 1305.2967*, 2013. [Online]. Available: <http://arxiv.org/abs/1305.2967>
- [73] M. Marques Ph.D. thesis, *Density Functional Theory for Superconductors, Exchange and Correlation Potentials for Inhomogeneous Systems*. Bayerische Julius-Maximilians Universität Würzburg, 1998. [Online]. Available: <http://katalog.bibliothek.uni-wuerzburg.de/InfoGuideClient.ubwsys/start.do?Login=igubwww&Language=de&Query=10=%22BV013730086%22>
- [74] L. Boeri, O. V. Dolgov, and A. A. Golubov, “Is LaFeAsO_{1-x}F_x an electron-phonon superconductor?” *Phys. Rev. Lett.*, vol. 101, p. 026403, Jul 2008. [Online]. Available: <http://link.aps.org/doi/10.1103/PhysRevLett.101.026403>
- [75] J. Paglione and R. Greene, “High-temperature superconductivity in iron-based materials,” *nature physics*, vol. 6, p. 645, 2010. [Online]. Available: <http://www.nature.com/nphys/journal/v6/n9/full/nphys1759.html>
- [76] R. van Leeuwen, “First-principles approach to the electron-phonon interaction,” *Phys. Rev. B*, vol. 69, p. 115110, Mar 2004. [Online]. Available: <http://link.aps.org/doi/10.1103/PhysRevB.69.115110>
- [77] L. G. Molinari, “Hedin’s equations and enumeration of feynman diagrams,” *Phys. Rev. B*, vol. 71, p. 113102, Mar 2005. [Online]. Available: <http://link.aps.org/doi/10.1103/PhysRevB.71.113102>
- [78] H. Englisch and R. Englisch, “Exact density functionals for ground-state energies ii. details and remarks,” *physica status solidi b*, vol. 124, pp. 373–379, 1984. [Online]. Available: <http://onlinelibrary.wiley.com/doi/10.1002/pssb.2221240140/abstract>
- [79] F. Tandetzky, J. Dewhurst, S. Sharma, and E. Gross, “Multiplicity of solutions to gw-type approximations,” *arXiv 1205.4274*, 2012. [Online]. Available: <http://arxiv.org/abs/1205.4274>
- [80] J. A. Hertz and D. M. Edwards, “Intermediate-coupling theory for itinerant ferromagnetism,” *Phys. Rev. Lett.*, vol. 28, pp. 1334–1337, May 1972. [Online]. Available: <http://link.aps.org/doi/10.1103/PhysRevLett.28.1334>
- [81] J. Hertz and D. Edwards, “Electron-magnon interactions in itinerant ferromagnetism. i. formal theory,” *Journal of Phys. F: Metal Physics*, vol. 3, p. 2174, 1973. [Online]. Available: <http://iopscience.iop.org/0305-4608/3/12/018>
- [82] E. Şaşıoğlu, A. Schindlmayr, C. Friedrich, F. Freimuth, and S. Blügel, “Wannier-function approach to spin excitations in solids,” *Phys. Rev. B*, vol. 81, p. 054434, Feb 2010. [Online]. Available: <http://link.aps.org/doi/10.1103/PhysRevB.81.054434>
- [83] F. Aryasetiawan and K. Karlsson, “Green’s function formalism for calculating spin-wave spectra,” *Phys. Rev. B*, vol. 60, pp. 7419–7428, Sep 1999. [Online]. Available: <http://link.aps.org/doi/10.1103/PhysRevB.60.7419>
- [84] A. Sanna, G. Profeta, A. Floris, A. Marini, E. K. U. Gross, and S. Massidda, “Anisotropic gap of superconducting CaC₆: A first-principles density functional calculation,” *Phys. Rev. B*, vol. 75, p. 020511, Jan 2007. [Online]. Available: <http://link.aps.org/doi/10.1103/PhysRevB.75.020511>

- [85] A. Floris, A. Sanna, S. Massidda, and E. K. U. Gross, “Two-band superconductivity in pb from *ab initio* calculations,” *Phys. Rev. B*, vol. 75, p. 054508, Feb 2007. [Online]. Available: <http://link.aps.org/doi/10.1103/PhysRevB.75.054508>
- [86] C. Bersier, A. Floris, A. Sanna, G. Profeta, A. Continenza, E. K. U. Gross, and S. Massidda, “Electronic, vibrational, and superconducting properties of CaBeSi: First-principles calculations,” *Phys. Rev. B*, vol. 79, p. 104503, Mar 2009. [Online]. Available: <http://link.aps.org/doi/10.1103/PhysRevB.79.104503>
- [87] G. Vignale and K. S. Singwi, “Effective two-body interaction in coulomb fermi liquids,” *Phys. Rev. B*, vol. 32, no. 4, pp. 2156–2166, Aug 1985. [Online]. Available: <http://link.aps.org/doi/10.1103/PhysRevB.32.2156>
- [88] A. Schindlmayr, T. J. Pollehn, and R. W. Godby, “Spectra and total energies from self-consistent many-body perturbation theory,” *Phys. Rev. B*, vol. 58, pp. 12 684–12 690, Nov 1998. [Online]. Available: <http://link.aps.org/doi/10.1103/PhysRevB.58.12684>
- [89] N. E. Bickers, D. J. Scalapino, and S. R. White, “Conserving approximations for strongly correlated electron systems: Bethe-Salpeter equation and dynamics for the two-dimensional hubbard model,” *Phys. Rev. Lett.*, vol. 62, pp. 961–964, Feb 1989. [Online]. Available: <http://link.aps.org/doi/10.1103/PhysRevLett.62.961>
- [90] R. Del Sole, L. Reining, and R. W. Godby, “*GW* γ approximation for electron self-energies in semiconductors and insulators,” *Phys. Rev. B*, vol. 49, pp. 8024–8028, Mar 1994. [Online]. Available: <http://link.aps.org/doi/10.1103/PhysRevB.49.8024>
- [91] V. P. Zhukov, E. V. Chulkov, and P. M. Echenique, “*GW* + *T* theory of excited electron lifetimes in metals,” *Phys. Rev. B*, vol. 72, p. 155109, Oct 2005. [Online]. Available: <http://link.aps.org/doi/10.1103/PhysRevB.72.155109>
- [92] M. S. Hybertsen and S. G. Louie, “Electron correlation in semiconductors and insulators: Band gaps and quasiparticle energies,” *Phys. Rev. B*, vol. 34, pp. 5390–5413, Oct 1986. [Online]. Available: <http://link.aps.org/doi/10.1103/PhysRevB.34.5390>
- [93] G. D. Mahan and B. E. Sernelius, “Electron-electron interactions and the bandwidth of metals,” *Phys. Rev. Lett.*, vol. 62, pp. 2718–2720, Jun 1989. [Online]. Available: <http://link.aps.org/doi/10.1103/PhysRevLett.62.2718>
- [94] A. Görling, “Density-functional theory for excited states,” *Phys. Rev. A*, vol. 54, pp. 3912–3915, Nov 1996. [Online]. Available: <http://link.aps.org/doi/10.1103/PhysRevA.54.3912>
- [95] C. Filippi, C. Umrigar, and X. Gonze, “Excitation energies from density functional perturbation theory,” *Journal of Chemical Physics*, vol. 107, p. 9994, 1997. [Online]. Available: http://jcp.aip.org/resource/1/jcpsa6/v107/i23/p9994_s1
- [96] J. P. Perdew and Y. Wang, “Accurate and simple analytic representation of the electron-gas correlation energy,” *Phys. Rev. B*, vol. 45, pp. 13 244–13 249, Jun 1992. [Online]. Available: <http://link.aps.org/doi/10.1103/PhysRevB.45.13244>
- [97] J. P. Perdew, K. Burke, and M. Ernzerhof, “Generalized gradient approximation made simple,” *Phys. Rev. Lett.*, vol. 77, pp. 3865–3868, Oct 1996. [Online]. Available: <http://link.aps.org/doi/10.1103/PhysRevLett.77.3865>
- [98] S. M. Shapiro, G. Shirane, and J. D. Axe, “Measurements of the electron-phonon interaction in nb by inelastic neutron scattering,” *Phys. Rev. B*, vol. 12, pp. 4899–4908, Dec 1975. [Online]. Available: <http://link.aps.org/doi/10.1103/PhysRevB.12.4899>

- [99] W. Meissner and R. Ochsenfeld, “Ein neuer Effekt bei Eintritt der Supraleitfähigkeit,” *Naturwissenschaften*, vol. 21, pp. 787–788, 1933. [Online]. Available: <http://link.springer.com/article/10.1007%2FBF01504252>
- [100] F. London and H. London, “The electromagnetic equations for the superconductor,” *Proceedings of the Royal Society of London*, vol. 149, pp. 71–88, 1935. [Online]. Available: <http://www.jstor.org/stable/96265>
- [101] H. F. Fong, B. Keimer, D. Reznik, D. L. Milius, and I. A. Aksay, “Polarized and unpolarized neutron-scattering study of the dynamical spin susceptibility of $\text{YBa}_2\text{Cu}_3\text{O}_7$,” *Phys. Rev. B*, vol. 54, pp. 6708–6720, Sep 1996. [Online]. Available: <http://link.aps.org/doi/10.1103/PhysRevB.54.6708>
- [102] D. Inosov, J. Park, P. Bourges, D. Sun, Y. Sidis, A. Schneidewind, K. Hradil, D. Haug, C. Lin, B. Keimer, and V. Hinkow, “Normal-state spin dynamics and temperature-dependent spin-resonance energy in optimally doped $\text{BaFe}_{1.85}\text{Co}_{0.15}\text{As}_2$,” vol. 6, pp. 178–181, 2009. [Online]. Available: <http://www.nature.com/nphys/journal/v6/n3/full/nphys1483.html>
- [103] T. A. Maier, S. Graser, D. J. Scalapino, and P. Hirschfeld, “Neutron scattering resonance and the iron-pnictide superconducting gap,” *Phys. Rev. B*, vol. 79, p. 134520, Apr 2009. [Online]. Available: <http://link.aps.org/doi/10.1103/PhysRevB.79.134520>
- [104] P. Romaniello, F. Bechstedt, and L. Reining, “Beyond the gw approximation: Combining correlation channels,” *Phys. Rev. B*, vol. 85, p. 155131, Apr 2012. [Online]. Available: <http://link.aps.org/doi/10.1103/PhysRevB.85.155131>
- [105] C. A. Kukkonen and A. W. Overhauser, “Electron-electron interaction in simple metals,” *Phys. Rev. B*, vol. 20, no. 2, pp. 550–557, Jul 1979. [Online]. Available: <http://link.aps.org/doi/10.1103/PhysRevB.20.550>
- [106] S. Yarlagadda and G. F. Giuliani, “Quasiparticle pseudo-hamiltonian of an infinitesimally polarized fermi liquid,” *Phys. Rev. B*, vol. 49, no. 12, pp. 7887–7897, Mar 1994. [Online]. Available: <http://link.aps.org/doi/10.1103/PhysRevB.49.7887>
- [107] C. Rostgaard, K. W. Jacobsen, and K. S. Thygesen, “Fully self-consistent GW calculations for molecules,” *Phys. Rev. B*, vol. 81, p. 085103, Feb 2010. [Online]. Available: <http://link.aps.org/doi/10.1103/PhysRevB.81.085103>
- [108] S. V. Faleev, M. van Schilfgaarde, and T. Kotani, “All-electron self-consistent GW approximation: Application to Si, MnO, and NiO,” *Phys. Rev. Lett.*, vol. 93, p. 126406, Sep 2004. [Online]. Available: <http://link.aps.org/doi/10.1103/PhysRevLett.93.126406>
- [109] M. Hellgren and U. von Barth, “Linear density response function within the time-dependent exact-exchange approximation,” *Phys. Rev. B*, vol. 78, p. 115107, Sep 2008. [Online]. Available: <http://link.aps.org/doi/10.1103/PhysRevB.78.115107>
- [110] A. Sanna Ph.D. thesis, *Application of Density Functional Theory for Superconductors to real materials*. Università degli Studi di Cagliari, 2007.
- [111] S. Kümmel and L. Kronik, “Orbital-dependent density functionals: Theory and applications,” *Rev. Mod. Phys.*, vol. 80, pp. 3–60, Jan 2008. [Online]. Available: <http://link.aps.org/doi/10.1103/RevModPhys.80.3>
- [112] M. Wierzbowska, “Effect of spin fluctuations on T_c from density-functional theory for superconductors,” *arXiv 0506262*, 2005. [Online]. Available: [arXiv:cond-mat/0506262](http://arxiv.org/abs/cond-mat/0506262)

- [113] I. I. Mazin, D. J. Singh, M. D. Johannes, and M. H. Du, “Unconventional superconductivity with a sign reversal in the order parameter of $\text{LaFeAsO}_{1-x}\text{F}_x$,” *Phys. Rev. Lett.*, vol. 101, p. 057003, Jul 2008. [Online]. Available: <http://link.aps.org/doi/10.1103/PhysRevLett.101.057003>
- [114] W. L. McMillan, “Transition temperature of strong-coupled superconductors,” *Phys. Rev.*, vol. 167, pp. 331–344, Mar 1968. [Online]. Available: <http://link.aps.org/doi/10.1103/PhysRev.167.331>
- [115] P. Morel and P. W. Anderson, “Calculation of the superconducting state parameters with retarded electron-phonon interaction,” *Phys. Rev.*, vol. 125, pp. 1263–1271, Feb 1962. [Online]. Available: <http://link.aps.org/doi/10.1103/PhysRev.125.1263>
- [116] D. J. Scalapino, J. R. Schrieffer, and J. W. Wilkins, “Strong-coupling superconductivity. i,” *Phys. Rev.*, vol. 148, pp. 263–279, Aug 1966. [Online]. Available: <http://link.aps.org/doi/10.1103/PhysRev.148.263>
- [117] P. B. Allen and R. C. Dynes, “Transition temperature of strong-coupled superconductors reanalyzed,” *Phys. Rev. B*, vol. 12, pp. 905–922, Aug 1975. [Online]. Available: <http://link.aps.org/doi/10.1103/PhysRevB.12.905>
- [118] G. R. Stewart, “Superconductivity in iron compounds,” *Rev. Mod. Phys.*, vol. 83, pp. 1589–1652, Dec 2011. [Online]. Available: <http://link.aps.org/doi/10.1103/RevModPhys.83.1589>
- [119] J. H. Tapp, Z. Tang, B. Lv, K. Sasmal, B. Lorenz, P. C. W. Chu, and A. M. Guloy, “ LiFeAs : An intrinsic FeAs -based superconductor with $T_c = 18$ K,” *Phys. Rev. B*, vol. 78, p. 060505, Aug 2008. [Online]. Available: <http://link.aps.org/doi/10.1103/PhysRevB.78.060505>
- [120] G. F. Chen, W. Z. Hu, J. L. Luo, and N. L. Wang, “Multiple phase transitions in single-crystalline $\text{Na}_{1-\delta}\text{FeAs}$,” *Phys. Rev. Lett.*, vol. 102, p. 227004, Jun 2009. [Online]. Available: <http://link.aps.org/doi/10.1103/PhysRevLett.102.227004>
- [121] S. V. Borisenko, V. B. Zabolotnyy, D. V. Evtushinsky, T. K. Kim, I. V. Morozov, A. N. Yaresko, A. A. Kordyuk, G. Behr, A. Vasiliev, R. Follath, and B. Büchner, “Superconductivity without nesting in LiFeAs ,” *Phys. Rev. Lett.*, vol. 105, p. 067002, Aug 2010. [Online]. Available: <http://link.aps.org/doi/10.1103/PhysRevLett.105.067002>
- [122] A. Tamai, A. Y. Ganin, E. Rozbicki, J. Bacsá, W. Meevasana, P. D. C. King, M. Caffio, R. Schaub, S. Margadonna, K. Prassides, M. J. Rosseinsky, and F. Baumberger, “Strong electron correlations in the normal state of the iron-based $\text{FeSe}_{0.42}\text{Te}_{0.58}$ Superconductor Observed by Angle-Resolved Photoemission Spectroscopy,” *Phys. Rev. Lett.*, vol. 104, p. 097002, Mar 2010. [Online]. Available: <http://link.aps.org/doi/10.1103/PhysRevLett.104.097002>
- [123] M. Yi, D. H. Lu, J. G. Analytis, J.-H. Chu, S.-K. Mo, R.-H. He, R. G. Moore, X. J. Zhou, G. F. Chen, J. L. Luo, N. L. Wang, Z. Hussain, D. J. Singh, I. R. Fisher, and Z.-X. Shen, “Electronic structure of the BaFe_2As_2 family of iron-pnictide superconductors,” *Phys. Rev. B*, vol. 80, p. 024515, Jul 2009. [Online]. Available: <http://link.aps.org/doi/10.1103/PhysRevB.80.024515>
- [124] D. Lu, M. Yi, S. Mo, A. Erickson, J. Analytis, J. Chy, D. Singh, Z. Hussain, T. Geballe, R. Fischer, and Z. Shen, “Electronic structure of the iron-based superconductor LaOFeP ,” pp. 81–84, 2008. [Online]. Available: <http://www.nature.com/nature/journal/v455/n7209/full/nature07263.html>
- [125] “Elk code.” [Online]. Available: <http://elk.sourceforge.net/>
- [126] S. J. Zhang, X. C. Wang, R. Sammynaiken, J. S. Tse, L. X. Yang, Z. Li, Q. Q. Liu, S. Desgreniers, Y. Yao, H. Z. Liu, and C. Q. Jin, “Effect of pressure on the iron arsenide superconductor Li_xFeAs ($x = 0.8, 1.0, 1.1$),” *Phys. Rev. B*, vol. 80, p. 014506, Jul 2009. [Online]. Available: <http://link.aps.org/doi/10.1103/PhysRevB.80.014506>

- [127] M. Gooch, B. Lv, J. Tapp, J. Tapp, Z. Tang, B. Lorenz, A. Guloy, and P. Chu, “Pressure shift of the superconducting T_c of LiFeAs,” *Europhysics Letters*, vol. 85, p. 27005, 2009. [Online]. Available: <http://iopscience.iop.org/0295-5075/85/2/27005/>
- [128] S. Margadonna, Y. Takabayashi, Y. Ohishi, Y. Mizuguchi, Y. Takano, T. Kagayama, T. Nakagawa, M. Takata, and K. Prassides, “Pressure evolution of the low-temperature crystal structure and bonding of the superconductor FeSe ($T_c = 37$ K),” *Phys. Rev. B*, vol. 80, p. 064506, Aug 2009. [Online]. Available: <http://link.aps.org/doi/10.1103/PhysRevB.80.064506>
- [129] R. Kumar, Y. Zhang, S. Sinogeikin, Y. Xiao, S. Kumar, P. Chow, A. Cornelius, and C. Chen, “Crystal and electronic structure of FeSe at high pressure and low temperature,” *J. Phys. Chem. B*, pp. 12 597–12 606, 2010. [Online]. Available: <http://pubs.acs.org/doi/abs/10.1021/jp1060446>
- [130] N. Jasmine, D. Phelana, E. Thomasb, J. Leãoa, and E. Carpentera, “Pressure-induced effects on the structure of the FeSe superconductor,” *Solid State Communications*, pp. 707–710, 2009. [Online]. Available: <http://dx.doi.org/10.1016/j.ssc.2009.02.011>
- [131] P. Giannozzi, S. Baroni, N. Bonini, M. Calandra, R. Car, C. Cavazzoni, D. Ceresoli, G. L. Chiarotti, M. Cococcioni, I. Dabo, A. Dal Corso, S. de Gironcoli, S. Fabris, G. Fratesi, R. Gebauer, U. Gerstmann, C. Gougoussis, A. Kokalj, M. Lazzeri, L. Martin-Samos, N. Marzari, F. Mauri, R. Mazzarello, S. Paolini, A. Pasquarello, L. Paulatto, C. Sbraccia, S. Scandolo, G. Sclauzero, A. P. Seitsonen, A. Smogunov, P. Umari, and R. M. Wentzcovitch, “Quantum espresso: a modular and open-source software project for quantum simulations of materials,” *Journal of Physics: Condensed Matter*, vol. 21, no. 39, p. 395502 (19pp), 2009. [Online]. Available: <http://www.quantum-espresso.org>
- [132] L. Ortenzi, I. I. Mazin, P. Blaha, and L. Boeri, “Accounting for spin fluctuations beyond local spin density approximation in the density functional theory,” *Phys. Rev. B*, vol. 86, p. 064437, Aug 2012. [Online]. Available: <http://link.aps.org/doi/10.1103/PhysRevB.86.064437>
- [133] Z. Yin, K. Haule, and G. Kotliar, “Kinetic frustration and the nature of the magnetic and paramagnetic states in iron pnictides and iron chalcogenides,” *Nature Materials*, vol. 10, pp. 932–935, 2011. [Online]. Available: <http://www.nature.com/nmat/journal/v10/n12/full/nmat3120.html>
- [134] G. Kotliar, S. Y. Savrasov, K. Haule, V. S. Oudovenko, O. Parcollet, and C. A. Marianetti, “Electronic structure calculations with dynamical mean-field theory,” *Rev. Mod. Phys.*, vol. 78, pp. 865–951, Aug 2006. [Online]. Available: <http://link.aps.org/doi/10.1103/RevModPhys.78.865>
- [135] S. Doniach, “Theory of inelastic neutron scattering in nearly ferromagnetic metals,” *Proceedings of the Physical Society*, vol. 91, pp. 86–96, 1967. [Online]. Available: <http://iopscience.iop.org/0370-1328/91/1/316>
- [136] P. Larson, I. I. Mazin, and D. J. Singh, “Magnetism, critical fluctuations, and susceptibility renormalization in Pd,” *Phys. Rev. B*, vol. 69, p. 064429, Feb 2004. [Online]. Available: <http://link.aps.org/doi/10.1103/PhysRevB.69.064429>
- [137] K. Umezawa, Y. Li, H. Miao, K. Nakayama, Z.-H. Liu, P. Richard, T. Sato, J. B. He, D.-M. Wang, G. F. Chen, H. Ding, T. Takahashi, and S.-C. Wang, “Unconventional anisotropic s -wave superconducting gaps of the LiFeAs iron-pnictide superconductor,” *Phys. Rev. Lett.*, vol. 108, p. 037002, Jan 2012. [Online]. Available: <http://link.aps.org/doi/10.1103/PhysRevLett.108.037002>
- [138] D. Evtushinsky, V. Zabolotnyy, T. Kim, A. Kordyuk, A. Yaresko, J. Maletz, S. Aswartham, S. Wurmehl, A. Boris, D. Sun, C. Lin, B. Shen, H. Wen, A. Varykhalov, R. Follath, B. Büchner, and S. Borisenko, “Strong pairing at iron $3d_{xz,yz}$ orbitals in hole-doped BaFe₂As₂,” *arXiv 1204.2432v1*, 2012. [Online]. Available: <http://arxiv.org/abs/1204.2432v1>

- [139] A. Sanna, S. Pittalis, J. K. Dewhurst, M. Monni, S. Sharma, G. Umrinario, S. Massidda, and E. K. U. Gross, “Phononic self-energy effects and superconductivity in CaC_6 ,” *Phys. Rev. B*, vol. 85, p. 184514, May 2012. [Online]. Available: <http://link.aps.org/doi/10.1103/PhysRevB.85.184514>
- [140] R. Jishi and D. Scalapino, “Contribution of the electron-phonon coupling to the pairing interaction in lifeas,” *arXiv 1306.2925*, 2013. [Online]. Available: <http://arxiv.org/abs/1306.2925>
- [141] P. Buczek Ph.D. thesis, *Spin dynamics of complex itinerant magnets*. Martin-Luther-Universität Halle-Wittenberg, 2009. [Online]. Available: <http://nbn-resolving.de/urn:nbn:de:gbv:3:4-552>
- [142] J. Cornwell, *Group Theory in Physics*. Academic Press, 1997.
- [143] H. B. Callen and T. A. Welton, “Irreversibility and generalized noise,” *Phys. Rev.*, vol. 83, pp. 34–40, Jul 1951. [Online]. Available: <http://link.aps.org/doi/10.1103/PhysRev.83.34>
- [144] G. Onida, L. Reining, and A. Rubio, “Electronic excitations: Density-functional versus many-body green’s-function approaches,” *Rev. Mod. Phys.*, vol. 74, pp. 601–659, Jun 2002. [Online]. Available: <http://link.aps.org/doi/10.1103/RevModPhys.74.601>
- [145] E. Runge and E. K. U. Gross, “Density-functional theory for time-dependent systems,” *Phys. Rev. Lett.*, vol. 52, pp. 997–1000, Mar 1984. [Online]. Available: <http://link.aps.org/doi/10.1103/PhysRevLett.52.997>
- [146] A. Linscheid Ph.D. thesis (to be submitted), *Density Functional Theory of Superconductivity in the Presence of a Magnetic Field*. Martin-Luther-Universität Halle-Wittenberg, 2014.
- [147] M. Sigrist and K. Ueda, “Phenomenological theory of unconventional superconductivity,” *Rev. Mod. Phys.*, vol. 63, pp. 239–311, Apr 1991. [Online]. Available: <http://link.aps.org/doi/10.1103/RevModPhys.63.239>
- [148] A. Kemper, T. Maier, S. Graser, H. Cheng, P. Hirschfeld, and D. Scalapino, “Sensitivity of the superconducting state and magnetic susceptibility to key aspects of electronic structure in ferropnictides,” vol. 12, p. 073030, 2010. [Online]. Available: <http://iopscience.iop.org/1367-2630/12/7/073030>
- [149] T. M. McQueen, A. J. Williams, P. W. Stephens, J. Tao, Y. Zhu, V. Ksenofontov, F. Casper, C. Felser, and R. J. Cava, “Tetragonal-to-orthorhombic structural phase transition at 90 K in the superconductor $\text{Fe}_{1.01}\text{Se}$,” *Phys. Rev. Lett.*, vol. 103, p. 057002, Jul 2009. [Online]. Available: <http://link.aps.org/doi/10.1103/PhysRevLett.103.057002>
- [150] H. Nakamura and M. Machida, “First-principles calculations of the effect of pressure on the iron-based superconductor LaFeAsO ,” *Phys. Rev. B*, vol. 80, p. 165111, Oct 2009. [Online]. Available: <http://link.aps.org/doi/10.1103/PhysRevB.80.165111>
- [151] F. Bruneval and M. Marques, “Benchmarking the starting points of the gw approximation for molecules,” *J. Chem. Theory Comput.*, pp. 324–329, 2013. [Online]. Available: <http://pubs.acs.org/doi/abs/10.1021/ct300835h>
- [152] R. M. Munroe, “the difference,” *xkcd 242*. [Online]. Available: <http://xkcd.com/242/>

Acknowledgments

In the end of such a long work, keeping me busy over many years, it is a pleasure to thank people who helped me on the way. I will enumerate the people in the order they come to my mind. Most likely I will also miss somebody and my deepest apologies for that. First I thank Hardy for giving me the opportunity to write the thesis at the Max-Planck-Institute. Hardy created a very relaxed and friendly working atmosphere and gave his [Ph.D.](#) students the freedom to find interesting projects. Every morning I was looking forward to go to the institute and work on my project.

Now I have to mention Andi who shared an office and a flat over the whole [Ph.D.](#) time with me. I think we were called “Frandy” for a reason in the office. But there was also a second [Ph.D.](#) student from the institute staying in our apartment: Kevin. Together we had the most “theoretical” flat in Halle or even Germany. I will never forget the endless cooking marathons in our kitchen or the shopping tours on Monday evenings at the worst supermarket.

When I arrived in Halle, I got in touch with Paweł and strongly benefited from his work on magnetic excitations in complex systems. For all the calculations I used his code and this work would be much poorer without his help. Via Paweł, I also meet Arthur and Leonid who are very different in nature, but are both great colleges. Both helped me a lot: Writing the paper on FeSe, understanding the [KKR](#) multiple scattering approach or discussing future projects. Besides an excellent group of scientists leading to fruitful collaborations, the institute also provided a very good infrastructure. Here I would like to mention Udo who kept, as a system administrator, the three high performance clusters and our desktop PCs running and Ina who organized all kinds of different things.

However, the [Ph.D.](#) in Halle was not a complete new beginning for me. From Hardy’s group in Berlin many familiar people joined the new group in Halle. Among them I would like to mention Sangeeta and Kay who became already colleges and friends while I did my Diploma at the Free University. Together we had very nice dinners and evenings together in Halle. Also Antonio moved from Berlin to Halle and was cooking excellent Italian food for everybody and laid out a herb garden in front of the Institute. Unfortunately the garden was destroyed by somebody for unknown reasons. Besides all that activities, he is the mastermind for [SCDFT](#) and it is fair to say that without him, there would be no successful [SCDFT](#) projects in the group.

After the version 1.0 of the thesis was written many people spend their precious time reading and correcting the manuscript. Here Julia, Falk, Andi, Antonio and Hardy helped a lot to bring the thesis in the current shape. I am really happy with the final result and could not imagine the outcome when I started the project more than three years ago. I will close the acknowledgments with thanking my parents who always encouraged me and my girlfriend who waited for me in Berlin. Thank you for the patience.

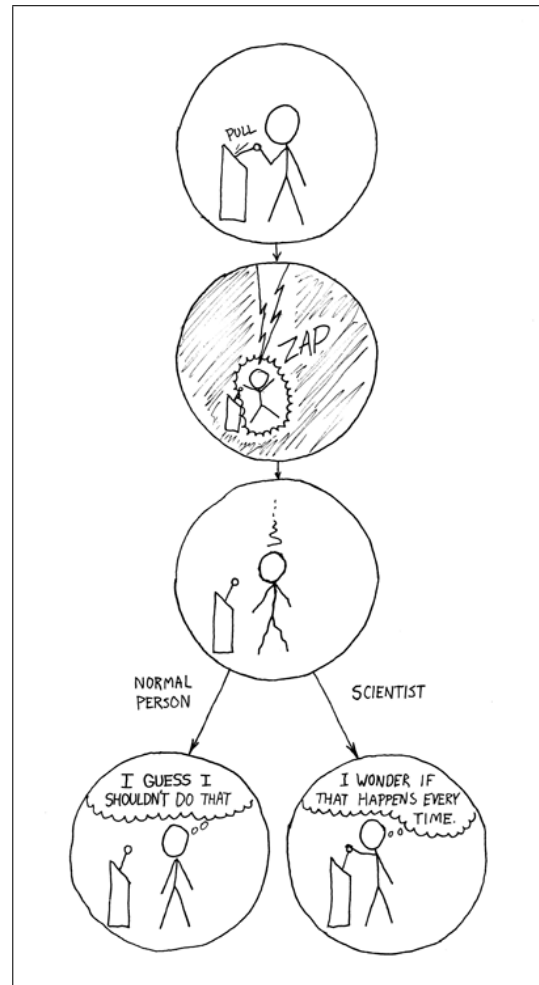


Figure E.4.: If you worked for a while in a physics institute you realize that there is some truth in this comic [152].

Curriculum Vitae

Personal Details

Name: Frank Essenberger

Address: Sophienstraße 1, 12203 Berlin

Born: 1984 in Berlin, Germany

Email: frank.essenberger@gmail.com

Citizenship: German

Marital Status: Unmarried

Education

1997 - 2004 High school

04/2005 - 04/2007 Prediploma in Physics – Freie Universität Berlin

04/2007 - 03/2010 Diploma in Physics – Freie Universität Berlin

Current Position

03/2010 - 04/2014 **Ph.D.** Student – MPI for Microstructure Physics in Halle (Saale)

Publications

- *Magnon spectrum of transition-metal oxides: Calculations including long-range magnetic interactions using the LSDA+U method*
F. Essenberger, S. Sharma, J. K. Dewhurst, C. Bersier, F. Cricchio, L. Nordström, and E. K. U. Gross
Phys. Rev. B 84, 174425 (2011)
- *Paramagnons in FeSe close to a magnetic quantum phase transition: ab initio study*
F. Essenberger, P. Buczek, A. Ernst, L. Sandratskii and E.K.U. Gross
Phys. Rev. B 86, 060412 (2012)

Eidesstattliche Erklärung

Hiermit erkläre ich gemäß §5 Abs. 4 der Promotionsordnung der Naturwissenschaftlichen Fakultät II – Chemie, Physik und Mathematik der Martin-Luther Universität Halle-Wittenberg vom August 2012, dass ich die vorliegende Arbeit selbständig und ohne fremde Hilfe verfasst habe. Es wurden keine, außer die angegebenen Quellen und Hilfsmittel benutzt und die den benutzten Werken wörtlich oder inhaltlich entnommenen Stellen wurden als solche kenntlich gemacht.

Desweiteren erkläre ich gemäß §5 Abs. 5 der Promotionsordnung, dass ich bisher keine vergeblichen Promotionsversuche an dieser oder einer anderen Fakultät unternommen habe.

Halle, den 25.11.2014

Frank Essenberger